

³¹P MAS NMR
INVESTIGATION OF SURFACE
ACIDITY ON SILICA-ALUMINA CATALYSTS
USING ADSORBED PHOSPHINES
AS NEW PROBES

by

BING HU

B.Sc. Nanjing University (China), 1983

M.Sc. Nanjing University (China), 1986

A THESIS SUBMITTED IN PARTIAL FULFILLMENT OF
THE REQUIREMENTS FOR THE DEGREE OF
DOCTOR OF PHILOSOPHY

in the Department of
Chemistry.

© BING HU 1997

Simon Fraser University

September 1997

All rights reserved. This work
may not be reproduced in whole or in part, by
photocopy or other means, without permission of the author.



National Library
of Canada

Acquisitions and
Bibliographic Services

395 Wellington Street
Ottawa ON K1A 0N4
Canada

Bibliothèque nationale
du Canada

Acquisitions et
services bibliographiques

395, rue Wellington
Ottawa ON K1A 0N4
Canada

Your file Votre référence

Our file Notre référence

The author has granted a non-exclusive licence allowing the National Library of Canada to reproduce, loan, distribute or sell copies of this thesis in microform, paper or electronic formats.

The author retains ownership of the copyright in this thesis. Neither the thesis nor substantial extracts from it may be printed or otherwise reproduced without the author's permission.

L'auteur a accordé une licence non exclusive permettant à la Bibliothèque nationale du Canada de reproduire, prêter, distribuer ou vendre des copies de cette thèse sous la forme de microfiche/film, de reproduction sur papier ou sur format électronique.

L'auteur conserve la propriété du droit d'auteur qui protège cette thèse. Ni la thèse ni des extraits substantiels de celle-ci ne doivent être imprimés ou autrement reproduits sans son autorisation.

0-612-24315-X

Canada

APPROVAL

Name: Bing Hu
Degree: Doctor of Philosophy
Title of Thesis: ^{31}P MAS NMR investigation of surface acidity on silica-alumina catalysts using adsorbed phosphines as new probes

Examining Committee:

Chairperson: Dr. B. M. Pinto

Dr. I. D. Gay (Senior Supervisor)

Dr. E. J. Wells

Dr. R. H. Hill

Dr. A. S. Tracey (Internal Examiner)

Dr. J. A. Ripmeester (External Examiner)

Date Approved: Sept 15, 1997

ABSTRACT

^{31}P solid state MAS NMR has been used to study the acidity on the surface of commercial silica-alumina cracking catalyst and novel monolayer Al_2O_3 catalyst coated with SiO_2 , using adsorbed solid bulky phosphines. Tricyclohexylphosphine (Cy_3P), tri-*p*-tolylphosphine ($(p\text{-Tol})_3\text{P}$), tri-*m*-tolylphosphine ($(m\text{-Tol})_3\text{P}$), triphenylphosphine (Ph_3P), tri-*p*-chlorophenylphosphine ($(p\text{-ClC}_6\text{H}_4)_3\text{P}$) and triphenylphosphine hydrobromide (Ph_3PHBr) have been widely studied in the thesis. Several model molecules (HCl , AlCl_3 , individual SiO_2 and Al_2O_3) were employed to characterize the species on the silica-alumina catalyst surface.

It was found that Cy_3P is a unique probe. Due to high basic strength, its measured Brønsted acid concentration is larger than with Me_3P and other phosphines. The bulky structure of Cy_3P is sensitive to different pore sizes. At submonolayer coverages, the molecules are highly mobile. At monolayer or higher coverages, the mobility of adsorbed species decreases. From this special property, we can observe some interesting results.

Using bulky arylphosphines, the maximum observed concentrations for Brønsted acid were controlled by the steric effects. At higher coverages a genuine decrease in the titration curves for Brønsted acid was observed. This phenomenon was explained by the presence of basic sites and the multilayers of physically adsorbed species at high surface coverages.

The new SiO_2 on Al_2O_3 catalyst (coated with 6.2 SiO_2 per nm^2) was prepared by a chemical vapor deposition method. It has a higher Brønsted acid concentration per nm^2 of the catalyst; more Lewis acid sites; and a larger pore size distribution than the commercial silica-alumina cracking catalyst.

Combining NMR results with net charge calculation, we suggest that catalytically active sites involve octahedral aluminum groups.

ACKNOWLEDGMENT

I wish to express my deep gratitude to Dr. I. D. Gay. It has been a great pleasure to work under his guidance. His continuous, patient and expert supervision has been proven extremely helpful. I thank Dr. T. Sheng for his beneficial assistance and discussion in the lab.

I would like to thank Dr. R. K. Pomeroy for his useful advice, encouragement and aryl phosphine samples. I thank Dr. E. J. Wells and Dr. R. H. Hill for their useful comments and time as members of my supervisory committee.

I thank Dr. B. Czajka for arranging measurement of the pore size distribution. The service of Mr. F. Chin, Mr. G. Owen, Mr. L. Wakida, Mr. G. Rynders and the other staff, especially secretaries is gratefully acknowledged.

Finally, I thank Dr. I. D. Gay, the Department of Chemistry and Simon Fraser University for the financial aid.

DEDICATION

to my wife Ning, my daughter Abby and my parents

TABLE OF CONTENTS

Title Page.....	i
Approval.....	ii
Abstract.....	iii
Acknowledgment.....	v
Dedication.....	vi
Table of Contents.....	vii
List of Schemes.....	x
List of Tables.....	xi
List of Figures.....	xii
Format.....	xxii
Symbols.....	xxv
Abbreviation.....	xxvi
Chapter 1 Solid-state NMR for adsorbed species and surfaces: Is it powerful?.....	1
1. Dipolar decoupling: This removes the (¹ H, ³¹ P) interaction.....	1
2. Magic Angle Spinning (MAS): Weapons for Chemical Shift Anisotropy (CSA) and weak dipolar interaction.....	5
3. Cross Polarization (CP): Borrowing proton magnetization greatly enhances signal-to-noise ratios.....	10
4. Extra Resolution Enhancement Techniques: Bonus from NMR to provide more information.....	23
5. References.....	30
Chapter 2 ³¹ P NMR to investigate acidity of the SiO ₂ -Al ₂ O ₃ catalysts: overview of related known facts.....	35
1. What is "Acidity"? definition and measurement.....	35

	2.	SiO ₂ -Al ₂ O ₃ is a mixed binary oxide: structure and acid property.....	37
	3.	NMR approaches to acid sites on silica-alumina surfaces by basic probes.....	47
	4.	References.....	56
Chapter 3		Still larger phosphines as ³¹ P NMR probes to investigate the acidity: the necessity, objectives and technical problems of this project.....	60
	1.	Remaining problems: why perform this project?.....	60
	2.	Electronic, Steric effects or both for acidity on a surface objectives.....	62
	3.	Technical problems: headaches not only from NMR.....	65
	4.	Experimental conditions: chemicals, apparatus, preparation procedures and measurement methods.....	74
	5.	References.....	80
Chapter 4		³¹ P NMR investigation of surface acidity using adsorbed tricyclohexylphosphine: an excellent new probe.....	82
	1.	Introduction: Why use Cy ₃ P?.....	82
	2.	Results and discussion: what we got.....	83
	3.	Conclusion.....	106
	4.	References.....	107
Chapter 5		³¹ P NMR investigation of surface acidity using adsorbed arylphosphines: strange titration curves.....	109
	1.	Introduction: why use more bulky aryl phosphines?.....	109
	2.	Results and Discussion: can these phosphines work?.....	109
	3.	Conclusion.....	169
	4.	References.....	170
Chapter 6		³¹ P NMR investigation of surface acidity of vapor deposited SiO ₂ on Al ₂ O ₃ monolayer catalyst: application to novel catalyst system.....	172
	1.	Introduction.....	172

2.	Results and Discussion.....	173
3.	Conclusion.....	215
4.	References.....	216
Chapter 7	Lewis acid sites using adducts of the phosphines and AlCl ₃ by ³¹ P NMR; poisoning effects of adsorbed phosphines on commercial silica-alumina catalyst using 1-butene isomerization reaction followed by GC, and the adsorbed (<i>p</i> -ClC ₆ H ₄) ₃ PO species by Mass Spectroscopy...217	
1.	Introduction.....	217
2.	Results and Discussion.....	219
3.	References.....	239
Chapter 8	³¹ P NMR investigation of surface basicity using adsorbed PPh ₃ HBr molecules.....	240
Chapter 9	Overall conclusion and future work.....	250
1.	Facts.....	250
2.	Argument.....	252
3.	Future work suggestions.....	253
4.	References.....	254

LIST OF SCHEMES

Scheme #		Page
6.1	Model of PH bond conversion.	193
6.2	Models of Brønsted acid sites for the monolayer Al ₂ O ₃ catalyst coated with SiO ₂ .	194

LIST OF TABLES

Table#		Page
1.1	Static Dipole Couplings in Selected Molecules	3
1.2	Static Dipole Coupling in Selected Phosphorous Molecules	4
1.3	An example of calculation of delay time for TOSS	22
1.4	Related Techniques for resolution enhancement	23
2.1	The techniques to measure the amount and strength of an acid	36
3.1	pKa and cone angle of the bulky phosphines	63
3.2	pKa and cone angle of previously studied phosphines	63
3.3	³¹ P chemical shifts of model compounds	71
3.4	J coupling constant of model compounds	73
3.5	³¹ P chemical shift on the SiO ₂ -Al ₂ O ₃ catalyst	74
5.1	³¹ P chemical shift of physically adsorbed Ph ₃ P species on SiO ₂ -Al ₂ O ₃	118
6.1	T ₁ values of Cy ₃ P on coated Al ₂ O ₃ monolayer catalyst	191
7.1	Results of fitting quadratic coupling experiments	231
7.2	Poisoning of 1-butene isomerization on the silica-alumina catalyst	233
7.3	MS results of the adsorbed phosphine and phosphine oxides	235
7.4	Literature MS results for Ph ₃ P and Ph ₃ PO	236
7.5	Theoretical isotope patterns of C ₁₈ H ₁₂ Cl ₃ P and C ₁₈ H ₁₂ Cl ₃ PO	237

LIST OF FIGURES

Figure#		Page
1.1	Non-dipolar decoupling ^{31}P NMR spectrum of pure Cy_3P	2
1.2	Non-spinning ^{31}P NMR spectrum of pure Cy_3P	5
1.3	Magic angle spinning and coordinates	8
1.4	^{31}P NMR spectrum of pure Cy_3P	9
1.5	Cross-Polarization pulse sequence using ^1H - ^{31}P as an example	11
1.6	Cross-Polarization flipback pulse sequence using ^1H - ^{31}P as an example	14
1.7	Dipolar dephasing pulse sequence using ^1H - ^{31}P as an example	16
1.8	^{31}P NMR spectra of $0.94 \mu\text{mol}/\text{m}^2$ Cy_3P on 6.2 SiO_2 per nm^2 Al_2O_3 monolayer catalyst adsorbed at 200°C .	18
1.9	Toss pulse sequence using ^1H - ^{31}P as an example	20
1.10	^{31}P NMR spectra of $1.33 \mu\text{mol}/\text{m}^2$ (<i>m</i> -Tol) $_3\text{P}$ on 6.2 SiO_2 per nm^2 Al_2O_3 monolayer catalyst adsorbed at 100°C	27
1.11	^{31}P NMR spectra of $0.38 \mu\text{mol}/\text{m}^2$ Cy_3P on 6.2 SiO_2 per nm^2 Al_2O_3 monolayer catalyst adsorbed at 100°C	29
2.1	The types of silanol groups on the silica surface	39
2.2	The reaction to form siloxane groups	40
2.3	Proposed models of surface OH groups on Al_2O_3 with the net charges and assigned OH IR frequencies.	42
2.4	Model A of the acid site structure of silica-alumina	45
2.5	Model B of the acid site of silica-alumina	45
2.6	Charge densities for models of silica-alumina	46
3.1	Y-shape tubing for sample preparing	68
3.2	Intensity of ^{31}P NMR spectra at various CP contact time	69
3.3	Reactor for the poisoning experiments by GC	79

4.1	^{31}P NMR spectra of pure Cy_3P for the T_1 measurement	84
4.2	Intensity of ^{31}P NMR spectra of pure Cy_3P versus delay time	85
4.3	^{31}P NMR spectra of pure Cy_3P and $0.38 \mu\text{mol}/\text{m}^2$ Cy_3P on silica gel	86
4.4	^{31}P NMR spectra of Cy_3P on silica gel with various coverage	88
4.5	^{31}P NMR spectra of Cy_3P on silica gel with higher coverages	89
4.6	^{31}P NMR spectra of $0.31 \mu\text{mol}/\text{m}^2$ Cy_3P on alumina	90
4.7	^{31}P NMR spectra of $1.01 \mu\text{mol}/\text{m}^2$ Cy_3P on alumina at low temperatures	91
4.8	^{31}P NMR spectra of $1.01 \mu\text{mol}/\text{m}^2$ Cy_3P on alumina adsorbed at 50°C with various recycle delay	92
4.9	Solution ^{31}P NMR spectra of pure Cy_3P and Cy_3PH^+ species	95
4.10	^{31}P NMR spectra of $1.27 \mu\text{mol}/\text{m}^2$ Cy_3P on silica-alumina with different pulse sequences and adsorbed at 200°C	97
4.11	^{31}P NMR spectra of $1.27 \mu\text{mol}/\text{m}^2$ Cy_3P on silica-alumina with different recycle delays and adsorbed at 200°C	98
4.12	^{31}P NMR spectra of $0.30 \mu\text{mol}/\text{m}^2$ Cy_3P on silica-alumina with different temperatures	99
4.13	^{31}P NMR spectra of Cy_3P on silica-alumina with different coverage and adsorbed at 200°C	100
4.14	^{31}P NMR spectra of Cy_3P on silica-alumina at higher coverages and adsorbed at 200°C	101
4.15	The concentration of Cy_3PH^+ on commercial silica-alumina at various coverages	103
4.16	The line widths of Cy_3P on silica-alumina catalyst as a function of surface coverages	105
5.1	^{31}P NMR spectra of pure Ph_3P and $0.92 \mu\text{mol}/\text{m}^2$ Ph_3P on silica gel	111
5.2	^{31}P NMR spectra of Ph_3P on silica gel with various coverages	112
5.3	^{31}P NMR spectra of $0.38 \mu\text{mol}/\text{m}^2$ Ph_3P on alumina	114

5.4	^{31}P NMR spectra of $0.33 \mu\text{mol}/\text{m}^2$ Ph_3P on commercial silica-alumina catalyst	115
5.5	^{31}P NMR spectra of $0.48 \mu\text{mol}/\text{m}^2$ Ph_3P on commercial silica-alumina catalyst with various recycle delay	116
5.6	^{31}P NMR spectra of Ph_3P at various coverages on commercial silica-alumina catalyst adsorbed at 200°C	120
5.7	^{31}P MAS NMR spectra of $0.11 \mu\text{mol}/\text{m}^2$ Ph_3P at various adsorption temperatures on silica-alumina	121
5.8	the concentrations of Ph_3PH^+ on commercial silica-alumina at various coverages.	122
5.9	^{31}P MAS NMR spectra of $0.19 \mu\text{mol}/\text{m}^2$ $(p\text{-Tol})_3\text{P}$ at various adsorption temperatures on silica	124
5.10	^{31}P MAS NMR spectra of $0.24 \mu\text{mol}/\text{m}^2$ $(p\text{-Tol})_3\text{P}$ at various adsorption temperatures on alumina	125
5.11	^{31}P MAS NMR spectra of $(p\text{-Tol})_3\text{P}$ at various coverages on alumina	126
5.12	^{31}P MAS NMR spectra of $(p\text{-Tol})_3\text{P}$ in HCl solution and $0.13 \mu\text{mol}/\text{m}^2$ on the silica-alumina surface	127
5.13	^{31}P MAS NMR spectra of $0.31 \mu\text{mol}/\text{m}^2$ $(p\text{-Tol})_3\text{P}$ on silica-alumina catalyst with various recycle delays	128
5.14	^{31}P MAS NMR spectra of $0.13 \mu\text{mol}/\text{m}^2$ $(p\text{-Tol})_3\text{P}$ at various adsorption temperatures on the silica-alumina catalyst	132
5.15	^{31}P MAS NMR spectra of $(p\text{-Tol})_3\text{P}$ at various coverages on silica-alumina adsorbed at 200°C	133
5.16	^{31}P MAS NMR spectra of $1.12 \mu\text{mol}/\text{m}^2$ $(p\text{-Tol})_3\text{P}$ on silica-alumina catalyst adsorbed at 200°C	134
5.17	the concentrations of $(p\text{-Tol})_3\text{PH}^+$ on commercial silica-alumina catalyst at various coverages	135

5.18.	^{31}P MAS NMR spectra of $0.19 \mu\text{mol}/\text{m}^2$ (<i>m</i> -Tol) $_3\text{P}$ on silica gel with various adsorption temperature	137
5.19	^{31}P MAS NMR spectra of (<i>m</i> -Tol) $_3\text{P}$ on silica gel with various degassing temperatures	138
5.20	^{31}P MAS NMR spectra of $0.29 \mu\text{mol}/\text{m}^2$ (<i>m</i> -Tol) $_3\text{P}$ on alumina surface	139
5.21	^{31}P MAS NMR spectra of $0.10 \mu\text{mol}/\text{m}^2$ (<i>m</i> -Tol) $_3\text{P}$ on silica-alumina catalyst with various adsorption temperatures	141
5.22	^{31}P MAS NMR spectra of (<i>m</i> -Tol) $_3\text{P}$ at various coverages on silica-alumina adsorbed at 200°C	142
5.23	^{31}P MAS NMR spectra of $1.33 \mu\text{mol}/\text{m}^2$ (<i>m</i> -Tol) $_3\text{P}$ on silica-alumina catalyst using 180° pulse-delay- 90° pulse program	143
5.24	the concentrations of (<i>m</i> -Tol) $_3\text{PH}^+$ on commercial silica-alumina catalyst at various coverages	145
5.25	^{31}P MAS NMR spectra of $0.16 \mu\text{mol}/\text{m}^2$ (<i>p</i> -ClC $_6\text{H}_4$) $_3\text{P}$ on the silica gel surface	147
5.26	^{31}P MAS NMR spectra of $0.12 \mu\text{mol}/\text{m}^2$ (<i>p</i> -ClC $_6\text{H}_4$) $_3\text{P}$ on the silica-alumina surface with various recycle delays	148
5.27	^{31}P MAS NMR spectra of $0.12 \mu\text{mol}/\text{m}^2$ (<i>p</i> -ClC $_6\text{H}_4$) $_3\text{P}$ on the silica-alumina surface with various adsorption temperatures	149
5.28	^{31}P MAS NMR spectra of (<i>p</i> -ClC $_6\text{H}_4$) $_3\text{P}$ on the silica-alumina surface with various surface coverages	150
5.29	^{31}P MAS NMR spectra of $0.28 \mu\text{mol}/\text{m}^2$ (<i>p</i> -ClC $_6\text{H}_4$) $_3\text{P}$ on the silica-alumina surface with various oxide species	151
5.30	^{31}P MAS NMR spectra of mixture of (<i>p</i> -ClC $_6\text{H}_4$) $_3\text{P}$ and Me $_3\text{NO}$ heated at 200°C for half an hour	152
5.31	the concentrations of (<i>p</i> -ClC $_6\text{H}_4$) $_3\text{PH}^+$ on commercial silica-alumina catalyst at various coverages	153

5.32	^{31}P MAS NMR spectra of pure (<i>o</i> -Tol) $_3\text{P}$ sample and (<i>o</i> -Tol) $_3\text{P}$ in the concentrated HCl	157
5.33	^{31}P MAS NMR spectra of $0.08 \mu\text{mol}/\text{m}^2$ (<i>o</i> -Tol) $_3\text{P}$ on the silica gel surface with different adsorption temperatures	158
5.34	^{31}P MAS NMR spectra of $0.17 \mu\text{mol}/\text{m}^2$ (<i>o</i> -Tol) $_3\text{P}$ on the alumina surface with different pulse programs	159
5.35	^{31}P MAS NMR spectra of $0.35 \mu\text{mol}/\text{m}^2$ (<i>o</i> -Tol) $_3\text{P}$ on the alumina surface	160
5.36	^{31}P MAS NMR spectra of $0.13 \mu\text{mol}/\text{m}^2$ (<i>o</i> -Tol) $_3\text{P}$ on the silica-alumina surface with different pulse programs	161
5.37	^{31}P MAS NMR spectra of liquid Me_2PhP sample	164
5.38	^{31}P MAS NMR spectra of $2.04 \mu\text{mol}/\text{m}^2$ Me_2PhP on silica gel	165
5.39	^{31}P MAS NMR spectra of $1.01 \mu\text{mol}/\text{m}^2$ Me_2PhP on the alumina surface	166
5.40	^{31}P MAS NMR spectra of $0.91 \mu\text{mol}/\text{m}^2$ Me_2PhP on the silica-alumina surface with difference pulse sequences	167
5.41	^{31}P MAS NMR spectra of $1.51 \mu\text{mol}/\text{m}^2$ Me_2PhP on the silica-alumina surface with difference pulse sequences	168
6.1.	^{31}P MAS NMR spectra of $0.40 \mu\text{mol}/\text{m}^2$ Ph_3P on Al_2O_3 monolayer catalyst with 6.2 SiO_2 per nm^2 with different pulse sequences	176
6.2	^{31}P MAS NMR spectra of $0.40 \mu\text{mol}/\text{m}^2$ Ph_3P on Al_2O_3 monolayer catalyst with 6.2 SiO_2 per nm^2 with different recycle delays	177
6.3	^{31}P MAS NMR spectra of $0.40 \mu\text{mol}/\text{m}^2$ Ph_3P on Al_2O_3 monolayer catalyst with 6.2 SiO_2 per nm^2 , with different adsorption temperatures	178
6.4	^{31}P MAS NMR spectra of Ph_3P on Al_2O_3 monolayer catalyst with 6.2 SiO_2 per nm^2 , with different coverages	179
6.5	the concentrations of Ph_3PH^+ on Al_2O_3 monolayer catalyst with 6.2 SiO_2 per nm^2 at various coverages	180

6.6	^{31}P MAS NMR spectra of $1.10 \mu\text{mol}/\text{m}^2$ Me_3P on Al_2O_3 monolayer catalyst with 6.2 SiO_2 per nm^2 , with different pulse sequences	183
6.7	^{31}P MAS NMR spectra of $1.10 \mu\text{mol}/\text{m}^2$ Me_3P on Al_2O_3 monolayer catalyst with 6.2 SiO_2 per nm^2 , with different recycle delays	184
6.8	^{31}P MAS NMR spectra of $1.10 \mu\text{mol}/\text{m}^2$ Me_3P on Al_2O_3 monolayer catalyst with 6.2 SiO_2 per nm^2 , with different τ values in the $(180^\circ-\tau-90^\circ(\text{FID})-\text{T}_d)_n$ pulse sequence (90° pulse)	185
6.9	Intensity of ^{31}P MAS NMR spectra versus delay time in the 90° sequence (the data were taken from Figure 6.8)	186
6.10	^{31}P MAS NMR spectra of $1.10 \mu\text{mol}/\text{m}^2$ Me_3P on Al_2O_3 monolayer catalyst with 6.2 SiO_2 per nm^2 , with different adsorption temperatures	187
6.11	^{31}P MAS NMR spectra of Me_3P on commercial silica-alumina catalyst with different adsorption temperatures	188
6.12	^{31}P MAS NMR spectra of $0.41 \mu\text{mol}/\text{m}^2$ Cy_3P on Al_2O_3 monolayer catalyst with 6.2 SiO_2 per nm^2 , with different adsorption temperatures	198
6.13	^{31}P MAS NMR spectra of $0.41 \mu\text{mol}/\text{m}^2$ Cy_3P on Al_2O_3 monolayer catalyst with 6.2 SiO_2 per nm^2 , with different recycle delays	199
6.14	^{31}P MAS NMR spectra of $0.41 \mu\text{mol}/\text{m}^2$ Cy_3P on Al_2O_3 monolayer catalyst with 6.2 SiO_2 per nm^2 , with different delays for the dipolar dephasing sequence	200
6.15	Intensity of ^{31}P MAS NMR spectra versus delay time in the dipolar dephasing sequence (The data were taken from adding of several groups of spectra like Figure 6.14).	201
6.16	Intensity of ^{31}P MAS NMR spectra versus delay time in the dipolar dephasing sequence (The data were taken from same sample with Figure 6.12b)	202
6.17	^{31}P MAS NMR spectra of $1.68 \mu\text{mol}/\text{m}^2$ Cy_3P on Al_2O_3 monolayer catalyst with 6.2 SiO_2 per nm^2 , with adsorption at different temperatures, 90° pulse	203

6.18	^{31}P MAS NMR spectra of $1.68 \mu\text{mol}/\text{m}^2$ Cy_3P on Al_2O_3 monolayer catalyst with 6.2 SiO_2 per nm^2 , with adsorption at different temperatures, CP	204
6.19	^{31}P MAS NMR spectra of $1.99 \mu\text{mol}/\text{m}^2$ Cy_3P on Al_2O_3 monolayer catalyst with 6.2 SiO_2 per nm^2 , with different pulse sequences	205
6.20	^{31}P MAS NMR spectra of $1.99 \mu\text{mol}/\text{m}^2$ Cy_3P on Al_2O_3 monolayer catalyst with 6.2 SiO_2 per nm^2 , with different pulse sequences	206
6.21	^{31}P MAS NMR spectra of $1.99 \mu\text{mol}/\text{m}^2$ Cy_3P on Al_2O_3 monolayer catalyst with 6.2 SiO_2 per nm^2 , with different pulse sequences	207
6.22	the concentrations of Cy_3PH^+ on Al_2O_3 monolayer catalyst with 6.2 SiO_2 per nm^2 at various coverages.	208
6.23	The concentrations of Cy_3PAI Lewis acid sites on Al_2O_3 monolayer catalyst with 6.2 SiO_2 per nm^2 at various coverages.	209
6.24	^{31}P MAS NMR spectra of $0.80 \mu\text{mol}/\text{m}^2$ (<i>p</i> - ClC_6H_4) $_3\text{P}$ on Al_2O_3 monolayer catalyst with 6.2 SiO_2 per nm^2 , with different adsorption temperatures	211
6.25	^{31}P MAS NMR spectra of $0.80 \mu\text{mol}/\text{m}^2$ (<i>p</i> - ClC_6H_4) $_3\text{P}$ on Al_2O_3 monolayer catalyst with 6.2 SiO_2 per nm^2 using cross-polarization flipback (except specified), with different adsorption temperatures	212
6.26	^{31}P MAS NMR spectra of $1.47 \mu\text{mol}/\text{m}^2$ (<i>p</i> - ClC_6H_4) $_3\text{P}$ on Al_2O_3 monolayer catalyst with 6.2 SiO_2 per nm^2 , with different adsorption temperature	213
6.27	^{31}P MAS NMR spectra of $1.47 \mu\text{mol}/\text{m}^2$ (<i>p</i> - ClC_6H_4) $_3\text{P}$ on Al_2O_3 monolayer catalyst with 6.2 SiO_2 per nm^2 using cross-polarization flipback, with different adsorption temperature	214
7.1	^{31}P NMR MAS spectra of Ph_3P and AlCl_3 mixture, 21% (mol) Ph_3P	223
7.2	^{31}P NMR MAS spectra of Ph_3P and AlCl_3 mixture, 28% (mol) Ph_3P	224
7.3	^{31}P NMR MAS spectra of Ph_3P and AlCl_3 mixture, 28% (mol) Ph_3P	225
7.4	^{31}P NMR MAS spectra of Ph_3P and AlCl_3 mixture, 50% (mol) Ph_3P	226
7.5	^{31}P NMR MAS spectra of (<i>m</i> - Tol) $_3\text{P}$ and AlCl_3 mixture	

	25% (mol) (<i>m</i> -Tol) ₃ P	227
7.6	³¹ P NMR MAS spectra of (<i>p</i> -Tol) ₃ P and AlCl ₃ mixture	
	12 % (mol) (<i>p</i> -Tol) ₃ P	228
7.7	³¹ P NMR MAS spectra of (<i>o</i> -Tol) ₃ P and AlCl ₃ mixture	
	10 % (mol) (<i>o</i> -Tol) ₃ P	229
7.8	the mass spectrum of desorption products from 0.34 μmol/m ² (<i>p</i> -ClC ₆ H ₄) ₃ P on the silica-alumina catalyst	238
8.1	³¹ P NMR MAS spectra of pure Ph ₃ PHBr, cross-polarization flipback	243
8.2	³¹ P NMR MAS spectra of 0.50 μmol/m ² Ph ₃ PHBr on silica gel	244
8.3	³¹ P NMR MAS spectra of 0.83 μmol/m ² Ph ₃ PHBr on alumina	245
8.4	³¹ P NMR MAS spectra of 0.40 μmol/m ² Ph ₃ PHBr on commercial silica-alumina catalyst with different recycle delay at 100°C	246
8.5	³¹ P NMR MAS spectra of 0.40 μmol/m ² Ph ₃ PHBr on commercial silica-alumina catalyst with different recycle delay at 150°C	247
8.6	³¹ P NMR MAS spectra of 0.80 μmol/m ² Ph ₃ PHBr on commercial silica-alumina catalyst	248

FORMAT

Since solid-state NMR is the prerequisite technique for this project, Chapter 1 discusses the general techniques of solid state NMR research for adsorbed species and surface systems. These techniques can also be used with other solid state systems. It is intended to provide a concise overview of the major theoretical and practical problems in performing this ^{31}P solid state NMR project (including decoupling, magic angle spinning, cross-polarization and other resolution enhancement techniques), with examples taken from research work. Among the NMR chemists, I believe that most of them are interested in using solid state NMR as an analysis tool, rather than figuring out the complicated, hard-to-understand solid state NMR theories. Thus a minimum amount of mathematics will be used. Also I am assuming that readers are familiar with basic liquid NMR ideas. For detailed solid-state NMR theories, the reader will be referred to many in-depth publications.

Chapter 2 gives an overview of the development of solid state NMR for research on surface acidity using basic molecules as probes, and related facts. The definition of acidity is clarified for myself and the readers. To show a clear picture of the research systems, structural facts (especially at a surface) about SiO_2 , Al_2O_3 and $\text{SiO}_2\text{-Al}_2\text{O}_3$ catalysts are summarized. For the purpose of comparison, a very brief description of techniques other than NMR is given. ^{13}C , ^{15}N , ^{31}P and ^1H NMR studies of acid sites on silica-alumina surfaces are reviewed, which are organized mainly by historic order. The material is also grouped by basic probes. Among them, pyridine and trimethylphosphine

are the molecules which people were very interested in. Thus more pages are used for them.

Chapter 3 describes the objectives of this research work including the practical problems that were encountered in the processes. The necessity and experimental parts of this project have also been addressed.

Chapter 4 discusses an excellent new probe, tricyclohexylphosphine and summarizes the ^{31}P NMR spectra of this probe on the SiO_2 , Al_2O_3 and commercial cracking SiO_2 - Al_2O_3 catalyst surfaces. The phosphine rotates on the silica surface. Lewis acid sites were observed on the alumina surface, but not on the silica-alumina surface. The Brønsted acid concentrations were saturated at higher surface coverages, which gives the maximum value of $0.26 \mu\text{mol}/\text{m}^2$.

Chapter 5 is about the aryl probes: triphenylphosphine, trimetatolylphosphine, triparatolylphosphine, trichlorophenylphosphine and other phosphines were used. At higher coverages a genuine decrease in the number of sites was observed for titration curves of Brønsted acid. This phenomenon was due to the multilayer of physically adsorbed species formed at higher coverage. The maximum apparent Brønsted acid concentrations were different and this is influenced by steric effects.

Chapter 6 describes the application of these new ^{31}P NMR probes to novel catalysts prepared by a chemical vapor deposition method. The results suggest this kind of catalyst is anticipated to be better than the commercial catalyst for cracking bulky material. Also, it is interesting to propose that the active centers of the catalyst are associated with the aluminum octahedral groups.

Chapter 7 shows the ^{31}P NMR results for adducts of the phosphines and AlCl_3 , which probably can help to identify the Lewis acid sites on the surface. The poisoning effect of adsorbed phosphines on the commercial silica-alumina catalyst is discussed. The adsorbed (*p*- C_6H_4) $_3\text{PO}$ species were further studied with MS.

Chapter 8 shows the surface basicity observed by using adsorbed PPh_3HBr . Basic OH groups are present on the silica-alumina surface.

Chapter 9 is a brief summary and gives a few suggestions for future work.

SYMBOLS

B_0	static magnetic field of NMR spectrometer
B_1	r.f. magnetic field of "irradiation"
h	Planck constant: 6.62620×10^{-34} J S
H_0	the Hammett function of the acid strength
H_{nmr}	Hamiltonian operator (in energy units)
I	signal intensity
\hat{I}_j	nuclear spin operator for nucleus j (component \hat{I}_{jz})
k	Boltzmann constant: 1.38062×10^{-23} J K ⁻¹
K_a	equilibrium constant of an acid
M	equilibrium macroscopic magnetization
N	total number of nuclei
P_f	the fraction of ions formed (in mol ratio)
r	distance
R	dipolar coupling constant
S_0	signal intensity
T	temperature
T_1	spin-lattice relaxation time
T_{1C}	spin-lattice relaxation time of crystalline species
T_{1H}	spin-lattice relaxation time of protonated species
T_{1L}	spin-lattice relaxation time of Lewis acid species
T_{1P}	spin-lattice relaxation time of physically adsorbed species
$T_{1\rho}$	spin-lattice relaxation time in the frame rotating with B_1
T_{2G}	Gaussian decay constant
T_{2L}	Lorentzian decay constant
T_{CP}	time constant for cross-polarization
T_d	recycle delay time
δ	the chemical shift
γ_X	magnetogyric ratio of nucleus X
$\Delta\sigma_j$	chemical shift range of j nucleus
$\Delta\omega^2$	second moment (Hz ²)
ϕ	polar angle
θ	angle-between a given vector and B_0
μ_0	permeability constant: $4\pi \times 10^{-7}$ kg ms ⁻² A ⁻²
ν_j	Larmor precession frequency of nucleus j (in Hz)
ν_r	rotor frequency (Hz)
τ	delay time before the pulse
Θ_H	the fraction of surface covered with protonated acid sites

ABBREVIATION

2D	two dimensional
BET	Brunauer, Emmett and Teller
CP	cross polarization
CRAMPS	combined rotation and multiple pulse spectroscopy
Cy ₃ P	tricyclohexylphosphine
DAS	dynamic angle spinning
DOR	double rotation
DTA	differential thermal analysis
Et ₃ P	triethylphosphine
FID	free induction decay
FT	Fourier Transform
GC	gas chromatography
IR	Infrared spectroscopy
LB	line broadening
MAS	magic angle spinning
Me ₃ P	trimethylphosphine
(<i>m</i> -Tol) ₃ P	trimetatolylphosphine
MS	mass spectroscopy
(<i>n</i> -Bu) ₃ P	tri- <i>n</i> -butylphosphine
NMR	nuclear magnetic resonance
(<i>o</i> -Tol) ₃ P	triorthotolylphosphine
(<i>p</i> -ClC ₆ H ₄) ₃ P	triparachlorophenylphosphine
Ph ₃ P	triphenylphosphine
ppm	parts per million, relative to 85% H ₃ PO ₄ in ³¹ P spectra
(<i>p</i> -Tol) ₃ P	triparatolylphosphine
r.f.	radio frequency
TG	thermogravimetry
TOSS	total suppression of spinning sidebands
TPD	temperature programmed desorption

Chapter 1 Solid-state NMR for adsorbed species and surfaces: Is it powerful?

In recent years, solid-state nuclear magnetic resonance (NMR) has emerged as a unique technique for the study of solid materials¹. Since the long-range disorder of amorphous materials precludes the use of diffraction techniques, NMR is uniquely able to provide information about both structure and dynamics. Even for crystalline solids, NMR can provide the bridge between the solid and liquid states. Progress in NMR with dipolar decoupling, magic angle spinning (MAS), cross polarization (CP) and other pulse programs has made studies of amorphous systems possible²⁻⁶. The field of adsorbed species and surfaces is a natural beneficiary of this development⁷⁻⁸. Molecules adsorbed on solid surfaces are intermediate between solids and liquids⁷. In order to achieve high-resolution spectra of such systems, similar solid-state NMR techniques to those used for amorphous solids are necessary.

Compared with FT-IR (Fourier Transform Infrared spectroscopy), which is the older-established, equally-useful spectroscopy for adsorbed species and surface systems), the analysis of NMR spectra is much easier and more straightforward. Also there are various NMR techniques for resolution enhancement (including multi-dimensional pulse sequences). This is really an advantage especially for complicated systems, such as biochemical molecules. But the sensitivity of NMR is lower. Thus the NMR experiments normally take more time. Also, as every chemist knows, NMR is much more expensive.

1. **Dipolar decoupling⁹⁻¹²: This removes the (¹H, ³¹P) interaction.**

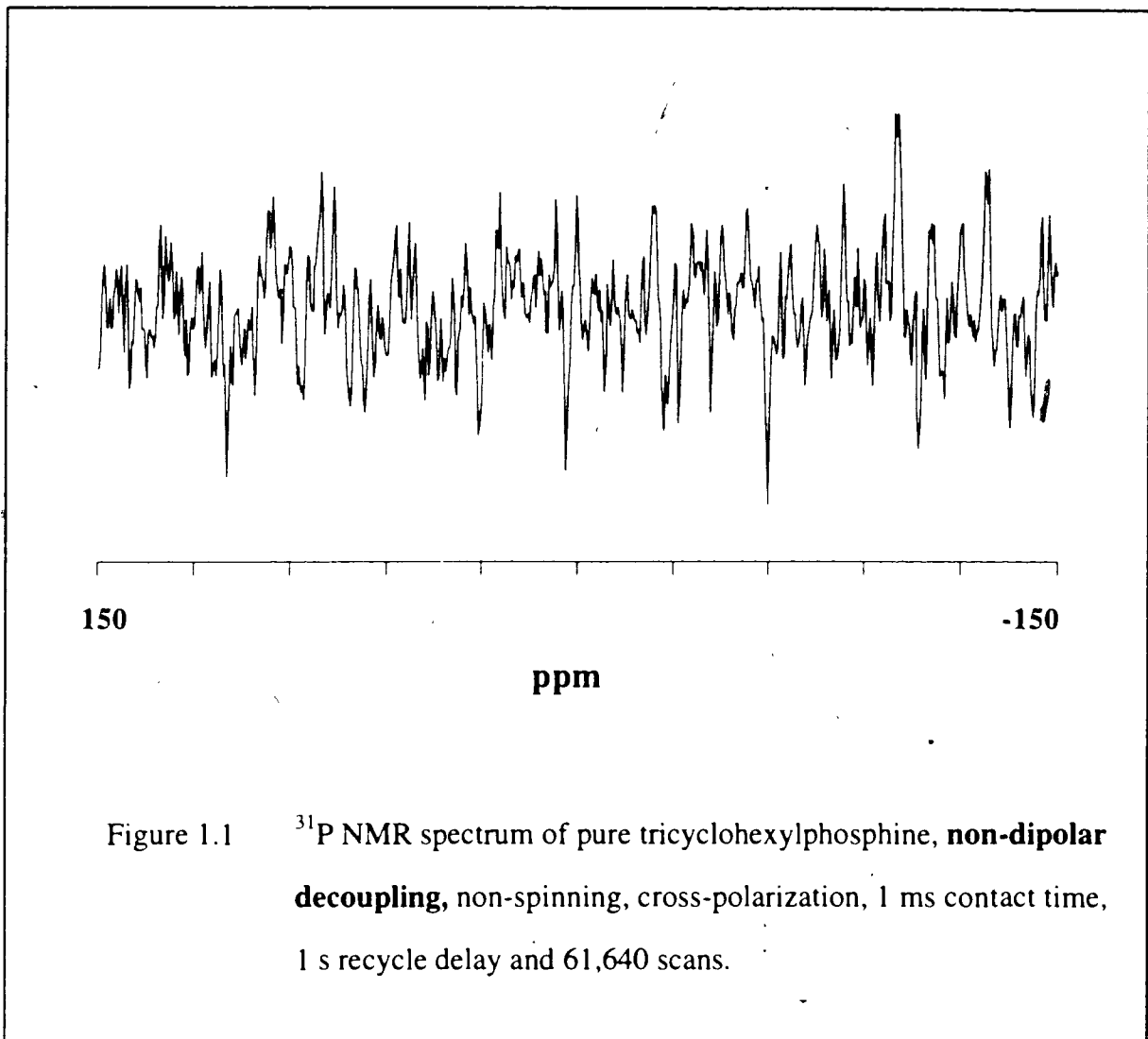


Figure 1.1 is the ^{31}P NMR spectrum of tricyclohexylphosphine. It is the spectrum recorded under conditions similar to normal liquid NMR: non-dipolar decoupling, non-spinning. Broad resonance lines arise primarily from the dipolar interactions between ^{31}P and ^1H nuclear spins.

For a heteronuclear two-spin system, we can use a truncated dipolar Hamiltonian⁴, which, for an AX spin system, is:

$$h^{-1}H_{nmr} = -(v_a \hat{I}_{az} + v_x \hat{I}_{xz}) + R \hat{I}_{az} \hat{I}_{xz} (1-3\cos^2\theta) \quad 1.1$$

where v_a and v_x are Larmor precession frequencies, and R is the dipolar coupling constant, $R = \gamma_a \gamma_x (h/4\pi^2) r_{ax}^{-3} \mu_0/4\pi$. From the R value, the dipolar coupling interaction is related to gyromagnetic ratios and internuclear distance as well. Since the ^1H has the highest γ value, ^1H - ^1H has the biggest dipolar interaction. Also, R is inversely proportional to the cube of internuclear distance. Thus pulse sequences were designed for discrimination experiments according to different internuclear distances. (see 3c, chapter 1). Typical values of the width at half height for the nearest neighbor interactions in the solid state for small molecules where the interaction will be relatively large are given in table 1.1¹³.

Table 1.1 Static Dipole Couplings in Selected Molecules¹³

X-X or A-X	Sample	Distance (nm)	$[\langle \Delta\omega^2 \rangle]^{1/2}$ (kHz)
^1H - ^1H	H_2	0.0746	194
	H_2O	0.151	23.4
	C_2H_4	0.182	13.4
	CH_2O	0.189	11.9
^{13}C - ^{13}C	$^{13}\text{C}_2\text{H}_2$	0.120	2.92
	$^{13}\text{C}_2\text{H}_4$	0.134	2.12
	$^{13}\text{C}_2\text{H}_6$	0.154	1.40
^1H - ^{13}C	$^{13}\text{C}_2\text{H}_2$	0.106	11.4
	HCOOH	0.109	10.5
	$^{13}\text{C}_2\text{H}_6$	0.111	9.9

Table 1.2 Static Dipole Coupling in Selected Phosphorous Molecules

H-P or C-P	Sample	Distance (nm)	$[\langle \Delta\omega^2 \rangle]^{1/2}$ (kHz)
$^1\text{H}-^{31}\text{P}$	PH_3	0.1415^{13a}	7.64
	$[\text{PH}_4]^+$	0.142^{13a}	7.56
$^{13}\text{C}-^{31}\text{P}$	$(\text{CH}_3)_3\text{P}$	0.187^{13a}	0.83
	PCy_3	0.187^{13b}	0.83

For homonuclear dipolar decoupling, special pulse sequences must be used¹⁴⁻¹⁵. In the heteronuclear case, it is easier to remove the dipolar interaction by double resonance¹⁶. For our $^{31}\text{P}-^1\text{H}$ system, typical values of the width at half height for the nearest neighbor interactions on the solid state for phosphorous molecules are calculated in table 1.2. While the ^{31}P resonance is detected using one radio-frequency, the protons are simultaneously subjected to strong on-resonance irradiation. A 45 kHz field was used to decouple the protons in our home-made NMR spectrometer. The (^{31}P , ^1H) indirect coupling interactions (termed spin-spin coupling, or scalar coupling^{2, 4}) are eliminated from the spectra as well.

Figure 1.2 shows the spectrum under the dipolar decoupling condition.

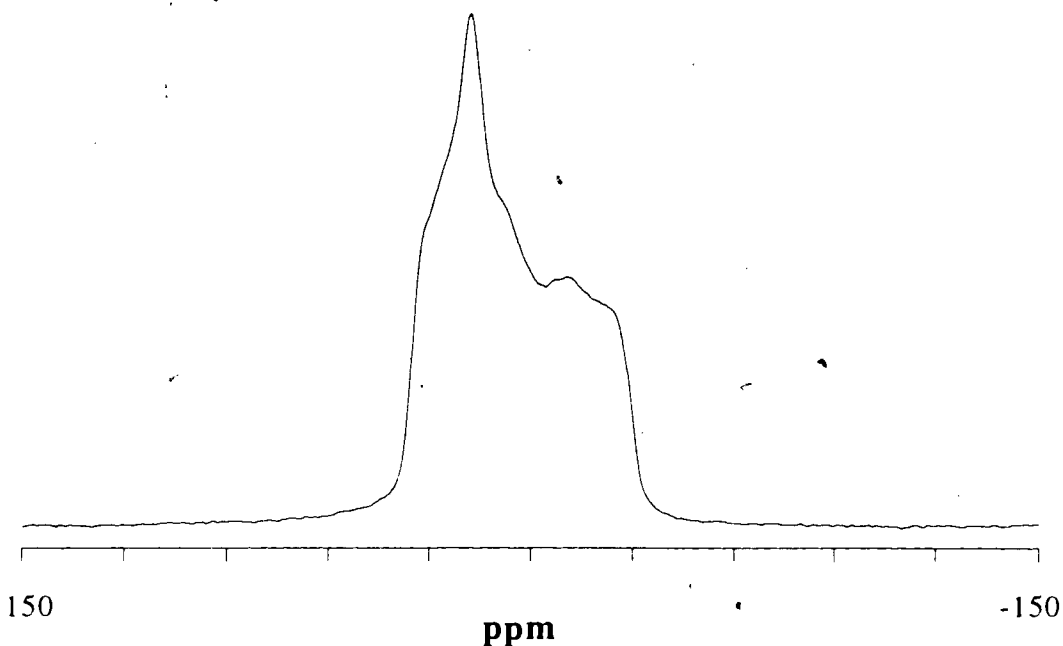


Figure 1.2 ^{31}P NMR spectrum of pure tricyclohexylphosphine, **dipolar decoupling, non-spinning**, cross-polarization flip back, 1 ms contact time, 1 s recycle delay and 77,330 scans.

Figure 1.2 is the spectrum of pure tricyclohexylphosphine under the conditions of decoupling. This spectrum is in agreement with¹⁷. Compared with the non-decoupled spectrum (no signal can be seen in Figure 1.1), a big gain in the resolution has been made. But the resonance still is very broad, and the chemical shift resolution not as good as that of the solution spectrum. This is due to chemical shift anisotropy. The chemical shift anisotropy can be eliminated by magic angle spinning. We will discuss this phenomenon in the following section.

2. Magic Angle Spinning (MAS)¹⁸⁻²⁰: **Weapon for Chemical Shift Anisotropy (CSA) and weak dipolar interaction.**

The chemical shift arises from the change in nuclear environment in the presence of an applied field. The nuclei are shielded by the presence of electrons. In solution, the chemical shift is an average over the isotropic motion of the molecules. In the solid state, since the molecules are not generally free to move, it will depend on the particular orientation of the molecule with respect to the magnetic field. The shielding is a second rank tensor quantity. Since vectors have 3 components, the chemical shift tensor σ can be represented by a matrix of 9 components:

$$\begin{pmatrix} \sigma_{11} & \sigma_{12} & \sigma_{13} \\ \sigma_{21} & \sigma_{22} & \sigma_{23} \\ \sigma_{31} & \sigma_{32} & \sigma_{33} \end{pmatrix}$$

The σ tensors appear symmetric, i.e. $\sigma_{12}=\sigma_{21}$. If there is an antisymmetric component, its effects are zero to first order¹². The antisymmetric component is a second order term, so it would be very small and hard to observe. It might be observable for a heavy metal⁶, but we do not know of any such observations. In such circumstances there are only 6 independent components to a symmetric σ tensor, and it is possible to choose axes in which σ is diagonal⁶:

$$\begin{pmatrix} \sigma_{11} & 0 & 0 \\ 0 & \sigma_{22} & 0 \\ 0 & 0 & \sigma_{33} \end{pmatrix}$$

The terms σ_{11} , σ_{22} and σ_{33} are called the principal components of the σ tensor. For external magnetic field B_0 chosen parallel to the z-axis, the shielding tensor element of interest is σ_{zz} ($\sigma_{zz} = \sigma_{obs}$). The observed chemical shift in a solid is given by²¹:

$$\sigma_{zz} = \sigma_{11} \sin^2 \theta \cos^2 \phi + \sigma_{22} \sin^2 \theta \sin^2 \phi + \sigma_{33} \cos^2 \theta \quad 1.2$$

where the angles θ and ϕ are the polar angles of B_0 with respect to the principal directions of σ .

In liquids, the isotropic motion of the molecules averages the $\cos^2 \theta$ to $1/3$. Also $\sin^2 \phi$, and $\cos^2 \phi$ both average to $1/2$. Hence the isotropic chemical shift is given by:

$$\sigma_{\text{liq}} = 1/3(\sigma_{11} + \sigma_{22} + \sigma_{33}) \quad 1.3$$

Therefore for solids, the experiment has to be devised to simulate the isotropic motion in the liquid state to obtain the spectra similar to the liquid state. It is necessary to make $\langle \cos^2 \theta \rangle = 1/3$. Then as in Figure 1.3, the solid sample is spun rapidly about an axis inclined at angle of 54.7° to the applied field. Thus just as for isotropic tumbling in the liquid state, $\langle \cos^2 \theta \rangle = 1/3$. 54.7° is called the magic angle.

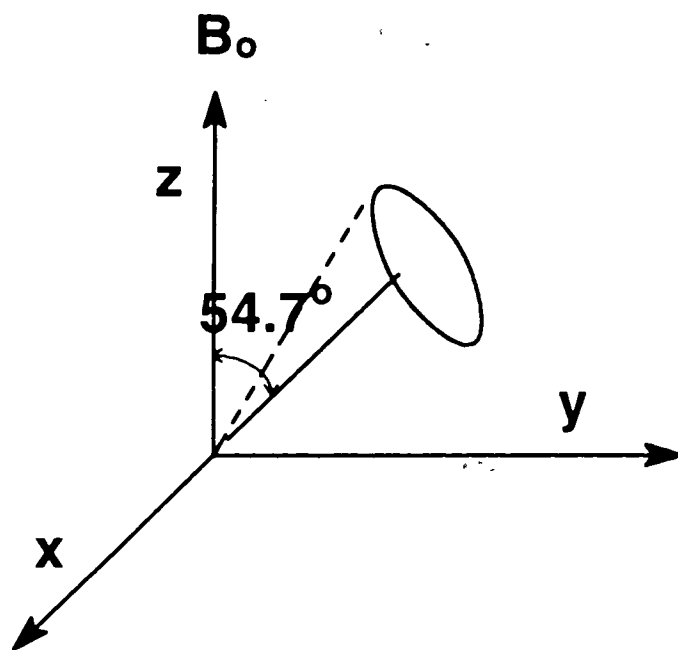
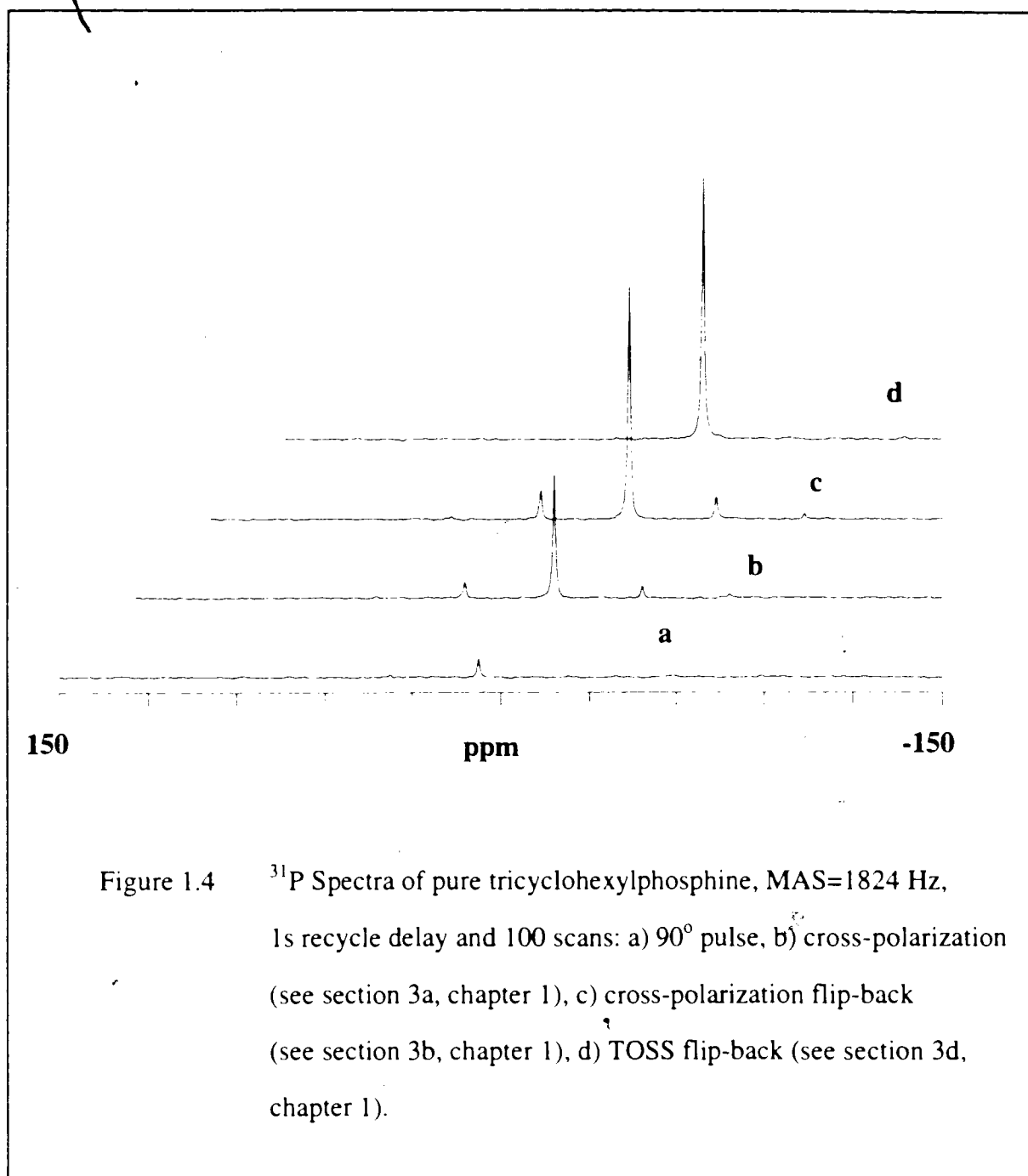


Figure 1.3 Magic angle spinning and coordinates.

When $\cos^2\theta = 1/3$, then according to equation 1.2, σ_{zz} becomes

$$\sigma_{zz} = 1/3 (2\sigma_{11}\cos^2\phi + 2\sigma_{22}\sin^2\phi + \sigma_{33}) \quad 1.4$$

If the sample spinning rate at the magic angle is sufficiently great, then $\sin^2\phi$ and $\cos^2\phi$ both average to $1/2$ and $\sigma_{zz} = \sigma_{\text{liq}}^{22}$. Also, weak dipolar interactions, such as ^{31}P - ^{13}C (Table 1.2), are eliminated from the spectra by the MAS. Figure 1.4 shows the spectrum of PCy_3 using dipolar decoupling and MAS techniques. The same y-axis scale was used to plot the intensities.



When the spinning rate is not large compared to chemical shift anisotropy in frequency units, a series of sidebands separated by the spinning frequency appear^{23, 24} (Figure 1.4a-1.4c). This is a disadvantage of using a very high magnetic-field

spectrometer for the experiments, since the intensity of spinning sidebands increases with the magnetic field²⁵. However, it may be useful to analyze the intensity of the sidebands to obtain additional information about the shielding tensor^{24a, 25-27}. For the species adsorbed on a surface, this may be used to get information about the molecule's mobility on the surface. We have used sideband intensities to conclude that the phosphine molecules move almost isotropically on the silica and silica-alumina surfaces at sub-monolayer coverages²⁸. Normally, analysis of the spinning sidebands only yields the principal values of the relevant tensor, the direction of the tensor requires work on single crystals²⁹.

It is not necessarily the situation that the centerband is the most intense peak. Since the center band position is invariant to spinning rate, the easiest way to identify the real centerband is to change the spinning speed. In order to eliminate the sidebands, TOSS (Total Suppression of Spinning Sidebands) techniques were introduced³⁰⁻³². Figure 1.4d shows the spectrum recorded under TOSS flip-back conditions. Compared with the spectrum of cross-polarization flip-back experiment (Figure 1.4c), the only difference is that the spinning sidebands are totally gone and the centreband is slightly larger. In Figure 1.4d, $\nu_r = 1824$ Hz, $\sigma_{11} = -30$ ppm, $\sigma_{22} = 18$ ppm, and $\sigma_{33} = 35$ ppm (Figure 1.2 and¹⁷), so $\Delta\sigma = 65$ ppm = 3930 Hz (for our ³¹P 60.457 MHz spectrometer). Thus $\Delta\sigma = 2.2 \nu_r$. The higher centreband in Figure 1.4d is in agreement with^{32a}: when $\Delta\sigma < 4 \nu_r$, the centreband of TOSS is higher than in the normal MAS spectrum.

3. Cross Polarization (CP)³³⁻³⁵: Borrowing proton magnetization greatly enhances signal-to-noise ratios.

a. Cross Polarization

The normal 90° pulse program, $(90^\circ(\text{FID}_1)-T_d-180^\circ-\tau-90^\circ(\text{FID}_2)-T_d)_n$ was used to minimize errors due to spectrometer drift and pulse feed through. The FID_1 was subtracted from FID_2 . Usually $\tau \ll T_1$ and T_d equals 3-5 T_1 . Since ^{31}P T_1 are often very long, this experiment could be very inefficient. For pure tricyclohexylphosphine, T_1 equals 22 seconds. But ^1H T_1 's are normally much shorter than ^{31}P T_1 's in the same compound.

The difficulty of long ^{31}P T_1 can be overcome by a technique which derives the magnetization from the ^1H spins. It is termed cross-polarization (CP). The pulse sequence is shown in Figure 1.5³⁴.

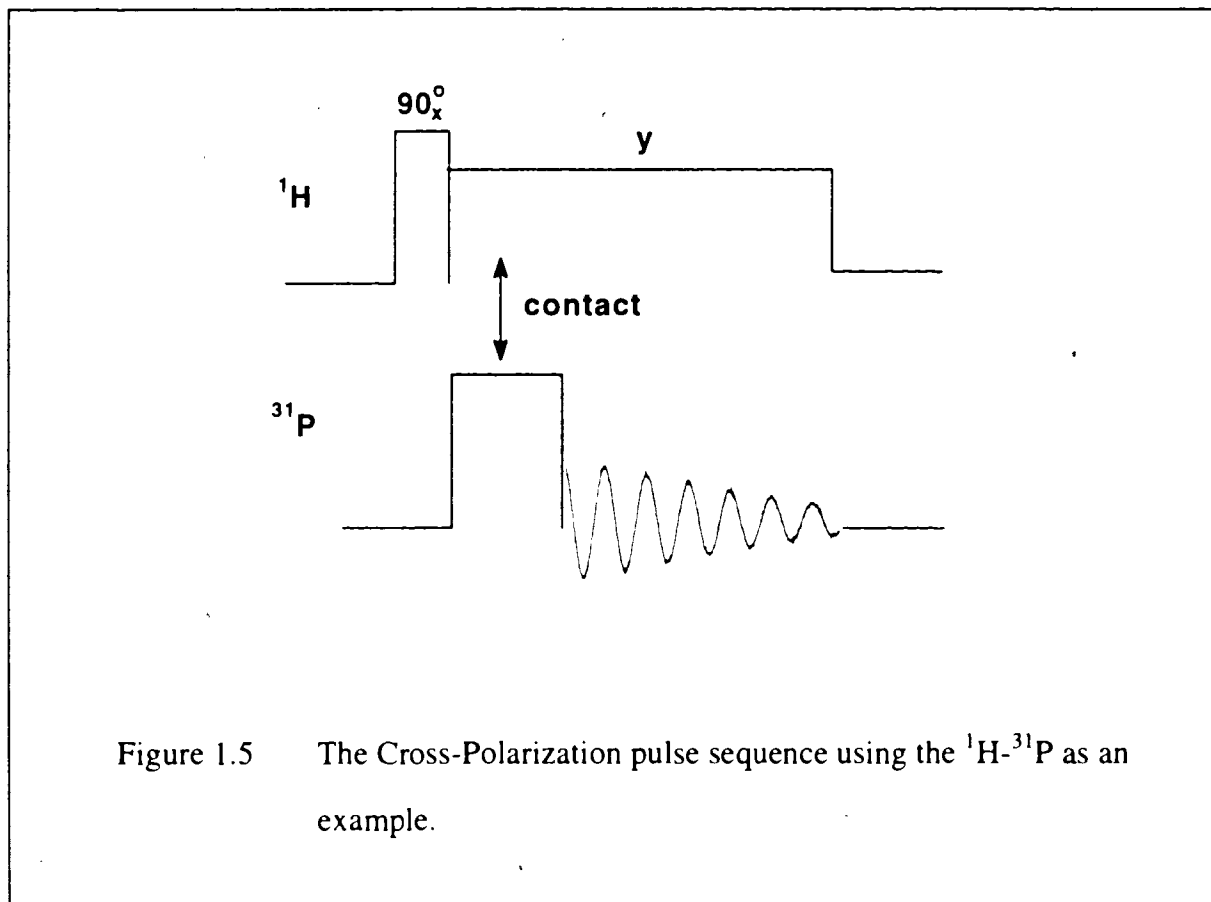


Figure 1.5 The Cross-Polarization pulse sequence using the ^1H - ^{31}P as an example.

The sequence is:

1. establish ^1H -spin polarization in \mathbf{B}_0 by 90°_x pulse
2. spin-lock ^1H -spin along $\mathbf{B}_{1\text{H}}$
3. contact ^1H and ^{31}P spins with a Hartmann-Hahn condition
4. record ^{31}P FID and decouple ^1H
5. relaxation delay
6. repeat

The sequence is based on the Hartmann-Hahn condition (Step 3), which is used for a period of double resonance with the radio-frequency magnetic fields matched according to the following equation³³:

$$\gamma_{\text{H}}B_{1\text{H}} = \gamma_{\text{P}}B_{1\text{P}} \quad 1.5$$

Cross-polarization can be explained by a simple thermodynamic picture³⁴. The equilibrium magnetization is given by the Curie law:

$$M = C B/T \quad 1.6$$

where $C = 1/4 \gamma^2 \hbar^2 N / (4k\pi^2)$. For ^1H initially at equilibrium in \mathbf{B}_0 , before step one:

$$M_{\text{H}(z)} = C_{\text{H}} B_0 / T_L \quad 1.7$$

where T_L is the lattice temperature. After steps one and two the ^1H magnetization has been transferred to the y direction. Thus:

$$M_{\text{H}(y)} = C_{\text{H}} B_{1\text{H}} / T_{\text{Hs}} = C_{\text{H}} B_0 / T_L \quad 1.8$$

where T_{H_s} is the spin temperature in the B_{1H} locking field. Since $B_{1H} \ll B_0$, T_s is very low. For the ^{31}P spins, before step three $M_{P(y)} = 0$, i.e. $T_{P_s} = \infty$. During step three, the ^{31}P is cooled by CP and both spins reach a common spin temperature T_s with conservation of energy:

$$C_H B_{1H}^2 / T_{H_s} = (C_H B_{1H}^2 + C_P B_{1P}^2) / T_s \quad 1.9$$

Since $C_H \gg C_P$ (for pure tricyclohexylphosphine $N_H \gg N_P$) and $B_{1H}/B_{1P} = \gamma_P/\gamma_H$ (from the Hartmann-Hahn condition), $C_H B_{1H}^2 \gg C_P B_{1P}^2$. Thus $T_s = T_{H_s}$. The resulting magnetization of the phosphorus is:

$$M(^{31}\text{P}) = C_P B_{1P} / T_s = C_P B_{1P} / T_{H_s} \quad 1.10$$

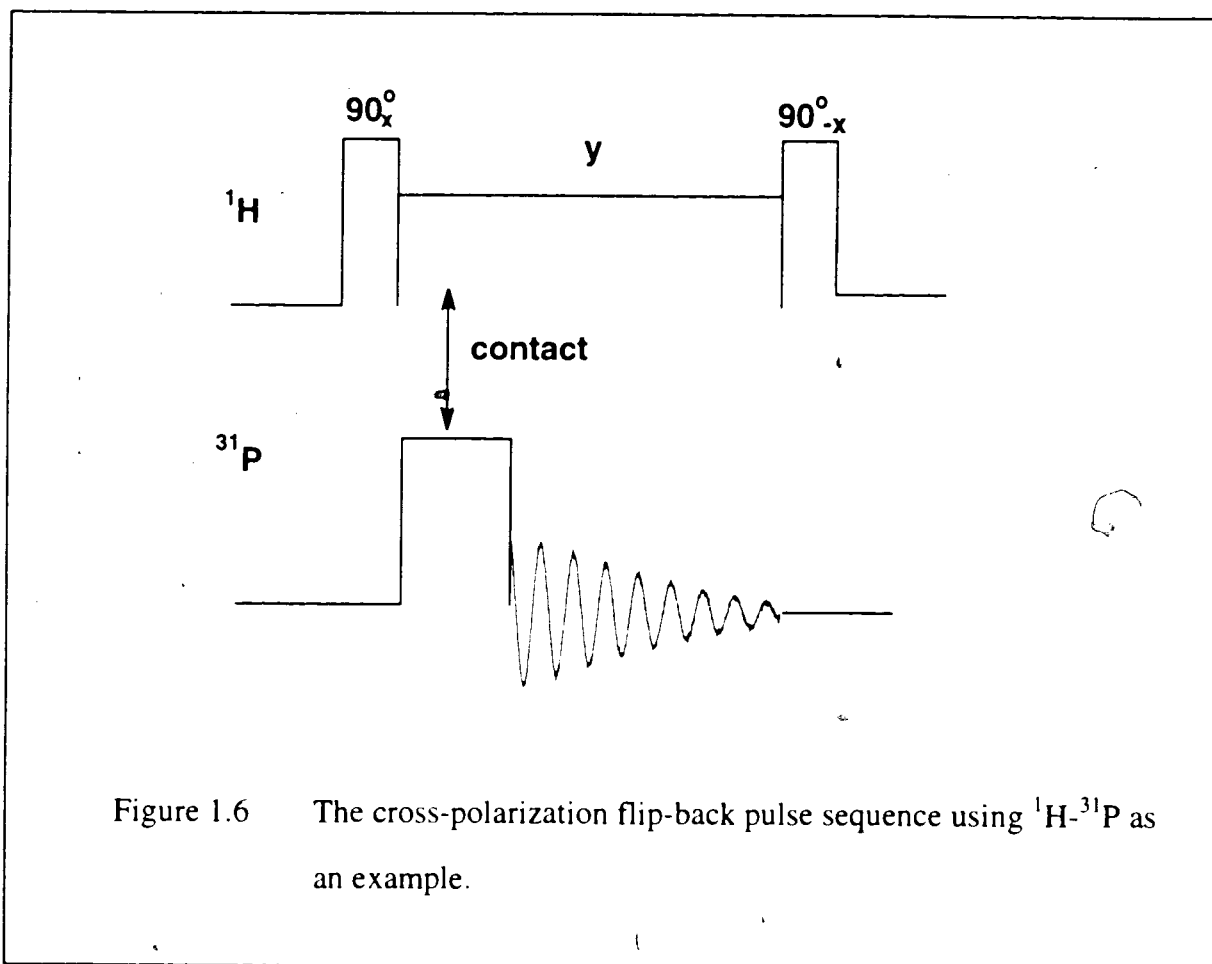
Substitution of equations 1.5 and 1.8 gives

$$M(^{31}\text{P}) = C_P (\gamma_H/\gamma_P) B_0 \sqrt{T_L} \quad 1.11$$

Compared with the normal phosphorus magnetization, $M_0(^{31}\text{P}) = C_P B_0 \sqrt{T_L}$. A gain of γ_H/γ_P is obvious. Figures 1.4a and 1.4b show us the change of the intensity using cross-polarization instead of 90° pulses. For tricyclohexylphosphine, the gain from the difference of relaxation times dominates. Since this sensitivity gain depends on natural abundance and magnetogyric ratios, the CP technique is even more attractive for dilute, low γ spins (such as ^{13}C , ^{15}N or ^{29}Si). Generally, the cross-polarization technique is useful for any spin $1/2$ nucleus except for ^1H and ^{19}F , in systems containing ^1H or ^{19}F . Since quadrupolar nuclei usually have short T_1 , the 90° pulse sequence is feasible. But CP experiments may provide additional information³⁵.

b. **Cross polarization flip-back**

Since T_1 (^{31}P) is irrelevant, for the CP sequence, the spectrum is considerably enhanced (Figure 1.4b). An alternative sequence, known as flip-back operation, is designed to use the residual ^1H magnetization at the end of the FID³⁶.



The sequence is:

1. establish ^1H -spin polarization in B_0 by 90°_x pulse
2. spin-lock ^1H -spin along $B_{1\text{H}}$
3. contact ^1H and ^{31}P spins with a Hartmann-Hahn condition

4. record ^{31}P FID and decouple ^1H
5. process residual ^1H magnetization back to B_0 by 90°_x pulse
6. relaxation delay
7. repeat

Step 5 is added to the sequence to process the residual ^1H magnetization back into z direction by a 90°_x ^1H pulse. Figure 1.4b and 1.4c show the difference between the normal CP sequence and the flip-back operation. The flip-back pulse sequence generally has better sensitivity than the normal CP one. These spectra in Figure 1.4b and 1.4c illustrate this.

c. Dipolar Dephasing

During the CP experiments, the magnetization of the proton can be transferred to the ^{31}P at a rate $1/T_{\text{CP}}$ as well as to the lattice at a rate $1/T_{1\rho}$. The kinetics of cross-polarization can be described by²:

$$S_{(t)}/S_0 = [1/(1-\lambda)] \{1 - \exp[(\lambda-1)t/T_{\text{CP}}]\} \exp(-t/T_{1\rho}) \quad 1.12$$

where S_0 is the hypothetical signal for total CP transfer, λ is $T_{\text{CP}}/T_{1\rho}$ and t is the contact time.

Cross-polarization is determined by the dipolar interactions. The rate therefore is dependent on the distance between A and X spins. We can discriminate different species by using a variable contact time³⁷.

The other typical discriminating experiment in CP MAS NMR is the dipolar dephasing technique (also known as delayed decoupling or nonquaternary suppression)³⁸.

This sequence can selectively suppress the signal from species with directly-bonded protons and is described in Figure 1.7.

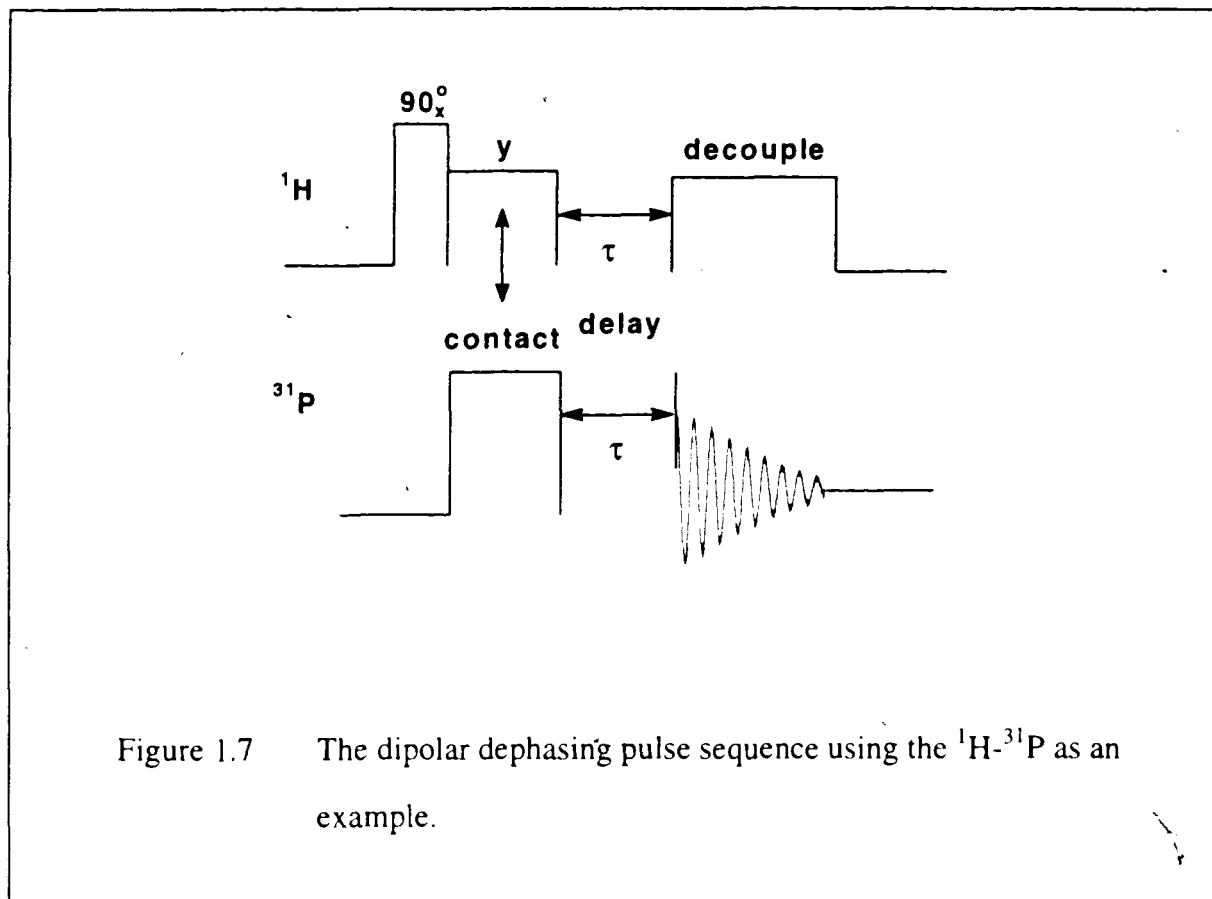


Figure 1.7 The dipolar dephasing pulse sequence using the ^1H - ^{31}P as an example.

The sequence is:

1. establish ^1H -spin polarization along B_0 by 90_x pulse
2. spin-lock ^1H -spin along $B_{1\text{H}}$
3. contact ^1H and ^{31}P spins with a Hartmann-Hahn condition
4. delay while the proton-decoupling field is off
5. record ^{31}P FID and decouple ^1H
6. relaxation delay
7. repeat

This sequence differs from that of a normal CP experiment in step 4, as a delay is inserted between the CP contact and the normal FID acquisition time. During the delay period, ^{31}P magnetization decays faster for phosphorus that is strongly coupled to protons. The typical time for the delay is 70 μs for our systems. Figure 1.8 shows the spectra of tricyclohexylphosphine on the 6.2 SiO_2 per nm^2 of Al_2O_3 monolayer catalyst. The 24.2, 7.6, and -3.7 ppm peaks are resonances of protonated, physically adsorbed, and Lewis-acid bound species respectively on the surface. Figure 1.8b shows that the signal from the protonated species (24.2 ppm) disappeared using the dipolar dephasing technique. According to equation 1.1, the dipolar coupling depends on r^{-3} . Therefore it is possible to select a delay time that eliminates directly bonded P-H signals without a large effect on other phosphorus species.

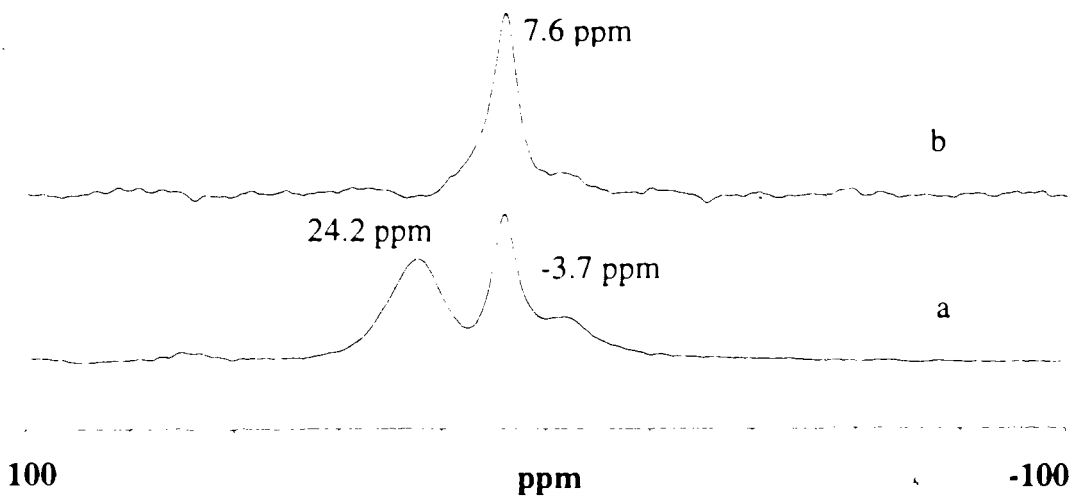


Figure 1.8 ^{31}P NMR spectra of $0.94 \mu\text{mol}/\text{m}^2$ tricyclohexylphosphine on 6.2 SiO_2 per nm^2 Al_2O_3 monolayer catalyst, adsorbed at 200°C one hour, the catalyst preheated at 450°C , 10^{-5} torr two hours; a) cross-polarization flip-back, MAS rate 1.77 kHz, contact time 1ms, recycle delay 1 second, scan 79410, and b) dipolar dephasing, MAS rate 1.83 kHz, delay time 70 μs , recycle delay 1 second, scans 12726.

The dipolar dephasing experiment has been widely used to assign the resonance signals of polymers, fossil fuels, wood samples and other complex materials²¹. Also the dipolar dephasing technique has been used to identify molecular motions by dipolar dephasing time measurements³⁹. The decrease of signal intensity during the dephasing

time t_{dd} is characterized by a constant T_2 . It has been shown⁴⁰ that strong dipolar coupling follows a Gaussian decay:

$$I_G = I_{oG} \exp(-t_{dd}^2/2T_{2G}^2) \quad 1.13$$

where I_{oG} is the signal intensity without dephasing ($t_{dd}=0$) and T_{2G} is the Gaussian decay constant. Weak dipolar interactions can be fitted by a Lorentzian decay:

$$I_L = I_{oL} \exp(-t_{dd}/T_{2L}) \quad 1.14$$

In some cases, the experimental data may be described by the equation

$$I = I_{oG} \exp(-t_{dd}^2/2T_{2G}^2) + I_{oL} \exp(-t_{dd}/T_{2L}) \quad 1.15$$

Since the molecular motion has a great impact on the dephasing⁴¹, T_{2G} and T_{2L} can be used to assign the motions.

In some cases inverted signals were observed^{40, 42}. Equations 1.13 to 1.15 cannot explain this phenomenon. Computer simulations have been used to explain the negative signals⁴².

d. TOSS

In the Figures (1.4a-c), the spinning sidebands arise from the chemical shift anisotropy and the magic angle spinning frequencies of the sample. Figure 1.4 is for a pure compound. In most cases, multiple resonances are present in the spectra and some of the isotropic resonances could overlap with the spinning side bands of others.

Therefore, spinning side bands can be a nuisance in a complicated spectrum where the isotropic chemical shift needs to be identified. Several techniques have been proposed for spinning sideband suppression³⁰. The TOSS sequence has been proven effective with all spinning side bands suppressed³⁰⁻³². The TOSS pulse sequence is shown in Figure 1.9:

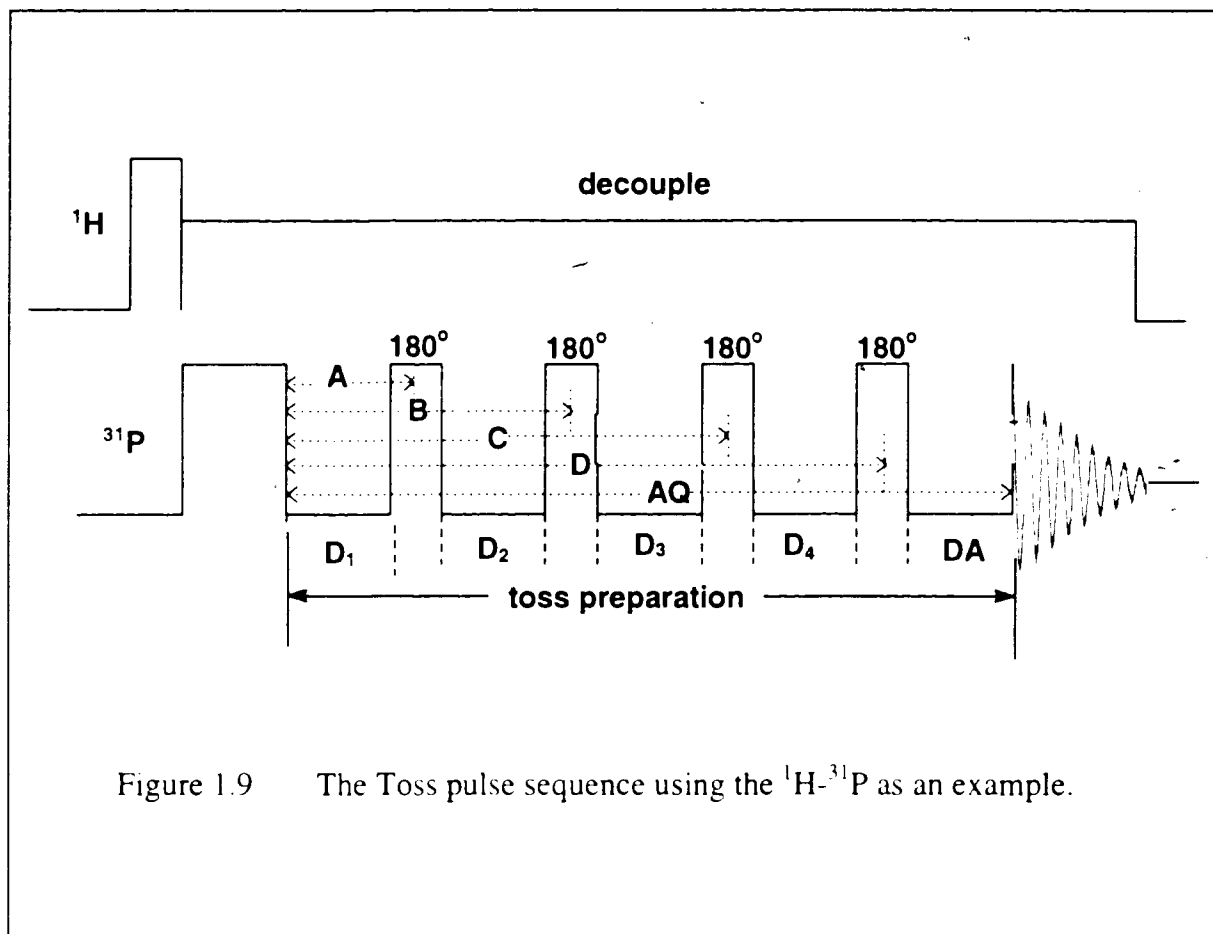


Figure 1.9 The Toss pulse sequence using the ^1H - ^{31}P as an example.

The sequence is:

1. establish ^1H -spin polarization in B_0 by 90°_x pulse
2. spin-lock ^1H -spin along $B_{1\text{H}}$
3. contact ^1H and ^{31}P spins with a Hartmann-Hahn condition
4. Toss preparation by four 180° pulses and five well defined delays
5. record ^{31}P FID and decouple ^1H

6. relaxation delay
7. repeat

Step 4 is a period in which the spin system is prepared for recording a TOSS spectrum. During this step, the four 180° pulses at well defined times t_1 , t_2 , t_3 , t_4 have been applied. The timing of the pulses is chosen in such a way that the magnetization components giving the spinning side bands in the spectrum interfere to give zero result during the FID acquisition, and the central isotropic resonance remains. A particular choice of delays in Figure 1.4d is shown in Table 1.3.

Table 1.3 An example of calculation of delay time for TOSS
 (τ_{180° :180° pulse time 10.2 μs and τ_v : rotor period 548.2 μs)

Rotor Revolution Fraction ^{32, 43a}	Between Pulse Fraction	Experiment Delay Calculation
A. 0.1226	A. 0.1226	$D_1 = A \times \tau_v - 0.5 \times \tau_{180^\circ}$ = 62.2 μs
B. 0.1999	B-A. 0.0773	$D_2 = (B-A) \times \tau_v - \tau_{180^\circ}$ = 32.2 μs
C. 0.4235	C-B. 0.2236	$D_3 = (C-B) \times \tau_v - \tau_{180^\circ}$ = 112.5 μs
D. 1.4668	D-C. 1.0433	$D_4 = (D-C) \times \tau_v - \tau_{180^\circ}$ = 562.1 μs
AQ. 2.2412	AQ-D. 0.7744	$DA = (AQ-D) \times \tau_v - \tau_{180^\circ}/2$ = 419.7 μs

The theoretical basis for the value of rotor revolution fraction in the TOSS pulse sequence can be found in^{32a, 43}

4. Extra Resolution Enhancement Techniques: Bonus from NMR to provide more information

Besides all the techniques previously discussed (dipolar decoupling, MAS, dipolar dephasing and spinning sideband suppression), there are various methods available to increase spectral resolution and obtain extra information. Table 1.2 lists some of these techniques related to our research systems.

a.	change temperature
b.	change pressure
c.	change field
d.	two-dimensional NMR
e.	relaxation rate studies
f.	mathematical enhancement

a. Temperature

New probes are available to perform variable temperature experiments. High temperature operation offers an attractive method of in-situ NMR studies of catalytic reactions⁴⁴⁻⁵⁰. Low temperature experiments may be used to detect molecular motions and exchange processes in terms of activation barriers⁵¹⁻⁵³.

We must be aware that $T_{1\rho}$, T_1 , T_2 , and T_{CP} depend on temperature. Line broadening or narrowing can occur. The experiments may become selective, thus making quantitative comparison difficult. For low temperature experiments, normally molecular motions with barriers less than 3 kcal/mol can be studied²¹. A laser heater was used for high temperature experiments⁵⁴. A laser heater might be used to change temperature and back in a few seconds. If this period can be shortened to a thousandth of a second or even smaller, we could add this temperature change block to a pulse sequence and design new selective experiments.

b. Pressure

High pressures are involved with many catalytic reactions. It should be possible to design a suitable NMR probe for in-situ NMR experiments.

c. Frequency and sideband suppression

For spin 1/2 nuclei there is a potential gain in sensitivity at higher magnetic fields⁵⁵⁻⁵⁷. Normally the sample must be spun faster in order to remove the spinning sidebands. It should be emphasized that the gain in sensitivity by higher fields justifies the trouble of using some sideband suppression pulse sequences, such as TOSS. It is found that TOSS causes centreband intensity to decrease if $\Delta\sigma > 4\nu_r$ ^{32a}. For our phosphine/silica-alumina system, chemical shift anisotropy has been greatly reduced by the molecular motions on the surfaces²⁸. Thus the higher fields may be used for sensitivity enhancement without the trouble of the spinning sideband suppression.

Further, for quadrupolar nuclei with non-integral spins (such as ²⁷Al and ¹⁷O), the second-order quadrupolar interaction is inversely field dependent. MAS experiments for

these nuclei will better be performed at a magnetic field as high as possible⁵⁶. Besides, the double rotation (DOR) and dynamic angle spinning (DAS) experiments can be used to average second-order as well as first-order interactions^{57a, b}. ¹⁷O DOR and DAS can distinguish the three inequivalent oxygen sites in CaMgSi₂O₆^{57c}. ²⁷Al DOR is capable of resolving aluminum sites in the AlPO₄ system^{57d}.

d. 2D NMR

Dipolar and anisotropic interactions give broad resonances. However these interactions contain considerable information about molecular structure. 2D NMR can separate the hetero-nuclear dipolar and chemical shift spectra into orthogonal dimensions⁵⁸⁻⁶⁰. Also 2D NMR is very valuable for spectral assignment. There is a good review about 2D NMR of particular interest for catalysis⁷. The chemical aspects of 2D NMR applications can be checked there.

e. Relaxation

Generally, T_1 and $T_{1\rho}$ for solids are long in the absence of any motion. The effect of motion can be checked by the T_1 value at different temperatures⁴.

In CP experiments, the rate of polarization varies as a function of the chemical environment and molecular motions. The differences can be used to enhance resolution by variable contact times⁶¹. Also more sophisticated pulse sequences have been developed to selectively excite different spins⁶². These experiments rely on the differences of T_1 , $T_{1\rho}$, T_2 of protons. A pre-contact delay has been used while spin-

locking is maintained in the proton channel⁶³. The $T_{1\rho H}$ is usually much smaller than $T_{1\rho P}$. Therefore a delay before contact has essentially the similar result as a long contact, but without the trouble of probe overheating. During the delay, the species of short $T_{1\rho H}$ lose magnetization preferentially, so that these species may be discriminated by suitable delay time.

Both CP and 90° pulse experiments are likely to be useful for discriminating species. Another experiment $(180^\circ-\tau-90^\circ(\text{FID})-T_d)_n$, which is normally used for T_1 measurement experiments by varying τ , can be of great use for discriminating the different species by different τ values. The greater the differences in T_1 's the better the discrimination. We have successfully separated the overlapping peaks of monolayer of physically-adsorbed species from multilayers by this technique using $\tau = 3$ and 0.1 seconds in the $(180^\circ-\tau-90^\circ(\text{FID})-T_d)_n$ pulse sequence (Figure 1.10). Figure 1.10b is the resonance of monolayer physically adsorbed species. Figure 1.10a arises from the multilayer physically-adsorbed ones. The uncertainty for the chemical shift measurement is less than 0.4 ppm, which is much smaller than the chemical shift differences between these two species.

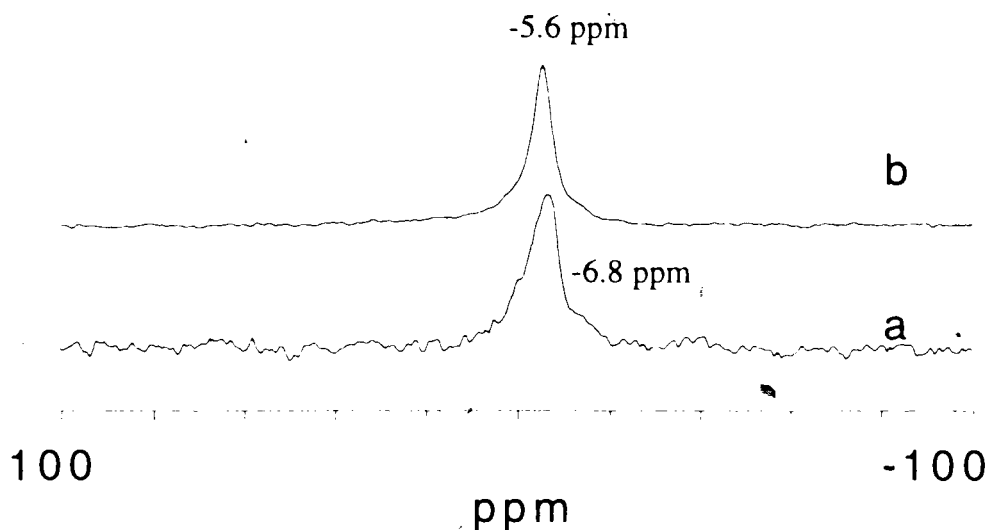


Figure 1.10 ^{31}P spectra of $1.33 \text{ } \mu\text{mol}/\text{m}^2$ trimetatholyphosphine on commercial $\text{SiO}_2\text{-Al}_2\text{O}_3$ catalyst, adsorption at 100°C one hour, preheat catalyst at 450°C , 10^{-5} torr two hours, using the $(180^\circ\text{-}\tau\text{-}90^\circ(\text{FID})\text{-}T_d)_n$ pulse sequence, spinning rate= 1.80 kHz . a). τ delay time 0.1 second, T_d recycle delay 1 second, scans 5976. b). τ delay time 3 seconds, T_d recycle delay 20 seconds, scans 6308.

f. Mathematical

We routinely enhance the sensitivity of the NMR spectra by multiplying the FID by a decaying exponential function prior to Fourier transformation. This will change the amplitudes and the widths of the peaks in the frequency domain. However, the relative areas are not altered. A broadening function is chosen which is much larger than the width of the high frequency noise, but smaller than the width of the real peaks. This results in a significant improvement in signal-to-noise ratio with a slight increase in the width of the resonance (Figure 1.11). In Figure 1.11, LB stands for line broadening. The exponential decay constant is determined by the LB. Resolution enhancement may be achieved by multiplying a negative LB exponential with a positive LB Gaussian function²¹.

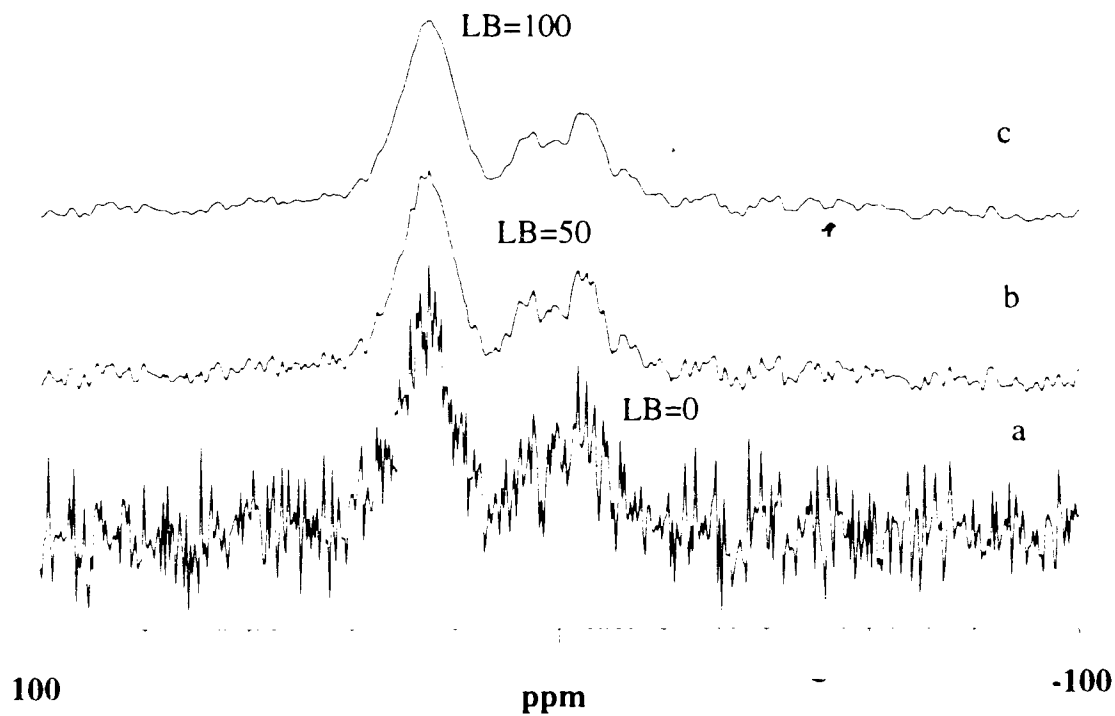


Figure 1.11 ^{31}P NMR spectra of $0.38 \mu\text{mol}/\text{m}^2$ tricyclohexylphosphine on the 6.2 SiO_2 per nm^2 of Al_2O_3 monolayer catalyst, adsorbed at 100°C one hour, preheat catalyst at 450°C , 10^{-5} torr two hours, 90° pulse, MAS rate 1.81 kHz, recycle delay 5 seconds, 10000 scans. a). normal FT, b). multiply the exponential function before FT, LB=50, and c) LB=100.

5. References:

1. C. A. Fyfe, "Solid State NMR for Chemists", CFC press (1984).
2. P. Granger and R. K. Harris (edited), "Multinuclear Magnetic Resonance in Liquids and Solids-Chemical Applications ", Kluwer Academic Publishers, The Netherlands (1990).
3. E. O. Stejskal and J. D. Memory, "High Resolution NMR in the Solid State", Oxford University Press (1994).
4. R. K. Harris, "Nuclear Magnetic Resonance Spectroscopy- A Physicochemical View", Pitman (1983).
5. A. Abragam, "Principles of Nuclear Magnetism", Oxford University Press (1961).
6. U. Haeberlen, "High Resolution NMR in Solids, Selective Averaging", Suppl 1, *Advances in Magnetic Resonance*, (1976).
7. A. T. Bell and A. Pines (edited), "NMR Techniques in Catalysis", Marcel Dekker, Inc, (1994).
8. G. Engelhardt and D. Michel, "High-Resolution Solid-State NMR of Silicates and Zeolites", John Wiley and Sons, (1987).
9. F. Bloch, *Phys. Rev.*, **111**, 841 (1948).
10. L. R. Sarles and R. M. Cotts, *Phys. Rev.*, **111**, 853 (1958).
11. G. Sinnig, M. Mehring, and A. Pines, *Chem. Phys. Lett.*, **43**, 382 (1976).
12. M. Mehring, *NMR Basic Principles and Progress*, **11** (1976).
13. T. M. Duncan and C. Dybowski, *Surface Science Reports*, **1**, 157 (1981).
- 13a. R. C. Weast (editor-in-chief), *CRC Handbook of Chemistry and Physics*, CRC Press, (1989-90).
- 13b. J. A. Davis, S. Dutremez and A. A. Pinkerton, *Inorg. Chem.*, **30**, 2380, (1991).

14. D. P. Burum and M. Linder and R. R. Ernst, *J. Magn. Reson.* **44**, 173 (1981).
15. M. E. Stoll, A. J. Vega and R. W. Vaughan, *J. Chem. Phys.*, **65**, 4093 (1976).
16. M. Mehring, A. Pines, W. K. Rhim and J. S. Waugh, *J. Chem. Phys.*, **54**, 3239 (1971).
17. G. H. Penner and R. E. Wasylshen, *Can. J. Chem.*, **67**, 1909 (1989).
18. E. R. Andrew, A. Bradbury and R. G. Eades, *Nature*, **182**, 1659 (1958).
19. E. R. Andrew, A. Bradbury and R. G. Eades, *Nature*, **183**, 1802 (1959).
20. I. J. Low, *Phys. Rev. Lett.*, **2**, 285 (1959).
21. D. E. Axelson, "Solid State Nuclear Resonance of Fossil Fuels", Multiscience Publications Limites, Canada (1985).
22. J. R. Lyerla, "Contemporary Topics in Polymer Science", **3**, 143 (1979).
23. J. Schaefer, E.O. Stejskal, R.A. McKay, *J. Magn. Reson.*, **25**, 269 (1977).
24. E. Lippmaa, M. Alla, T. Tuherm, *XIX Congress Ampere*, Heidelberg, (1976).
- 24a. M. M. Maricq, J. S. Waugh, *J. Chem. Phys.*, **70**, 3300 (1979).
25. J. Herzfeld, A. E. Berger, *J. Chem. Phys.*, **73**, 6021 (1980).
26. N. J. Clayden, C.M. Dobson, L. Lian, D. J. Smith, *J. Magn. Reson.*, **69**, 476 (1986).
27. R. K. Harris, L. H. Merwin, G. Hagele, *J. Chem. Soc. Faraday 1*, **85**, 1409 (1989).
28. B. Hu, I. D. Gay, *Langmuir*, **11**, 3845 (1995).
29. Y. He, M. Sc. thesis, Simon Fraser University (1988).
30. W. T. Dixon, *J. Magn. Reson.*, **44**, 220 (1981).
31. W. T. Dixon, *J. Chem. Phys.*, **70**, 3300 (1979).

32. W. T. Dixon, J. Schaefer, M. D. Sefcik, E. O. Stejskal, R. A. McKay, *J. Magn. Reson.*, **49**, 341 (1982).
- 32a. D. P. Raleigh, E. T. Olejniczak, and R. G. Griffin *J. Chem. Phys.*, **89**, 1333 (1988).
33. S. R. Harmann, E. L. Hahn, *Phys. Rev.*, **128**, 2042 (1952).
34. A. Pines, M. G. Gibby and J. S. Waugh, *J. Chem. Phys.* **59**, 569 (1973).
35. R. K. Harris and G. J. Nesbitt, *J. Magn. Reson.* **78**, 245 (1988).
36. J. Tegenfeldt and U. Haerberlen, *J. Magn. Reson.* **36**, 453 (1979).
37. C. J. Clemett, E. G. Smith, R. K. Harris, A. M. Kenwright and K. J. Packer, *Polymer Comm.* **28**, 137 (1987).
38. S. J. Opella, M. H. Frey, *J. Am. Chem. Soc.* **101**, 5854 (1979).
39. Y. Huang, D. F. R. Gilson, I. S. Butler, and F. Morin, *J. Phys. Chem.* **95**, 2151 (1991).
40. L. B. Alemany, D. M. Grant, T. D. Alger, and R. J. Pugmire, *J. Am. Chem. Soc.* **105**, 6697 (1983).
41. M. Alla, and E. Lippmaa, *Chem. Phys. Lett.* **37**, 260 (1976).
42. R. H. Newman, *J. Mag. Reson.* **86**, 176 (1990).
43. W. T. Dixon, *J. Chem. Phys.*, **77**, 1800 (1982).
44. F. G. Oliver, E. J. Munson and J. F. Haw, *J. Phys. Chem.*, **96**, 8106 (1992).
45. M. W. Anderson, M. L. Odelli, and J. Klinowski, *J. Phys. Chem.*, **96**, 388 (1992).
46. J. L. White, L. M. Beck and J. F. Haw, *J. Am. Chem. Soc.*, **114**, 6182 (1992).
47. J. F. Haw, B. R. Richardson, I. S. Oshiro, N. D. Lazo and J. A. Speed, *J. Am. Chem. Soc.*, **111**, 2052 (1989).
48. D. K. Murray, J.-W. Chang and J. F. Haw, *J. Am. Chem. Soc.* **115**, 4732 (1993).
49. I. T. Ali, Ph. D. thesis, Simon Fraser University, (1982).
50. S. H. C. Liang, Ph. D. thesis, Simon Fraser University, (1985).

51. J. R. Lyerla, C. A. Fyfe and C. S. Yannoni, *J. Am. Chem. Soc.*, **101**, 1351 (1979).
52. C. S. Yannoni, V. Macho and P.C. Myhre, *J. Am. Chem. Soc.*, **104**, 907 (1982).
53. C. S. Yannoni, V. Macho and P.C. Myhre, *J. Am. Chem. Soc.*, **104**, 7380 (1982).
54. F. Taulelle, J. P. Coutures, D. Massiot, and J. P. Rifflet, *Bull. Magn. Reson.*, **11**, 318 (1989).
55. Y. Ohtsuka, T. Nozawa, A. Tomita, Y. Tamai, M. Hatano, *Fuel*, **63**, 1363 (1984).
56. C. A. Fyfe, G. C. Gobbi, J. S. Hartman, R. E. Lenkinski, J. H. O'Brien, E. R. Beauge and M. A. R. Smith, *J. Mag. Res.*, **47**, 168 (1982).
57. M. T. Sullivan, G. E. Maciel, *Anal. Chem.*, **54**, 1615 (1982).
- 57a A. Llor and J. Virlet, *Chem. Phys. Lett.*, **152**, 248 (1988).
- 57b A. Samoson, E. Lippmaa and A. Pines, *Mol. Phys.*, **65**, 1013 (1988).
- 57c B. F. Chmelka, K. T. Mueller, A. Pines, J. Stebbins, Y. Wu and J. W. Zwanziger, *Nature*, **339**, 42 (1989).
- 57d Y. Wu, B. F. Chmelka, A. Pines, M. E. Davis, P. J. Grobet, P. A. Jacobs, *Nature*, **346**, 550 (1990).
58. M. G. Munowitz, R. G. Griffin, G. Bodenhausen and T. H. Huang, *J. Am. Chem. Soc.*, **103**, 2529 (1981).
59. M. G. Munowitz and R. G. Griffin, *J. Chem. Phys.*, **76**, 2848 (1982).
60. M. G. Munowitz and R. G. Griffin, *J. Chem. Phys.*, **77**, 2217 (1982).
61. C. J. Clemett, E. G. Smith, R. K. Harris, A. M. Kenwright and K. J. Packer, *Polymer Comm.* **28**, 137 (1987).
62. N. Zumbulyadis, *J. Mag. Res.*, **53**, 486 (1983).

63. R. S. Aujla, R. K. Harris, K. J. Packer, M. Parameswaran, B. J. Say,
Polym. Bull. **8**, 253 (1982).

Chapter 2 ³¹P NMR to investigate acidity of the SiO₂-Al₂O₃ catalysts: A overview of related known facts.

1. What is "Acidity"?: definition and measurement

Before the study of the acidity on a surface, we should clarify the definition of this term in the thesis. Here the "acidity" is the amount of acid on a surface obtained by the reaction of a base with the solid surface. It is expressed as the number of moles of acid sites per unit surface area of the catalyst.

Besides the acid amount, the acid strength can be used to describe the acidic properties. It is defined as the ability of the surface to convert an adsorbed neutral base into its conjugate acid. The Hammett function H_0 can be used to express the acid strength¹,

$$H_0 = pK_a + \log [B] / [A] \quad 2.1$$

where [B] is the concentration of the neutral base. [A] is the concentration of its conjugate acid or Lewis acid.

There are a number of ways to measure acid amount and strength. The main methods are listed in Table 2.1.

Table 2.1 The techniques to measure the amount and strength of an acid

a	Titration
b	TPD (temperature programmed desorption)
c	DTA (differential thermal analysis)
d	TG (thermogravimetry)
e	IR
f	NMR
g	Catalytic activity

The number of acid sites on a solid surface can be titrated in benzene with *n*-butylamine using an indicator². The use of indicators with different pK_a values can determine the amount of acid at various acid strengths by amine titration. The amount of acid is the sum of the both Brønsted and Lewis acid, since the Brønsted acid and Lewis acid sites on the surface will react with either the indicator or the amine.

TPD (temperature programmed desorption) of basic molecules can be used to characterize the acid strength and acid amount in a surface. Ammonia, pyridine, *n*-butylamine are extensively used as basic probe molecules. Since a base is more stable on stronger sites, the basic molecules at weaker sites will be desorbed earlier when raising the temperature. Thus, the temperature of the TPD peaks can show the acid strength³. The adsorption heat of various bases is also a measurement of the acid strength on a solid surface^{2,4}. DTA (differential thermal analysis) and TG (thermogravimetry) can be used to

estimate the acid amount and strength as well². These methods have the advantage that the measurement occurs at high temperatures, which is closer to their real working conditions as a catalyst. The disadvantages are a) it is hard to get the amount of acid at various strengths, and b) difficult to know the nature of the adsorbed species.

The IR method for measurement of acid strength and number of surface hydroxyl groups is well known⁵⁻⁷. It has been shown that IR is effective for acidic properties of hydroxyl groups. The different Lewis acid sites can also be characterized by the shift of the fundamental stretching vibrations of adsorbed H₂ at low temperature. Recently, progress in solid-state NMR has made quantitative studies of acidic properties possible. We will discuss the details in section 3 of this chapter.

The surface areas of some catalysts are so small that an adsorption method is not feasible for the determination of acidity⁸⁻⁹. Therefore the catalytic activity for the dehydration of isopropyl alcohol or the isomerization of butene has been used to measure the acidity and acid strength. Besides, any kind of acid-catalyzed reactions, such as cracking of cumene, alkylation of benzene with propene, isomerization of cyclopropane, etc., can be used for the measurement of the acidic property on a catalyst¹⁰. It should be mentioned that it is not easy to distinguish the acid strength and acid amount by this method.

2. SiO₂-Al₂O₃ is a mixed binary oxide: structure and acid property.

SiO₂-Al₂O₃ is a mixed catalyst which is composed of SiO₂ and Al₂O₃ oxides. Thus we have to understand the individual structure of SiO₂ and Al₂O₃ oxides before we study the properties of these chemically mixed catalysts.

There are various forms of silica including crystalline and non-crystalline types. Here we are only interested in porous silica (also termed silica gel). Limited information on the structure of porous silica is available. We have to refer to non-porous crystalline forms which have the same bulk composition but known crystal structures. The Si-O bond length is about 0.162 nm, which is much smaller than the sum of covalent radii (0.191 nm)¹¹. This accounts for the partially ionic character of the Si-O bond. Each silicon atom is normally surrounded by four oxygen atoms, which forms the tetrahedral [SiO₄]¹². The Si-O-Si bond angles have been measured by diffraction. Bond angles of 144° and 147° were found for α-quartz and α-cristobalite respectively¹¹.

The surface of porous silica is covered by silanol groups (SiOH) and physically adsorbed water. In order to remove the physically adsorbed water, the drying temperature range needs to be between 423 and 573 K under vacuum, depending on the type of silica¹³. Silanol groups are left on the silica surface mainly as three types, i.e. isolated (a), geminal (b) and vicinal (c) groups (Figure 2.1).

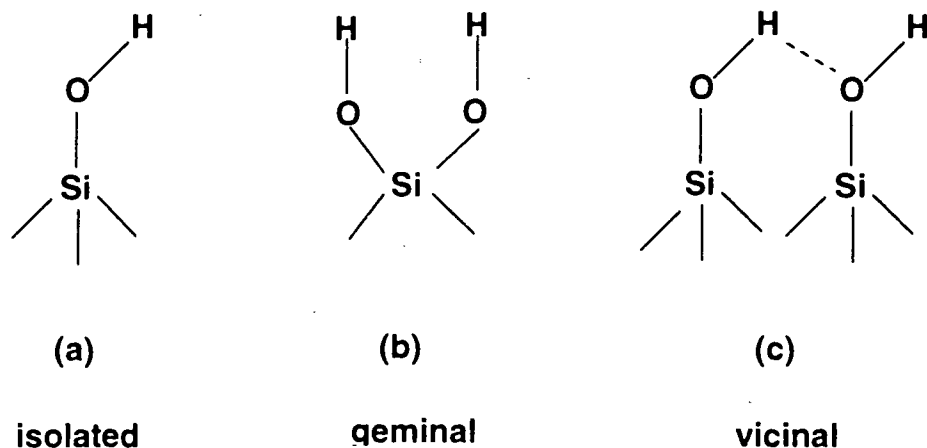


Figure 2.1 The types of silanol groups on the silica surface.

^{29}Si CP-MAS spectra of silica gel show three peaks¹⁴. They are assigned as $(-\text{O}-)_4\text{Si}$, $(-\text{O}-)_3\text{SiOH}$ ((a) in Figure 2.1) and $(-\text{O}-)_2\text{Si}(\text{OH})_2$ ((b) in Figure 2.1) based on the variable contact time CP experiments and the spectra of silicic acid solutions.

It should be noted that although Si is also present within the bulk, all the protons are essentially at the surface. CP experiments are based on the ^1H - ^{29}Si dipolar interaction. The dipolar coupling varies as the inverse cube of the H-Si internuclear distance. Hence, the CP experiment can be used to discriminate in favor of the surface nuclei (not only ^{29}Si , but also ^{27}Al , ^{17}O etc.).

Dehydration at 473 K of silica will be accompanied by dehydroxylation of vicinal hydroxyl groups (Figure 2.2).

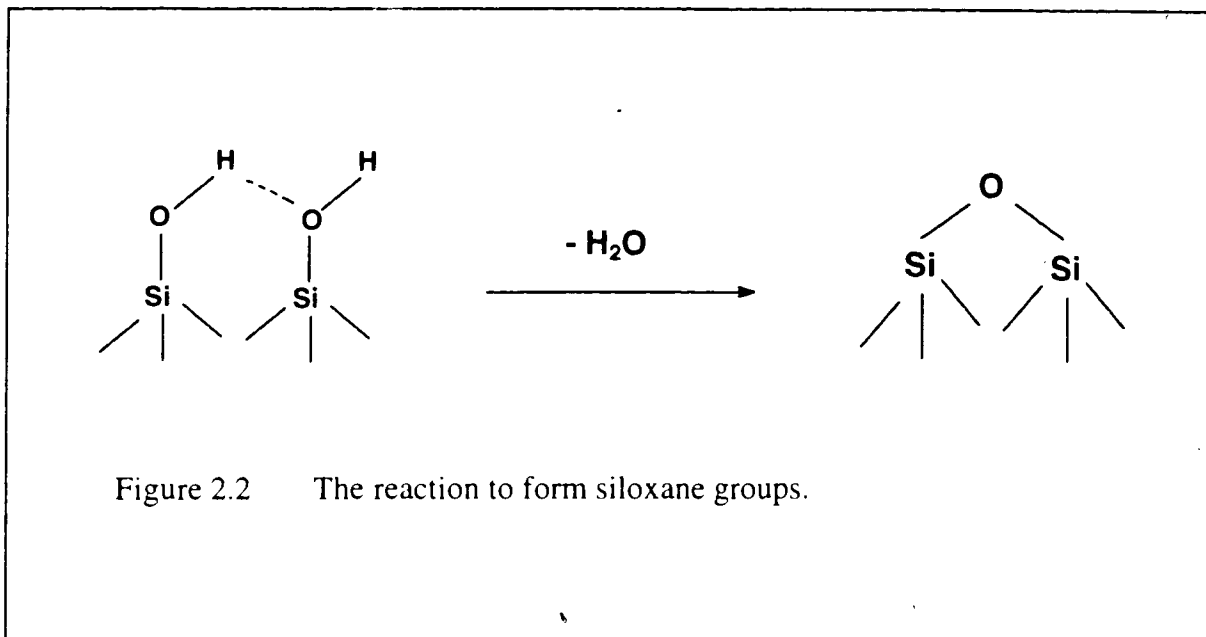


Figure 2.2 The reaction to form siloxane groups.

The product of this reaction is at least a part of the species detected as $(-\text{O}-)_4\text{Si}$ using NMR. The amount of $(-\text{O}-)_4\text{Si}$ by NMR increases as contact time is increased. This suggests that deeper Si can be seen with a sufficiently long contact time. This reaction proceeds at higher temperature. At about 773 K^3 , the vicinal hydroxyl groups are completely condensed. The number of silanol groups on silica gel can be estimated by various techniques. The surface concentration of silanol groups is a function of the temperature of heat-treatment under vacuum¹⁵. We pretreated the silica gel at 450°C under vacuum. The concentration of silanol groups on silica gel treated at 450°C is about $4 \pm 1\ \mu\text{mol}/\text{m}^2$ ¹⁵.

The pK_a value of the surface silanol group is determined to be 7.1 ¹⁶⁻¹⁷.

Alumina Al_2O_3 has various crystallographic forms. Among them, the γ - and η -alumina are most important as catalysts. Both γ - and η -alumina possess defect spinel lattices¹⁸. The average Al-O bond length in γ -alumina was calculated as $0.1820\text{-}0.1818\text{ nm}$, which is smaller than in η -alumina ($0.1838\text{-}0.1825\text{ nm}$)¹⁹. The aluminas are built

primarily of tetrahedral $[\text{AlO}_4]$ and octahedral $[\text{AlO}_6]$ groups. The surface of these aluminas consists of (100), (110), and (111) planes²⁰.

Water adsorbs on the surface of alumina both physically (desorbing at 373-393 K) and chemically (desorption starting at about 573 K). The surface area of γ -, η -alumina are usually $100\text{-}300\text{ m}^2\text{g}^{-1}$. The number of OH groups left on the alumina is a function of the drying temperature¹². The values of OH concentrations from different laboratories scatter around the curve to fairly considerable degrees. At 450°C , the concentration of OH on alumina is about $8\text{ }\mu\text{mol/m}^2$ ^{2, 20}.

Two models have been proposed to describe the partially dehydroxylated surface of alumina. Both reasonably explain the IR bands of the surface OH groups. The earlier model considered the surface of the alumina to be only the (100) plane¹³. The IR frequency of OH groups was influenced by the inductive effect from the adjacent oxide ions. In the later model, the IR frequency of the OH groups is influenced by their net charges²⁰. The net charge can be calculated by the Pauling's electrostatic valence rule²¹. The (111), (110) and (100) surface planes of alumina are considered. Examples of proposed models and the net charges and assigned IR frequencies are shown in Figure 2.3.

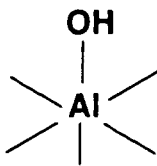
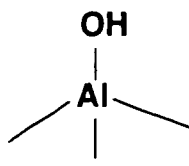
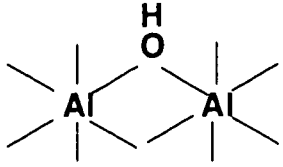
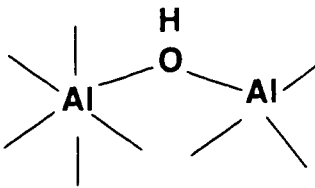
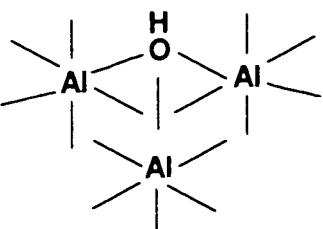
Proposed Model	ν_{OH} (cm^{-1})	Net Charge at OH
	3785-3800	-0.5
	3760-3780	-0.25
	3740-3745	0
	3730-3735	+0.25
	3700-3710	+0.5

Figure 2.3 Proposed models of surface OH groups on Al_2O_3 with the net charges and assigned OH IR frequencies²⁰.

The number of Lewis acid sites produced by the process of dehydroxylation is of the order of magnitude of 10^{14} cm^{-2} ²⁰. The number of catalytically active sites is one to two order of magnitude lower. The number of active sites has been estimated to be 10^{13} cm^{-2} for dehydration of 1-butanol, $8 \times 10^{12} \text{ cm}^{-2}$ for isomerization of cyclohexane and $5 \times 10^{12} \text{ cm}^{-2}$ for $\text{CH}_4\text{-CD}_4$ isotopic exchange²⁴. It must be concluded that Lewis acid sites produced during the regular dehydroxylation process can hardly be involved in catalytic reactions as active sites. The active sites may be identified with defects, with multiple vacancies and/or cluster of oxygen atoms in a certain special environment²⁰. **The use of suitable specific probe molecules can provide us with information about such sites.**

The surface of alumina has both acid and basic sites. This is confirmed by adsorption of basic and acidic molecules or by poisoning experiments^{15, 22}. Most experiments agree that the IR does not detect any protonated species, but only Lewis acid sites¹⁷. This is in agreement with our NMR results for tricyclohexylphosphine²³. 4-methyl and 2,6-dimethyl pyridine react more weakly than pyridine with the alumina surface, even though they are stronger bases^{18, 24}. **This indicates the presence of steric effects for bulky molecules (including 4-methyl and 2,6-dimethyl pyridine) during the adsorption processes on the surface.**

Silica-alumina is an acidic oxide which has been extensively studied. The acidic centers on the surfaces are the catalytically active sites. The following are the primary reasons why the surface acid sites are the catalytically active sites².

a). The existence of acid sites has been confirmed by various methods we mentioned in section 1 of this chapter, also the catalytic activities correlate with the number of acid sites.

b). The catalytic activity of the catalyst is poisoned by adsorbed basic molecules (see Chapter 7).

c). Studies of the reaction mechanism indicate that reaction intermediates are cations formed by the acid sites.

Both Brønsted and Lewis acid are formed on the silica-alumina surfaces. The acid sites on the surface are stronger than $H_0 = -8.2$ ²⁵. The number of Lewis acid sites increases when the pretreating temperature is raised. Good correlations between the number of acid sites and catalytic activities are observed in many catalytic reactions (including propene polymerization, cumene cracking, and *o*-xylene isomerization)²⁶. The butene isomerization on the silica-alumina surface has been extensively studied. The active sites are Brønsted acid sites²⁷⁻²⁹.

The structures of acid sites of silica-alumina have been proposed³⁰⁻³². One model (A) is shown in Figure 2.4³¹. A tetrahedral aluminum atom is inserted in to the silica structures. The AlO_4 part is unsatisfied by a whole valence unit. Thus a proton must be associated with a unit to balance the charge.

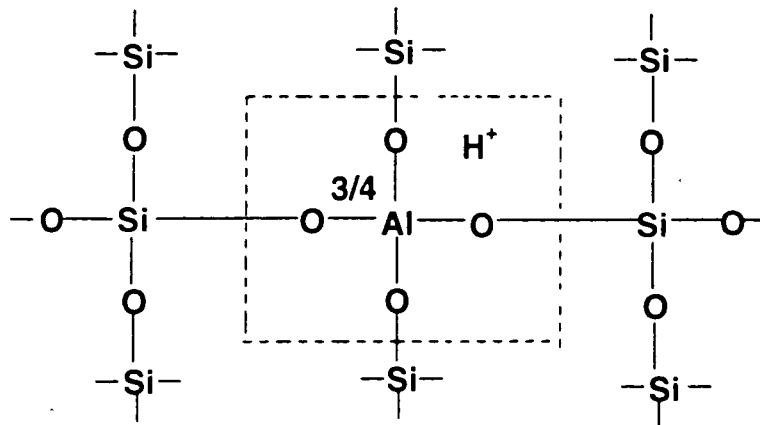


Figure 2.4 Model A of the acid site structure of silica-alumina.

The other model (B) is shown in Figure 2.5³². This model shows the Lewis acid structure as well.

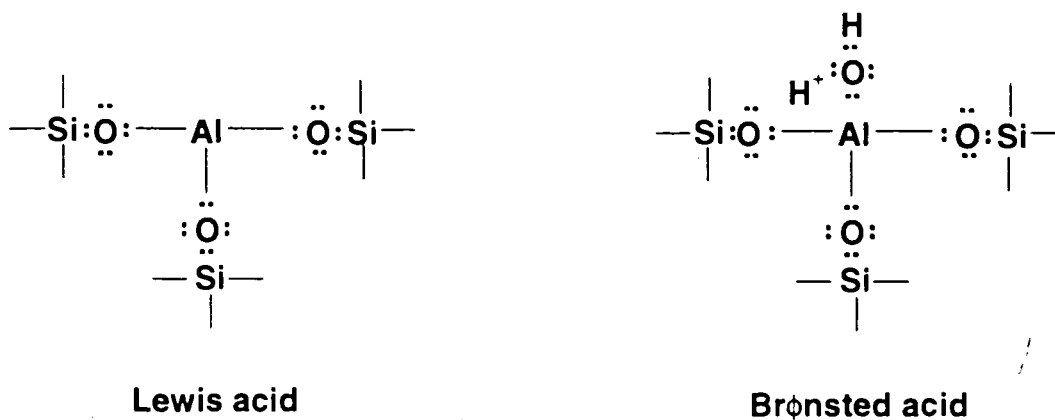


Figure 2.5 Model B of the acid site structure of silica-alumina.

Because of the amorphous structure of silica-alumina, it is hard to identify the acid site. Calculations of cluster models have been applied to the silica-alumina system. The cluster models are shown in Figure 2.6 with charge densities³³. One hydrogen is attached to O_b to balance the charge and make the most stable structure. This hydrogen has the highest positive charge in the model, which is comparable to H_3O^+ (+0.32).

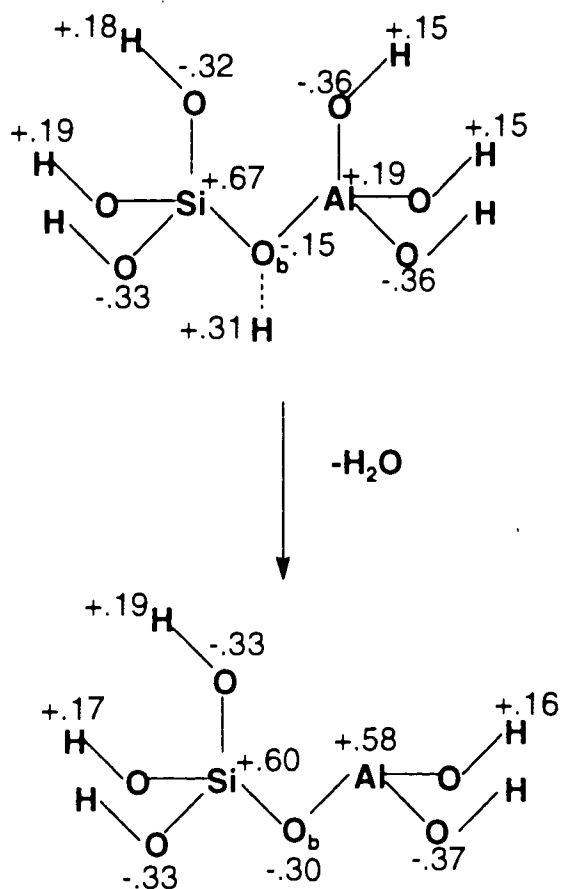


Figure 2.6 Charge densities calculated for models of silica-alumina.

The cluster models have been recently reviewed³⁴. The Brønsted acid sites have been summarized as bridged hydroxyl groups and water molecules coordinated on a trigonal aluminum atom.

3. NMR approaches to acid sites on silica-alumina surfaces: basic probes.

The acidity on a surface is of great interest in the area of surface catalysis (for example, see section 2). Besides NMR, many experimental methods have been developed to address the surface sites (see section 1). Here, we will discuss the NMR approaches using basic probes. It should be pointed out that the pioneering contributions of my supervisor in this area of NMR spectroscopy have been recognized³⁵⁻³⁶.

a. ¹³C and ¹⁵N studies of acid sites: by pyridine, *n*-butylamine, ammonia CH₃¹³CN, ¹⁵N₂O and ¹³CO.

a1. Pyridine

The formation of protonated organic compounds on a surface has been studied by ¹³C and ¹⁵N NMR spectroscopy. The pyridine and substituted aromatic bases were first used as NMR probes to study the surface acidity³⁷⁻³⁹. The pK_a of pyridine is 5.23³⁵. The pyridinium ions formed on the surface undergo a fast equilibrium with pyridine. Thus the observed chemical shift difference, $\delta_2 - \delta_3$ (between C₂ and C₃), can be used to calculate the fraction of ions formed (P₁)³⁷:

$$\delta_2 - \delta_3 = (1-P_1) (\delta_{2M} - \delta_{3M}) + P_1 (\delta_{2I} - \delta_{3I}) \quad 2.2$$

where $(\delta_{2M} - \delta_{3M})$ and $(\delta_{2I} - \delta_{3I})$ represent the differences of chemical shifts for the individual pyridine (M) and the pyridinium ion (I) without exchange. The formation of pyridium ions can be observed by adding HCl and pyridine to silica gel. Obviously these values of chemical shift difference are the same for different catalysts. Therefore this technique can be applied to the study of the acidity of various solid surfaces, for example zeolites⁴⁰. Also, it was observed that the molecular mobility of these probes is more strongly reduced for alumina than for silica surfaces³⁸.

In the earlier work, the MAS technique was not used. The chemical shift anisotropy causes overlap and a broad spectrum, even at high surface coverages. This makes the quantitative measurement difficult and results have wider uncertainty. Later the ¹³C CP-MAS spectrum of pyridine was completely resolved at 0.05 monolayer coverage on γ -alumina⁴¹. The separate resonances of the three types of carbon have the same chemical shifts as liquid pyridine within experimental error. The lines are 3-4 ppm broad. The use of 90% ¹⁵N enriched material reduced the linewidth of the α carbon by approximately 30% relative to normal >99.7% ¹⁴N material. This may be explained by the quadrupole effect, which interferes with MAS averaging of ¹³C-¹⁴N dipolar interactions³⁵. The residual linewidths probably are due to heterogeneity of the surface acid sites, or to site diffusion between chemi-sites or physi-sites on the surface.

Later ¹⁵N NMR was applied to study pyridine adsorbed on alumina samples⁴². It was shown that Brønsted acid species are not present on the alumina surface. Also two kinds of the Lewis acid sites were found on the surface.

The pyridine/alumina system has been studied in more detail⁴³. The ¹⁵N spectra showed two Lewis acid peaks, which were hypothesized to be the two resonances associated with octahedral and tetrahedral sites on the surface. The γ -Al₂O₃ surface was

demonstrated to contain an equal mixture of (111) and (110) planes. This conflicts with previous studies with the IR, which showed that the combination of (110), (111), and (100) planes probably gives a description of the surfaces²⁰ (see section 2).

The combination of ¹³C and ¹⁵N spectroscopy provides more information on the pyridine probe on silica-alumina⁴⁴. Hydrogen bonding is shown to be the dominant interaction at high coverages (0.5-1 statistical monolayer). The pyridine is very mobile for this coverage range, and exchanging species are observed. At lower coverages, a Lewis acid site was observed where pyridine is significantly less mobile. The assignment of the Lewis acid sites is based on the dynamics of exchange processes, which were not verified experimentally. Protonated pyridine species were found after the surface was treated with HCl. Later the same group used the competitive adsorption of ¹⁵N enriched pyridine and natural-abundance *n*-butylamine to study the silica-alumina surfaces⁴⁵. The *n*-butylamine is a stronger base than pyridine, with a pK_a of 10.61³⁵. It was found that at the low coverages (0.082 monolayer) the pyridine was protonated without the added butylamine. The addition of 0.4-0.8 equivalent of natural-abundant *n*-butylamine (relative to the adsorbed pyridine coverage) makes adsorbed pyridine shift to Lewis acid sites. Spectra of more than 1 equivalent butylamine show a relatively sharp peak, which was assigned as the hydrogen bonded species. 11 equivalents of *n*-butylamine (about 1 monolayer) showed a shift to the intermediate between hydrogen-bonded and liquid pyridine. It seems that the coadsorption is an excellent technique to investigate the different adsorbed forms on the surface.

a2. *n*-butylamine

n-butylamine is a very strong base. Besides the coadsorption studies with the pyridine on the silica-alumina surface, the adsorption of *n*-butylamine on γ -Al₂O₃ has been investigated⁴⁶. The ¹³C NMR spectrum contains four peaks for the α and β carbons of the alkyl group, which clearly shows two different sites on the alumina surface. The two solid adducts, HCl and BCl₃ of *n*-butylamine, have been used to assign the two sites. They concluded that the two sites are probably arising from Brønsted and Lewis acid sites, in which the Lewis acid site is stronger than the BCl₃, based on the chemical shift change. It is interesting to observe a conformational effect for *n*-butanol (natural isotopic abundance) adsorbed on MgO⁴⁷, which was suggested to explain two peaks for β carbon of *n*-butanol. Also the majority of the literature agrees that the Brønsted acid sites are not produced on an alumina surface (see section 2). Therefore, we cannot eliminate the argument of only Lewis acid complexes on the surface, which showed four peaks for α and β carbons of *n*-butylamine by a conformational effect.

a3 Ammonia

Ammonia has a pK_a of 9.25³⁵. The adsorption of ammonia on acid zeolites shows the formation of ammonium ions at low coverages (less than 4 molecules per supercage)⁴⁸. On alumina surfaces, however, even with MAS technique the ¹⁵N resonance is too broad to be used as a probe⁴⁹. It was suggested that ND₃ would be a good choice for an ammonia probe. The reason is that the ²H spectra can reveal the mobility of the species, and obviously motions of NH₄⁺ should be quite different from NH₃ bound to a Lewis acid site.

a4 CH₃CN, ¹⁵N₂O, and ¹³CO

¹⁵N NMR of acetonitrile probes can be used to detect the Lewis acid sites in Y zeolites⁴⁹. The electron acceptor strength of Lewis acid sites has been shown to increase with increasing of activation temperature.

¹⁵N₂O has been used to probe Lewis acid sites on alumina surface⁵⁰. This probe is sensitive to the Lewis acid sites (variations of the chemical shifts under different conditions), but insensitive to the Brønsted acid sites on the silica surface treated by acid (same chemical shifts under different conditions).

¹³CO is also used to elucidate the Lewis acid sites⁵¹. These three probes have smaller molecular sizes and thus probably have easier access to Lewis acid sites than bulky probes. **It appears that the steric effects of various probes can provide detailed information about the Lewis acid sites on the surfaces. Systematic studies of steric effects are needed.**

b. ³¹P studies of acid sites: by (CH₃)₃P, (CH₃CH₂)₃P, (CH₃CH₂CH₂CH₂)₃P, (CH₃)₃PO, (CH₃CH₂)₃PO and (*n*-octyl)₃PO.

The ³¹P nucleus has 100% natural abundance, a spin 1/2 quantum number and higher magnetogyric ratio than ¹³C or ¹⁵N. Thus ³¹P NMR is a useful technique for studying acid sites on surfaces.

b1. (CH₃)₃P

Trimethylphosphine ((CH₃)₃P) was first demonstrated as a useful probe for the acid sites in zeolites⁵²⁻⁵³. A phosphonium ion is found with well resolved J_{P-H} coupling and a shift of -4 ppm. A number of ³¹P resonances were found (-32, -44, -47, -50, -54 and -58 ppm) that were assigned to Lewis sites. The -58 ppm peak was also ascribed to the presence of Al₂O₃ in the zeolite. Physisorbed species also were detected. The (CH₃)₃P was adsorbed on γ-Al₂O₃ at two surface coverages⁵⁴. The CP-MAS spectra show that the presence of Brønsted acid (-4 ppm), Lewis acid (-48 ppm) sites and physisorbed phosphine (-58 ppm). The small CP contact time (<1 ms) can discriminate strongly against the physisorbed species. The presence of Brønsted acid on the γ-Al₂O₃ contradicts the results of our lab⁵⁵, in which the spectrum of γ-Al₂O₃ shows little or no Brønsted acid on the surface. Also we found that the Lewis acid sites are centered at -48 ppm, with the same separation (300 Hz) of Al-P coupling sub-peaks as in⁵⁶ for (CH₃)₃P interacting with AlCl₃ in zeolite Y.

The quantitative measurements of acidity were carried out on the commercial silica-alumina and Al₂O₃ monolayer catalysts coated by SiO₂⁵⁵. The physically-adsorbed peak grows and shifts upfield as coverage increases, and finally converts to the chemical shift found on SiO₂. The shift of the peak is explained by the assumption that a fraction of the protonated molecules can exchange rapidly with physically adsorbed phosphine. The observed shift of the coverage-dependent peak is a mole-fraction-weighted average of the -4.9 ppm shift associated with PMe₃H⁺ and -62 ppm of physisorbed species. The mole fraction of protonated phosphine can be calculated:

$$\text{fraction protonated} = \frac{\text{observed ppm} - (-62 \text{ ppm})}{-4.9 \text{ ppm} - (-62 \text{ ppm})} \quad 2.3$$

The maximum concentration of $0.21 \mu\text{mol}/\text{m}^2$ of protonated phosphine on commercial silica-alumina catalyst was calculated by this equation. A lower limit of $0.08 \mu\text{mol}/\text{m}^2$ of Lewis acid concentration on the same catalyst was obtained at $0.23 \mu\text{mol}/\text{m}^2$ total phosphine coverage.

The same type of exchange phenomenon was observed for SiO_2 on Al_2O_3 monolayer catalysts. The results of Brønsted acid of varying SiO_2 levels can be understood by a simple quantitative model. The model assumes:

- a). SiO_2 covers bare Al_2O_3 or previously deposited SiO_2 .
- b). Brønsted acid formation requires bare Al_2O_3 and adjacent SiO_2 on bare Al_2O_3 .
- c.) Brønsted acid sites could be covered by SiO_2 with equal probability.

The model well explains the change of Brønsted acidity with the coated SiO_2 on the monolayer alumina catalysts.



b2. $(\text{CH}_3\text{CH}_2)_3\text{P}$ and $(\text{CH}_3\text{CH}_2\text{CH}_2\text{CH}_2)_3\text{P}$

$(\text{CH}_3\text{CH}_2)_3\text{P}$ was also used as a NMR probe, adsorbed on a silica-alumina over a range of surface coverage⁵⁷. At low surface coverage (0.06 layers), only the Brønsted acid was observed. At higher coverages, two additional peaks were observed, which partly overlapped. The higher frequency peaks were assigned to Lewis acid sites, and the lower

frequency one is assigned to physically adsorbed species. The phosphines adsorbed on silica gel are essentially physically adsorbed species.

Similarly, $(\text{CH}_3\text{CH}_2\text{CH}_2\text{CH}_2)_3\text{P}$ was also studied as a probe⁶⁰. Apparent Brønsted acid concentrations were 0.23, 0.19 and 0.15 mmol H^+ per gram of silica-alumina for trimethylphosphine, triethylphosphine and tri-*n*-butylphosphine respectively. **The different values of concentrations may indicate either steric or basic strength factors.**

b3. $(\text{CH}_3)_3\text{PO}$, $(\text{CH}_3\text{CH}_2)_3\text{PO}$ and $(n\text{-octyl})_3\text{PO}$.

Some phosphine oxides have also been chosen as NMR probes for acidity studies on surfaces⁵⁴. The CP-MAS ^{31}P spectra of $(\text{CH}_3)_3\text{PO}$ and $(\text{CH}_3\text{CH}_2)_3\text{PO}$ show three separate peaks: the Brønsted acid, the Lewis acid and the physically adsorbed species. The spectra obtained with a 90° pulse have poorer resolution than by CP. It is not easy to make a quantitative measurement. However, $(\text{CH}_3\text{CH}_2)_3\text{PO}$ has better resolution than $(\text{CH}_3)_3\text{PO}$. This suggests that variation of R in the R_3PO might produce better probes. $(n\text{-octyl})_3\text{PO}$ is such a molecule that gives better peak separation³⁵. Also this probe shows steric effects. It cannot penetrate the HY zeolite structure, but the spectrum of $(\text{CH}_3)_3\text{PO}$ can give the peaks of acid species with the same zeolite.

c. ^1H NMR studies of acid sites

If the protons are sufficiently dilute on the surfaces and not in clusters, the dipolar broadening can be averaged by MAS (greater than 10 kHz)⁵⁸. To remove ^1H - ^1H dipolar

effects, CRAMPS (combined Rotation and Multiple Pulse Spectroscopy) can be applied⁵⁹. Although there is an extensive literature on the study of silica-alumina systems using ^1H NMR⁶⁰⁻⁶¹, this subject has huge uncertainties associated with the effects of dynamics at surfaces³⁵.

4. References

- 1 L. P. Hammett, and A. J. Deyrup, *J. Am. Chem. Soc.*, **54**, 2721 (1932).
- 2 K. Tanabé, *Solid Acids and Bases*, Kodansha, Tokyo and Academic Press, (1970).
- 3 G. Wang, H. Itoh, H. Hattori, and K. Tanabe, *J. Chem. Soc., Faraday Trans. 1*, **79**, 1373 (1983).
- 4 K. Tsutsumi, H. Q. Koh, S. Hagiwaja, and H. Takahashi, *Bull. Chem. Soc. Jpn.*, **48**, 3576 (1975).
- 5 J. B. Peri, *J. Phys. Chem.*, **69**, 211, 220 (1965).
- 6 L. M. Kustov, V. Yu. Borovkov, V. M. Kazanski, *J. Catal.*, **72**, 149 (1981).
- 7 V. B. Kazanski, L. M. Kustov, and V. Yu. Borovkov, *Zeolites*, **3**, 77 (1983).
- 8 M. Ai, S. Suzuki, *J. Catal.*, **30**, 362 (1973).
- 9 M. Ai, *Bull. Chem. Soc. Jpn.*, **50**, 2579 (1977).
- 10 M. Guisnet, in: *Catalysis by Acids and Bases*, (B. Imelit et al., eds.), Elsevier, Amsterdam, (1985).
- 11 A. F. Wells, *Structural Inorganic Chemistry*, Clarendon Press, (1975).
- 12 K. K. Unger, *Porous Silica-Its Properties and Use as Support in Column Liquid Chromatography*, Elsevier, (1979).
- 13 J. B. Peri, *J. Phys. Chem.*, **68**, 220, (1965).
- 14 G. E. Maciel and D. W. Sindorf, *J. Am. Chem. Soc.*, **102**, 7606 (1980).

- 15 K. Tanabe, M. Misono, Y. Ono, and H. Hattori, *New solid acids and bases-their Catalytic Properties*, Kodansha and Elsevier, (1989).
- 16 D. N. Strazhesko, V. B. Strelko, V. N. Belyakov, S. C. Rubank, *J. Chromatography*, **102**, 191 (1974).
- 17 M. L. Hair, and W. Hertl, *J. Phys. Chem.*, **74**, 91 (1970).
- 18 B. C. Lippens and J. J. Steggerda, in B. G. Linsen(editor), *Physical and Chemical Aspects of Adsorbents and Catalysts*, Academic Press, (1970).
- 19 A. J. Leonard, P. N. Semaille, and J. J. Fripiat, *Proc. Br. Ceram. Soc.*, 103 (1969) (cited from reference 20).
- 20 H. Knözinger and P. Ratnasamy, *Catal. Rev.-Sci. Eng.*, **17(1)**, 31 (1978).
- 21 L. Pauling, *The Nature of the Chemical Bond*, Cornell Univ. Press, (1960).
- 22 H. Knözinger, *Adv. Catal. Relat. Subj.*, **25**, 184, (1976).
- 23 B. Hu, I. D. Gay, *Langmuir*, **11**, 3845 (1995).
- 24 A. Corma, C. Rodellas, and V. Fornes, *J. Catal.*, **88**, 374 (1987).
- 25 H. A. Benesi, *J. Am. Chem. Soc.*, **78**, 5490 (1956).
- 26 J. Ward, and R. C. Hansford, *J. Catal.*, **13**, 354 (1969).
- 27 J. W. Hightower, W. K. Hall, *J. Am. Chem. Soc.*, **89**, 7778 (1967).
- 28 J. W. Hightower, H. R. Gerberich, and W. K. Hall, *J. Catal.*, **35**, 225 (1974).
- 29 J. W. Hightower, and W. K. Hall, *J. Phys. Chem.*, **71**, 1015 (1967).
- 30 R. C. Hansford, *Ind. Eng. Chem.*, **39**, 39 (1947).
- 31 C. L. Thomas, *Ind. Eng. Chem.*, **41**, 2564 (1949).
- 32 K. Tamele, *Disc. Faraday Soc.*, **8**, 270 (1950).

- 33 W. Grabowski, M. Misono, Y. Yoneda, *J. Catal.*, **61**, 103 (1980).
- 34 G. M. Zhidomirov, V. B. Kazansky, *Adv. Catal.*, **34**, 131 (1986).
- 35 G. E. Maciel, and P. D. Ellis, in " NMR techniques in Catalysis ", (A. T. Bell and A. Pines, editors), Marcel Dekker, Inc, (1994).
- 36 G. Engelhardt and D. Michel, " High-Resolution Solid-State NMR of Silicates and Zeolites ", John Wiley and Sons, (1987).
- 37 I. D. Gay, *J. Catal.*, **48**, 430 (1977).
- 38 I. D. Gay and S. H. Liang, *J. Catal.*, **44**, 306 (1976).
- 39 S. H. Liang and I. D. Gay, *J. Catal.*, **66**, 294 (1980).
- 40 H. J. Rauscher, D. Miichel, D. Deininger and D. Geschke, *J. Mol. Catal.*, **9**, 369 (1980).
- 41 W. H. Dawson, S. W. Kaiser, P. D. Ellis, and R. R. Inners, *J. Phys. Chem.*, **86**, 867 (1982).
- 42 J. A. Ripmeester, *J. Am. Chem. Soc.*, **105**, 2295 (1983).
- 43 P. D. Majors and P. D. Ellis, *J. Am. Chem. Soc.* **109**, 1648 (1987).
- 44 G. E. Maciel , J. F. Haw, I. S. Chung, B. L. Hawkins, T. A. Early, D. R. McKay and L. Petrakis, *J. Am. Chem. Soc.*, **105**, 5529 (1983).
- 45 J. F. Haw, I-S. Chung, B. L. Hawkins, and G.E. Maciel, *J. Am. Chem. Soc.*, **105**, 7206 (1983).
- 46 W. H. Dawson, S. W. Kaiser, P. D. Ellis, and R. R. Inners, *J. Am. Chem. Soc.*, **103**, 6780 (1981).
- 47 S. H. C. Liang and I. D. Gay, *J. Catal.*, **101**, 293 (1986).
- 48 D. Michel, A. Germanus and H. Pfeifer, *J. Chem. Soc., Faraday Trans.*

- 78**, 237 (1982).
- 49 P. D. Majors, T. E. Raidy, and P. D. Ellis, *J. Am. Chem. Soc.*, **108**, 8123 (1986).
- 50 V. M. Mastikhin, I. L. Mudrakovsky, and S. V. Filimonova. *Chem. Phys. Lett.*, **149**, 175 (1988).
- 51 A. Michel, W. Meiler, D. Michel, and H. Pfeifer, *J. Chem. Soc. Faraday Trans.* **82**, 3053 (1986).
- 52 W. R. Rothwell, W. X. Shen and J. H. Lumsford, *J. Am. Chem. Soc.*, **106**, 2452 (1984).
- 53 J. H. Lunsford, W. P. Rothwell and W. X. Shen, *J. Am. Chem. Soc.*, **107**, 1540 (1985).
- 54 L. Baltusis, J. S. Frye, and G. E. Maciel, *J. Am. Chem. Soc.* **109**, 40 (1987).
- 55 T.-C. Sheng and I. D. Gay, *J. Catal.*, **145**, 10 (1994).
- 56 P.-J. Chu, J. H. Lunsford, and D. J. Zalewski, *J. Mag. Res.* **87**, 68 (1990).
- 57 L. Baltusis, J. A. Frye and G. E. Maciel, *J. Am. Chem. Soc.*, **109**, 40 (1987).
- 58 R. Eckman, *J. Chem. Phys.* **76**, 2767 (1982).
- 59 C. E. Bronnimann, B. L. Hawkins, M. Zhang, and G. E. Maciel, *Anal. Chem.*, **60**, 1743 (1988).
- 60 C. E. Bronnimann, R. C. Zeigler, and G. E. Maciel, *J. Am. Chem. Soc.*, **110**, 2023, (1988).
- 61 H. Pfeifer, *Colloids. and Surfaces.*, **36**, 169 (1989).

Chapter 3 Still larger phosphines as ^{31}P NMR probes to investigate the acidity: the necessity, objectives and technical problems of this project

1. Remaining problems: why perform this project?

The literature overview of Chapter 2 has shown that NMR of the adsorbed basic molecules does yield valuable information on acidic sites. Compared with techniques of TPD, DTA, TG, titration and activity measurement, NMR can provide the nature of adsorbed molecule sites. In other words, it is possible for NMR to distinguish Brønsted and Lewis acid sites. Compared with IR, the quantitative determination of acidic sites using NMR is possible and easier. Since NMR has simpler spectra, the intensity measurements should be easier and more accurate than IR. Also with IR the relative extinction coefficients of different surface species must be known. However, there is no way to determine these independently, and nonsurface systems are often used, which will obviously bring inaccuracy. Besides, path length is difficult to determine and Beer's law has to be obeyed even around the monolayer coverages, which should be used for a measurement of saturated acidic concentration.

Among the various nuclei of NMR probes, ^{31}P is an excellent choice. ^{31}P has 100% natural abundance, $\frac{1}{2}$ spin quantum number and higher gyromagnetic ratio than ^{13}C or ^{15}N . For quantitative measurement of acidity, 90° degree pulse excitation is necessary. Therefore, using ^{31}P is really an advantage for the reason of sensitivity.

However, ^{31}P NMR tells the information about acid strength very slowly. Each phosphine probe can only detect the acidity corresponding to its pK_a value. Hence, the profile of phosphines with various basic strength (pK_a) is necessary. As in 3-b2, chapter 2, apparent Brønsted acid concentrations were 0.23, 0.19 and 0.15 mmol H^+ per gram of silica-alumina for trimethylphosphine, triethylphosphine and tri-*n*-butylphosphine respectively. These molecules not only have different basic strength, but also have different sizes. The influence of steric effects is uncertain. Thus these different values of H^+ concentration reflect basic strength, steric effects or both. Therefore still larger molecules with various pK_a values are necessary to figure out the variation of H^+ concentrations.

From Section 2. Chapter 2, previous studies showed that 4-methyl and 2,6-dimethyl pyridine reacted more weakly than pyridine with the alumina surface, even though they are stronger bases. Also from section 3-a4, chapter 2, CH_3CN , $^{15}\text{N}_2\text{O}$ and ^{13}CO were used to detect Lewis acid sites. These all have smaller sizes and probably easier access to Lewis acid sites than bulky probes. Are steric effects involved in the determination of acid sites? If there are steric effects, how do they influence the acidity? To answer these questions, systematic studies using still larger phosphines are necessary.

Again from section 2, chapter 2, the catalytically active sites were proposed as defects with multiple vacancies and/or clusters of oxygen atoms in a certain environment. The use of these bulky phosphines may help us to better understand these active sites.

Silica-alumina is active for many catalytic reactions. Some of them use bulky starting materials, such as catalytic cracking reactions etc. In this case, the larger the phosphines, the better they reflect the real catalytic processes. Acidity measurement using these phosphines seems more valuable than with smaller molecules.

2. **Electronic, steric effect or both for acidity on a surface: objectives**

Several kinds of solid bulky phosphines have been chosen as the probes. Among them, the following are widely studied in this thesis: tricyclohexylphosphine (Cy_3P), triparatolylphosphine ($(p\text{-Tol})_3\text{P}$), trimetatolylphosphine ($(m\text{-Tol})_3\text{P}$), triphenylphosphine (Ph_3P) and triparachlorophenylphosphine ($(p\text{-ClC}_6\text{H}_4)_3\text{P}$). The properties of the phosphines are listed in Table 3.1¹⁻².

Table 3.1 pK_a and cone Angle of the bulky phosphines

Probe	pK_a	Cone Angle (degrees)
Cy_3P	9.70	170
$(p-Tol)_3P$	3.84	145
$(m-Tol)_3P$	3.30	
Ph_3P	2.73	145
$(p-ClC_6H_4)_3P$	1.03	145

Table 3.2 pK_a and cone angle of previously studied phosphines

Probe	pK_a	Cone Angle (degrees)
Et_3P^{2a}	8.69	132
$Me_3P^{2b-2d, 5, 8}$	8.65	118
$(n-Bu)_3P^{2a, 8}$	8.43	132

R_3PO molecules have not been used since the poor peak separation will make a quantitative measurement difficult (see 3-b3, chapter 2). For comparison, the physical properties of phosphines which were previously studied as NMR probes are also listed in Table 3.2¹⁻².

Here, pK_a (values for R_3PH^+) has been used as a measure of the basicities of the phosphines. The electronic properties of the phosphorus compounds are commonly divided into σ -donicity and π -acidity or π -basicity³ in the field of inorganic chemistry. The cone angles represent the steric parameters. They have been routinely used to qualitatively explain the reactivity patterns of certain organometallic complexes. The steric parameters, cone angles for symmetric molecules (all three substituents the same) are the apex angle of a cylindrical cone, centered 2.28 Å from the center of the P atom, which just touches the Van der Waals radii of the outermost atoms⁴.

Comparing Table 3.1 with 3.2, we find out: a) the phosphines in Table 3.1 cover much wider range of basic strength (pK_a from 1.0 to 9.7), whereas in Table 3.2 only 8.4 to 8.7. b) the molecules in Table 3.1 are much bulkier (substituents have six carbon rings and also bigger cone angles). Hopefully, these bulky phosphines with wider ranges of basic strength will help us to explain the phenomenon of the acid measurements.

3. **Technical problems: headaches not only from NMR**

We have already discussed the general NMR techniques in the first chapter. Here, the problems of sample preparation, NMR peak identity and quantitative NMR measurement will be addressed.

a. **Sample preparation**

The process of sample preparation involves glass blowing. The NMR tube was sealed under vacuum. The glass tubing with special shapes (Figure 3.1) was made and connected to the vacuum line. After a few weeks' practice, I eventually could do the connections, make the tubings and seal them.

Due to its high vapor pressure, Me_3P can be put on the surface in the gaseous state. The amount of Me_3P can be determined by measuring the pressure change after adsorption on the surface and calculating the number of moles from the known volume of the vacuum line⁵. However, the phosphines in Table 3.1 have very low vapor pressures. For example, Ph_3P has a vapor pressure of 5 torr at 200°C and 0.6 torr at 150°C^{6,7}.

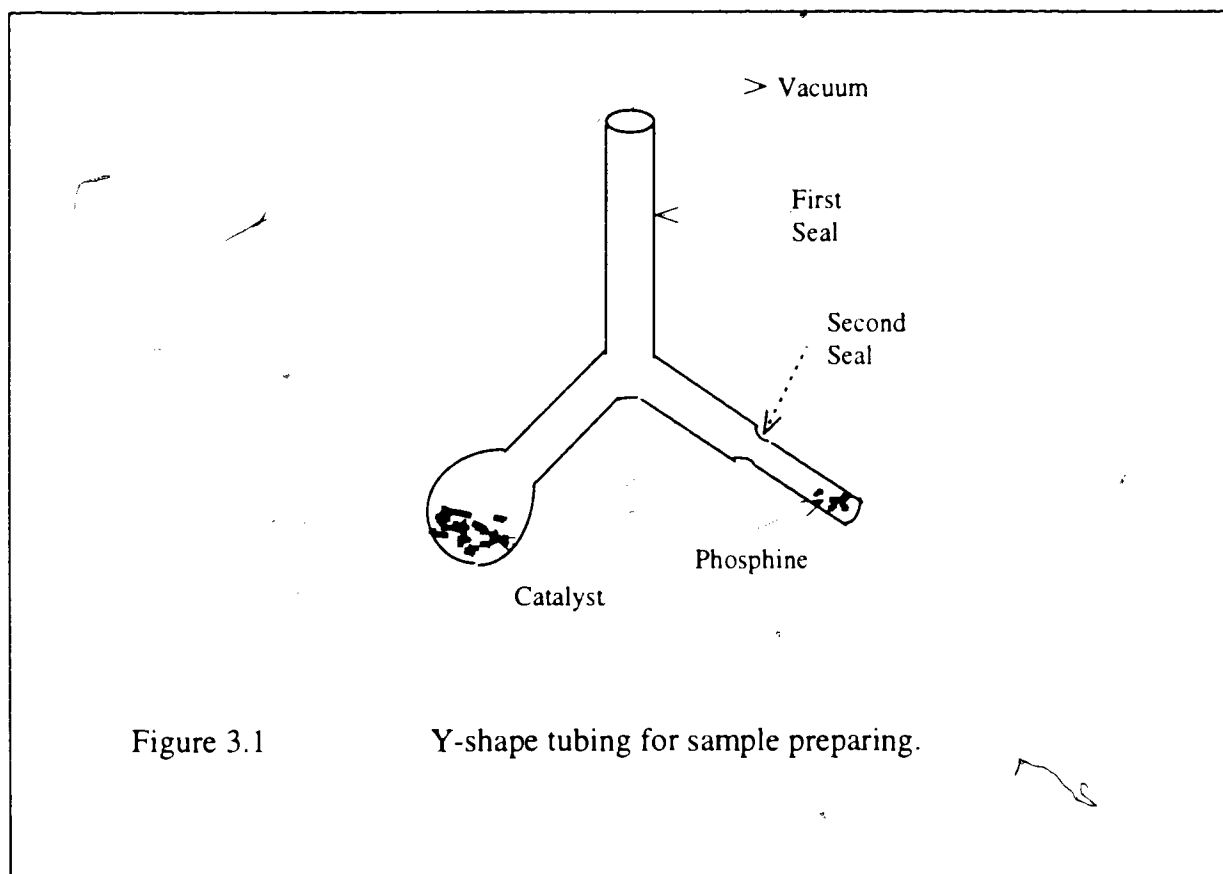
Our initial try to introduce the phosphines used a solution. The procedure was as follows. The catalyst was treated at 450°C. The desired amount of phosphine was added to a solvent. The resulting solution was added to the catalyst under nitrogen. The solvent was

then evaporated under vacuum. This is the traditional way to put low volatility compounds on a surface⁸. But the initial experiment failed in the process of evaporating the solvent. When vacuum was applied, a part of the catalyst with the solvent was suddenly pumped into the vacuum line. The vacuum line could be modified to use milder conditions to pump the solvent. However, the questionable problems of this method still remain: a) Can the solvent be 100% pumped away from the surface? Will it affect the acid measurement, if there is remaining solvent? b) How much impurity is in the nitrogen gas or the solvent? Will this affect the surface structures of the catalyst?

In order to avoid these problems, we explored other ways to prepare the samples. A new way which keeps all the preparing processes under vacuum was found out⁹. We used a Y-shaped tube (Figure 3.1). One leg of the Y was sealed to a 5 mm o.d. by 5.5 cm long NMR tube, the other to a 2 cm o.d. bulb; the open end was connected to the vacuum line. The oxides and phosphines were put into the two ends of the tube (in a glove bag under N₂ or Ar for air sensitive Cy₃P) with the phosphine in the NMR tube. The tube was then quickly connected to the vacuum line. The oxides were treated at 450°C for two hours in 10⁻⁵ torr vacuum in the bulb while the phosphine remained in vacuum at room temperature. Then the oxides were cooled to room temperatures and the open end of the tube was sealed under vacuum. Finally the oxides and phosphines were mixed under vacuum and sealed in the NMR tube. After heating, ³¹P NMR measurements were carried out at room temperature. The samples were then heated to 150°C and 200°C, followed in

each case by NMR measurements at room temperature. Higher temperatures were not used, because the phosphines reacted above 200°C.

You may ask: were the phosphines lost by pumping at room temperature? The answer is no. A simple experiment was done to check the weight of Ph_3P . After pumping at 10^{-5} torr and even 80°C for two hours, the weight of Ph_3P was the same within the weighing error. The vapor pressure at 25°C was also estimated as 1×10^{-4} torr by the Clausius-Clapeyron equation⁶. This value explains why there is no loss of phosphines by this preparation method.



b. Quantitative measurement

^{31}P NMR experiments involve molecular motion. Some species will be less mobile as a result of strong adsorption to the catalyst surface (such as Lewis acid species). Other species may rotate on the surface. The motion normally will be rapid enough to make the ^{31}P NMR properties intermediate between solutionlike and solidlike behavior. CP spectra may reflect different distribution in enhancements, and thus cannot be suited for quantitative measurement. This problem is illustrated by the graphs of cross-polarization data in Figure 3.2.

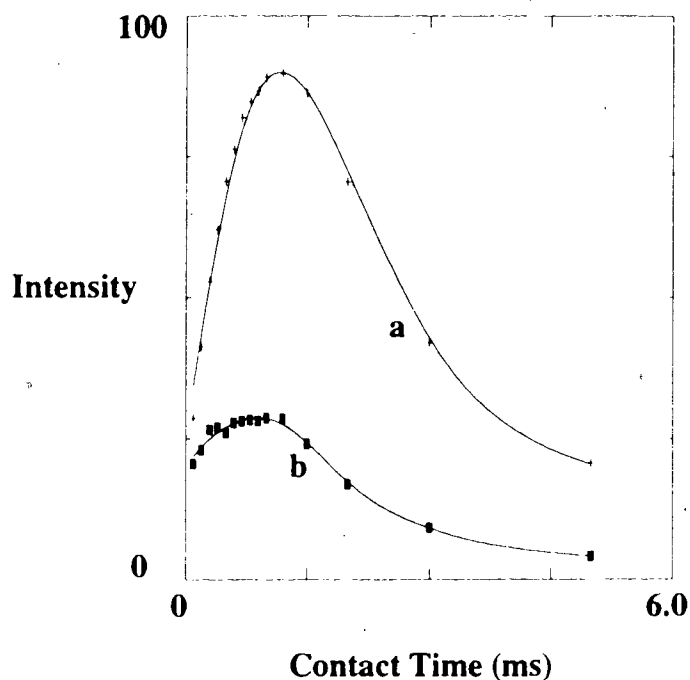


Figure 3.2 Intensity of $1.27 \mu\text{mol}/\text{m}^2$ Cy_3P ^{31}P NMR spectra on silica-alumina catalyst at various CP contact time, adsorbed at 200°C one hour, catalyst was degassed at 450°C and 10^{-5} torr two hours, cross-polarization flip-back, MAS rate 1.82 kHz, recycle delay 1 second, scans 4000; a) physically adsorbed species, and b) protonated species.

In Figure 3.2 Cy_3P was adsorbed onto a sample of commercial silica-alumina catalyst and sealed under vacuum, then heated to 200°C , forming protonated and physically adsorbed species. The CP/MAS behavior of this sample was then investigated. Any arbitrary but reasonable choice of a contact time is likely to produce a quantitative error. For example, 1 ms or 2 ms will give a ratio of 0.33 or 0.25 respectively for these two species. Compared with a ratio of 0.12 from a 90° pulse experiment, this will cause a mistake of a factor of two or three. Indeed, in this example shown in Figure 3.2, cross-polarization will discriminate against the physically adsorbed species by different degrees for all choices of contact time, since cross-polarization is determined by the dipolar interaction (see 3c, chapter 1). Thus, quantitative measurements should be made using 90° pulse experiments. For this kind of experiment, the recycle delay should be sufficiently long. We repeated the spectra with at least a 2-fold change of recycle delay time, to verify that peak intensity ratios were almost the same.

c. Peak Identity

In order to characterize the ^{31}P NMR parameters of the R_3P species expected on the silica-alumina surface, several model molecules were employed. Reaction of phosphines with concentrated HCl will produce the analogue of protonated phosphines on the catalyst. Lewis acid complexes were modeled by the reaction products of phosphines with AlCl_3 . Phosphines were also adsorbed on the individual SiO_2 or Al_2O_3 oxides, which

will show the physically adsorbed and Lewis acid species. The chemical shifts of model compounds are collected in Table 3.3.

Species	R_3P	R_3P	R_3P	$\text{R}_3\text{P-Al}$	$\text{R}_3\text{P-AlCl}_3$	R_3PH^+
State	Solid	on Silica Physisorbed	on $\gamma\text{-Al}_2\text{O}_3$ Physisorbed	on $\gamma\text{-Al}_2\text{O}_3$ Lewis acid	Solid	Solution
C_3P	7.5	8-10	6.5	-7,-22		31.3
$(p\text{-Tol})_3\text{P}$	-10.3	-8.3	-10.1	-12	-15.8	4.4
$(m\text{-Tol})_3\text{P}$	-6.7	-5.3 -5.8	-7.2	-9	-17	5.0
Ph_3P	-9.1	-5.4 -7.2	-6.2 -7.2	-10, -16	-8.4	4.2
$(\text{Cl-C}_6\text{H}_4)_3\text{P}$	-4.0	-10.5			4.9	6.7

The chemical shifts are reported relative to external 85% H_3PO_4 . The reproducibility of chemical shift measurements on different days is better than 0.4 ppm. Since some of these chemical shifts are coverage dependent, the ranges of values are given in Table 3.3 and 3.5. For the $\text{R}_3\text{P-AlCl}_3$ and R_3PH^+ in solution, the central peaks are shown in Table 3.3. The separation of sub-peaks, which is due to J coupling is given in Table 3.4. The systematic trend of J coupling values is due to dipolar interactions to

quadrupolar nuclei, which cannot be completely averaged by MAS. The theory of quadrupolar effects transferred to spin-1/2 MAS spectra was reviewed by Harris and Olivieri^{9a}, which also discussed how to get shielding, dipolar, indirect coupling and quadrupolar interaction tensors from the spectra. The $\text{C}_3\text{H}_7\text{P}-\text{AlCl}_3$ and $(\text{Cl}-\text{C}_6\text{H}_4)_3\text{P}-\text{AlCl}_3$ J couplings are not observed by directly mixing these two solids together.

Table 3.4 J Coupling Constant of Model Compounds

Species	$R_3P-AlCl_3$ P-Al splitting (Hz)	R_3PH^+ J_{P-H} (Hz)
Cy_3P		464
$(p-Tol)_3P$	105,196,280,293,306	488
$(m-Tol)_3P$	220,244,269,281,305	366
Ph_3P	220,244,244,269,317	416
$(P-ClC_6H_4)_3P$		513

The ^{31}P NMR parameters of phosphines on the silica-alumina surface are summarized in Table 3.5. Besides the R_3PH^+ analogues in solution, the dipolar dephasing sequence can help us to assign the R_3PH^+ on the surface by suppressing the signal from these protonated species (see 3c, Chapter 1). The Lewis acid is hardly observed on the catalyst surface.

Table 3.5 ^{31}P Chemical Shifts on the $\text{SiO}_2\text{-Al}_2\text{O}_3$ Catalyst

Species	R_3P	$\text{R}_3\text{P-Al}$	R_3PH^+
State	Physisorbed	Lewis Acid	Brønsted Acid
Cy_3P	8.3-9.6		28
$(p\text{-Tol})_3\text{P}$	-6.0- -8.1		4.6-6.5
$(o\text{-Tol})_3\text{P}$	-28- -30	-8	-11
$(m\text{-Tol})_3\text{P}$	-4.6- -5.5		7.2-7.8
Ph_3P	-5.2- -7.0	-12	6.9-8.4
$(\text{Cl-C}_6\text{H}_4)_3\text{P}$	-7.3- -8.5		4.0-4.4

4. Experimental conditions: chemicals, apparatus, preparation procedures and measurement methods.

a. Chemicals

The sample of silica-alumina is a grade-980, 25% (weight) alumina product from Davison company. The pore size distribution, determined by N_2 adsorption, showed a

maximum at a radius of 17.5 Å. All pores are larger than 15 Å, and 90% of the pore volume is in pores smaller than 50 Å. This sample was ground to 20-40 mesh before the adsorption processes. The surface area was determined to be 400 m²/g by the BET method using nitrogen. The main impurities in this catalyst consist of 0.05% Fe₂O₃ and 0.04% Na₂O from manufacturer's analysis¹⁰.

For distinguishing different species on the catalyst surface, the following model samples were used: Davison high purity silica gel, grade 923, 100-200 mesh, 484 m²/g; Harshaw γ -Al₂O₃, grade Al-3945 E, 40-60 mesh, 225 m²/g; 55% of the pore volume is between 30 Å and 45 Å in radius. 90% of the pore volume is in pores smaller than 60 Å. 12 M HCl from Anachemia, AC-4955, UN-1789. Aluminum chloride was from Anachemia, AC-370, UN-1726. Tricyclohexylphosphine was from Strem Chemicals, 97%, grade 15-6150. Trimetatolylphosphine and Triparacholorophenylphosphine were also from Strem Chemicals, grade 15-8100 and 15-6050 respectively. We thank Dr. Roland K. Pomeroy for providing the arylphosphines.

b. Apparatus

The solid-state NMR spectrometer is a home-made instrument constructed by Dr. Ian D. Gay. A 3.5 T Nalorac cryomagnet is used for NMR. The ³¹P resonance frequency is 60.5 MHz. The spinner was designed by Dr. Ian D. Gay¹¹, which can be spun up to 4 kHz for a sealed 5 mm o.d. by 5.5 cm long NMR tube. The spectrometer is controlled by

two PC computers. The hardware is directly controlled by a 386 computer. A 486 computer is used for processing. The software is written and regularly upgraded by Dr. Ian D. Gay.

Mass spectroscopy experiments were run by Mr. G. Owen using a Hewlett Packard 5985 GC-mass spectrometer.

Gas chromatography experiments were carried out for the poisoning effects of phosphines using a Microtek D99-161 GC with the Gow-Mac thermistor detector. The column was packed with Porasil C silica gel modified with 10% Na_3PO_4 ¹².

c. Preparation procedures

The phosphine/oxide samples were prepared as described in section 3a of this chapter. The phosphine/aluminum chloride samples were prepared in a vacuum line. The weighed aryl phosphines and aluminum chloride were put into the NMR tube. Then it was connected to the vacuum line and sealed under vacuum. The NMR tubes were heated at 100°C for one hour. After heating ³¹P NMR measurement were carried out at room temperature. Two different ways were used to prepare the tricyclohexyl phosphine/aluminum chloride samples. The first way was using a Y-shaped tube. The procedures were similar to the preparation of $\text{C}_6\text{H}_5\text{P}$ /oxide samples (see 3a) except AlCl_3 was treated at 100°C for one hour (whereas oxides at 450°C for two hours). The second

way was used to avoid the possible exposure of the phosphine to HCl, which may be a product during the heating. AlCl_3 was individually treated at 100°C for one hour in 10^{-5} torr vacuum. Then it was cooled to room temperature and sealed under vacuum. The AlCl_3 was mixed into a NMR tube with Cy_3P in a glove bag under an Ar atmosphere. The tube was then quickly connected to the vacuum and sealed under vacuum. Finally the mixtures were heated at 100°C for one hour before the NMR measurement.

SiO_2 on Al_2O_3 monolayer catalysts were prepared using a fluidized-bed method. This method was devised by our lab⁵. A sample of 2 grams of 60-80 mesh Al_2O_3 was placed on a fritted glass disk in a vertical Pyrex tube. The alumina was first dried by heating to 400°C in the dried flowing N_2 for one hour at a flow rate of 500 ml/min. After drying the temperature was decreased to 320°C . The N_2 flow was accompanied by vapor from $\text{Si}(\text{OCH}_3)_4$ maintained at 0°C . The $\text{Si}(\text{OCH}_3)_4/\text{N}_2$ vapor was flowed for an hour. The sample was then cooled to room temperature in flowing N_2 . Finally it was calcined in air at 500°C for three hours. The amount of silica was determined from the final weight increase, in comparison with the Al_2O_3 weight after the drying. The calculated coverage was 6.2 SiO_2 per nm^2 of Al_2O_3 .

The modified silica gel was used as the GC column. The column material was prepared as in reference¹². A weighed portion of Porasil C was added to the 10% (weight) aqueous Na_3PO_4 to form a heavy slurry. The slurry was quickly dried by rotary vacuum evaporation and the resulting material was sieved to 80-120 mesh.

d. Measurement methods

Quantitative NMR measurements were made using 90° pulse experiments. Protons were decoupled with a 45 kHz field, except when J_{P-H} coupling was required for assignments. cross-polarization pulses were used to assign the peaks. The total amount of phosphine in each sample was determined by weight measurements when the samples were prepared. The number of acid species was determined from the spectra. It was calculated from the relative areas in the integrated spectra.

By GC, 1-butene isomerization was used to assess the poisoning effects of the phosphines on the catalyst surfaces. The phosphine/catalyst was prepared in the same way as in 3c. 0.2 g of the catalysts coated with phosphines was put into the reactor in a glove bag under Ar pressure. The reactor (see Figure 3.3) was connected to the GC system. 30 μ l 1-butene was injected through a six-port valve by a He flow at a speed of 20 ml/min. Several temperatures were adjusted for the reactor between room temperature and 120°C . The GC column temperature was controlled at 60°C . The recorder's speed was 0.5 inch/min.

The specific surface areas of the adsorbents were measured by the BET method^{12a}.

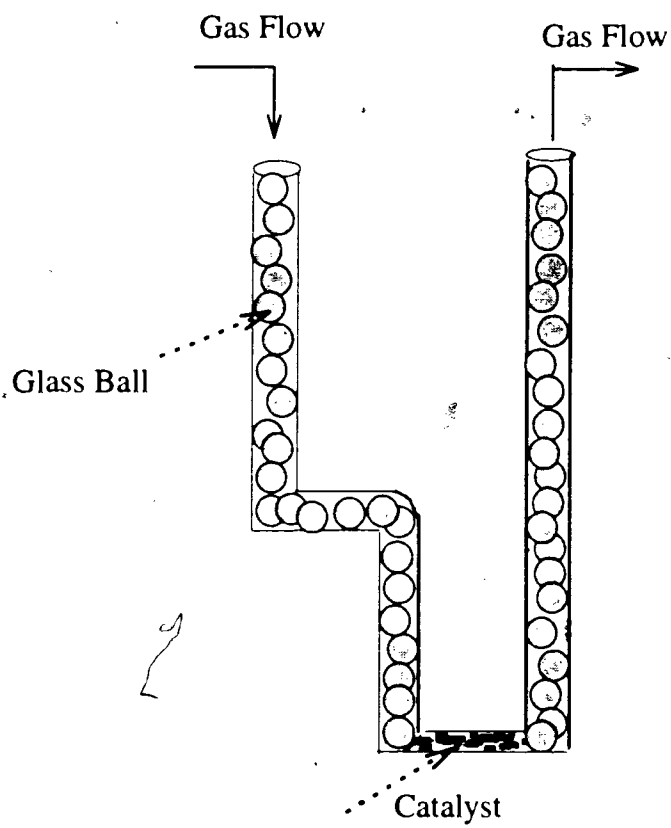


Figure 3.3 Reactor for the poisoning experiments by GC.

5. References:

1. M. N. Golovin, M. M. Rahman, J. E. Belmonte and W. D. Giering, *Organometallics*, **4**, 1981 (1985).
2. T. Allman and R. G. Goel, *Can. J. Chem.*, **60**, 716 (1982).
- 2a. C. E. Bronnimann, B. L. Hawkins, M. Zhang, and G. E. Maciel, *Anal. Chem.*, **60**, 1743 (1988).
- 2b. W. R. Rothwell, W. X. Shen and J. H. Lunsford, *J. Am. Chem. Soc.*, **106**, 2452 (1984).
- 2c. J. H. Lunsford, W. P. Rothwell and W. X. Shen, *J. Am. Chem. Soc.*, **107**, 1540 (1985).
- 2d. P-J Chu, J. H. Lunsford, and D. J. Zalewski, *J. Mag. Res.* **87**, 68 (1990).
3. F. A. Cotton and G. W. Wilkinson, *Advanced Inorganic Chemistry*, Wiley-Interscience (1980).
4. C. A. Tolman, *Chem. Rev.*, **77**, 313, (1977).
5. T. C. Sheng, and I. D. Gay, *J. Catal.*, **145**, 10 (1994).
6. M. V. Forward, S. T. Bowden and W. J. Jones, *J. Chem. Soc.*, S121 (1949).
7. A. A. Grigorev, Y. V. Konchractev, and A. V. Siworov, *Zh. Obsch. Kh.* **54**, 1935 (1984).
8. For an example: L. Baltusis, J. S. Frye and G. E. Maciel, *J. Am. Chem. Soc.*, **109**, 40 (1987).

9. B. Hu and I. D. Gay, *Langmuir*, **11**, 3845 (1995).
- 9a. R. K. Harris and A. Olivieri, *Prog. in NMR Spect.*, **24**, 435, (1992).
10. S. H. C. Liang, M. Sc. thesis, Simon Fraser University (1978).
11. I. D. Gay, *J. Magn. Reson.*, **58**, 413 (1984).
12. A. F. Isbell, Jr., and D. T. Sawyer, *Anal. Chem.*, **41**, 1381 (1969).
- 12a. B. G. Linsen and etal (edited), "Physical and Chemical Aspects of Adsorbents and Catalysts", Academic Press, (1970).

Chapter 4 ^{31}P NMR investigation of surface acidity using adsorbed tricyclohexylphosphine: an excellent new probe¹

1. Introduction: why use Cy_3P ?

Surface acidity of silica-alumina catalysts is required for cracking, isomerization, dehydration and polymerization reactions^{1a}. Thus it is important to count the acid sites on the catalyst surface. Solid state ^{31}P MAS NMR has been successfully used to study adsorption sites on the surfaces of silica-alumina and zeolite catalysts²⁻⁵. Trimethylphosphine has been used as an NMR probe for the titration of acid sites^{2,3}. Baltusis *et al.*^{4,5} also used triethylphosphine, tri-*n*-butylphosphine and phosphine oxides as NMR probes. While studies of small phosphine probes by ^{31}P NMR on oxides of aluminum and silicon have yielded information about the types of surface acid sites and the numbers of these sites, the apparent acid concentration is dependent upon the choice of probe molecules. Saturation Brønsted acid concentrations were 0.23, 0.19 and 0.15 mmol H^+ per gram of silica-alumina for Me_3P , Et_3P and $(n\text{-Bu})_3\text{P}$ respectively⁵. This may indicate that a) some of the Brønsted sites may be accessible only to small phosphines, b) Brønsted sites may be clustered, or c) different base strengths may have an effect. Since many catalytic reactions involve large molecules, it is interesting to study the surface sites by still larger phosphine probes. Bulky probes will provide more information about whether steric factors are important.

Silica-alumina catalyst is active for many reactions. Some of these involve bulky starting reagents, such as the cracking of petroleum⁶. In this study, tricyclohexylphosphine (Cy_3P) has been chosen as a probe to study surface acidity. Cy_3P is interesting for the following reasons: first, it is a very strong base, in solution $\text{p}K_a=9.70$

(compared to Me_3P $\text{pK}_a=8.75^7$) secondly, it has a bulky structure⁸, with a cone angle of 170° .⁷ Here, we report the titration of Brønsted acid concentrations on the silica-alumina catalyst surface by the Cy_3P probe using different adsorption temperatures.

2. Results and discussion: what we got

a. Pure sample and on the silica surface

Figure 4.1 shows the spectra of pure solid Cy_3P for the T_1 experiment. 200 second recycle delay was used to make a full magnetization relaxation. Intensity as a function of τ was used to calculate T_1 . Here, τ refers to the delay time in the $(90^\circ(\text{FID}_1)-T_d-180^\circ-\tau-90^\circ(\text{FID}_2)-T_d)_n$ pulse sequence (see page 11, chapter 1). The logarithm of intensities in Figure 4.1 were plotted against the delay time (Figure 4.2), from which the T_1 of pure Cy_3P was calculated as 22 seconds.

Figure 4.3a shows the spectrum of pure solid Cy_3P at 1.89 kHz MAS speed. The centre band resonance position, 7.5 ppm, is close to literature values of 7.5 ppm and 7.0 ppm,^{12,13} but different from 9.28 ppm reported in reference⁸. Figure 4.3b to 4.3d are the spectra of $0.38 \mu\text{mol}/\text{m}^2$ Cy_3P on silica gel after treatment at 100°C , 150°C and 200°C respectively. We refer to the species present as 'physically adsorbed'. Absence of spinning side bands suggests that the apparent chemical shift anisotropies are greatly reduced by rotation of the Cy_3P molecules on the surface. From the static spectrum of pure Cy_3P at room temperature (see Figure 1.2), we find $\sigma_{11}=-30$ ppm, $\sigma_{22}=18$ ppm and $\sigma_{33}=35$ ppm in agreement with reference¹³. The side band intensities in Figure 1a are in agreement with calculated intensities¹⁴ based on these principal values. It should be noted

that the rotation of Cy_3P on SiO_2 must be nearly isotropic, and not simply a rotation about the 3-fold axis. In the

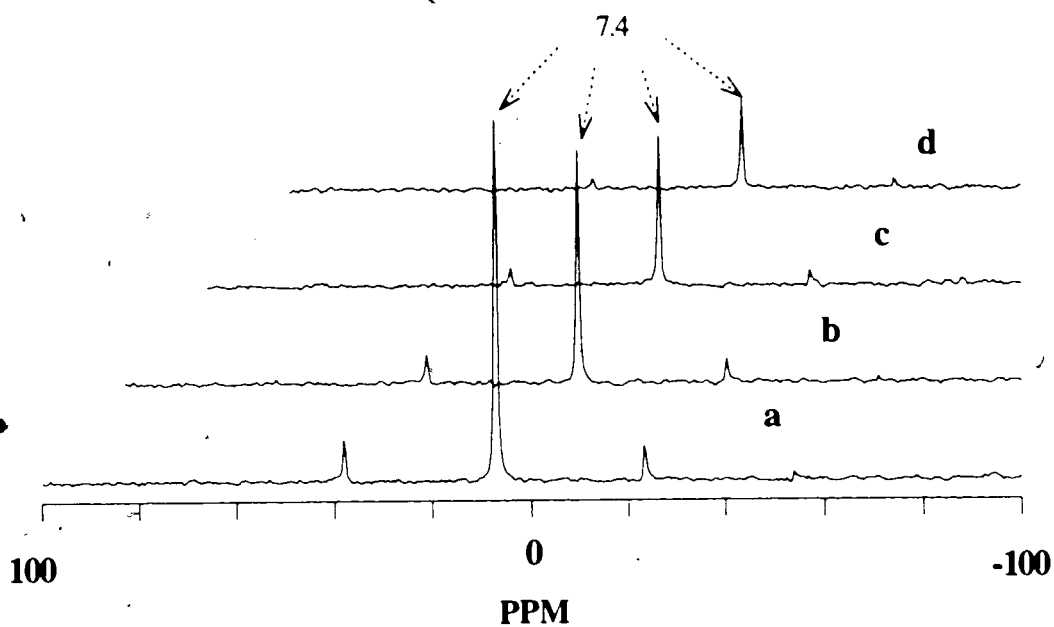


Figure 4.1 ^{31}P MAS NMR spectra of pure Cy_3P for the T_1 measurement experiment, 90° pulse, 1.85 kHz MAS rate, 200 s recycle delay, 20 scans. a) $\tau = 1$ s (delay time, see page 11, chapter 1). b) $\tau = 11$ s. c) $\tau = 21$ s. and d) $\tau = 31$ s.

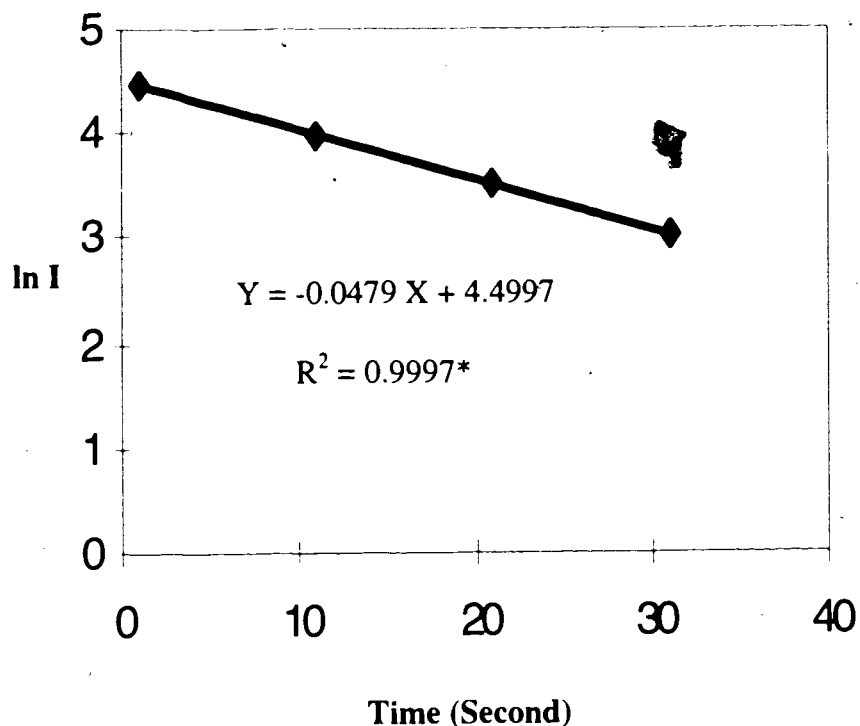


Figure 4.2 Intensity of ^{31}P MAS NMR spectra of pure Cy_3P versus delay time. (The data were taken from Figure 4.1). *R-squared value is a calculated value that indicates how valid a trendline is for forecasting. The R-squared value helps determine the line of best fit. An R-squared value near 0 indicates a poor fit, a value near 1 indicated a good fit and therefore a meaningful trendline.

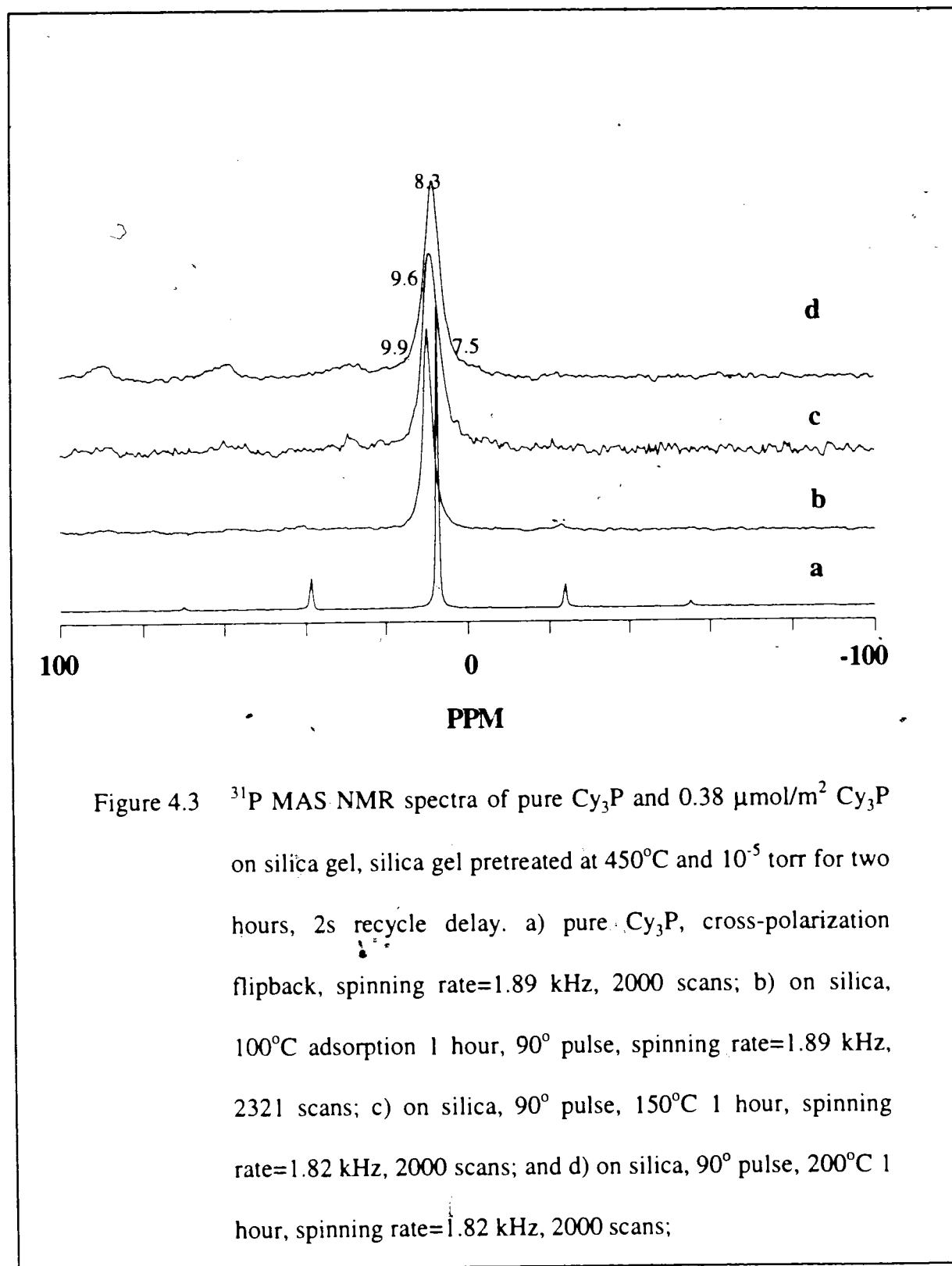


Figure 4.3 ^{31}P MAS NMR spectra of pure Cy_3P and $0.38 \mu\text{mol}/\text{m}^2$ Cy_3P on silica gel, silica gel pretreated at 450°C and 10^{-5} torr for two hours, 2s recycle delay. a) pure Cy_3P , cross-polarization flipback, spinning rate=1.89 kHz, 2000 scans; b) on silica, 100°C adsorption 1 hour, 90° pulse, spinning rate=1.89 kHz, 2321 scans; c) on silica, 90° pulse, 150°C 1 hour, spinning rate=1.82 kHz, 2000 scans; and d) on silica, 90° pulse, 200°C 1 hour, spinning rate=1.82 kHz, 2000 scans;

latter case, spinning sidebands corresponding to an averaged axially symmetric shielding tensor would be observed.

There are two kinds of silanol groups (SiOH) on the silica gel surface after heating at 450°C in vacuum. They are isolated and geminal groups¹⁵. The concentrations of silanol groups on silica gel treated at 450°C are roughly 3-4 $\mu\text{mol}/\text{m}^2$.⁶ Because there are lone pair electrons on the P atoms of the phosphines, they are preferably connected to the H atoms on the surface by H bonds. The chemical shifts from Fig. 1b to Fig. 1d are 9.9, 9.6 and 8.3 ppm respectively. The reproducibility of chemical shift measurement on different days is better than 0.4 ppm, suggesting that the H bonding interaction may be slightly modified by different temperatures.

Figure 4.4 shows the spectra of Cy_3P at higher coverages on silica after treatment at 100°C for one hour. The spectra were recorded several times during three days following the adsorption until they did not change. Figure 4.4a, b are similar to Figure 4.3b. Cy_3P appears isotropic due to the motion on the silica gel. When the coverages were increased to 1.87 $\mu\text{mol}/\text{m}^2$ (4.4c), a new peak with spinning side bands appeared at 7.5 ppm. This is the same shift as pure Cy_3P , and is obviously different from the peaks of sub-monolayer coverages (4.4a). 1.8 $\mu\text{mol}/\text{m}^2$ is of the order of one monolayer, based on the dimension of the Cy_3P molecules.⁸ When the coverages are higher than one monolayer, a non-rotating species is clearly present which might arise either from multilayer adsorption or from non-adsorbed crystalline Cy_3P . Coverages for Figure 4.4d, e exceed two and three statistical layers respectively.

Figure 4.5 shows the spectra of Cy_3P at higher coverages on silica immediately after the adsorption at 100°C for one hour. We detected new peaks which resonated around 8.2 ppm, with spinning sidebands (4.5a to 4.5c). These peaks totally disappeared

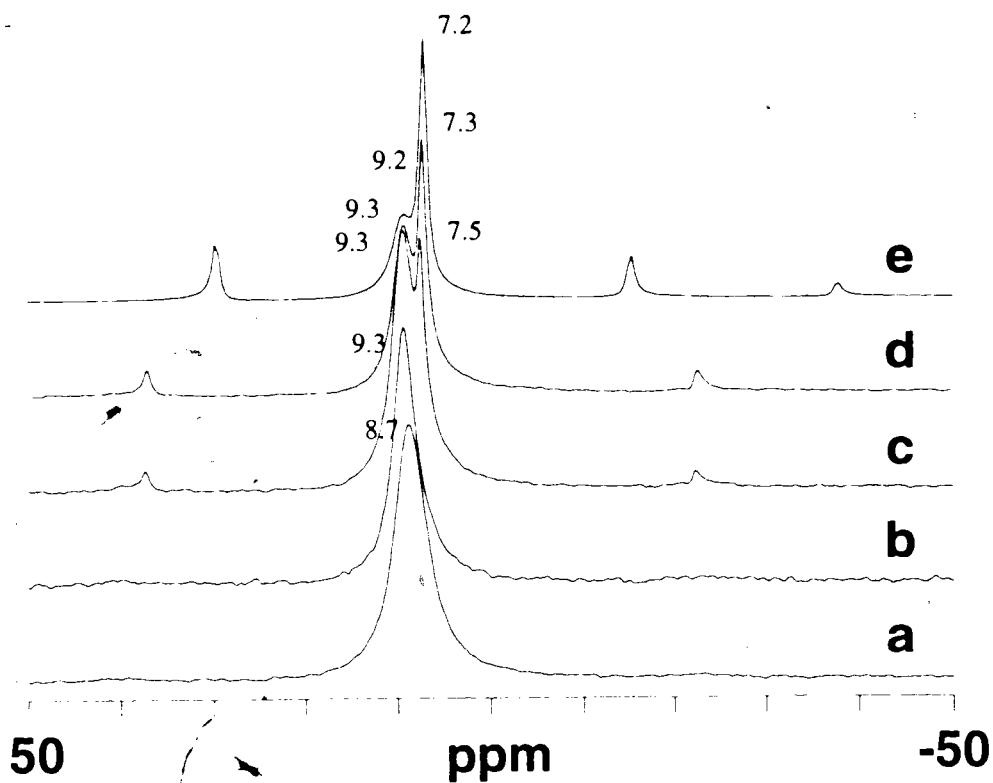


Figure 4.4 ^{31}P MAS NMR spectra of Cy_3P on silica gel, silica gel pretreated at 450°C and 10^{-5} torr for two hours, adsorbed at 100°C for one hour, 90° pulse, 10 s recycle delay.

- a) $1.32 \mu\text{mol}/\text{m}^2$, spinning rate= 1.81 kHz , 536 scans;
- b) $1.68 \mu\text{mol}/\text{m}^2$, spinning rate= 1.80 kHz , 340 scans;
- c) $1.87 \mu\text{mol}/\text{m}^2$, spinning rate= 1.80 kHz , 200 scans;
- d) $4.28 \mu\text{mol}/\text{m}^2$, spinning rate= 1.80 kHz , 200 scans; and
- e) $6.68 \mu\text{mol}/\text{m}^2$, spinning rate= 1.35 kHz , 8954 scans.

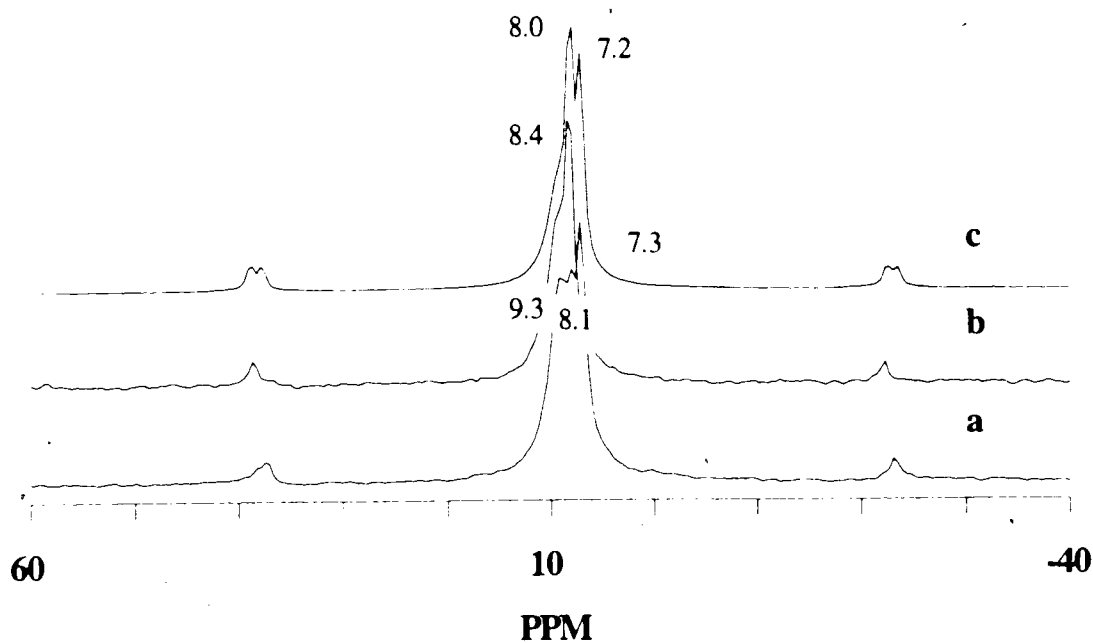


Figure 4.5 ^{31}P MAS NMR spectra of Cy_3P on silica gel with higher coverages recorded immediately after sample preparation, silica gel pretreated at 450°C and 10^{-5} torr for two hours, adsorbed at 100°C for one hour, 90° pulse. a) $4.28 \mu\text{mol}/\text{m}^2$, spinning rate= 1.82 kHz , 140 scans, 10 s recycle delay; b) $6.68 \mu\text{mol}/\text{m}^2$, spinning rate= 1.84 kHz , 1 s recycle delay, 314 scans; and c) $6.68 \mu\text{mol}/\text{m}^2$, spinning rate= 1.85 kHz , 7730 scans, 10 s recycle delays.

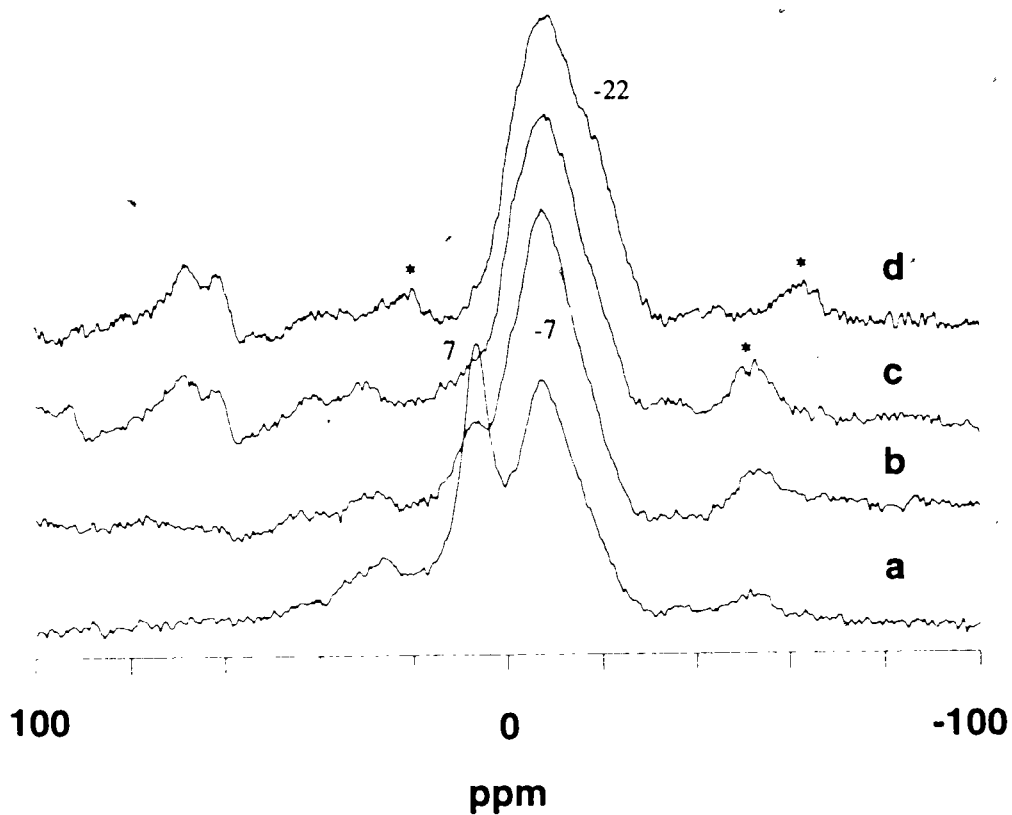


Figure 4.6 ^{31}P MAS NMR spectra of $0.31 \mu\text{mol}/\text{m}^2$ Cy_3P on alumina, alumina pretreated at 450°C and 10^{-5} torr for two hours, adsorbed 1 hour, cross-polarization flipback, 1ms contact time, 1s recycle delay. a) 100°C , spinning rate=1.89 kHz, 55670 scans; b) 150°C , spinning rate=1.87 kHz, 54800 scans; c) 200°C , spinning rate=1.87 kHz, 53996 scans, and d) 200°C , spinning rate= \approx 2.42 kHz, 42876 scans. The small peaks around 60-70 ppm in c) and d) arise from $\text{Cy}_3\text{P}=\text{O}$.

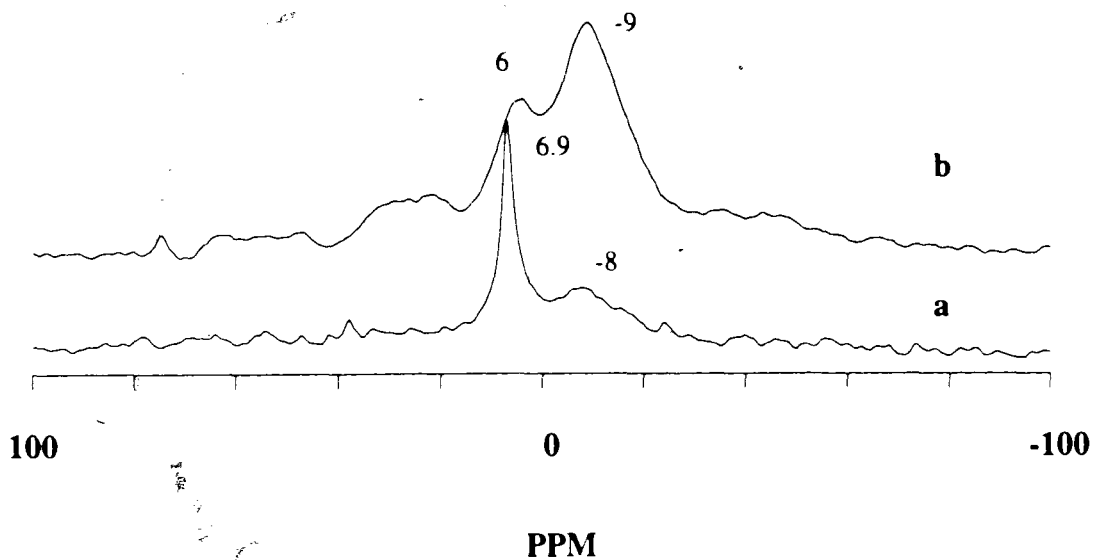


Figure 4.7 ^{31}P MAS NMR spectra of $1.01 \mu\text{mol}/\text{m}^2$ Cy_3P on alumina treated at low temperatures, alumina pretreated at 450°C and 10^{-5} torr for two hours, adsorbed 1 hour. a) adsorbed at room temperature, cross polarization flipback, 1 ms contact time, 1.87 kHz MAS rate, 1s recycle delay, 790 scans; and b) adsorbed at 50°C , 90° pulse, 1.70 kHz MAS rate, 16 s recycle delay, 9514 scans.

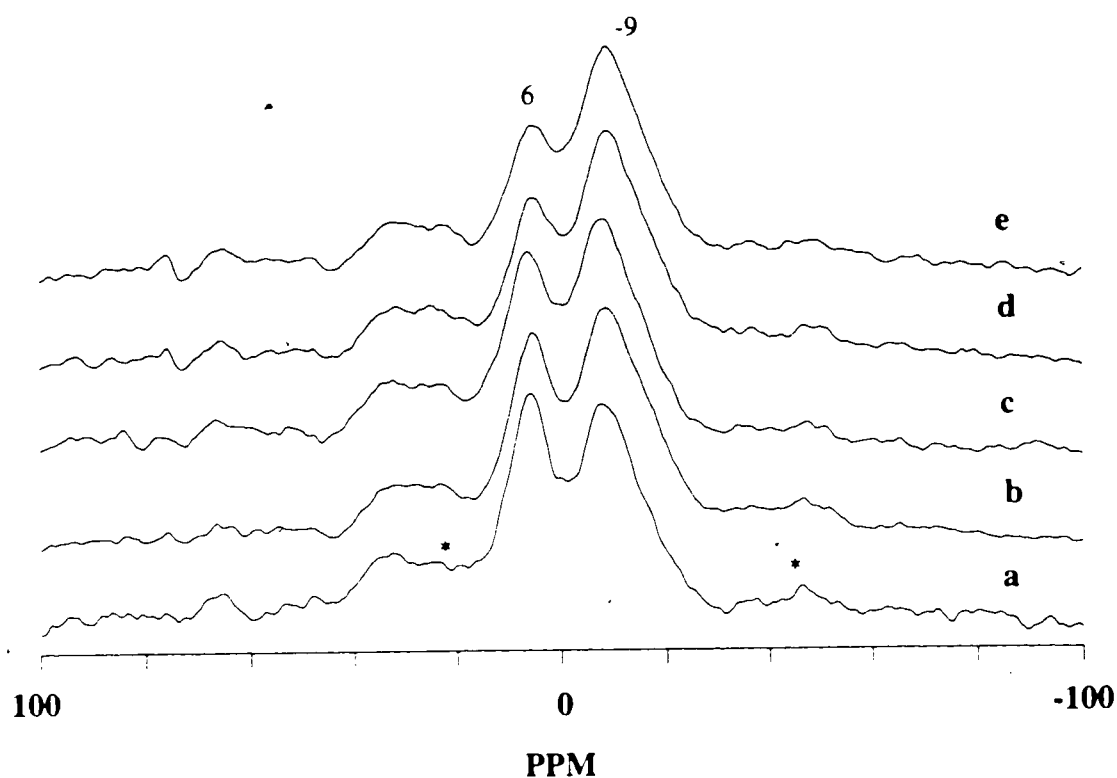


Figure 4.8 ^{31}P MAS NMR spectra of $1.01 \mu\text{mol}/\text{m}^2$ Cy_3P on alumina with various recycle delays, alumina pretreated at 450°C and 10^{-5} torr for two hours, adsorbed at 50°C 1 hour, 90° pulse. a) 1.68 kHz MAS rate, 1 s recycle delay, 108324 scans; b) 1.68 kHz MAS rate, 2 s recycle delay, 23762 scans; c) 1.69 kHz MAS rate, 4 s recycle delays; d) 1.69 kHz MAS rate, 8 s recycle delay, 8888 scans; and e) 1.70 kHz MAS rate, 16 s recycle delay, 9514 scans.

in several days at room temperature (see 4.4c to 4.4e). 8.2 ppm peaks did not appear following treatment at 150°C or 200°C. The peaks may be caused by Cy₃P clusters of two or more molecules which slowly disperse on the surface.

b On the alumina surface

Figure 4.6 shows the spectra of 0.31 $\mu\text{mol}/\text{m}^2$ Cy₃P on alumina, with different adsorption temperatures. Figure 4.6a is the spectrum after 100°C adsorption. The peak around 7 ppm arises from the 'physically adsorbed' species. The species changed to more stable ones after further heating at 150°C (Figure 4.6b) and 200°C (Figure 4.6c, 4.6d). From¹⁵, the chemical shift of the Me₃AlPCy₃ complex is -4 ppm. So the peak around -7 ppm is probably due to Lewis-bound species. Thus in spite of its large size, Cy₃P can access Lewis sites on Al₂O₃, which other works^{16,17} have found to be inaccessible to 2,6-dimethyl pyridine. It is clear from the spinning side bands (Figure 4.6c, 4.6d), that the broad peak around -7 ppm actually consists of at least two peaks: one is around -7 ppm; the other is around -22 ppm and gives rise to the spinning side bands. This probably results from interaction of Cy₃P with different types of Lewis sites.

Figure 4.7 shows the spectra of 1.01 $\mu\text{mol}/\text{m}^2$ Cy₃P on alumina, with lower adsorption temperatures. Figure 4.7a is the spectrum without any further treatment after the mixing. It is interesting to notice that -8 ppm (Lewis acid) and 6.9 ppm (physically adsorbed) peaks have been formed even on mixing at room temperature under vacuum. This suggests that the diffusion of Cy₃P on alumina is very rapid. Figure 4.7b shows the spectrum after treatment at 50°C for one hour. Similarly to Figure 4.6, more Lewis acid species were formed after the heating. The Lewis acid concentration was calculated as 0.9 $\mu\text{mol}/\text{m}^2$ from total phosphine coverage and the ratio of the integrated areas. Compared

with the saturation value of $1.3 \mu\text{mol}/\text{m}^2$ by Me_3P on the same alumina, there seems little difficulty for the Cy_3P molecules to access the Lewis acid sites on the alumina surface.

Figure 4.8 shows the spectra of $1.01 \mu\text{mol}/\text{m}^2$ Cy_3P on alumina, with various recycle delays. A long enough recycle delay will reflect the real distribution of different species on the surface. These spectra showed that the relative intensity of -9 ppm peaks (Lewis acid species) increases with longer recycle delays. The ratios of integrated areas between Lewis acid and physically adsorbed species (6 ppm) are 1.3, 1.6, 1.6, 1.9 and 2.0 for Figure 4.8a to 4.8e respectively. The difference among these numbers is because Lewis acid species on the alumina surface have a longer T_1 than the physically adsorbed species. This is reasonable, since Lewis acid sites obviously have stronger bondings than physically adsorbed species. The mobility of the Lewis acid species will be limited. T_1 for the Lewis acid species should be longer than for mobile species.

c. On the commercial silica-alumina catalyst surface

Figure 4.9 shows the spectra of Cy_3P and Cy_3PH^+ species in a solution. Figure 4.9a and 4.9b show the resonances of pure Cy_3P in the different solvents: 10.0 and 11.6 ppm for C_6D_6 and CDCl_3 respectively. The difference of 2 to 4 ppm for the chemical shifts between the solid state (Figure 4.3a) and solution spectra of this phosphine depends on the choices of solvents. In Figure 4.9c, 31.4 ppm is the resonance of Cy_3PH^+ , which is confirmed by running the same sample with decoupler off (Figure 4.9d). The J_{PH} coupling value of Cy_3PH^+ is 464 Hz, which is close to the value of 445 Hz reported in fluorosulfuric acid¹⁸. The 83 ppm peak in Figure 4.9c and 4.9d probably arises from the species of $\text{Cy}_3\text{P}=\text{O}\cdot\text{HCl}$ in the aqueous solution. The resonance of $\text{Cy}_3\text{P}=\text{O}\cdot\text{HCl}$ is not

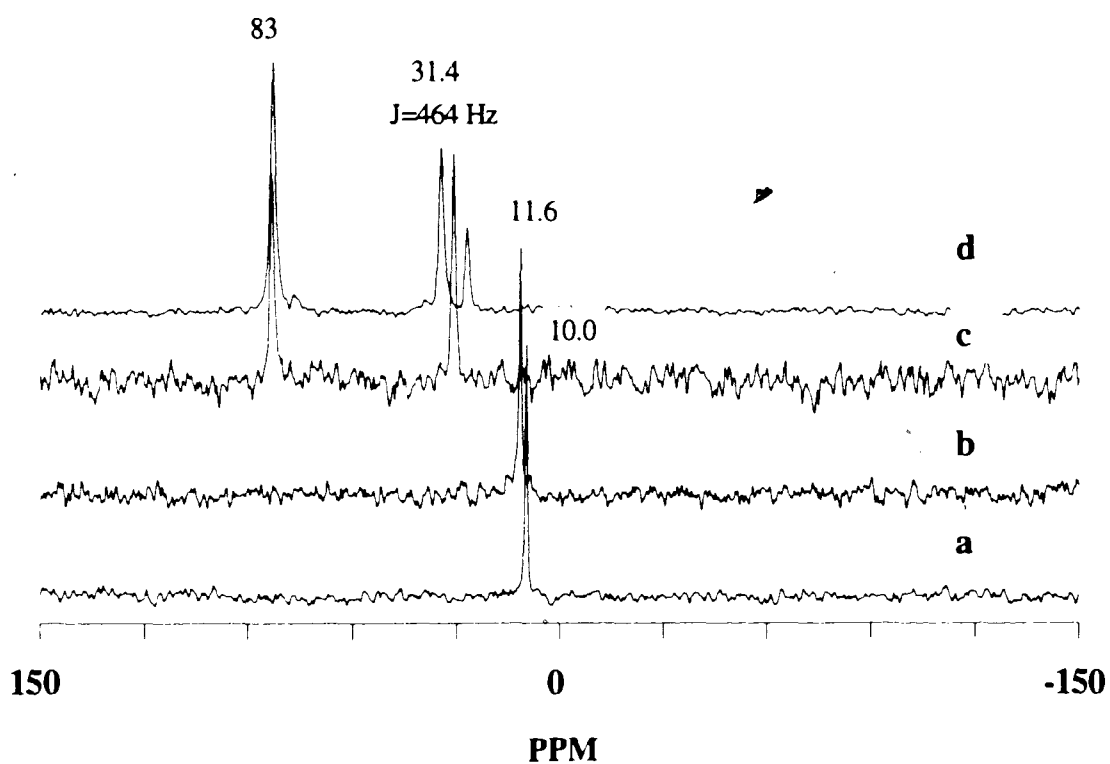


Figure 4.9 Solution ^{31}P NMR spectra of Cy_3P and Cy_3PH^+ species, Cy_3P and solvent were mixed in a glove bag under N_2 atmosphere and sealed, 90° pulse. a) Cy_3P in C_6D_6 solution, 1s recycle delay, 416 scans; b) Cy_3P in CDCl_3 solution, 1 s recycle delay, 231 scans; c) Cy_3P in HCl solution, 2 s recycle delay, 3780 scans; and d) Cy_3P in HCl solution, 2 s recycle delay, decoupler off, 2000 scans.

available from the literature. The simple $\text{Cy}_3\text{P}=\text{O}$ molecule could be the real candidate but this is not right, since it only gave a value of 50 ppm for chemical shift¹⁹. $\text{Ph}_3\text{P}=\text{O}\cdot\text{HCl}$ (44 ppm) and $\text{Ph}_3\text{P}=\text{O}\cdot\text{HBr}$ (54 ppm) have 20-30 ppm higher values of chemical shifts than $\text{Ph}_3\text{P}=\text{O}$ (23-27 ppm) in the solution¹⁹. Therefore, we suggest that the 83 ppm probably is the resonance of $\text{Cy}_3\text{P}=\text{O}\cdot\text{HCl}$ species.

Figure 4.10 shows the spectra of $1.27 \mu\text{mol}/\text{m}^2$ Cy_3P adsorbed on silica-alumina catalyst after treatment at 200°C , using different pulse programs. In Figure 4.10a, the protonated species (27 ppm peak) disappeared using the dipolar dephasing sequence with 70 μs delay (section 3c, chapter 1). The spectrum of Figure 4.10b using 90° pulse sequence reflects the real ratios between the protonated species and physically adsorbed sites (we will discuss the effect of recycle delay time in figure 4.11). The cross-polarization sequence enhances the peak of protonated species in figure 4.10c. The effect of contact time in the sequence has been discussed in figure 3.2, chapter 3.

Figure 4.11 shows the spectra of $1.27 \mu\text{mol}/\text{m}^2$ Cy_3P adsorbed on silica-alumina catalyst after treatment at 200°C , with different recycle delay time. The area ratios between physically adsorbed sites and Brønsted acid species are 3.4, 3.3 and 3.3 respectively for figure 4.11a to 4.11c. This indicates that 1 second is long enough for the quantitative measurements of the acidity on the commercial silica-alumina catalyst.

Figure 4.12 shows the spectra of Cy_3P at $0.30 \mu\text{mol}/\text{m}^2$ coverage adsorbed on commercial $\text{SiO}_2\text{-Al}_2\text{O}_3$ cracking catalyst after treatment at 100°C , 150°C and 200°C for one hour. The total phosphorus detected in each spectrum is constant within the experimental error, independent of heat treatment. We find that protonated Cy_3P in concentrated HCl resonates at 31.4 ppm (Figure 4.9c and 4.9d), close to 32.7 ppm reported in fluorosulfuric acid¹⁸. So around 28 ppm are the peaks arising from Brønsted

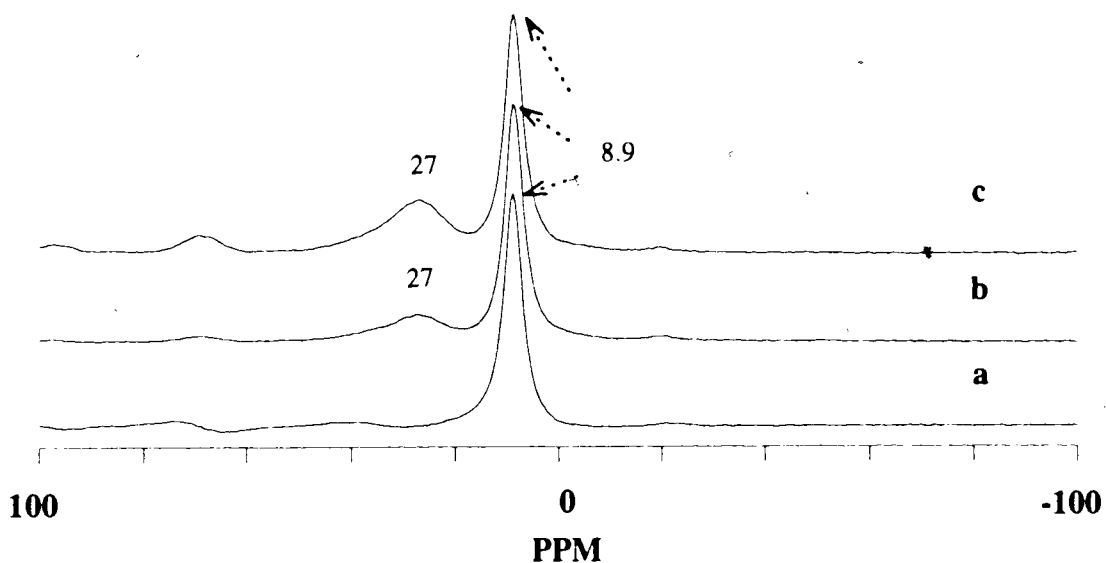


Figure 4.10 ^{31}P MAS NMR spectra of $1.27 \mu\text{mol}/\text{m}^2$ Cy_3P on silica-alumina catalyst using different pulse sequences, the catalyst was pretreated at 450°C and 10^{-5} torr for two hours, adsorption was at 200°C for 4 hours, 1.68 kHz MAS rate, 1 s recycle delay. a) dipolar dephasing, 70 μs delay, 69191 scans; b) 90° pulse, 67337 scans; and c) cross-polarization flipback, 26221 scans.

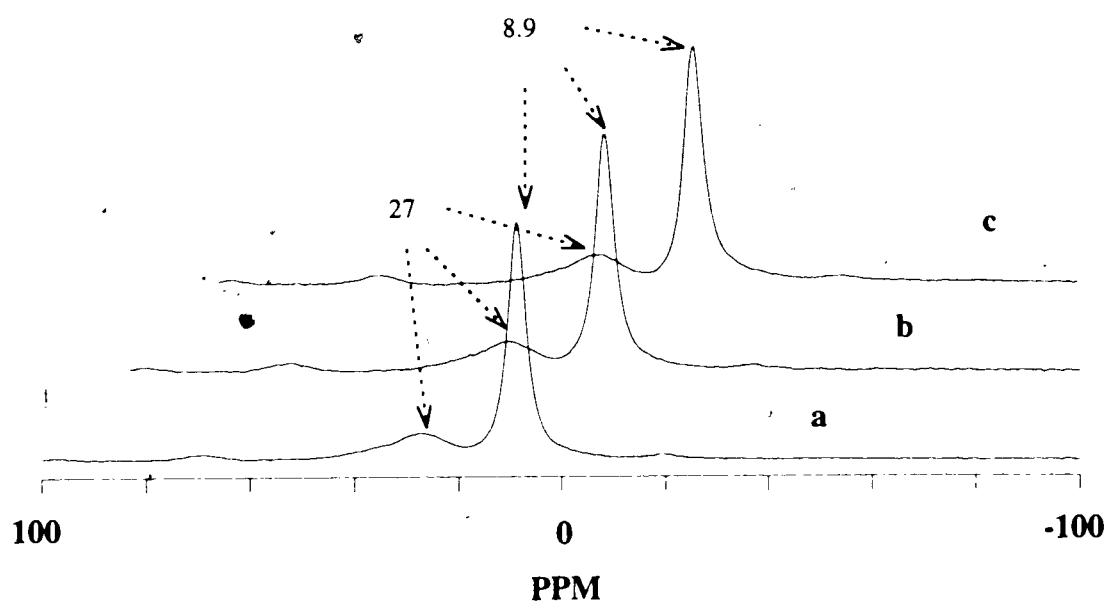


Figure 4.11 ^{31}P MAS NMR spectra of $1.27 \mu\text{mol}/\text{m}^2$ Cy_3P on silica-alumina catalyst with different recycle delay displaced along the x axis, the catalyst was pretreated at 450°C and 10^{-5} torr for two hours, adsorbed at 200°C for 4 hour, 90° pulse, 1.68 kHz MAS rate. a) 1 s recycle delay, 67337 scans; b) 4 s recycle delay, 9795 scans; and c) 8 s recycle delay, 10332 scans.

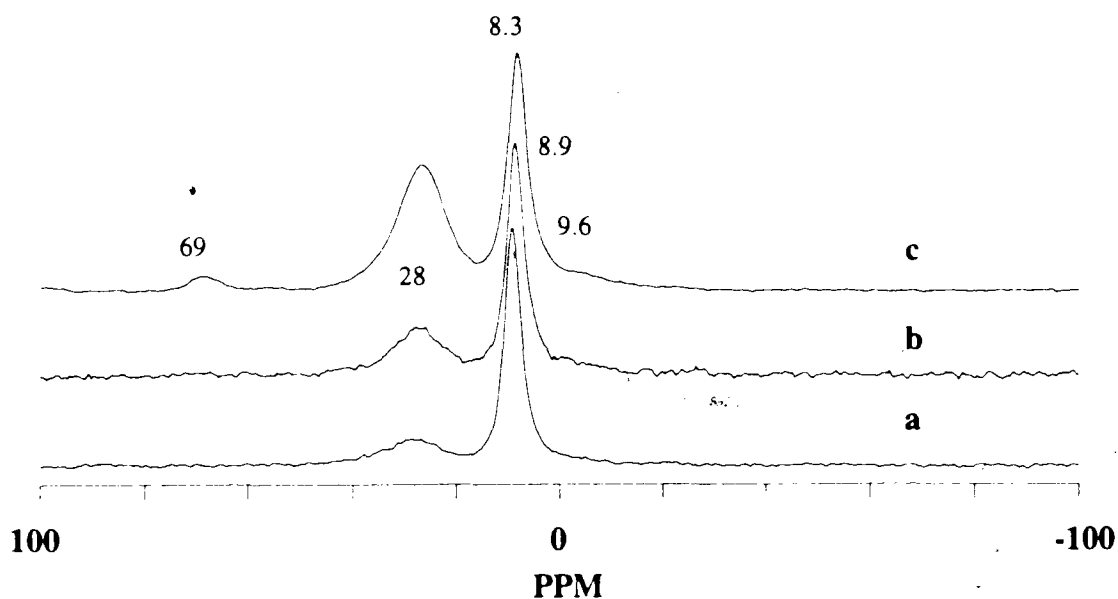


Figure 4.12 ^{31}P MAS NMR spectra of $0.30 \mu\text{mol}/\text{m}^2$ Cy_3P on silica-alumina catalyst, the catalyst was pretreated at 450°C and 10^{-5} torr for two hours, 90° pulse, 1s recycle delay. a) 100°C 1 hour, 1.87 kHz MAS rate, 9550 scans; b) 150°C 1 hour, 1.90 kHz MAS rate, 3338 scans; and c) 200°C 1 hour, 1.89 kHz MAS rate, 90350 scans. The peak around 69 ppm in c) arises from $\text{Cy}_3\text{P}=\text{O}$.

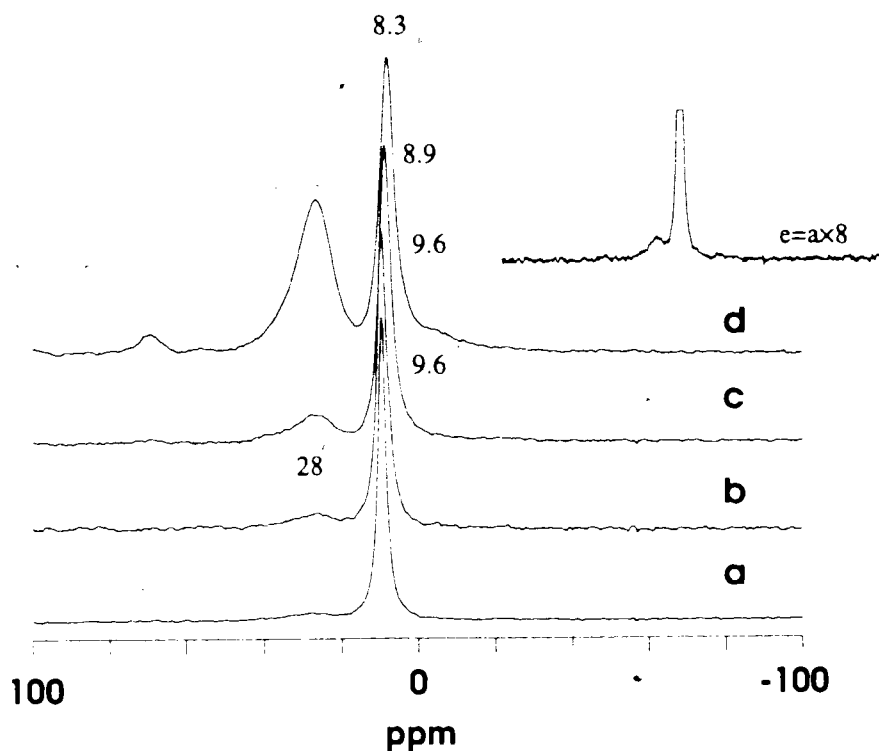


Figure 4.13 ^{31}P MAS NMR spectra of Cy_3P at various coverages on silica-alumina catalyst, the catalyst was pretreated at 450°C and 10^{-5} torr for two hours, adsorbed at 200°C for 1 hour, 90° pulse, 1s recycle delay. a) $2.15 \mu\text{mol}/\text{m}^2$, 1.86 kHz MAS rate, 740 scans; b) $1.82 \mu\text{mol}/\text{m}^2$, 1.86 kHz MAS rate, 1080 scans; c) $1.30 \mu\text{mol}/\text{m}^2$, 1.82 kHz MAS rate, 3690 scans; and d) $0.30 \mu\text{mol}/\text{m}^2$, 1.89 kHz MAS rate, 90350 scans.

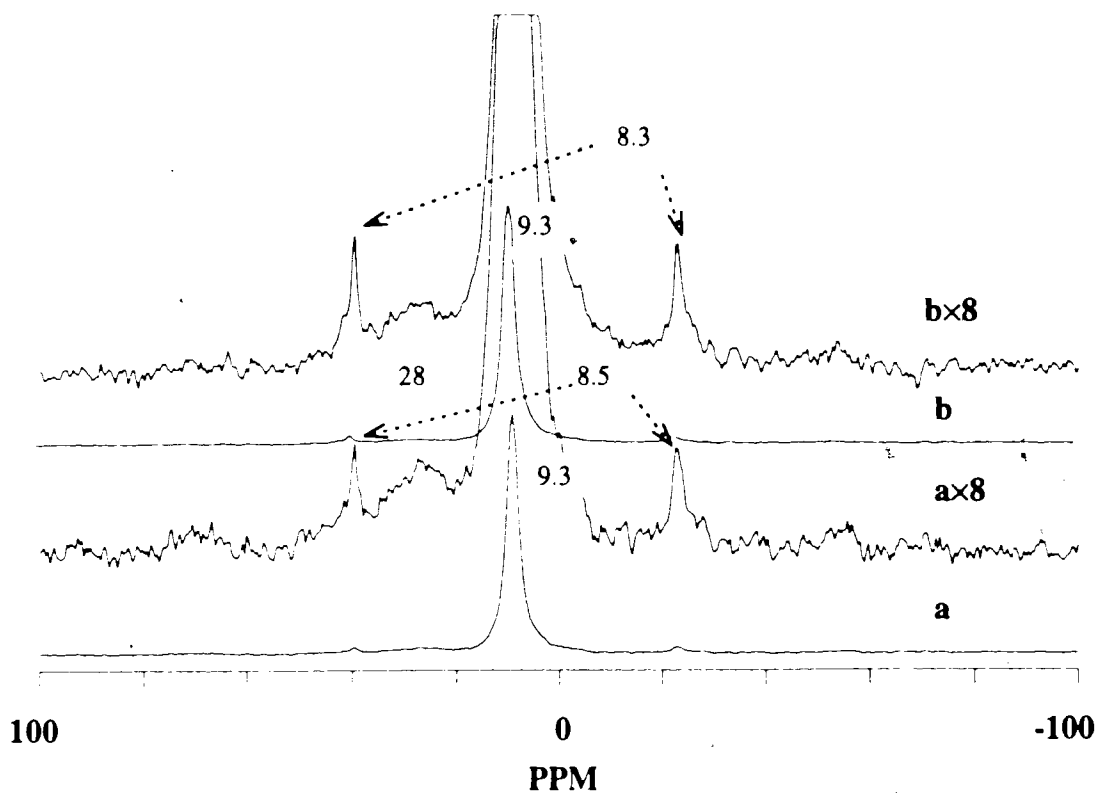


Figure 4.14 ^{31}P MAS NMR spectra of Cy_3P at high coverages (more than monolayer) on silica-alumina catalyst, the catalyst was pretreated at 450°C and 10^{-5} torr for two hours, adsorption at 200°C for 1 hour, 90° pulse, 1.89 kHz MAS rate, 1s recycle delay. a) $3.01 \mu\text{mol}/\text{m}^2$, 700 scans; b) $4.47 \mu\text{mol}/\text{m}^2$, 1550 scans;

acid species. The results of Figure 4.12a to 4.12c indicate that the higher the treatment temperature, the more protonated phosphine appears. The resonances of physically adsorbed species were at 9.6, 8.9 and 8.3 ppm respectively, which are similar to the shifts in Figure 4.3b to 4.3d on silica gel. No peaks were found from -4 to -20 ppm. So the Lewis sites of the silica-alumina catalyst, which are detected³ by Me_3P , are not detected by the Cy_3P probe. These Lewis sites must therefore be more hindered than those found on pure Al_2O_3 .

Figure 4.13 summarizes the spectra of Cy_3P at various coverage adsorbed on commercial silica-alumina cracking catalyst after treatment at 200°C . At the higher coverages, 4.13a and 4.13b, the resonances of the physically adsorbed phosphine are at 9.6 ppm. This value is roughly the same for monolayer Cy_3P on silica gel. Figure 4.8a was amplified (Figure 4.8e) to show the protonated species present at this coverage.

Figure 4.14 show the spectra of Cy_3P adsorbed on the silica-alumina catalyst at two coverages obviously higher than one monolayer. A line of 9.3 ppm in both spectra was about the same as in Figure 4.14a, b. A second peak (resonating at 8.5 and 8.3 ppm respectively for Figure 4.9a and 4.9b) was calculated from the spinning side bands. It is about the same as the 8.2 ppm peak on silica gel in Figure 4.5. We previously suggested these may be caused by Cy_3P clusters of two or more molecules. But the peaks on the silica gel can only be observed immediately after the sample preparation. On the silica-alumina surface, they probably hardly disperse on the surface. Combining Figure 4.14 with Figure 4.13, we figure out that the monolayer coverage on the silica-alumina surface should be between 2.2 and $3.0 \mu\text{mol}/\text{m}^2$, which is larger than $1.8 \mu\text{mol}/\text{m}^2$ on the silica gel. This probably is due to the silica-alumina catalyst having a larger average pore size than the silica gel. The surface areas of small pores could be accessed by N_2 , but not by Cy_3P .

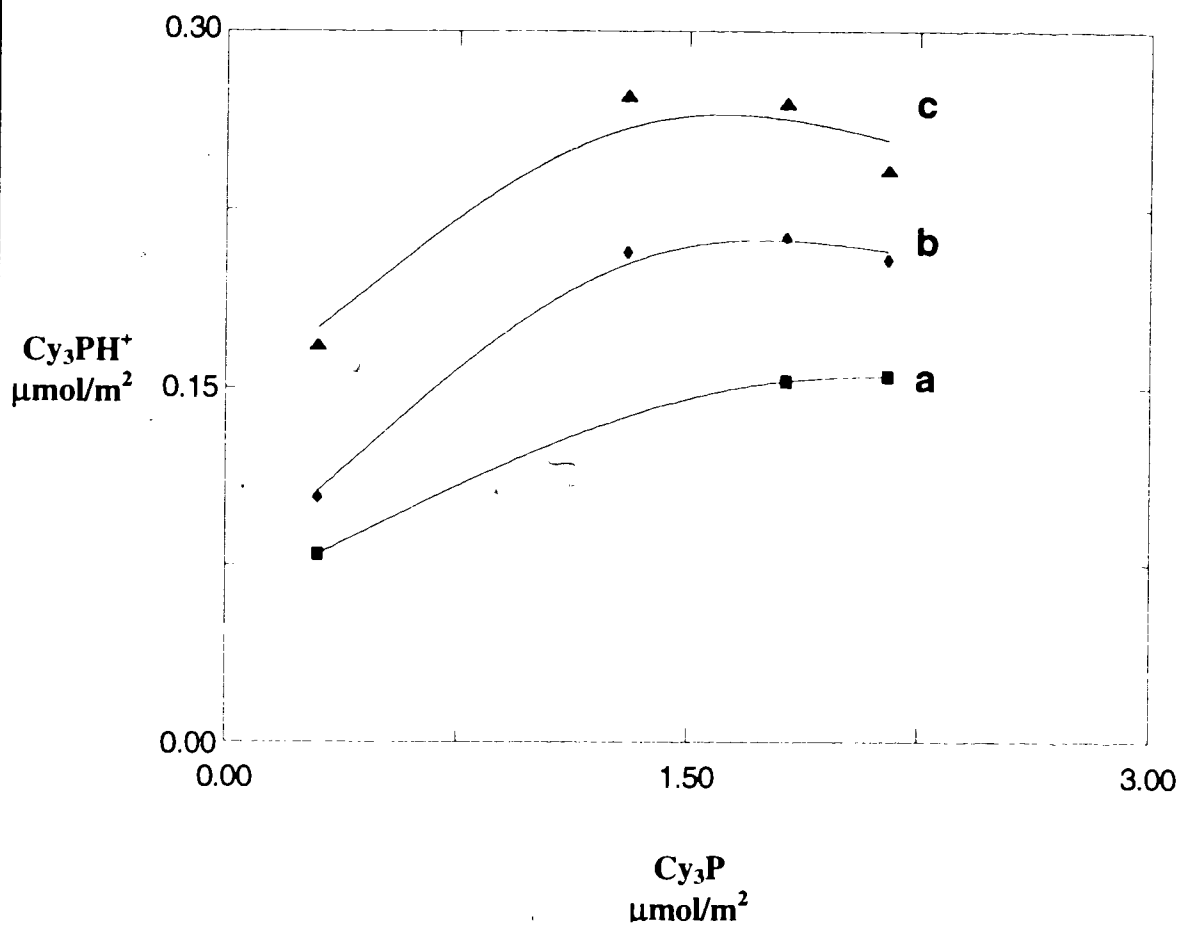


Figure 4.15 the concentrations of Cy_3PH^+ on commercial silica-alumina at various coverages. a) 100°C ; b) 150°C and c) 200°C .

Figure 4.15 shows the concentrations of Cy_3PH^+ on commercial $\text{SiO}_2\text{-Al}_2\text{O}_3$ cracking catalyst at various total phosphine coverages, for different adsorption temperatures. To measure total protonated phosphine, the fraction of the total area in the Cy_3PH^+ peak, together with the total adsorbed amount, leads to the results of Figure 15. Due to the uncertainties of integration, the concentration uncertainty is about ± 10 to 15%. It can be seen that the Cy_3PH^+ concentration tends to saturate with increasing phosphine coverage.

From Figure 4.15 the maximum concentration of Cy_3PH^+ is around $0.26 \mu\text{mol/m}^2$. This is higher than the value of $0.21 \mu\text{mol/m}^2$ found with the trimethylphosphine probe on the same catalyst.³ The higher apparent Brønsted acid concentration may occur for one of the following reasons: a) Since Cy_3P is a stronger base than Me_3P ,⁷ additional reaction with weaker sites may occur or b) since Me_3P was studied only by room temperature adsorption there might be sites only accessible by high temperature diffusion. To test b) we heated several of the samples used in reference³ to a temperature of 100°C , and found no change in Me_3PH^+ concentration. This result favors explanation a).

Figure 4.15 also indicates that apparent Brønsted acid concentrations are increased by higher adsorption temperatures. This is probably due to either a) activated diffusion or b) activated proton transfer. The latter might occur if the base cannot approach H^+ closely enough on the surface. The pore size measurements on this catalyst suggest that the pores are not too small to admit Cy_3P , but this does not preclude activated diffusion in the adsorbed layer. A similar activated process for NH_3 on the Al_2O_3 surface has been observed.²⁰

The line widths of adsorbed species on silica-alumina as a function of surface coverage are summarized in Figure 16. We see that the Brønsted acid peak is much

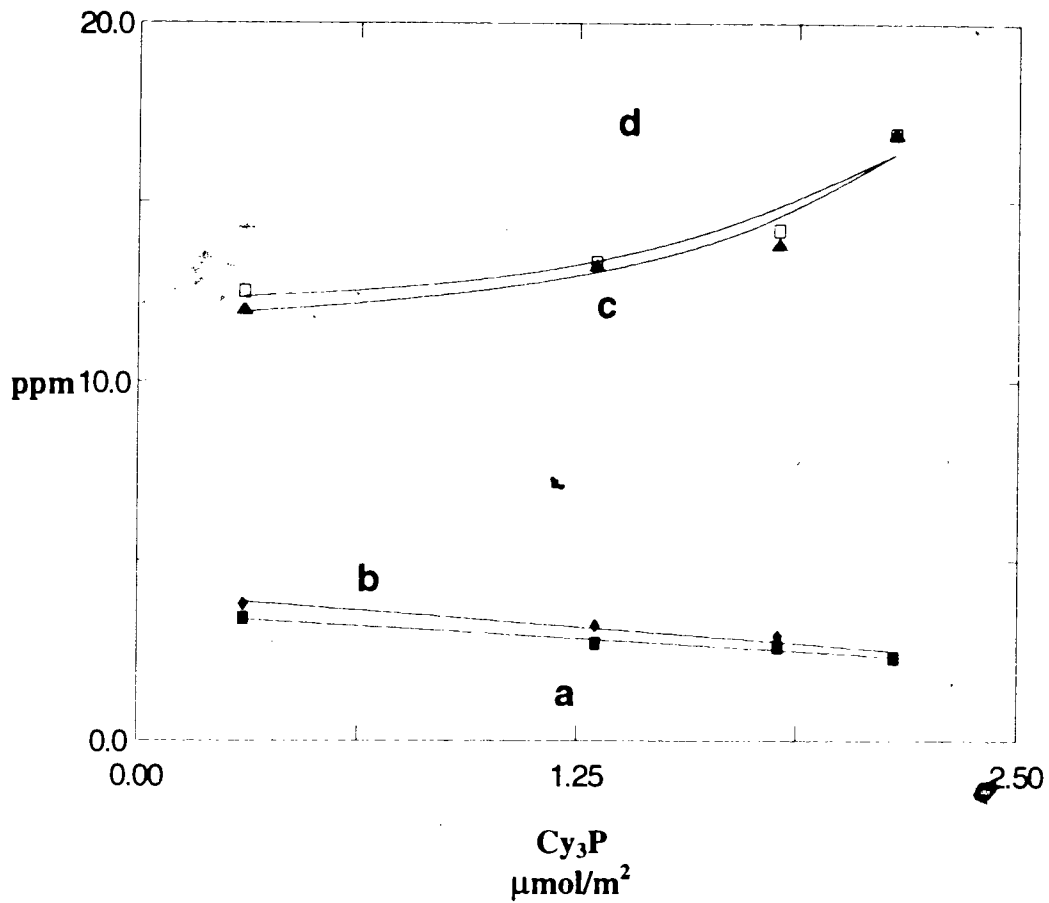


Figure 4.16 the line widths of Cy_3P on silica-alumina catalyst as a function of surface coverages. a) physisorbed peak 150°C adsorption; b) physisorbed peak, 200°C; c) Brønsted peak, 200°C and d) Brønsted acid peak, 150°C.

broader than that of the physically adsorbed species. Chemical shift variations among slightly differing Brønsted states may account for this. It can be seen that different adsorption temperatures give essentially the same line width, probably indicating that the motional state has not changed.

3. Conclusion

A new probe molecule (tricyclohexylphosphine) has been used to study acidity on silica, alumina and silica-alumina catalyst surfaces. It was found that tricyclohexylphosphine ($\text{C}_6\text{H}_{11}\text{P}$) rotates on the SiO_2 surface at room temperature, and the motion is nearly isotropic in the first adsorbed layer. Larger amounts of $\text{C}_6\text{H}_{11}\text{P}$ on silica are solid-like. Lewis sites were detected on alumina, but not on a silica-alumina catalyst. This is probably due to steric effects. On the silica-alumina catalyst, the concentrations of Brønsted acid sites were determined. These appeared to increase on raising the adsorption temperature. At 200°C , the maximum concentration of $\text{C}_6\text{H}_{11}\text{P}^+$ found is $0.26 \mu\text{mol}/\text{m}^2$.

4. References:

1. B. Hu, I. D. Gay, *Langmuir*, **11**, 3845 (1995).
- 1a. K. Tanabe, *Solid Acids and Bases*, Academic Press: New York, 1970.
2. J. H. Lunsford, W.P. Rothwell, and W. X. Shen, *J. Am. Chem. Soc.*, **107**, 1540 (1985).
3. T. C. Sheng, and I. D. Gay, *J. Catal.* **145**, 10 (1994).
4. L. Baltusis, J. S. Frye, and G. E. Maciel, *J. Am. Chem. Soc.*, **108**, 7119. (1986).
5. L. Baltusis, J. S. Frye, and G. E. Maciel, *J. Am. Chem. Soc.*, **109**, 40. (1987).
6. K. Tanabe, M. Misono, Y. Ono, and H. Hattori, *New Solid Acids and Bases*, Elsevier, New York, (1989).
7. N. Golovin, M. M. Rahman, J. E. Belmonte, and W. D. Giering, *Organometallics*, **4**, 1981 (1985).
8. J. A. Davies, S. Dutremez, and A. A. Pinkerton, *Inorg. Chem.*, **30**, 2380 (1991).
9. M. V. Forward, S. T. Bowden, and W. J. Jones, *J. Chem. Soc.*, **3**, S121 (1949)..
10. A. A. Grigorev, Y. V. Konchractev, and A. V. Siworov, *Zh. Obsch. Kh.*, **54**, 1935 (1984).

11. I. D. Gay, *J. Magn. Reson.* **58**, 413 (1984).
12. L. Beml, H. C. Clark, J. A. Davis, C. A. Fyfe, R. E. Wasylshen, *J. Am. Chem. Soc.*, **104**, 438 (1982).
13. G. H. Penner, and R. E. Wasylshen, *Can. J. Chem.*, **67**, 1909 (1989).
14. J. Herzfeld, and A. E. Berger, *J. Chem. Phys.*, **73**, 6021 (1980).
15. A. R. Barron, *J. Chem. Soc. Dalton Trans.*, 3047 (1988).
16. I. D. Gay, S. H. Liang, *J. Catal.*, **44**, 306 (1976).
17. H. A. Benesi, *J. Catal.*, **28**, 176 (1973).
18. G. A. Olah, and C. W. McFarland, *J. Org. Chem.*, **34**, 1832 (1969).
19. M. M. Crutchfield, C. H. Dungan, J. H. Letcher, V. Mark and J. R. Van Wazer, *P³¹ Nuclear Magnetic Resonance*, John Wiley & Sons, 1967.
20. J. Medema, J. J. G. M. Van Bokhoven, A. E. T. Kuiper, *J. Catal.*, **25**, 238 (1972).

Chapter 5 ^{31}P NMR investigation of surface acidity using adsorbed arylphosphines: strange titration curves

1. Introduction: why more bulky aryl phosphines?

Trimethylphosphine and tricyclohexylphosphine have been successfully used as probes to study catalyst acidity by means of ^{31}P MAS NMR spectroscopy¹⁻² (Chapter 4). Triethylphosphine, tri-*n*-butylphosphine and phosphine oxides have also been used as ^{31}P NMR probes³⁻⁴. It has been found that the apparent Brønsted acid concentration is dependent upon the choice of probe molecules⁴. Large molecules are involved in many catalytic reactions. Still larger phosphines are better probes to check steric effects on surface acidity. In our initial work⁵ (chapter 4), bulky tricyclohexylphosphine (Cy_3P) was chosen as a probe. Cy_3P is a very strong base, in solution $\text{p}K_{\text{a}}=9.70$ ⁶. Since many reactions involve less basic starting materials, it is interesting to choose bulky, less basic phosphines as new ^{31}P NMR probes. In this chapter the following phosphine probes are discussed: tri-*p*-tolylphosphine ($(p\text{-Tol})_3\text{P}$), tri-*m*-tolylphosphine ($(m\text{-Tol})_3\text{P}$), triphenylphosphine (Ph_3P), tri-*p*-chlorophenylphosphine ($(p\text{-ClC}_6\text{H}_4)_3\text{P}$), tri-*o*-tolylphosphine ($(o\text{-Tol})_3\text{P}$) and dimethylphenylphosphine (Me_2PhP). Aryl molecules are involved in many catalytic processes. Thus it is interesting to use these aryl phosphines as new probes. The Brønsted acid concentrations on the silica-alumina catalyst surface are titrated with these phosphines.

2. Results and Discussion: can these phosphines work?

Table 3.3 (Chapter 3) includes the chemical shifts of phosphine probes. Pure $(p\text{-Tol})_3\text{P}$ resonated at -10.3 ppm, which is roughly the same as -10.2, -10.4 ppm in

references^{10, 11}. -6.7 ppm for pure (*m*-Tol)₃P is close to -7.0 ppm in reference¹¹. -9.1 ppm for pure Ph₃P differs from -7.2, -10.3 ppm in^{10, 11}.

a. Ph₃P

Figure 5.1 shows the spectra of pure Ph₃P and 0.92 μmol/m² Ph₃P on SiO₂. The spinning side bands were observed in Figure 5.1a due to the chemical shift anisotropy of pure Ph₃P. After the adsorption on SiO₂, those spinning side bands disappeared in Figure 5.1b using the same MAS speed as Figure 5.1a. This indicates that the apparent chemical shift anisotropies were greatly reduced after adsorption on SiO₂. Similar results were observed for tricyclohexylphosphine⁵. Using a lower MAS rate (0.70 kHz), the results are shown in Figure 5.1c. Chemical shift anisotropies of pure Ph₃P were reported as δ₁₁=-42.0, δ₂₂=9.0 and δ₃₃=9.0 ppm¹¹. Thus for MAS equals 1.82 kHz, μ=1.7 and ρ=-1.0¹²; the theoretical I₊₁/I₀=0.08 and I₋₁/I₀=0.12¹², based on chemical shift anisotropies of pure Ph₃P. These values are similar to experimental results in Figure 1a (I₊₁/I₀=0.07 and I₋₁/I₀=0.09). When MAS was changed to 0.70 kHz, μ=4.4, then theoretically I₊₁/I₀=0.4 and I₋₁/I₀=1.2¹². (These are close to experimental results for pure Ph₃P, I₊₁/I₀=0.5 and I₋₁/I₀=1.0). Both theoretical calculation and experimental values indicate that crystalline Ph₃P should have high degrees of chemical shift anisotropy. For the physically adsorbed species, we find I₊₁/I₀=0.03 and I₋₁/I₀=0.04 at 0.70 kHz (Figure 5.1c). The spinning side band intensities have been reduced over 95%. These much smaller intensities indicate a great decrement of chemical shift anisotropy, suggesting the motion of Ph₃P on SiO₂ is nearly isotropic. Without MAS, the spectra on SiO₂ (Figure 5.1d) had a similar shape to those using MAS, which further confirmed the isotropic motions on the surface. The motion was not around the 3-fold axis of Ph₃P molecules, since the chemical shift anisotropies corresponding to an axially symmetric shielding tensor were not observed.

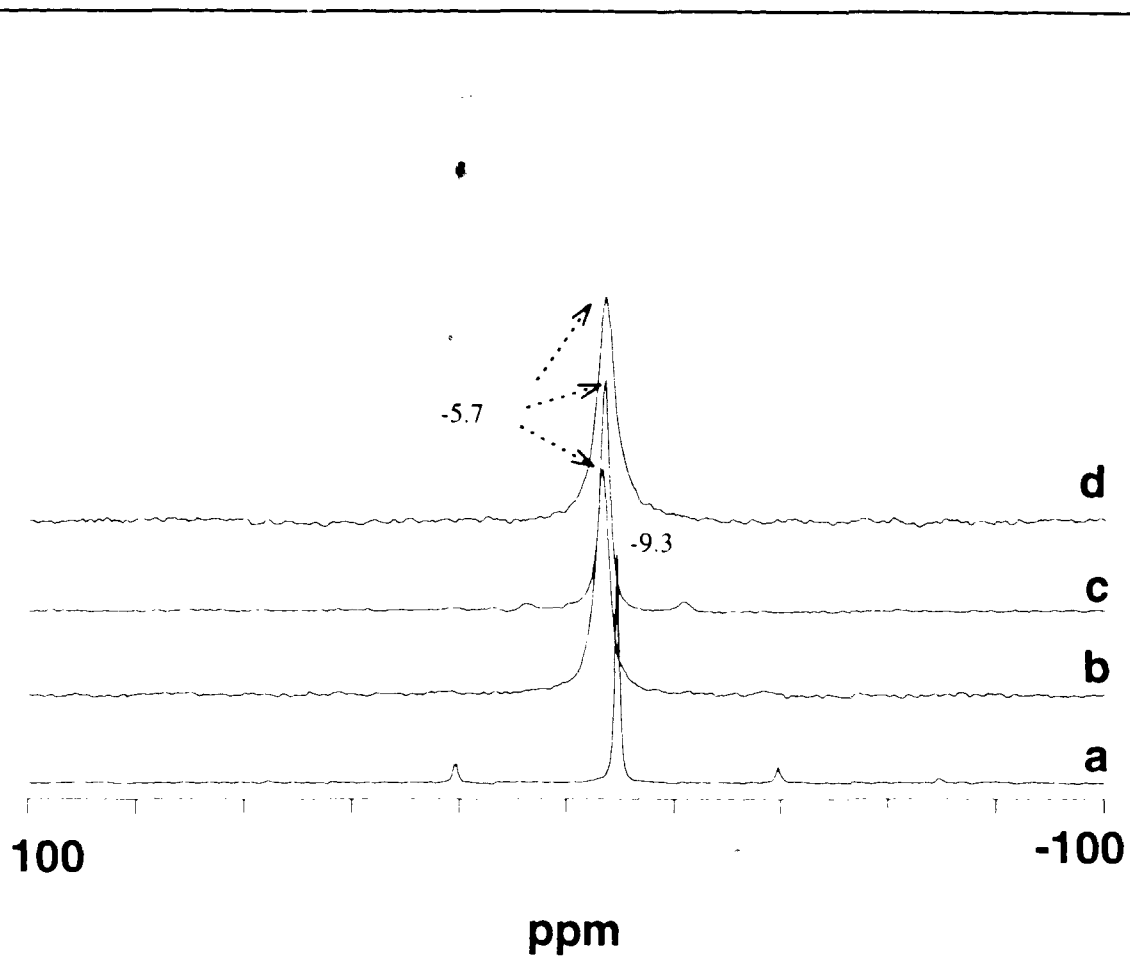


Figure 5.1. ^{31}P MAS NMR spectra of pure Ph_3P and $0.92 \mu\text{mol}/\text{m}^2$ Ph_3P on silica gel, silica was pretreated at 250°C , 10^{-5} torr for two hours, Ph_3P was adsorbed on silica at 200°C for one hour. a) pure PPh_3 , spinning rate: 1.82 K, 1 s recycle delay, 5756 scans; b) on silica, spinning rate: 1.82 K, 2 s recycle delay, 800 scans; c) on silica, spinning rate: 0.70 K, 1 s recycle delay, 1556 scans; and d) on silica, spinning rate: 0 K, 1 s recycle delay, 788 scans.

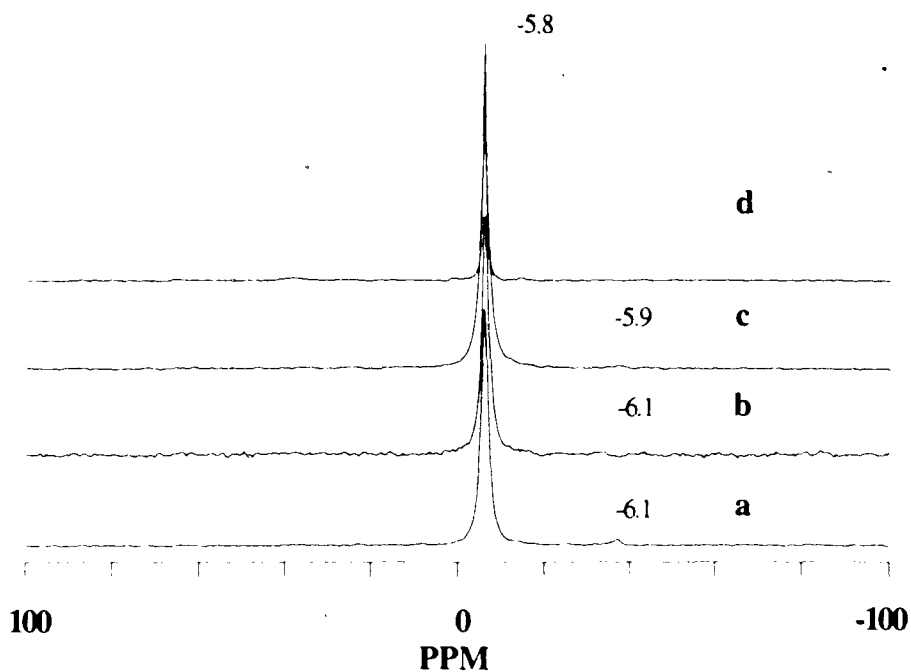


Figure 5.2 ^{31}P MAS NMR spectra of Ph_3P on silica gel with various coverages, silica pretreated at 250°C (if not specified), 10^{-5} torr for two hours, Ph_3P adsorbed at 100°C one hour (if not specified). a) $0.25 \mu\text{mol}/\text{m}^2$, 1.85 kHz MAS rate, 2 s recycle delay, 26120 scans; b) $0.41 \mu\text{mol}/\text{m}^2$, adsorbed at 150°C , 1.65 kHz MAS rate, 2 s recycle delay, 800 scans; c) $0.92 \mu\text{mol}/\text{m}^2$, 1.84 kHz MAS rate, 2 s recycle delay, 800 scans; and d) $1.68 \mu\text{mol}/\text{m}^2$, pretreated at 450°C , 1.80 kHz MAS rate, 1 s recycle delay, 800 scans.

Figure 5.2 shows the spectra of Ph_3P on SiO_2 , at various coverages. The chemical shifts of these peaks were all around -6.0 ppm within the experimental error. However, small changes of chemical shifts were observed for Cy_3P molecules on the silica surface (Figures 4.3, chapter 4). Here the constant chemical shift suggests that differences of H bonding do not exist, or can not be detected with Ph_3P probes.

Figure 5.3 shows the spectra of $0.38 \mu\text{mol}/\text{m}^2$ Ph_3P on alumina, with various adsorption temperatures. Figure 5.3a shows the physically adsorbed species at 100°C , which resonated around -6.4 ppm (similar to -6.0 ppm in Figure 5.2). Checking the spectrum of 100°C adsorption using cross-polarization (Figure 5.3b), at least one more new peak appeared (probably around -16 ppm). This peak probably arises from Lewis acid species. At higher adsorption temperatures (Figure 5.3c-5.3e), the physically adsorbed species convert to Lewis acid species (one of them resonated at -10 ppm). The Lewis acid complexes obviously have stronger bonding than physically adsorbed species on the alumina surfaces, so the changes from the physically adsorbed to Lewis acid species are reasonable and seem to be controlled by diffusion processes.

Figure 5.4 shows the spectra of $0.33 \mu\text{mol}/\text{m}^2$ Ph_3P on silica-alumina catalyst, with various adsorption temperatures. The peak of Ph_3P on SiO_2 resonated at -6.0 ppm, so the peaks around -6.2 ppm in Figure 5.4a to 5.4d are due to physically adsorbed species. PPh_3H^+ in concentrated HCl resonates at 4.2 ppm, close to the peaks around 7.2 ppm in Figure 5.4b to 5.4d. These Brønsted acid species were further confirmed by a delayed-decoupled spectrum (Figure 5.4a). The results of Figure 5.4b to 5.4d also indicate that the higher the treatment temperature, the more protonated phosphine appears. Other peaks were not seen in these spectra at this coverage.

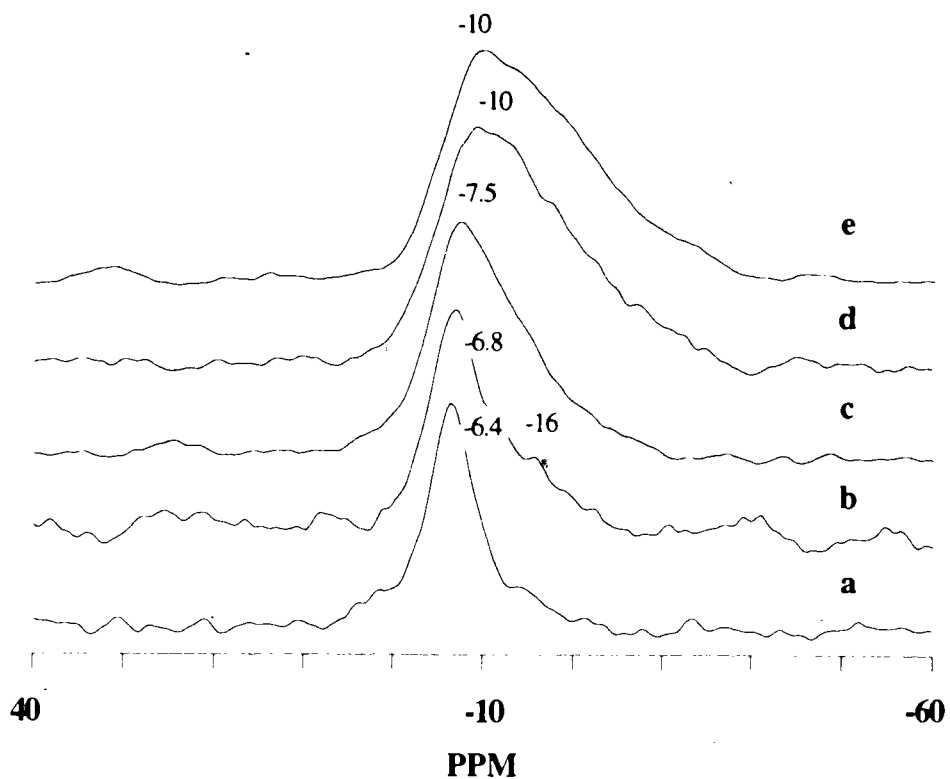


Figure 5.3 ^{31}P MAS NMR spectra of $0.38 \mu\text{mol}/\text{m}^2$ Ph_3P on alumina, alumina was pretreated at 450°C , 10^{-5} torr for two hours, with various adsorption temperatures, cross-polarization (if not specified), 1.86 kHz MAS rate, 2 s recycle delay. a) adsorbed at 100°C for one hour, 90° pulse, 2000 scans; b) adsorbed at 100°C for one hour, 3000 scans; c) adsorbed at 150°C for one hour, 5000 scans; d) adsorbed at 200°C for one hour, 5000 scans; and e) adsorbed at 200°C for two hours, 70450 scans.

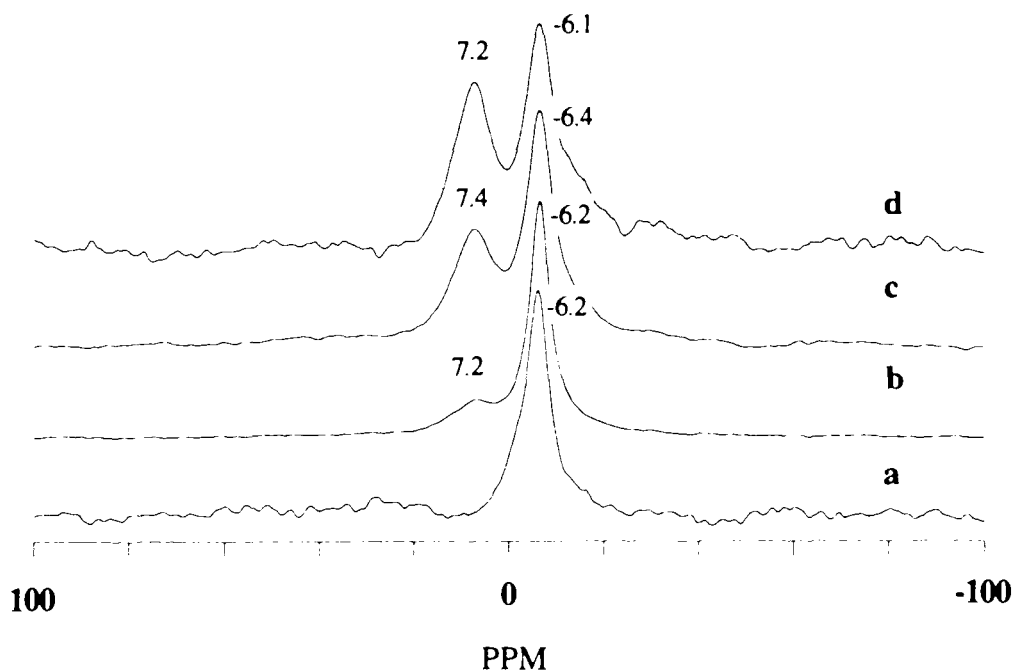


Figure 5.4 ^{31}P MAS NMR spectra of $0.33 \mu\text{mol}/\text{m}^2$ Ph_3P on commercial silica-alumina catalyst, catalyst was pretreated at 450°C , 10^{-5} torr for two hours, with various adsorption temperatures, 90° pulse (if not specified), 1 s recycle delay. a) 100°C for one hour, dipolar dephasing, $70 \mu\text{s}$ delay, 1.0 kHz MAS rate, 10118 scans; b) 100°C for one hour, 1.83 kHz MAS rate, 46318 scans; c) 150°C for one hour, 1.83 kHz MAS rate, 56458 scans; and d) 200°C for one hour, 1.85 kHz MAS rate, 9100 scans.

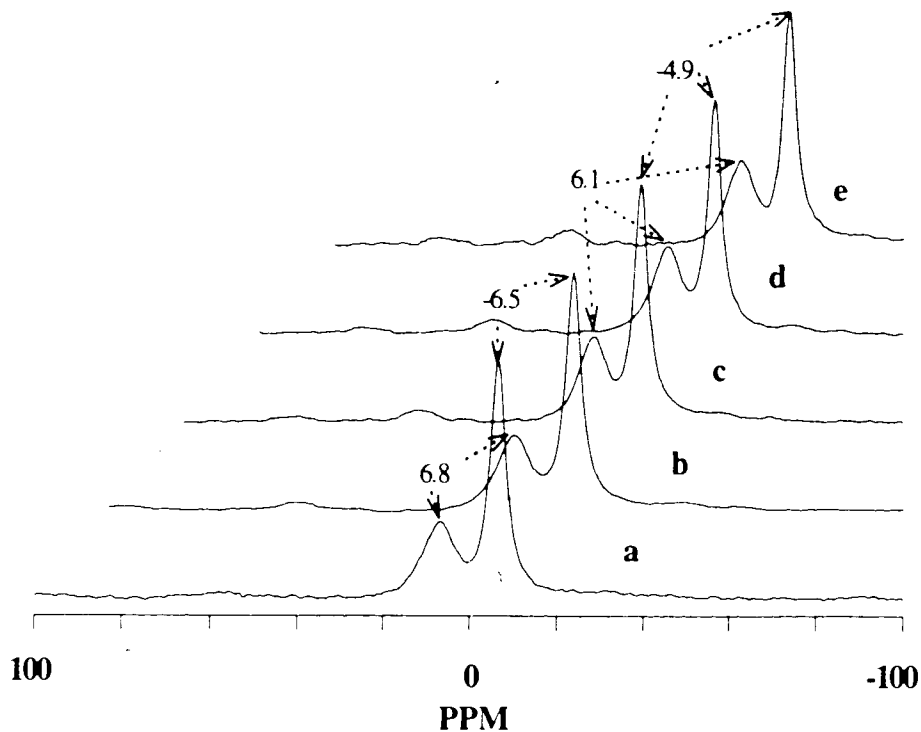


Figure 5.5 ^{31}P MAS NMR spectra of $0.48 \mu\text{mol}/\text{m}^2$ Ph_3P on commercial silica-alumina catalyst with various recycle delays, catalyst was pretreated at 450°C , 10^{-5} torr for two hours, adsorption at 200°C for two hours, 90° pulse. a) 1.83 kHz MAS rate, 1 s recycle delay, 7600 scans; b) 1.83 kHz MAS rate, 2 s recycle delay, 30030 scans; c) 1.74 kHz MAS rate, 4 s recycle delay, 12904 scans; d) 1.73 kHz MAS rate, 8 s recycle delay, 17723 scans; and e) 1.71 kHz MAS rate, 16 s recycle delay, 4470 scans.

Figure 5.5 shows the spectra of $0.48 \mu\text{mol}/\text{m}^2 \text{Ph}_3\text{P}$ on silica-alumina catalyst, with various recycle delays. The integrated areas of each spectrum were checked to determine the recycle delay for quantitative measurement. The ratios of integrated areas between physically adsorbed species (-5 to -6 ppm) and Brønsted acid (6-7 ppm) were 1.7, 1.5, 1.7, 1.8 and 1.7 for Figure 5.5a to 5.5e respectively. These values are about the same since the integration errors can be around 10% to 15%, so the 1 s is long enough for quantitative determination. It is interesting to notice that the values of chemical shifts in Figure 5.5c to 5.5e are slightly different from those in Figure 5.5a and 5.5b. Figure 5.5a and 5.5b were measured about the time of the sample preparation, however, Figure 5.5c to 5.5e were checked three years later. After three years these two kinds of species may be slightly different since the difference of the chemical shifts became smaller.

Figure 5.6 shows the results for Ph_3P at different coverages on the silica-alumina catalyst surface after adsorption at 200°C . The peaks around -6.0 ppm in Figure 5.6b to 5.6e are due to physically adsorbed species. The broad peaks in the range of 0 to -20 ppm in Figure 5.7a probably were from Lewis acid species, which will be further discussed in Figure 5.7. The peaks around 7-8 ppm in Figure 5.6a to 5.6e are the Brønsted acid species, confirmed by delayed-decoupled experiments. The chemical shifts of the physically adsorbed peaks are summarized in Table 5.1. The Brønsted acid concentrations decrease in Figure 5.6d, e based on the integrated areas. The detailed data of Brønsted concentrations as a function of coverage and adsorption temperature are summarized in Figure 5.8.

TABLE 5.1

³¹P Chemical Shifts (ppm) of Physically Adsorbed Species from Ph₃P on SiO₂-Al₂O₃

Coverage $\mu\text{mol}/\text{m}^2$	100°C	150°C	200°C
0.11	-6.0		
0.18	-5.2		
0.24	-6.2		
0.30	-6.2		
0.33	-6.2	-6.2	-6.1
0.48	-6.6	-6.1	-6.1
0.77	-6.9	-6.7	-6.7
0.94	-7.2	-6.9	-6.8

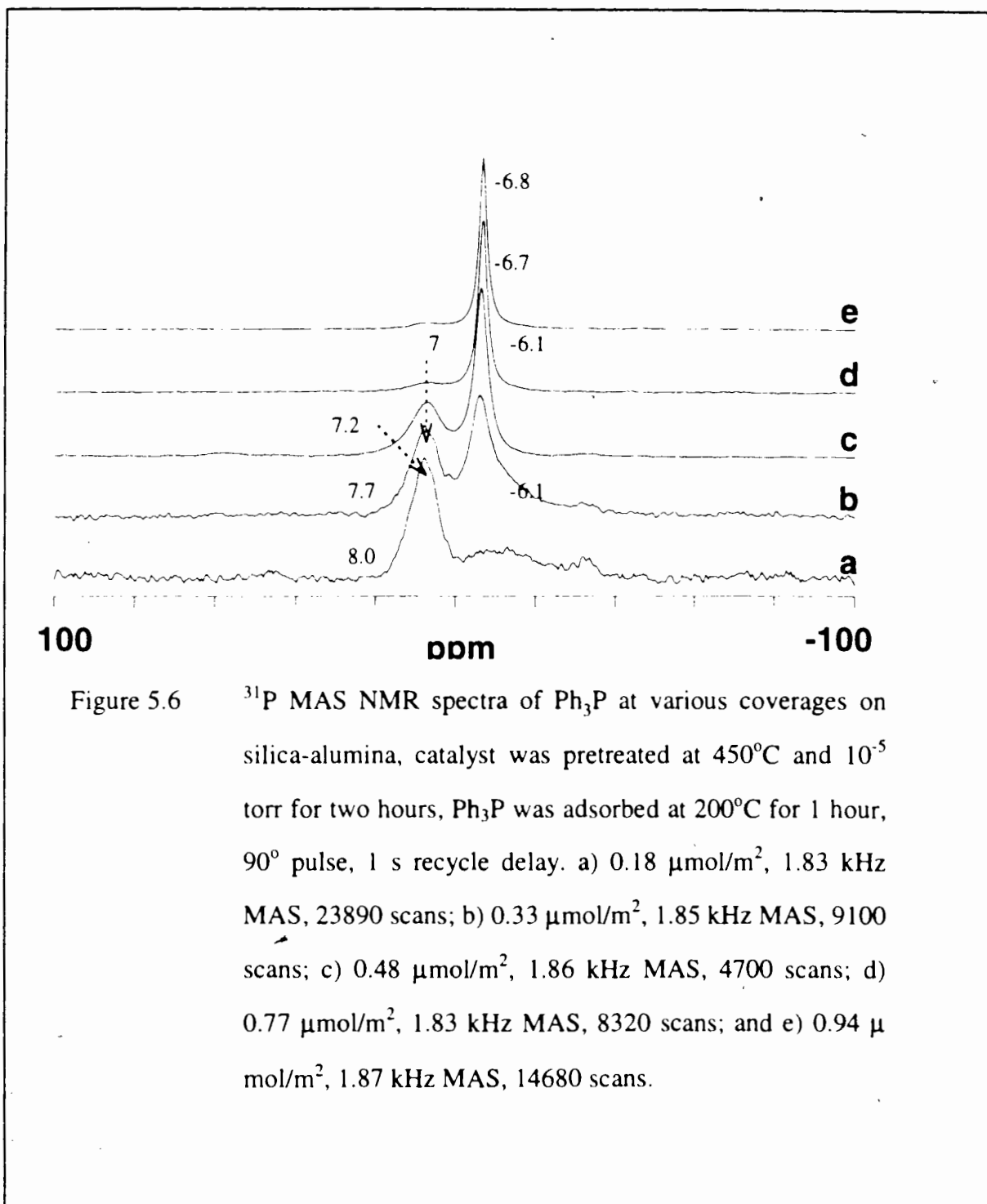
In Table 5.1, the physical adsorption peaks of Ph₃P species were summarized. At higher coverages the chemical shifts (-7.0 ppm) are slightly greater than those on SiO₂ (-6.0 ppm). The peaks around -7.0 ppm with not much spinning side bands are definitely not crystalline species (-9.3 ppm with spinning side bands, Figure 5.1a). The peaks are probably not Lewis acid sites either, otherwise they should be much broader (see Figure 5.3). Thus we suggest the peaks were caused by multilayer physically adsorbed species at higher coverages.

Figure 5.7 shows ³¹P MAS NMR spectra of 0.11 $\mu\text{mol}/\text{m}^2$ Ph₃P at various adsorption temperatures on the silica-alumina surface. The results of the spectra were similar to the 0.18 $\mu\text{mol}/\text{m}^2$ coverage sample in Figure 5.6a. At 100°C adsorption temperature (Figure 5.7a), physically adsorbed species were detected (-6.0 ppm). At

150°C (Figure 5.7b), the physically adsorbed peak changed to a new peak or peaks (at least one around -12 ppm). The new (-12 ppm) peak becomes more visible at 200°C (Figure 5.7c, d). This phenomenon with the variation of temperatures is quite similar to that in Figure 5.3 (which was suggested as the shift to Lewis acid sites). Here, the broad peaks (may be around -12 ppm) were believed to Lewis acid sites too. Since the Lewis acid sites involved at least two overlapped broad peaks, the exact peak positions were hard to figure out.

Figure 5.8 summarizes the variation of Brønsted acid concentration with the coverages at various adsorption temperatures. The maximum concentration of Ph_3PH^+ is around $0.17 \mu\text{mol}/\text{m}^2$ in Figure 5.8c, d, which is much smaller than those using Cy_3P and Me_3P (0.26 and $0.21 \mu\text{mol}/\text{m}^2$). Cy_3P and Me_3P ($\text{pK}_a=9.70$ and 8.65 respectively⁶) are much stronger bases than Ph_3P ($\text{pK}_a=2.73$ ^{6,13}). The more basic phosphines can react with more acidic sites on the surface. Here the electronic effects play a role and cause the differences. In references^{2,5}, the amounts of protonated Cy_3P and Me_3P appear to saturate at higher coverages. But a genuine decrease as in Figure 9a to 9c of Brønsted acid species at higher coverages is abnormal. An exchange process could explain the decrease of apparent concentrations of protonated species at high coverages². From Figure 5.1 and 5.2, the chemical shift of the physically adsorbed species on silica is at -5.9 ppm. If the exchange happened, at low coverages the chemical shifts of the physically adsorbed species on the silica-alumina catalyst should shift to higher frequency. However, this is not the case with Ph_3P (Table 5.1). Partial multilayer physical adsorption could have an effect at higher coverages, since the chemical shifts of the physically adsorbed species actually shift to lower frequency (Table 5.1), in other words toward the direction of crystalline Ph_3P (-9.3 ppm). The multilayer adsorbed species would result in the uneven phosphine adsorption on the surface, so Ph_3P molecules might have fewer opportunities

to approach Brønsted acid sites. Thus a decrease of Ph_3PH^+ species could happen at higher coverages.



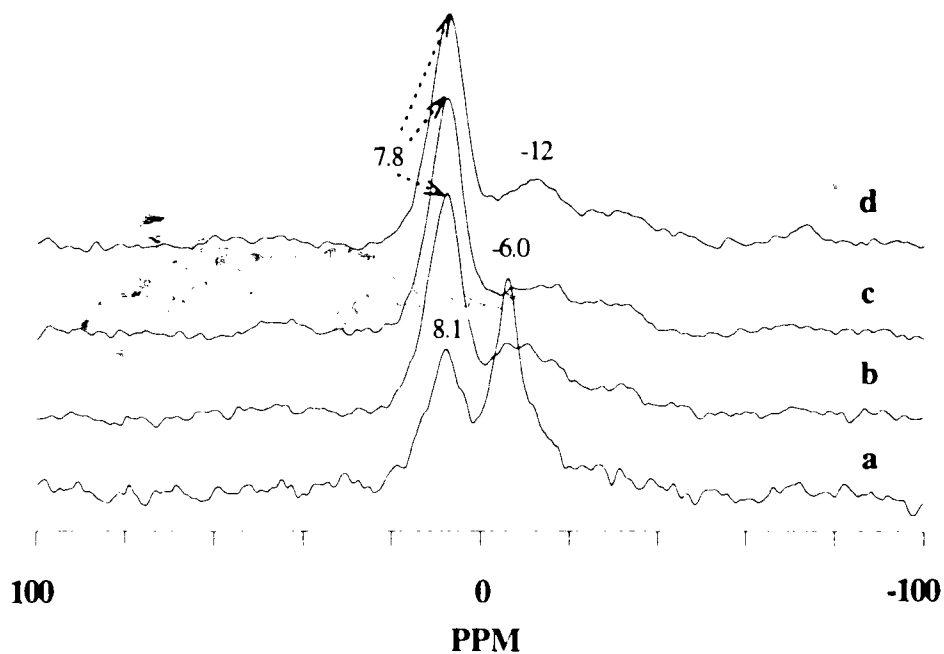


Figure 5.7 ^{31}P MAS NMR spectra of $0.11 \mu\text{mol}/\text{m}^2$ Ph_3P at various adsorption temperatures on silica-alumina, catalyst was pretreated at 450°C and 10^{-5} torr for two hours, 90° pulse, 2 s recycle delay. a) 100°C adsorbed for one hour, 1.86 kHz MAS rate, 46828 scans; b) 150°C adsorbed for one hour, 1.90 kHz MAS rate, 32888 scans; c) 200°C adsorbed for one hour, 1.83 kHz MAS rate, 32566 scans; and d) 200°C adsorbed for two hour, 1.86 kHz MAS rate, 49388 scans;

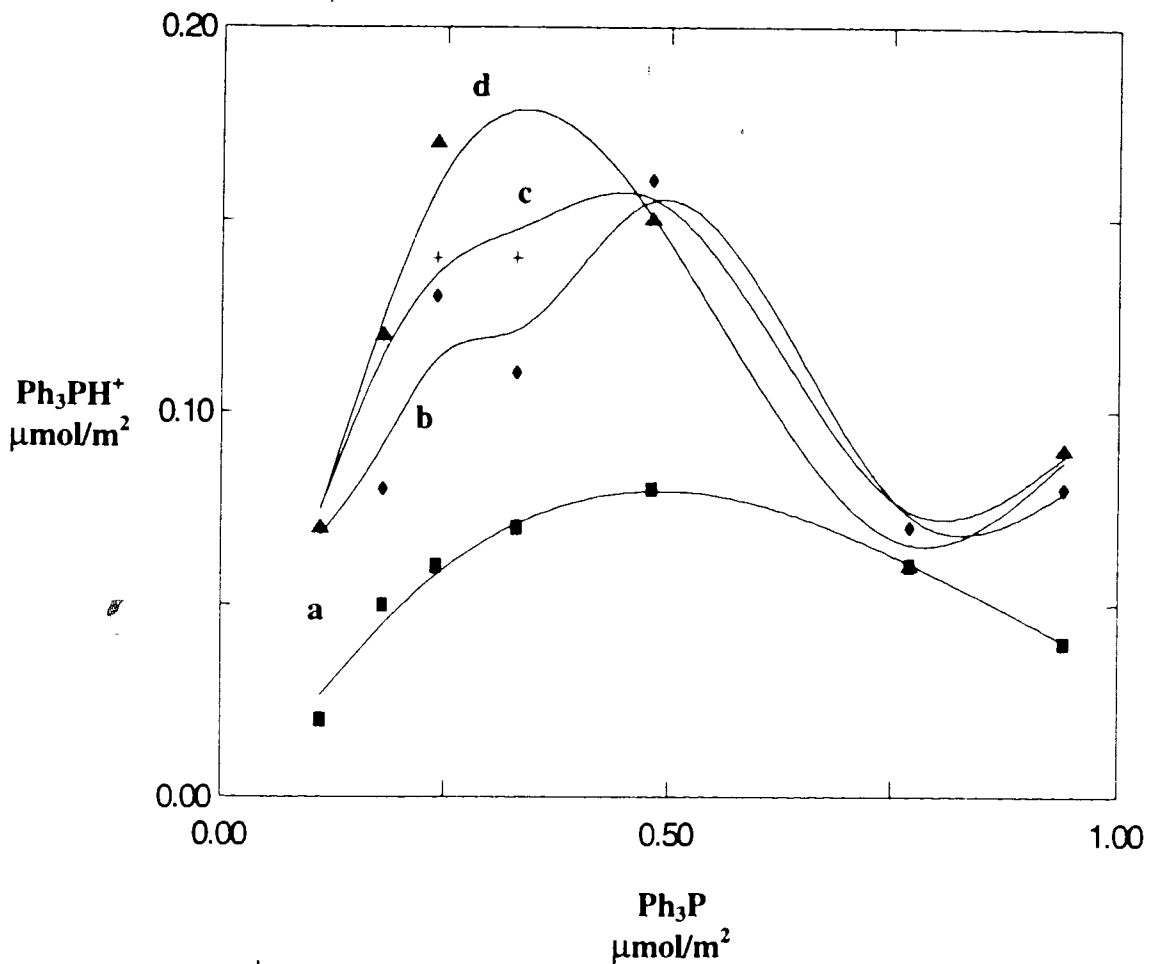


Figure 5.8 the concentrations of Ph_3PH^+ on commercial silica-alumina at various coverages. a) 100°C one hour(■); b) 150°C one hour(◆); c) 200°C one hour(+ and d) 200°C two hours(▲).

b. (p-Tol)₃P

Figure 5.9 shows the spectra of 0.19 $\mu\text{mol}/\text{m}^2$ (p-Tol)₃P on the silica surface for various adsorption temperatures. The resonances of physically adsorbed species were all around -8.3 ppm. The silica was pretreated at 450°C for two hours under vacuum. These results are similar to those on the silica pretreated at 250°C using Ph₃P, unlike Cy₃P probes. In the latter case, a small variation of chemical shift for physically adsorbed species was observed.

Figure 5.10 shows the spectra of 0.24 $\mu\text{mol}/\text{m}^2$ (p-Tol)₃P on the Al₂O₃ surface. Figure 5.10a is the result after 100°C adsorption. The -8.3 ppm peak in Figure 2a corresponds to the physically adsorbed species on Al₂O₃. After 150°C treatment, the peak shifted upfield to -12 ppm and became wider. The higher temperatures overcome the diffusion barrier; then shorter range interactions between (p-Tol)₃P and Al₂O₃ were observed. Thus Figure 5.10b probably is the result of Lewis acid species on the Al₂O₃ surface. Figure 5.10c shows the spectrum after 200°C adsorption. It is similar to Figure 2b. This indicates that 150°C is high enough to overcome the diffusion barriers.

Figure 5.11 shows the spectra of 0.19 and 0.63 $\mu\text{mol}/\text{m}^2$ (p-Tol)₃P on the Al₂O₃ surface. Figure 5.11a was similar to the spectra in Figure 5.10b and 5.10c, arising from the Lewis acid species. However, when the coverage was increased to 0.63 $\mu\text{mol}/\text{m}^2$ (Figure 5.11b, 5.11c), the resonances were at -8.5 ppm which is the same as the value on the silica gel (Figure 5.9). A recycle delay of ~~16~~ seconds is long enough for the quantitative measurement on the alumina surface (Figure 4.8). Therefore the physically adsorbed species were the main component for 0.63 $\mu\text{mol}/\text{m}^2$ coverage. The temperature

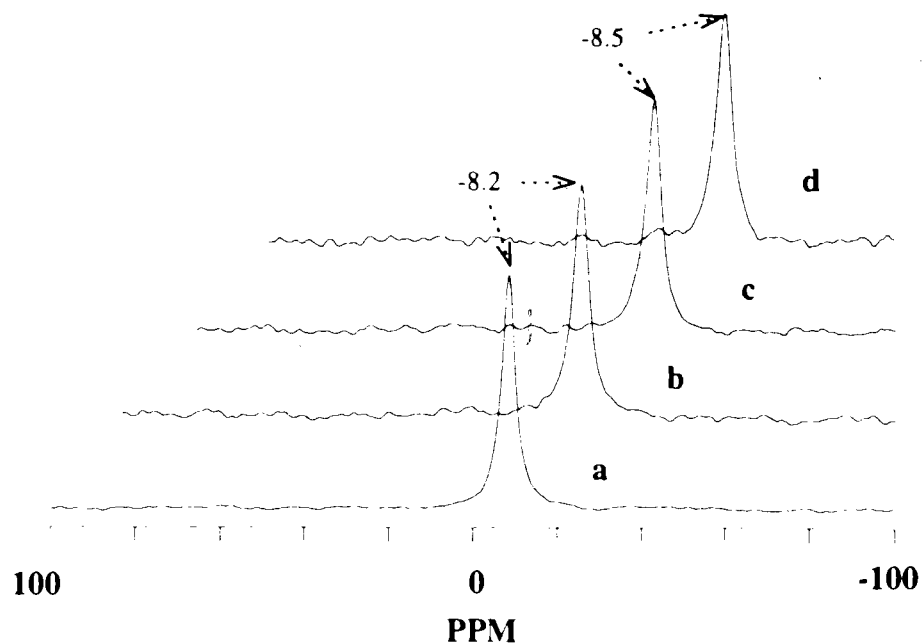


Figure 5.9 ^{31}P MAS NMR spectra of $0.19 \mu\text{mol}/\text{m}^2$ (*p*-Tol) $_3\text{P}$ at various adsorption temperatures on silica, silica was pretreated at 450°C and 10^{-5} torr for two hours, 90° pulse, 2 s recycle delay. a) 100°C one hour, 2.11 kHz, 24700 scans; b) 150°C one hour, 1.80 kHz, 2000 scans; c) 200°C one hour, 2.07 kHz, 2000 scans; and d) 250°C one hour, 1.86 kHz, 2000 scans.

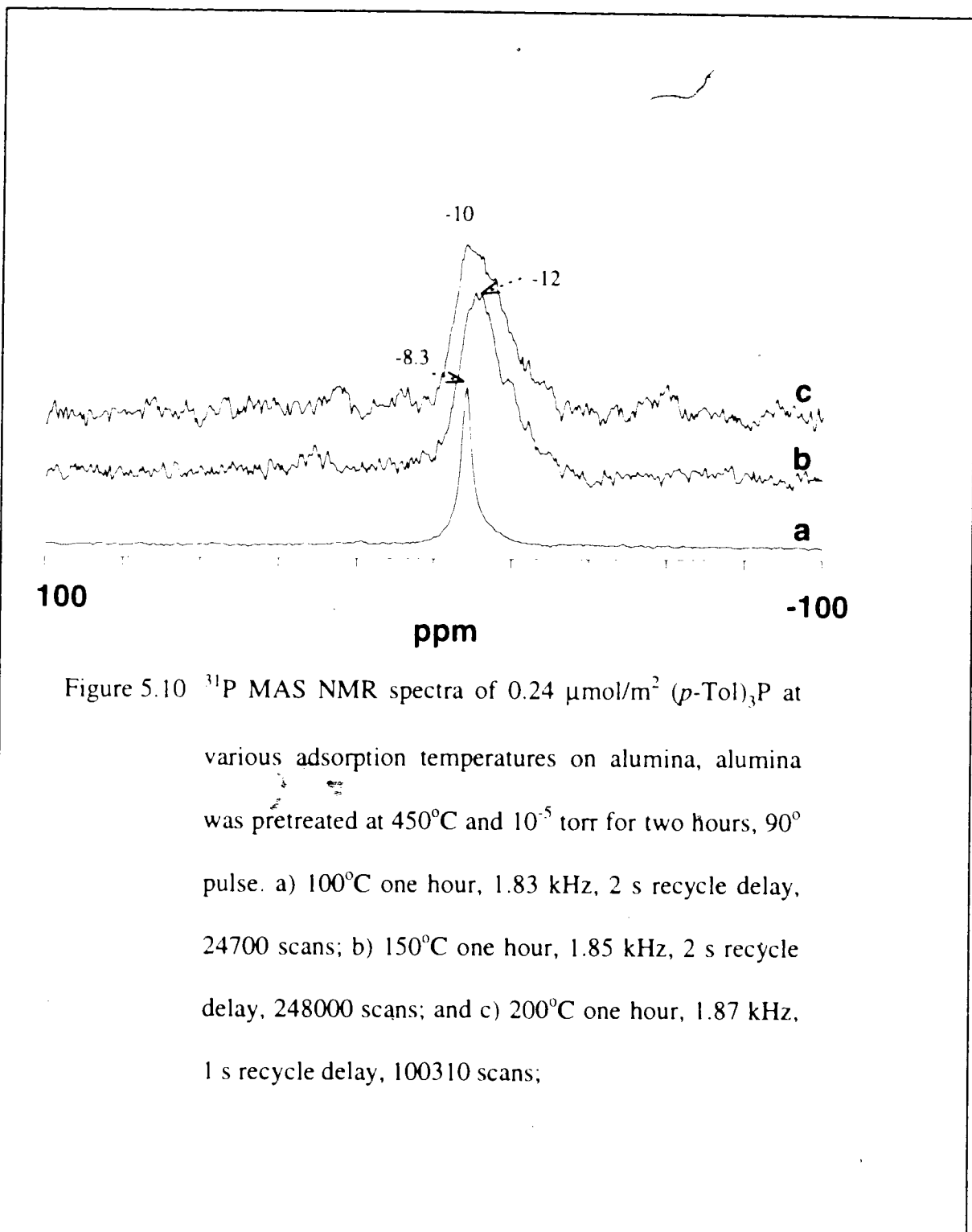


Figure 5.10 ^{31}P MAS NMR spectra of $0.24 \mu\text{mol}/\text{m}^2$ (*p*-Tol) $_3\text{P}$ at various adsorption temperatures on alumina, alumina was pretreated at 450°C and 10^{-5} torr for two hours, 90° pulse. a) 100°C one hour, 1.83 kHz, 2 s recycle delay, 24700 scans; b) 150°C one hour, 1.85 kHz, 2 s recycle delay, 248000 scans; and c) 200°C one hour, 1.87 kHz, 1 s recycle delay, 100310 scans;

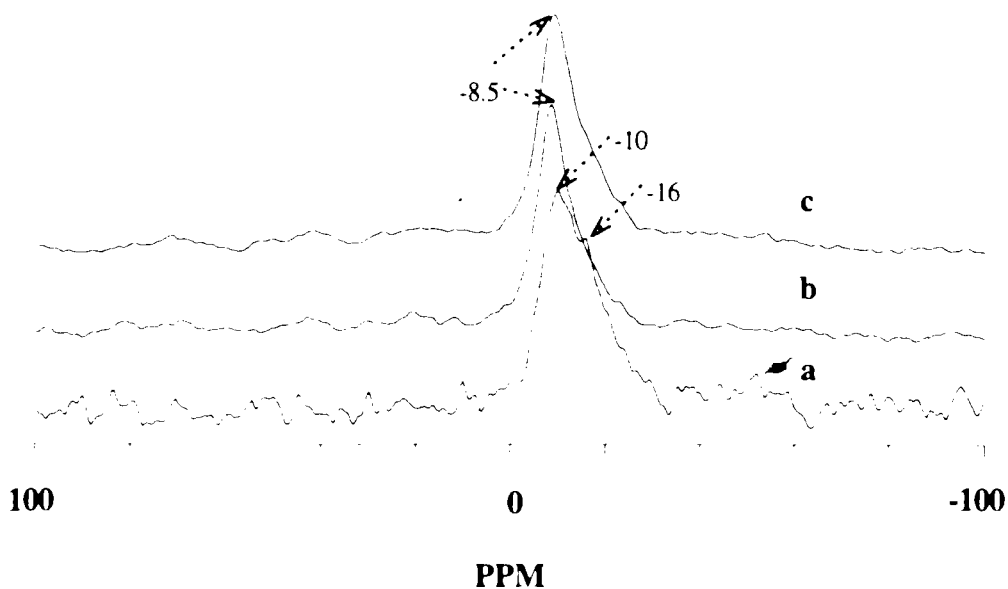


Figure 5.11 ^{31}P MAS NMR spectra of $(p\text{-Tol})_3\text{P}$ at various coverages on alumina, alumina was pretreated at 450°C and 10^{-5} torr for two hours. a) $0.19 \mu\text{mol}/\text{m}^2$, 100°C one hour, 1.83 kHz MAS rate, 90° pulse, 2 s recycle delay, 125150 scans; b) $0.63 \mu\text{mol}/\text{m}^2$, 200°C one hour, 1.74 kHz MAS rate, 90° pulse, 16 s recycle delay, 883 scans; and c) $0.63 \mu\text{mol}/\text{m}^2$ 200°C one hour, 1.74 kHz, cross-polarization flipback, 16 s recycle delay, 944 scans;

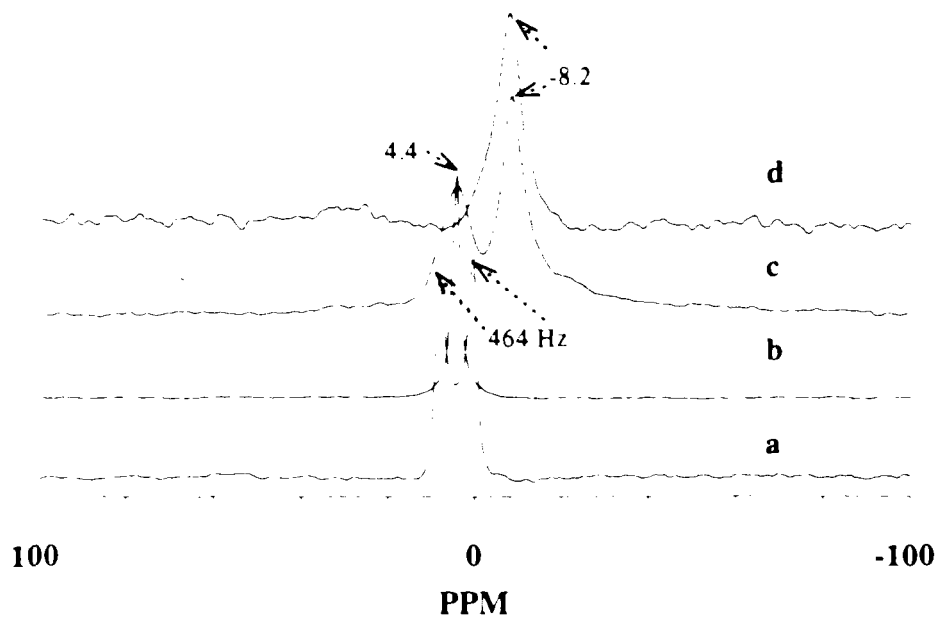


Figure 5.12 ^{31}P MAS NMR spectra of $(p\text{-Tol})_3\text{P}$ in HCl solution and $0.13 \mu\text{mol}/\text{m}^2$ on the silica-alumina surface. The catalyst was pretreated at 450°C and 10^{-5} torr for two hours, adsorbed at 150°C for one hour, 90° pulse (if not specified). a) in HCl, decoupler off, 1 s recycle delay, 5596 scans; b) in HCl, 1 s recycle delay, 9490 scans; c) on the catalyst, 2 s recycle delay, 1.80 kHz MAS rate, 72000 scans; and d) on the catalyst, dipolar dephasing, 1.80 kHz MAS rate, 2 s recycle delay, 5000 scans.

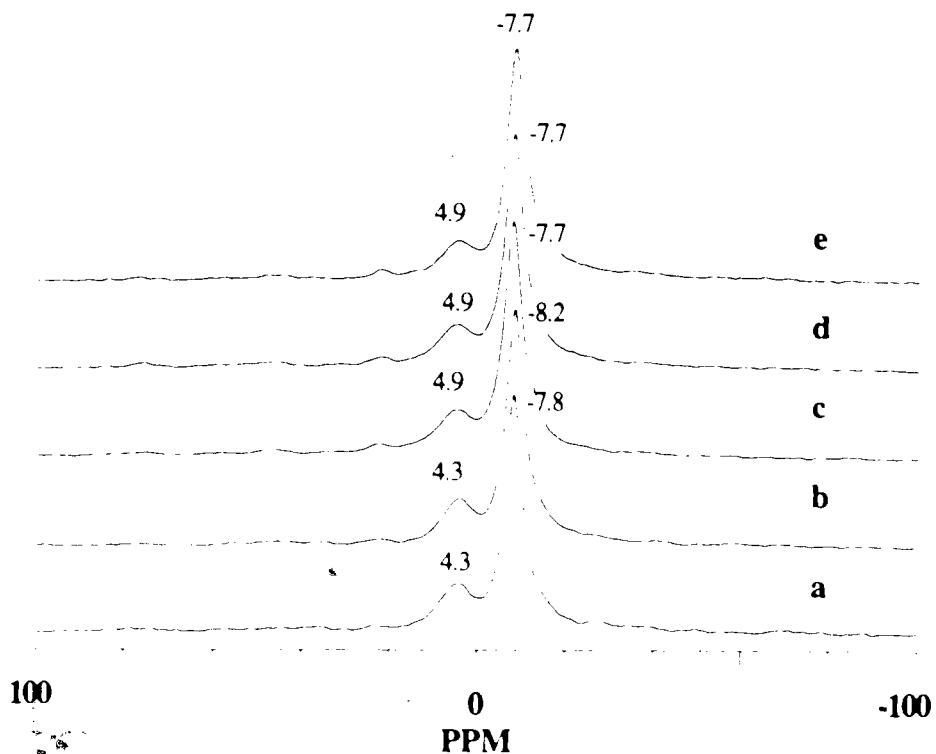


Figure 5.13 ^{31}P MAS NMR spectra of $0.31 \mu\text{mol}/\text{m}^2$ $(p\text{-Tol})_3\text{P}$ on silica-alumina catalyst with various recycle delays, the catalyst was pretreated at 450°C and 10^{-5} torr for two hours, adsorption at 200°C for two hours. a) 1.85 kHz MAS rate, 1 s recycle delay, 15666 scans; b) 1.85 kHz MAS rate, 2 s recycle delay, 30110 scans; c) 1.74 kHz MAS rate, 4 s recycle delay, 34330 scans; d) 1.74 kHz MAS rate, 8 s recycle delay, 8487 scans; and e) 1.74 kHz MAS rate, 16 s recycle delay, 5428 scans.

of 150°C is high enough to overcome the diffusion barriers between physically adsorbed species and Lewis acid species (Figure 5.10), so the apparent Lewis acid concentration saturated at this coverage. The maximum apparent concentration of Lewis acid should be between 0.24 and 0.63 $\mu\text{mol}/\text{m}^2$ using (*p*-Tol)₃P probe. This value is much smaller than measured with Cy₃P (>0.9 $\mu\text{mol}/\text{m}^2$ from Figure 4.8) and with Me₃P (1.3 $\mu\text{mol}/\text{m}^2$).

Figure 5.12 shows the spectra of protonated species of (*p*-Tol)₃P in HCl solution and on the silica-alumina surface. The resonance of protonated (*p*-Tol)₃P in concentrated HCl is 4.4 ppm (Figure 5.12b), with J_{P-H} coupling of 464 Hz (Figure 5.12a). This value of chemical shift is about the same with the Brønsted acid species of 0.13 $\mu\text{mol}/\text{m}^2$ (*p*-Tol)₃P on the silica-alumina surface (Figure 5.12c). The protonated species were further confirmed by dipolar dephasing sequences (Figure 5.12d). Under the conditions of dipolar dephasing, the protonated species was almost gone using a 70 μs delay time.

Figure 5.13 shows the spectra of (*p*-Tol)₃P with different recycle delays. The ratios of integrated areas between physically adsorbed species (-7.8 ppm) and Brønsted acid (4.5 ppm) were 4.1, 3.8, 4.3, 3.7 and 4.0 for Figure 5.13a to 5.13e respectively. These values are not significantly different since integrated errors can be around 10% to 15%, so the 1 s is long enough for quantitative determination.

Figure 5.14 shows the spectra of 0.13 $\mu\text{mol}/\text{m}^2$ (*p*-Tol)₃P at various adsorption temperatures on the silica-alumina catalyst. The peaks around -8.0 ppm were from the physically adsorbed species, which were very close to the chemical shifts (-8.4 ppm) with the phosphine on the silica gel (Figure 5.9). The resonances around 4.5 ppm arise from Brønsted acid species, which has been confirmed in Figure 5.12. Similarly to Cy₃P and Ph₃P probes, the higher the adsorption temperature, the more protonated phosphine appears. It is interesting to find out that no other peaks were observed at this coverage

even after 200°C adsorption. However, with the Ph_3P probe the Lewis acid sites were detected using the similar coverage (0.11 and 0.18 $\mu\text{mol}/\text{m}^2$ in Figure 5.6a and 5.7 respectively). The Lewis acid sites, which were accessible to the Ph_3P molecules, cannot be approached by $(p\text{-Tol})_3\text{P}$ probes on the silica-alumina surface. Since these two kinds of molecules have the same cone angles (145°) and $(p\text{-Tol})_3\text{P}$ ($\text{p}K_a = 3.84$) even has stronger basic strength than Ph_3P ($\text{p}K_a = 2.73$) (Table 3.1, Chapter 3), the extra methyl groups on the tolyl-phosphine make the difference. These suggest that some Lewis acid sites are only accessible by molecules which have sizes between the tolyl-phosphines and triphenylphosphine and most of the Lewis acid sites are hindered to molecules of the dimension of the tolylphosphine.

Figure 5.15 shows the results of $(p\text{-Tol})_3\text{P}$ at various coverages on commercial silica-alumina cracking catalyst after treatment at 200°C for one hour. The $(p\text{-Tol})_3\text{PH}^+$ species in HCl resonate at 4.4 ppm (Figure 5.12), So the peaks around 4.6 ppm for Figure 5.15a to 5.15d were from Brønsted acid species. The peak of -8.3 ppm was $(p\text{-Tol})_3\text{P}$ on SiO_2 (Figure 5.9). Therefore the peaks around -8.0 ppm in Figure 5.15a to 5.15c were arising from the physically adsorbed species. A new peak of -10.1 ppm in Figure 5.15d will be discussed with reference to Figure 5.16. Lewis acid species do not appear in Figure 5.15.

Figure 5.16 shows the spectrum of 1.12 $\mu\text{mol}/\text{m}^2$ $(p\text{-Tol})_3\text{P}$ on silica-alumina catalyst after treatment at 200°C (Figure 5.15d) using the cross-polarization program. The central highest peak resonated at -10.1 ppm, which is almost the same as pure $(p\text{-Tol})_3\text{P}$ peak (-10.3 ppm). But this peak is much broader and accompanying spinning side bands are smaller than the pure sample's. Besides, this sample has the higher coverage than the others in Figure 5.15. Hence we suggest the peak was caused by multilayer $(p\text{-Tol})_3\text{P}$

physically adsorbed on the catalyst surface. A similar argument was proposed for Ph_3P based on the results of chemical shifts (Table 5.1).

Figure 5.17 summarizes the $(p\text{-Tol})_3\text{PH}^+$ concentration with the coverages at various adsorbed temperatures. The maximum Brønsted acid concentration of $(p\text{-Tol})_3\text{PH}^+$ is around $0.09 \mu\text{mol}/\text{m}^2$ in Figure 5.17b and 5.17c. Similar to Ph_3P molecules (Figure 5.8) a genuine decrease of Brønsted acid species at higher coverages is observed. It can also be explained by the partial multilayer of physically adsorbed species, since this kind of $(p\text{-Tol})_3\text{P}$ species was claimed to exist at the higher coverages too (Figure 5.16). Compared with Ph_3P probe, the apparent maximum Brønsted acid concentration with $(p\text{-Tol})_3\text{P}$ is only about half of the amount with Ph_3P ($0.17 \mu\text{mol}/\text{m}^2$ in Figure 5.8), even though $(p\text{-Tol})_3\text{P}$ is a stronger base (Table 3.1, chapter 3). This obviously should be a steric effect. Some Lewis acid sites were observed only by Ph_3P , not by $(p\text{-Tol})_3\text{P}$ (Figure 5.6a, 5.7 and 5.14). Here, the extra methyl group on the tolylphosphine may play a role again. Maybe, about $0.08 \mu\text{mol}/\text{m}^2$ Brønsted acid sites were accessed by Ph_3P , but are inaccessible to $(p\text{-Tol})_3\text{P}$.

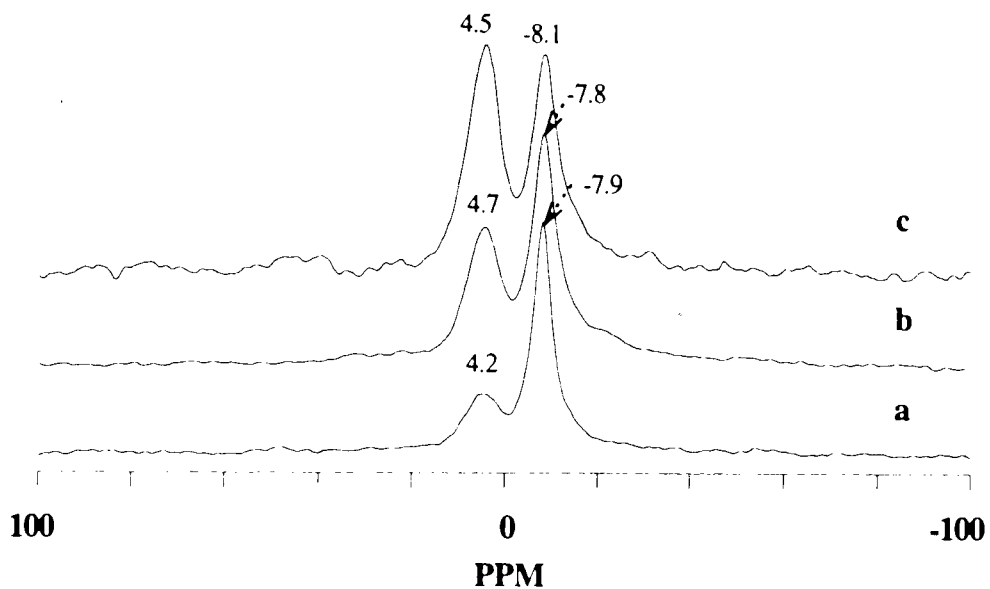


Figure 5.14 ^{31}P MAS NMR spectra of $0.13 \mu\text{mol}/\text{m}^2$ (*p*-Tol) $_3\text{P}$ at various adsorption temperatures on the silica-alumina catalyst, catalyst was pretreated at 450°C and 10^{-5} torr for two hours, 90° pulse, 2 s recycle delay. a) 100°C one hour, 1.99 kHz MAS rate, 22260 scans; b) 150°C one hour, 1.80 kHz MAS rate, 72000 scans; and c) 200°C one hour, 2.06 kHz MAS rate, 25000 scans;

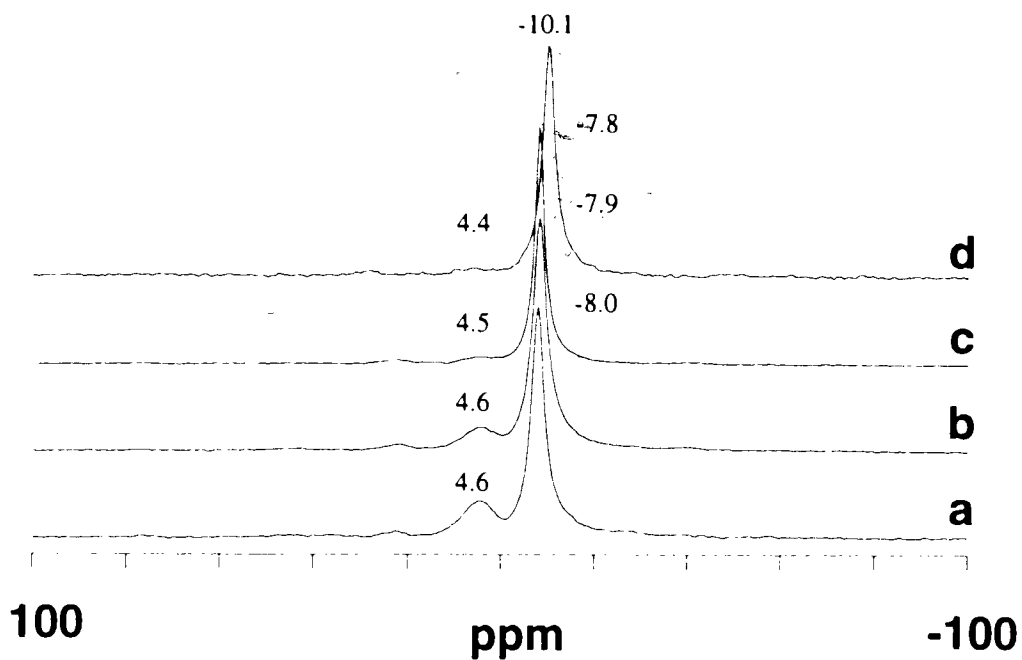


Figure 5.15 ^{31}P MAS NMR spectra of $(p\text{-Tol})_3\text{P}$ at various coverages on silica-alumina adsorbed at 200°C for 1 hour, the catalyst was degassed at 450°C and 10^{-5} torr for two hours, 90° pulse, 1.87 kHz MAS rate, 1 s recycle delay. a) $0.31 \mu\text{mol}/\text{m}^2$, 49720 scans; b) $0.56 \mu\text{mol}/\text{m}^2$, 56860 scans; c) $0.94 \mu\text{mol}/\text{m}^2$, 10628 scans; and d) $1.12 \mu\text{mol}/\text{m}^2$, 6830 scans.

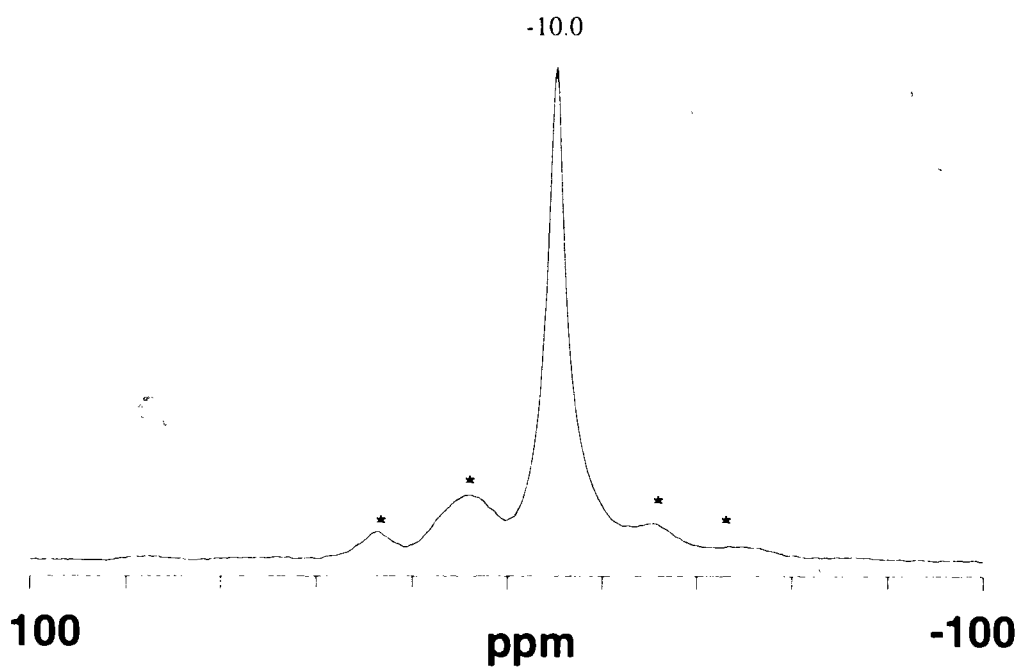


Figure 5.16 ^{31}P MAS NMR spectra of $1.12 \mu\text{mol}/\text{m}^2$ (*p*-Tol) $_3\text{P}$ on silica-alumina catalyst, adsorbed at 200°C for 1 hour, catalyst was degassed at 450°C and 10^{-5} torr for two hours, spinning rate: 1.12 kHz, cross-polarization flipback, 1 s recycle delay, 82888 scans. *: spinning side bands.

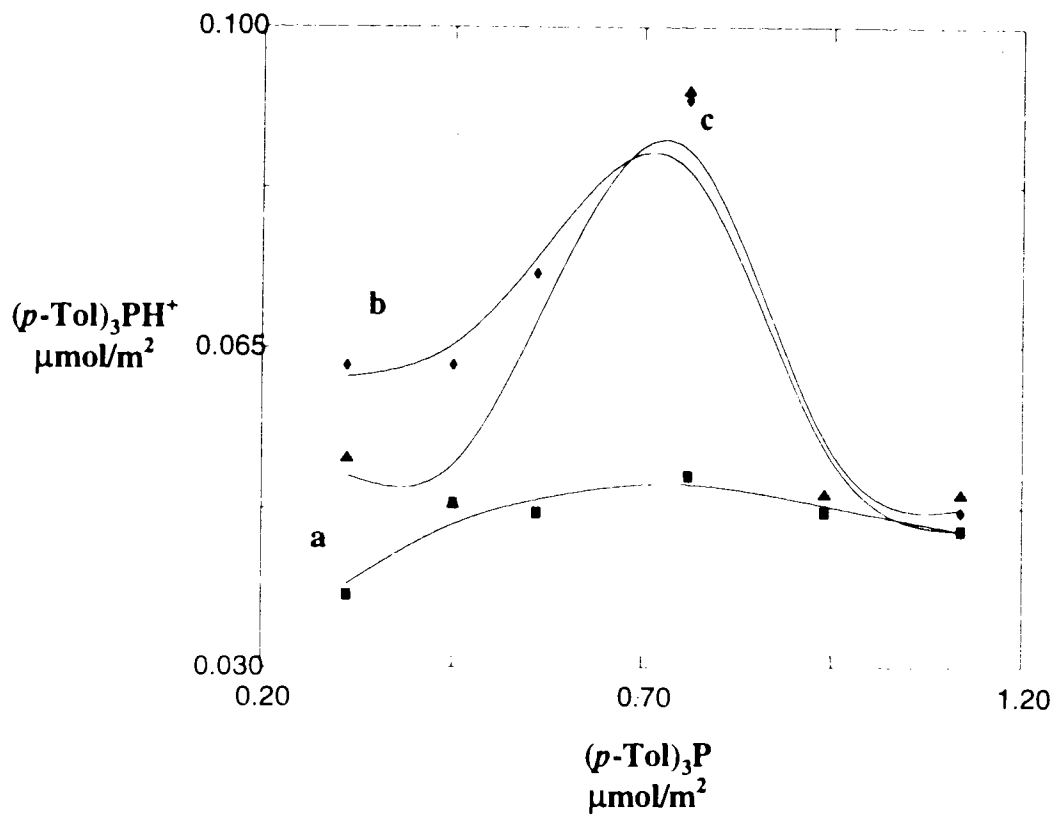


Figure 5.17 the concentrations of $(p\text{-Tol})_3\text{PH}^+$ on commercial silica-alumina catalyst at various coverages. a) 100°C one hour (■); b) 150°C one hour (◆); and c) 200°C one hour (▲).

c. $(m\text{-Tol})_3\text{P}$

Figure 5.18 shows the spectra of $0.19 \mu\text{mol}/\text{m}^2$ $(m\text{-Tol})_3\text{P}$ on the silica surface at various adsorption temperatures. The resonances of physically adsorbed species were all around -5.7 ppm. The silica was pretreated at 450°C for two hours under vacuum. These results are similar to those on silica using $(p\text{-Tol})_3\text{P}$ and Ph_3P molecules, with which no variation of chemical shifts for physically adsorbed species was observed.

Figure 5.19 shows the spectra of $(m\text{-Tol})_3\text{P}$ on the silica surface at various degassing temperatures. The resonances were about the same (around -5.3 ppm). The values were the same as those in Figure 5.18 within experimental errors. A different degassing temperature under vacuum will change the concentration of OH groups on the silica surface (Section 2, Chapter 2). The constant chemical shifts in Figure 5.19 indicate that the H bonding between the tolylphosphine and OH groups did not show any differences with the various OH coverages on the surface.

Figure 5.20 shows the spectra of $0.29 \mu\text{mol}/\text{m}^2$ $(m\text{-Tol})_3\text{P}$ on alumina surface adsorbed at 100°C obtained with different pulse programs. The peaks were around -7 ppm, were broader and shifted to lower frequency than the physically adsorbed species in Figure 5.19 and 5.20. They probably were Lewis acid species. The shapes of the peaks were similar to the Lewis acid species in Figure 5.3b-5.3e, 5.10b and 5.10c: shoulder peaks on the right. These also suggest more than one resonance was present for these Lewis sites.

Figure 5.21 shows the spectra of $0.10 \mu\text{mol}/\text{m}^2$ $(m\text{-Tol})_3\text{P}$ on commercial $\text{SiO}_2\text{-Al}_2\text{O}_3$ cracking catalyst with different adsorption temperatures. At each temperature the

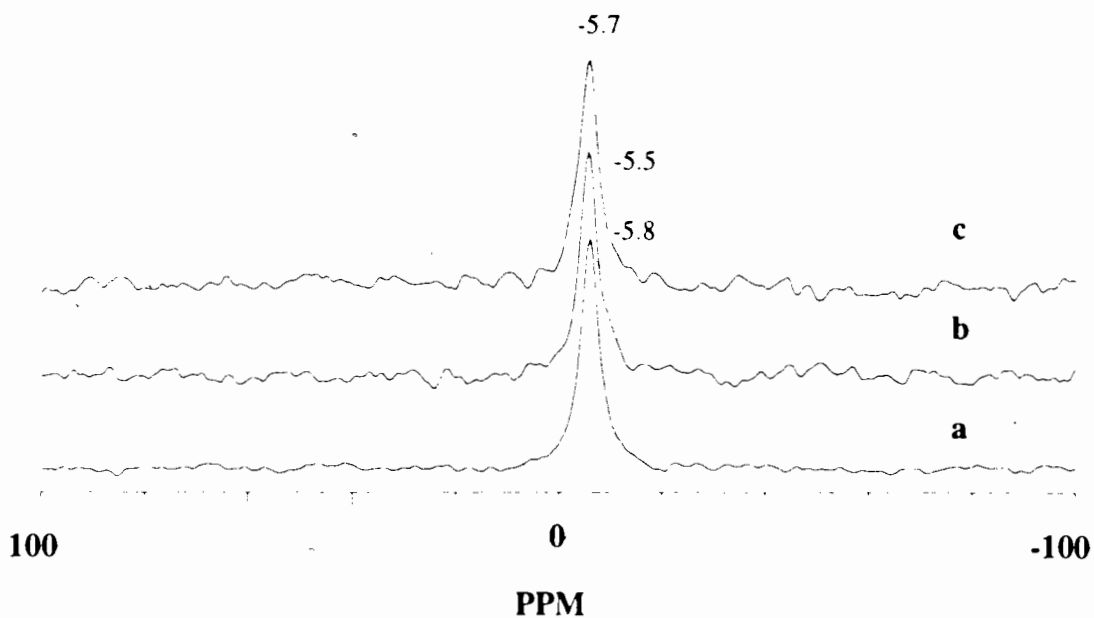


Figure 5.18. ^{31}P MAS NMR spectra of $0.19 \mu\text{mol}/\text{m}^2$ (*m*-Tol) $_3\text{P}$ on silica gel with various adsorption temperature, silica was pretreated at 450°C , 10^{-5} torr for two hours, 90° pulse, 2 s recycle delay. a) 100°C adsorption for 1 hour, spinning rate: 2.07 KHz, 25780- scans; b) 150°C adsorption for 1 hour, spinning rate: 2.05 KHz, 2000 scans; and c) 200°C adsorption for 1 hour, spinning rate: 1.80 kHz, 2000 scans;

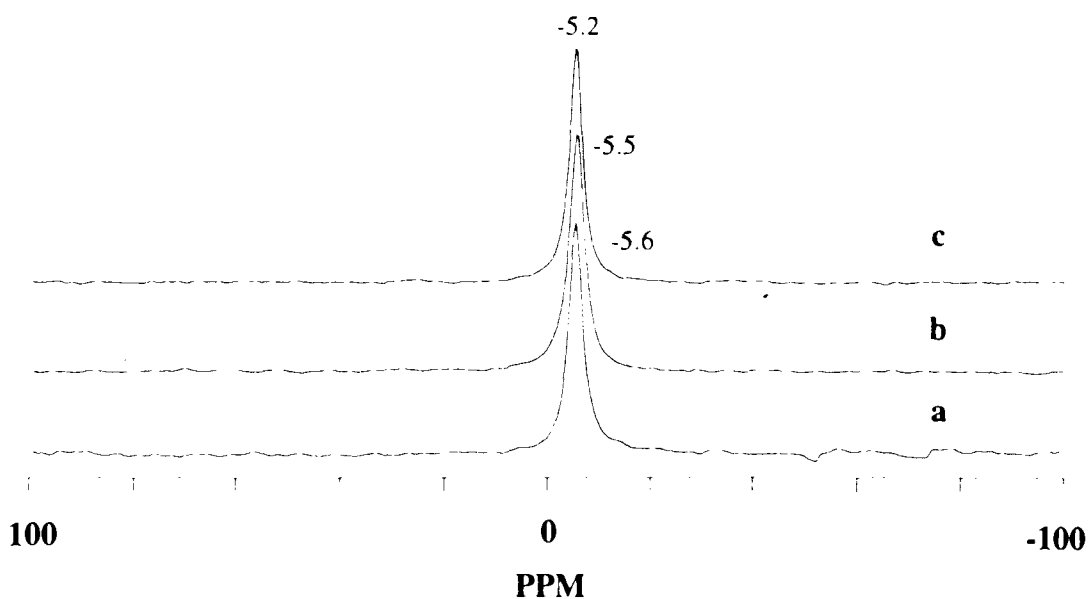


Figure 5.19 ^{31}P MAS NMR spectra of $(m\text{-Tol})_3\text{P}$ on silica gel with various degassing temperatures, silica was degassed at 10^{-5} torr for two hours, adsorption at 100°C for one hour, 90° pulse, 2 s recycle delay, 2000 scans. a) $0.32 \mu\text{mol}/\text{m}^2$, 250°C degassing temperature, spinning rate: 1.83 KHz; b) $0.29 \mu\text{mol}/\text{m}^2$, 450°C degassing temperature, spinning rate: 1.87 KHz; and c) $0.39 \mu\text{mol}/\text{m}^2$, 650°C degassing temperature*, spinning rate: 1.80 KHz. *: a ceramic stove was used.

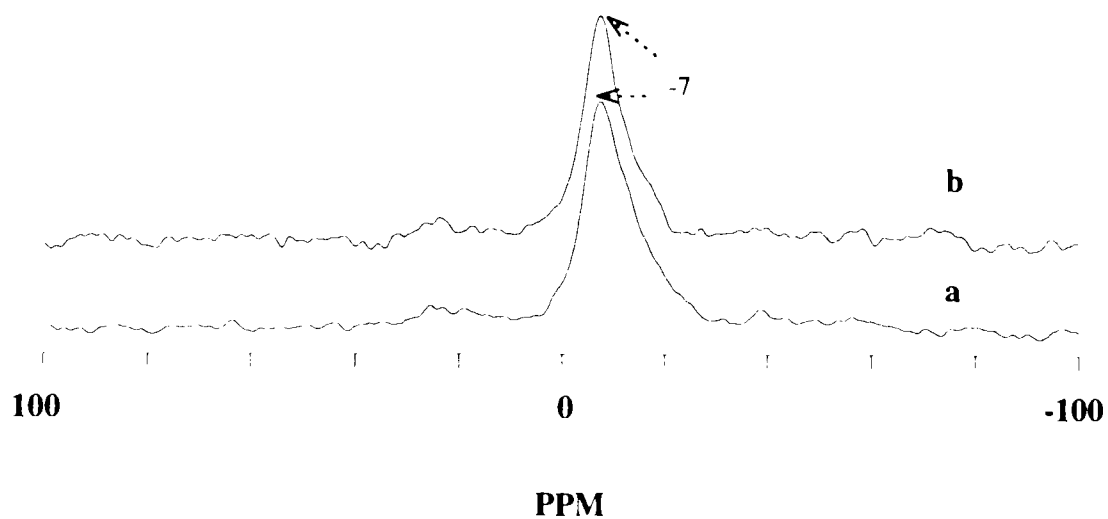


Figure 5.20 ^{31}P MAS NMR spectra of $0.29 \mu\text{mol}/\text{m}^2$ (*m*-Tol) $_3\text{P}$ on alumina surface, alumina was degassed at 450°C and 10^{-5} torr for two hours, adsorption at 100°C for one hour, 1.87 kHz MAS rate, 2 s recycle delay, 5000 scans. a) cross-polarization flipback; and b) 90° pulse.

total phosphine signal is constant within experimental error. (*m*-Tol)₃P on SiO₂ resonates at -5.5 ppm (Figure 5.18 and 5.19), so the right peaks around -5.3 ppm are due to physically adsorbed species. The left peaks in Figure 5.20a to 5.20c are around 5.6 ppm, which close to 5.0 ppm of protonated (*m*-Tol)₃P in concentrated HCl (Table 3.3, Chapter 3). The delayed-decoupled pulse program confirmed that the left peaks in Figure 5.20 a to 5.20 c arise from the (*m*-Tol)₃PH⁺ species. The spectra in Figure 5.21 clearly indicate the apparent Brønsted Acid concentrations are increased by higher adsorption temperatures. With Ph₃P, (*p*-Tol)₃P and Cy₃P phosphines, similar results have also been found. The higher temperatures probably either activated diffusion or activated proton transfer⁵.

Figure 5.22 shows the spectra of (*m*-Tol)₃P at various coverages adsorbed at silica-alumina catalyst at 200°C. As in Figure 5.21, the peaks around -5.2 ppm are from physically adsorbed species, wherea those around 5.0 ppm are from Brønsted acid species. The Lewis acid sites were not observed from Figure 5.22.

Figure 5.23 (same as Figure 1.10) shows spectra of 1.33 μmol/m² (*m*-Tol)₃P on silica-alumina catalyst using 180° pulse-delay-90° pulse program. This program (section 4e, chapter 1) can discriminate the different species by different delay values based on differences in T₁. At this high surface coverage, the resonance in Figure 5.23b was at -5.6 ppm with 0.1 second delay, which is the same value as on the silica surface (Figure 5.18 and 5.19). Here the physically adsorbed species is the main one detected. However, with a longer (3 seconds) delay, the chemical shift was -6.8 ppm (Figure 5.23a). This is almost the same as the value of crystalline pure (*m*-Tol)₃P sample (-6.7 ppm in Table 3.3, chapter 3). But this resonance does not arise from crystalline species: a) the peak was much wider than that from the crystalline sample; and b) there are no spinning side bands

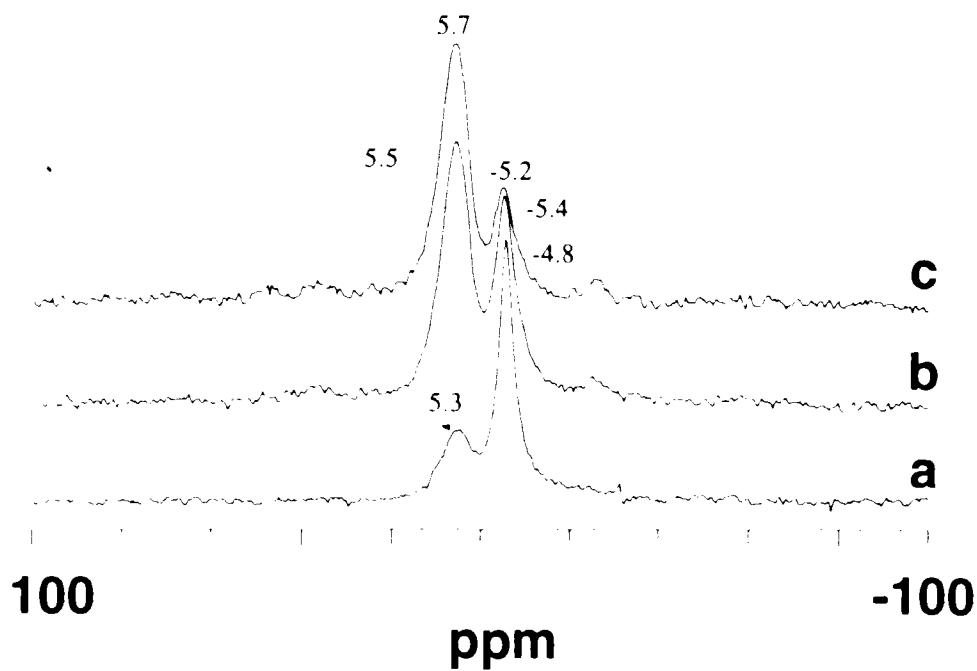


Figure 5.21 ^{31}P MAS NMR spectra of $0.10 \mu\text{mol}/\text{m}^2$ (*m*-Tol) $_3\text{P}$ on silica-alumina catalyst with various adsorption temperatures, the catalyst was degassed at 450°C and 10^{-5} torr for two hours, 90° pulse, 1.84 kHz MAS rate, 1 s recycle delay. a) 100°C 1 hour, 24000 scans; b) 150°C 1 hour, 81866 scans; and c) 200°C 1 hour, 21720 scans.

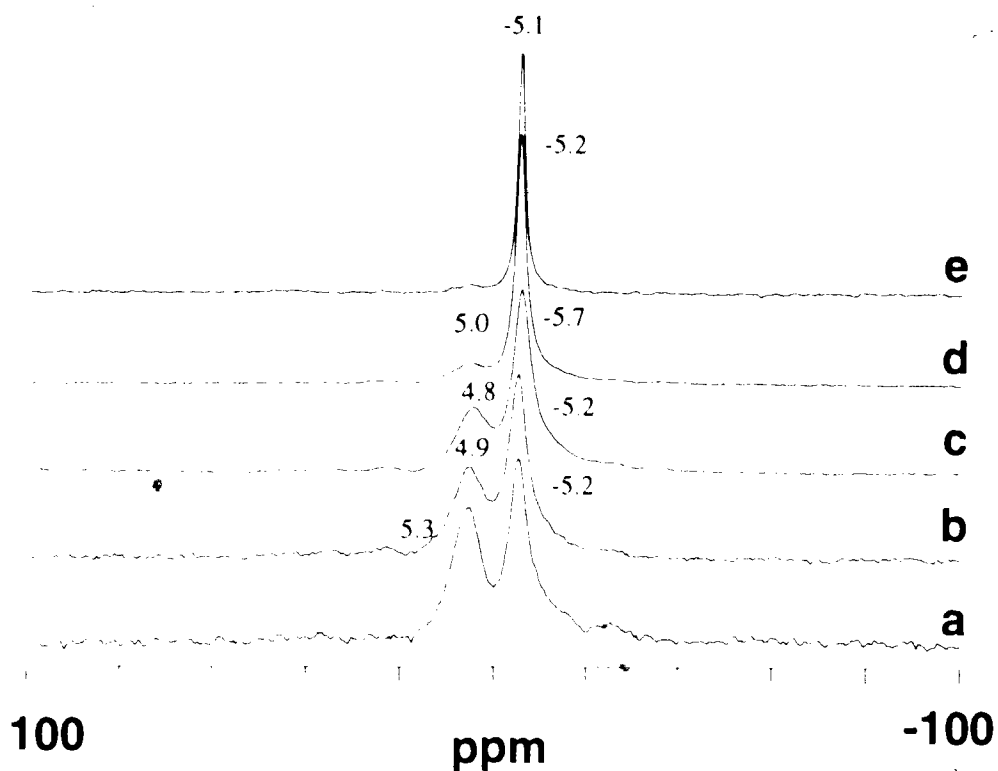


Figure 5.22 ^{31}P MAS NMR spectra of $(m\text{-Tol})_3\text{P}$ at various coverages on silica-alumina adsorbed at 200°C for 1 hour, the catalyst was degassed at 450°C and 10^{-5} torr for two hours, 90° pulse, 1.84 kHz MAS rate, 1 s recycle delay. a) $0.18 \mu\text{mol}/\text{m}^2$, 26050 scans; b) $0.32 \mu\text{mol}/\text{m}^2$, 74460 scans; c) $0.42 \mu\text{mol}/\text{m}^2$, 69500 scans; d) $0.47 \mu\text{mol}/\text{m}^2$, 18150 scans; and e) $0.56 \mu\text{mol}/\text{m}^2$, 5260 scans.

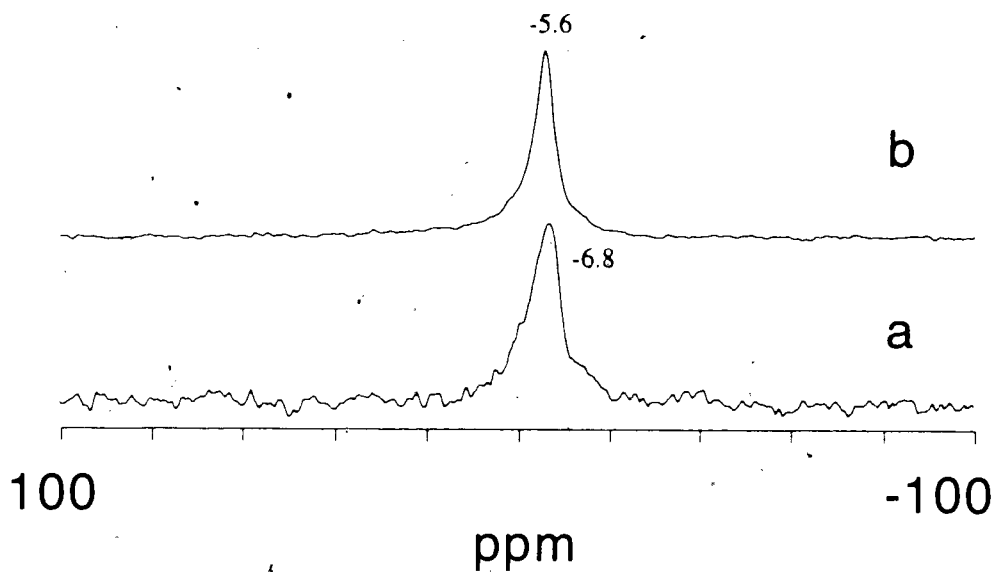


Figure 5.23 ^{31}P MAS NMR spectra of $1.33 \mu\text{mol}/\text{m}^2$ (*m*-Tol) $_3\text{P}$ on silica-alumina catalyst using 180° pulse-delay- 90° pulse program, the catalyst was degassed at 450°C and 10^{-5} torr for two hours, adsorbed at 200°C for one hour, 1.87 kHz MAS rate. a) 3 s delay, 20 s recycle delay, 4686 scans; and b) 0.1 s delay, 1 s recycle delay, 1072 scans.

using 1.87 kHz MAS rate in Figure 5.23 (while with crystalline sample, spinning side bands were observed even using over 2 kHz MAS rate). Also this peak does not arise from Lewis acid species: a) we did not detect Lewis acid species even at $0.10 \mu\text{mol}/\text{m}^2$ coverage (Figure 5.21) using this phosphine; and b) Lewis acid peaks are wider and have shoulders on the right like Figure 5.20. Therefore, we suggest the species in Figure 5.23a were mainly from a multilayer of physically adsorbed species. The same argument was proposed for Ph_3P and $(p\text{-Tol})_3\text{P}$. It seems all these aryl phosphines preferred to form multilayer species rather than monolayers at higher coverages. The benzene rings are not on the same plane for crystalline Ph_3P based on the x-ray structure^{13a}. However, this cannot exclude the argument that these kinds of species may be stabilized by forming 3 groups of strong π bonds between adjacent layers with the corresponding benzene rings.

Figure 5.24 summarizes the $(m\text{-Tol})_3\text{PH}^+$ concentration with the coverages at various adsorbed temperatures. The maximum Brønsted acid concentrations of $(m\text{-Tol})_3\text{PH}^+$ is around $0.15 \mu\text{mol}/\text{m}^2$ in Figure 5.24d. Similar to $(p\text{-Tol})_3\text{P}$ and Ph_3P molecules (Figure 5.8 and 5.17) a genuine decrease of Brønsted acid species at higher coverages was observed. It can also be explained by the partial multilayer of physically adsorbed species, since this kind of $(m\text{-Tol})_3\text{P}$ species was suggested to explain the peak in Figure 5.23a. Compared with the other two aryl phosphine probes, the apparent maximum Brønsted acid concentration with $(m\text{-Tol})_3\text{P}$ was between these two probes ($0.17 \mu\text{mol}/\text{m}^2$ with Ph_3P in Figure 5.8 and $0.09 \mu\text{mol}/\text{m}^2$ with $(p\text{-Tol})_3\text{P}$ in Figure 5.17). $(m\text{-Tol})_3\text{P}$ is a stronger base than Ph_3P , but weaker than $(p\text{-Tol})_3\text{P}$ (Table 3.1, chapter 3). The cone angle of $(m\text{-Tol})_3\text{P}$ is not available from the literature, but it is reasonable to assume that the value is same as $(p\text{-Tol})_3\text{P}$ or Ph_3P (145°). Here, the position of methyl groups in $(m\text{-Tol})_3\text{P}$ molecules makes the molecule harder than Ph_3P , but easier than $(p\text{-Tol})_3\text{P}$ to access the acidic sites. Hence its maximum Brønsted acid concentration was higher than $(p\text{-Tol})_3\text{P}$, but a little smaller than Ph_3P .

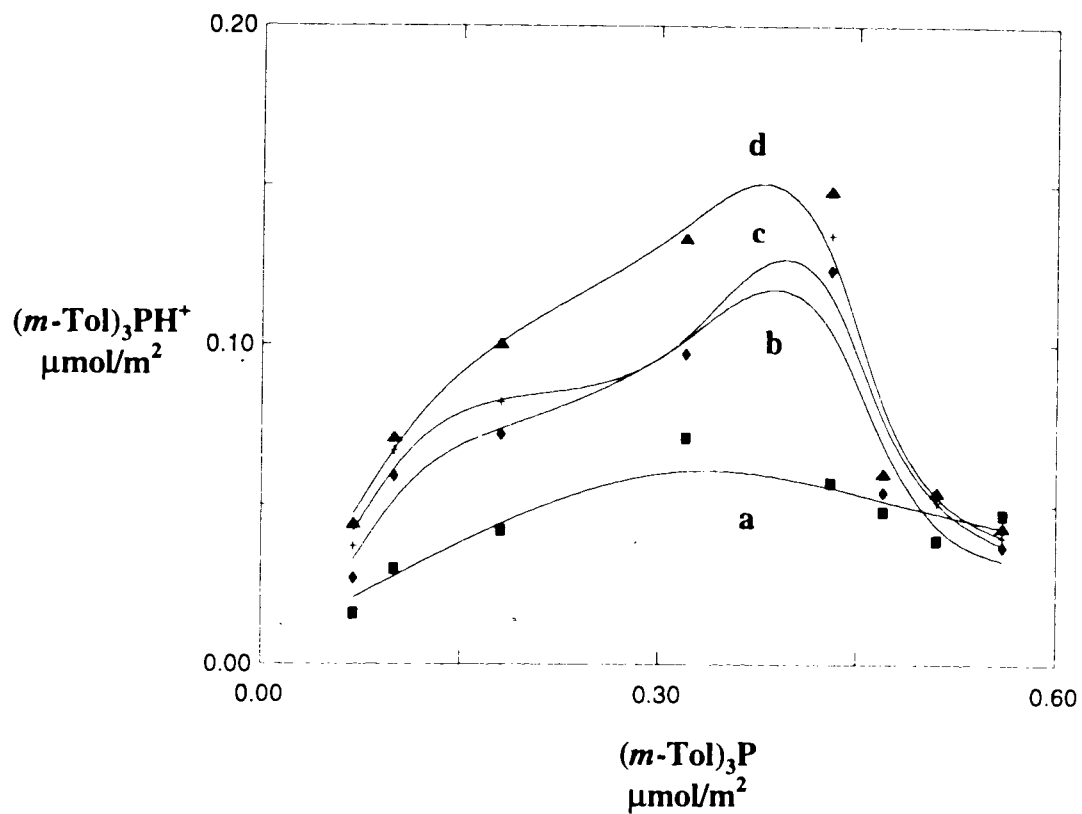


Figure 5.24 the concentrations of $(m\text{-Tol})_3\text{PH}^+$ on commercial silica-alumina catalyst at various coverages. a) 100°C one hour; b) 150°C one hour; c) 200°C one hour; and d) 200°C two hours

d $(p\text{-ClC}_6\text{H}_4)_3\text{P}$

Figure 5.25 shows the spectra of $0.16 \mu\text{mol}/\text{m}^2$ $(p\text{-ClC}_6\text{H}_4)_3\text{P}$ on the silica gel surface. It gave a resonance of -8.5 ppm, which was from the physically adsorbed species of $(p\text{-ClC}_6\text{H}_4)_3\text{P}$ species on the silica surface.

Figure 5.26 shows the spectra of $0.12 \mu\text{mol}/\text{m}^2$ $(p\text{-ClC}_6\text{H}_4)_3\text{P}$ on the silica-alumina surface recorded with various recycle delays. The protonated $(p\text{-ClC}_6\text{H}_4)_3\text{P}$ in concentrated HCl resonates at 4.4 ppm ($J_{\text{H-P}} = 391$ Hz), so the peaks around 4.3 ppm arise from Brønsted acid species. The resonances at -8.5 ppm were physically adsorbed phosphine, which were not far away from the resonances on the silica (Figure 5.25). The ratios of integrated areas between physically adsorbed species (-8.5 ppm) and Brønsted acid (4.3 ppm) were 0.69 , 0.73 and 0.70 for Figure 5.26a to 5.26c respectively. Thus the 1 s recycle delay is good enough to measure the acid concentration.

Figure 5.27 shows the spectra of $0.12 \mu\text{mol}/\text{m}^2$ $(p\text{-ClC}_6\text{H}_4)_3\text{P}$ on the silica-alumina catalyst surface with different adsorption temperatures. Similar to the other phosphines, more Brønsted acid species were observed at higher adsorption temperatures.

Figure 5.28 shows the spectra of $(p\text{-ClC}_6\text{H}_4)_3\text{P}$ on the silica-alumina surface with various surface coverages. Besides protonated and physically adsorbed $(p\text{-ClC}_6\text{H}_4)_3\text{P}$ species, three new peaks were also observed. They resonated around 23.2 , 26.0 and 42 ppm. The chemical shift of $(p\text{-ClC}_6\text{H}_4)_3\text{PO}$ was found to be around 23 or 22.7 ppm in solution¹⁴⁻¹⁵. Later, the sample was exposed to air for a long time (Figure 5.29b-5.29d). The resonances at 23 and 42 ppm still remained. Thus these species should be associated with the phosphine oxides. We also prepared the phosphines oxides

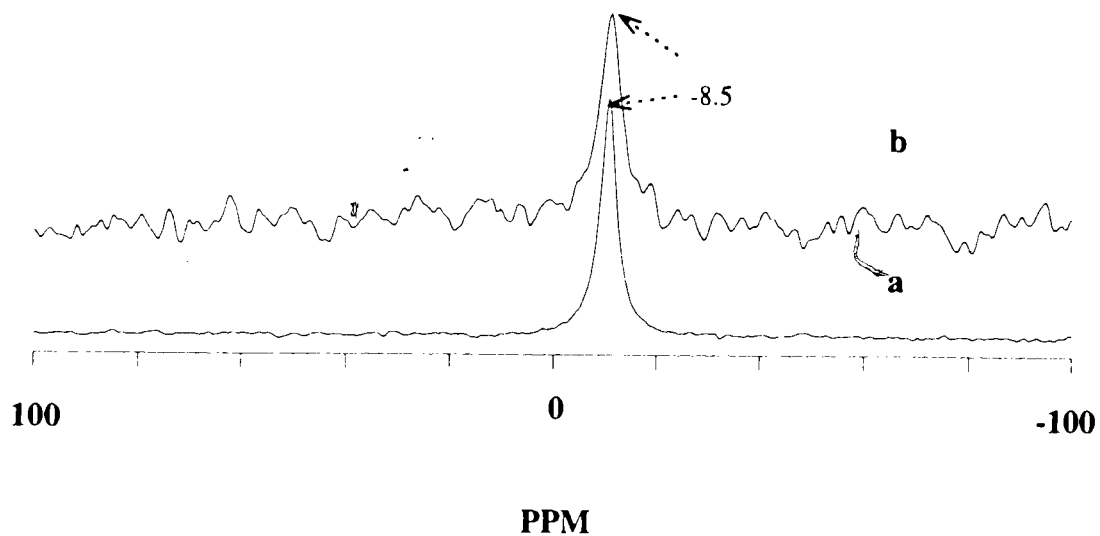


Figure 5.25 ^{31}P MAS NMR spectra of $0.16 \mu\text{mol}/\text{m}^2$ (*p*-ClC₆H₄)₃P on the silica gel surface, the silica was degassed at 450°C and 10^{-5} torr for two hours, adsorbed at 100°C for one hour, 1 s recycle delay. a) 90° pulse, 1.90 kHz MAS rate, 54878 scans; and b) cross-polarization flipback, 1.80 kHz, 1.80 kHz MAS rate, 7510 scans.

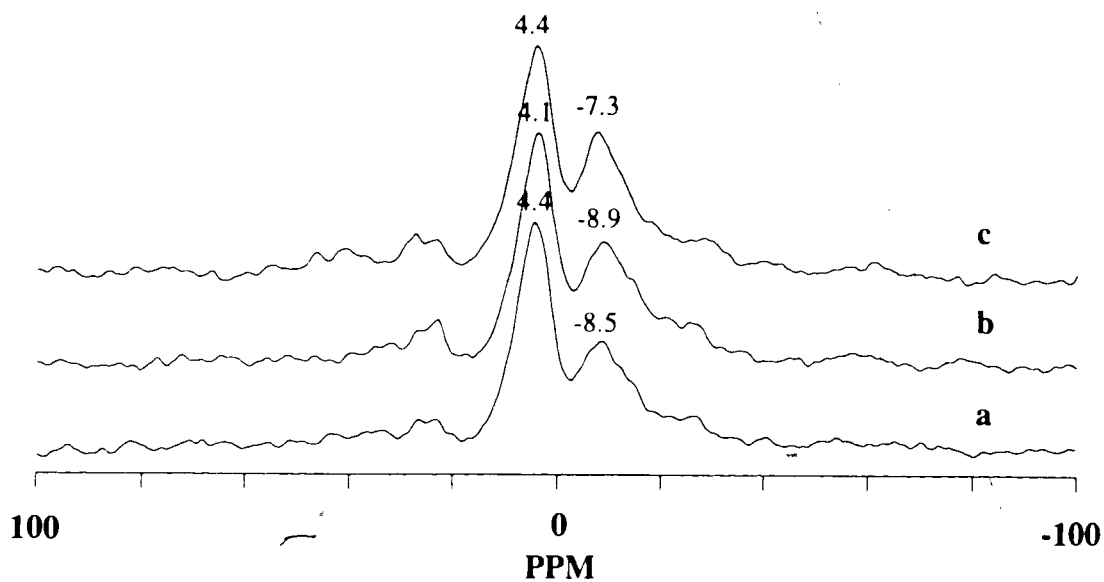


Figure 5.26 ^{31}P MAS NMR spectra of $0.12 \mu\text{mol}/\text{m}^2$ (*p*-ClC₆H₄)₃P on the silica-alumina surface with various recycle delays, the catalyst was degassed at 450°C and 10^{-5} torr for two hours, adsorption at 200°C for two hours, 90° pulse. a) 1.80 kHz MAS rate, 77560 scans, 1 s recycle delay; b) 1.80 kHz MAS rate, 35660 scans, 2 s recycle delay; and c) 2.03 kHz MAS rate, 33386 scans, 4 s recycle delays.

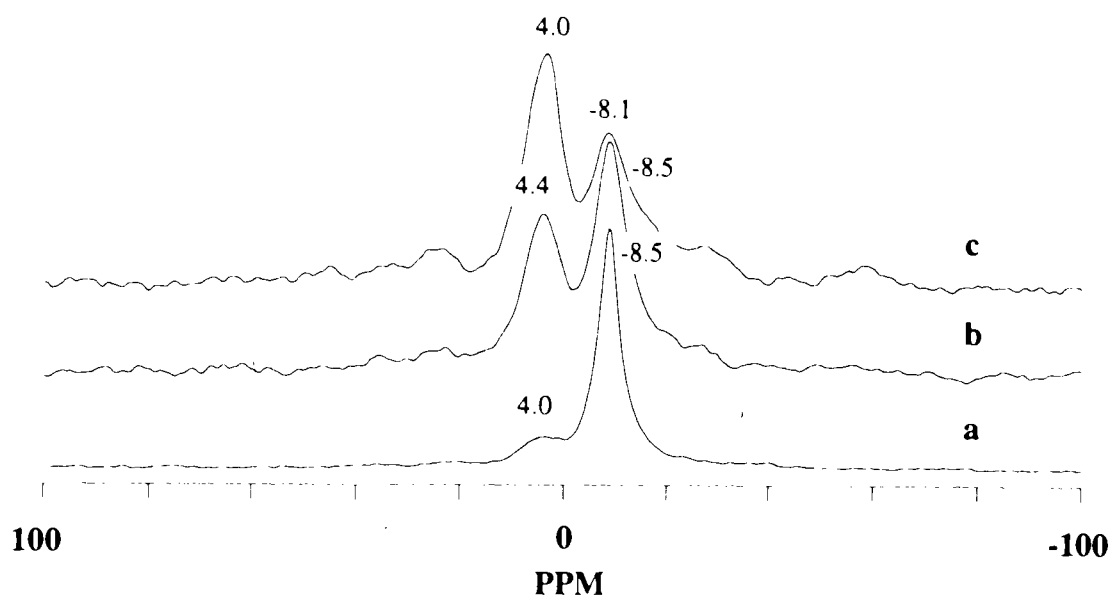


Figure 5.27 ^{31}P MAS NMR spectra of $0.12 \mu\text{mol}/\text{m}^2$ (*p*-ClC₆H₄)₃P on the silica-alumina surface with various adsorption temperatures, the catalyst was degassed at 450°C and 10^{-5} torr for two hours, 90° pulse, 1.85 kHz MAS rate, 2 s recycle delays. a) 100°C for one hour, 85930 scans; b) 150°C for one hour, 30256 scans; and c) 200°C for one hour, 45990 scans.

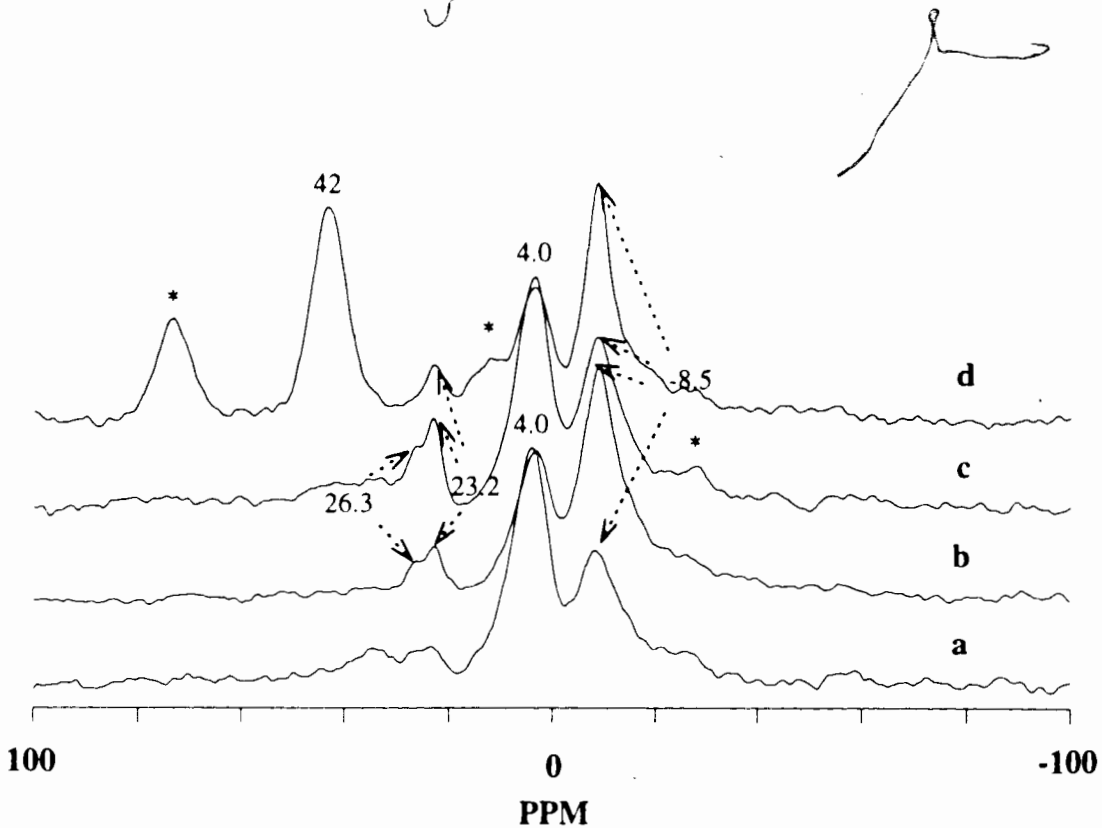


Figure 5.28 ^{31}P MAS NMR spectra of $(p\text{-ClC}_6\text{H}_4)_3\text{P}$ on the silica-alumina surface with various surface coverages, the catalyst was degassed at 450°C and 10^{-5} torr for two hours, adsorption at 200°C for one hour, 90° pulse, 1.83 kHz MAS rate, 1 s recycle delays. a) $0.12 \mu\text{mol}/\text{m}^2$, 64800 scans; b) $0.17 \mu\text{mol}/\text{m}^2$, 85900 scans; c) $0.24 \mu\text{mol}/\text{m}^2$, 55146 scans; and d) $0.28 \mu\text{mol}/\text{m}^2$, 27412 scans. *: spinning side bands.

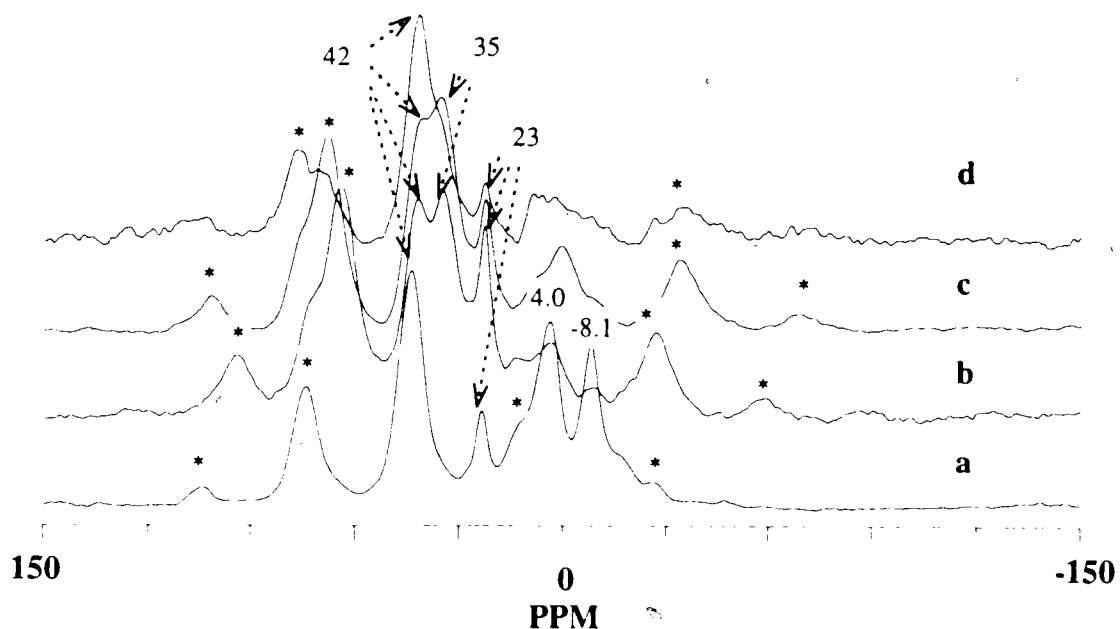


Figure 5.29 ^{31}P MAS NMR spectra of $0.28 \mu\text{mol}/\text{m}^2$ $(p\text{-ClC}_6\text{H}_4)_3\text{P}$ on the silica-alumina surface with various oxide species, the catalyst was initially degassed at 450°C and 10^{-5} torr for two hours, adsorbed at 200°C for one hour, sample was exposed in air for two years (if not specified), cross-polarization flipback (if not specified) 1 s recycle delay. a) sample was under vacuum, 1.83 kHz MAS rate, 56670 scans; b) 1.81 kHz MAS rate, 74662 scans; c) 2.04 kHz MAS rate, 167014 scans; and d) 90° pulse, 2.04 kHz MAS rate, 77916 scans.

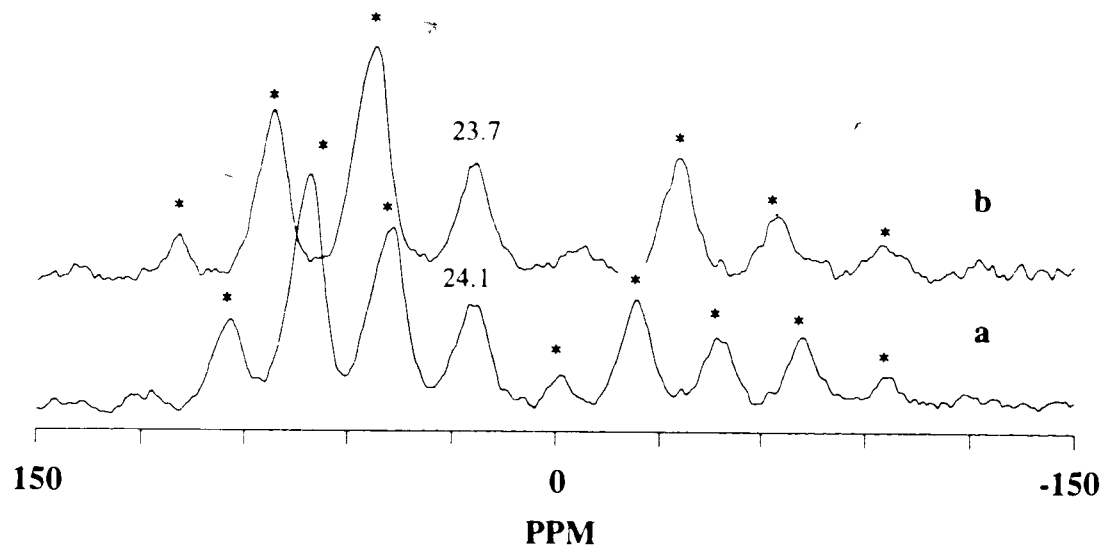


Figure 5.30 ^{31}P MAS NMR spectra of mixture of $(p\text{-ClC}_6\text{H}_4)_3\text{P}$ and Me_3NO heated at 200°C for half an hour, cross-polarization flipback, 1 s recycle delay. a) 1.42 kHz MAS rate, 165600 scans; and b) 1.76 kHz MAS rate, 61611 scans.

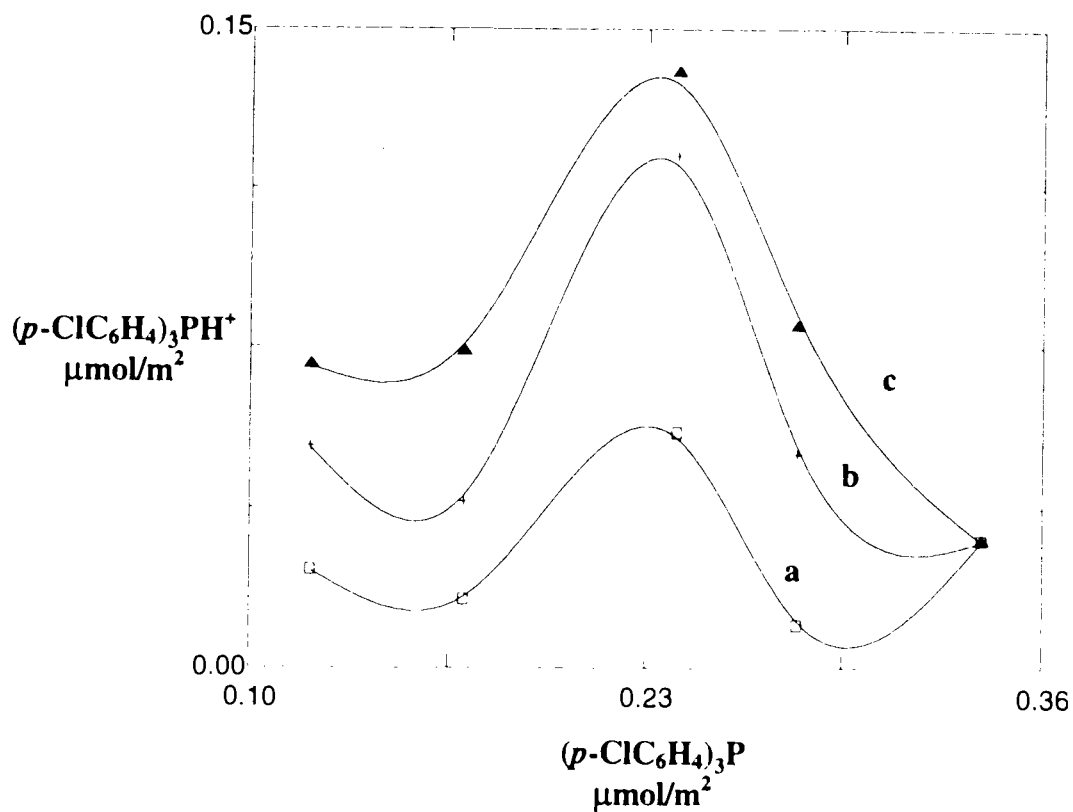


Figure 5.31 the concentrations of $(p\text{-ClC}_6\text{H}_4)_3\text{PH}^+$ on commercial silica-alumina catalyst at various coverages. a) 100°C one hour (\square); b) 150°C one hour ($+$); c) 200°C one hour (\blacktriangle).

by mixing (*p*-ClC₆H₄)₃P and Me₃NO in air (Figure 5.30). Again the 23.9 ppm peaks were found with a lot of spinning side bands. In reference³, 40 ppm (physically adsorbed and crystalline species), 53 ppm (Lewis acid sites) and 65 ppm (Brønsted acid site) were assigned for species of (CH₃)₃PO on the silica-alumina surface. Similarly, 50 ppm (physically adsorbed species and crystalline species), 63 ppm (Lewis acid species) and 76 ppm (Brønsted acid site) were also assigned as the various (C₂H₅)₃PO species on the silica-alumina surfaces. Combining all this information, we assigned the resonances of 23 ppm to be multilayer physically adsorbed (*p*-ClC₆H₄)₃PO species (crystalline species probably not present at the 0.2 μmol/m² coverages), 26 ppm to be monolayer physically adsorbed (*p*-ClC₆H₄)₃PO species, and 42 ppm to be Brønsted acid sites of (*p*-ClC₆H₄)₃PO species. The resonances at 35 ppm in Figure 5.29 b to 5.29 d may arise from the Lewis acid sites of (*p*-ClC₆H₄)₃PO. The Lewis acid sites could be penetrated by (*p*-ClC₆H₄)₃PO molecules during these two years period. (*p*-ClC₆H₄)₃PO seems good to measure the Lewis acid sites on the surface. We can solve the troubles of spinning side bands by using faster MAS rates or TOSS experiments. If (*p*-ClC₆H₄)₃PO is put on the surface, the spinning side bands may be smaller since the mobility of adsorbed species could be increased.

Figure 5.31 summarizes the results for the variation of (*p*-ClC₆H₄)₃PH⁺ concentration with the coverages at various adsorption temperatures. The maximum Brønsted acid concentration of (*p*-ClC₆H₄)₃PH⁺ is around 0.12 μmol/m² in Figure 5.31c. As observed for other aryl phosphine molecules, a genuine decrease of Brønsted acid species at higher coverages was observed. Compared with the other three aryl phosphines, the apparent maximum Brønsted acid concentration with (*p*-ClC₆H₄)₃P was intermediate for these three probes (0.17 μmol/m² with Ph₃P in Figure 5.8, 0.09 μmol/m² with (*p*-Tol)₃P in Figure 5.17 and 0.15 μmol/m² with (*m*-Tol)₃P in Figure 5.24). (*p*-ClC₆H₄)₃P is the weakest base among these phosphines (Table 3.1, chapter 3). The cone angle of

$(p\text{-ClC}_6\text{H}_4)_3\text{P}$ is also equal to 145° . Again, among these aryl phosphine probes, the apparent maximum Brønsted acid concentration is controlled by steric effects. The $(p\text{-ClC}_6\text{H}_4)_3\text{P}$ seems to access the Brønsted acid sites more easily than $(p\text{-Tol})_3\text{P}$. However, $(p\text{-ClC}_6\text{H}_4)_3\text{P}$ is still more hindered than $(m\text{-Tol})_3\text{P}$ and Ph_3P .

e. (*o*-Tol)₃P

Figure 5.32 shows spectra of pure (*o*-Tol)₃P sample and (*o*-Tol)₃P in concentrated HCl. It is interesting to observe two resonances at -27.2 and -32.8 ppm for the pure sample (Figure 5.32a), which arise from two magnetically different sites in the unit cell of the crystalline species. (*o*-Tol)₃P in concentrated HCl resonated at -12.9 ppm, which will help to locate the Brønsted acid species on the catalyst surface.

Figure 5.33 shows the spectra of (*o*-Tol)₃P on the silica gel. The physically adsorbed species resonate at -29.8 ppm, consistently with different adsorption temperatures and pulse programs.

Figure 5.34 shows the spectra of 0.17 μmol/m² (*o*-Tol)₃P on the alumina surface obtained with different pulse programs. The right peaks at -28.3 ppm, close to the value (-29.8 ppm) on the silica gel in Figure 5.33, arise from physically adsorbed species. The left peaks around -8 ppm peak are suggested to be Lewis acid species, since the dipolar dephasing sequence (Figure 5.34c) did not discriminate against this peak. The ratios of peak heights for physically adsorbed and Lewis acid species are 5.3 and 4.9 for Figure 5.34c and 5.34 b respectively. The two ratios are close to each other. The -8 ppm in Figure 5.34a was less visible using the 90° pulse program. This could be explained by a) discrimination against physically adsorbed species using cross polarization experiments; or b) the different T₁ values between Lewis acid and physically adsorbed species. The Lewis acid complex is probably closer to the surface (and hydroxyl groups at the same time) than the physically adsorbed species. Hence cross polarization may discriminate against the physically adsorbed species. A recycle delay of 2 s was used in figure 5.34a. This value probably did not reflect the real distribution of these two species in the alumina surface (see Figure 4.8, chapter 4). Since Lewis acid species have a longer

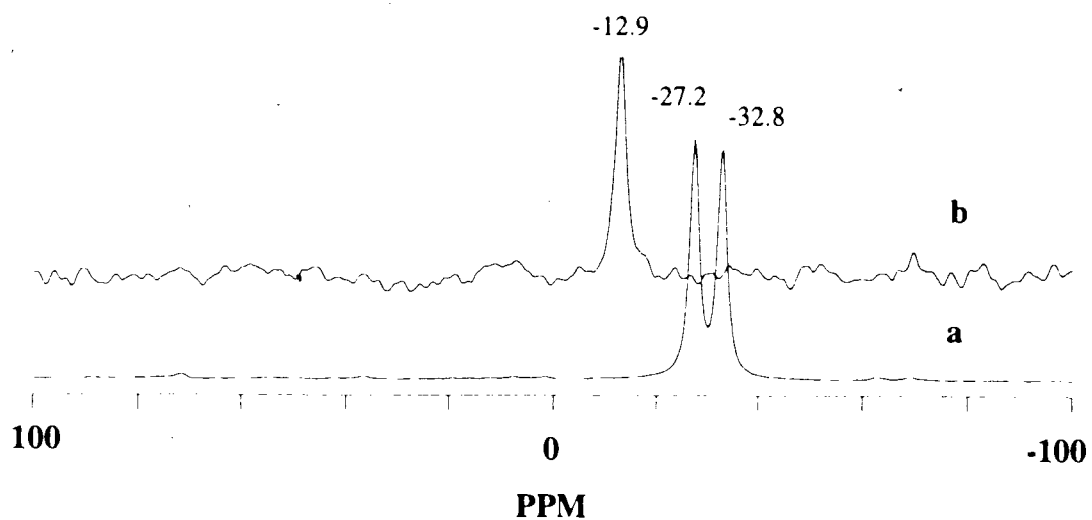


Figure 5.32 ^{31}P MAS NMR spectra of pure (*o*-Tol) $_3\text{P}$ sample and (*o*-Tol) $_3\text{P}$ in the concentrated HCl, 2 s recycle delay. a) pure sample, cross-polarization flipback, 2.13 kHz MAS rate, 3000 scans; and b) in HCl, 90° pulse, 1000 scans.

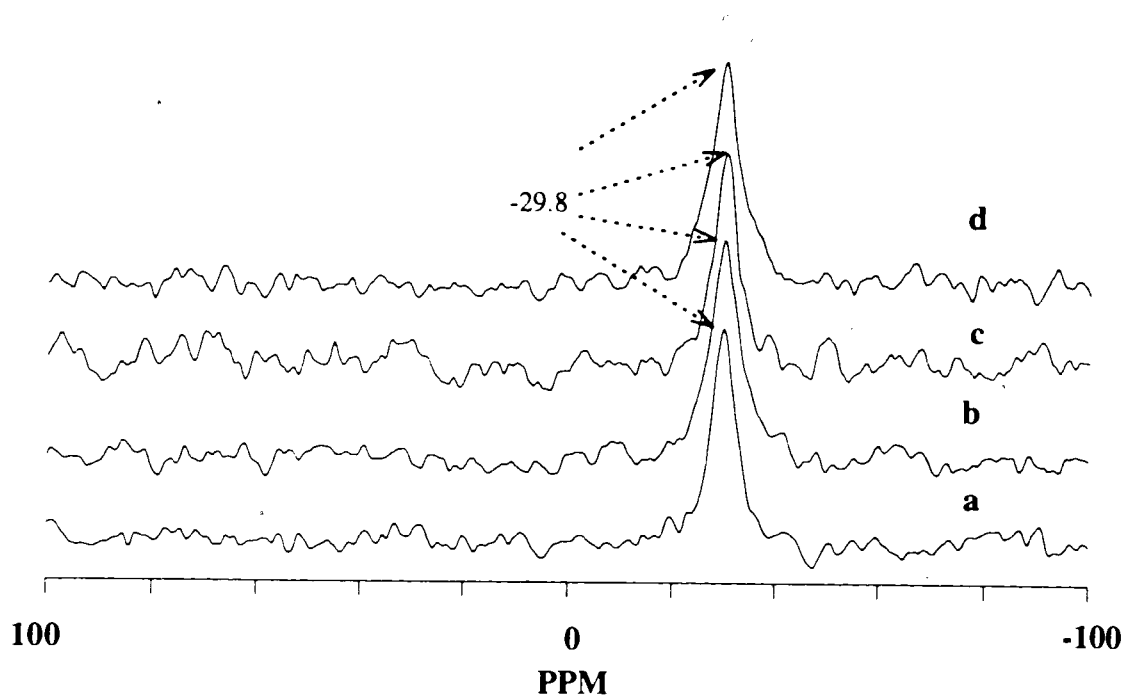


Figure 5.33 ^{31}P MAS NMR spectra of $0.08 \mu\text{mol}/\text{m}^2$ (*o*-Tol) $_3\text{P}$ on the silica gel surface with different adsorption temperatures, the silica was degassed at 450°C and 10^{-5} torr for two hours, 2 s recycle delay. a) 100°C , one hour, 90° pulse, 2.07 kHz MAS rate, 25210 scans; b) 100°C one hour, cross-polarization flipback, 2.08 kHz MAS rate, 5000 scans; c) 150°C one hour, 90° pulse, 1.78 kHz MAS rate, 5000 scans; and d) 150°C one hour, cross-polarization flipback, 1.78 kHz MAS rate, 3000 scans.

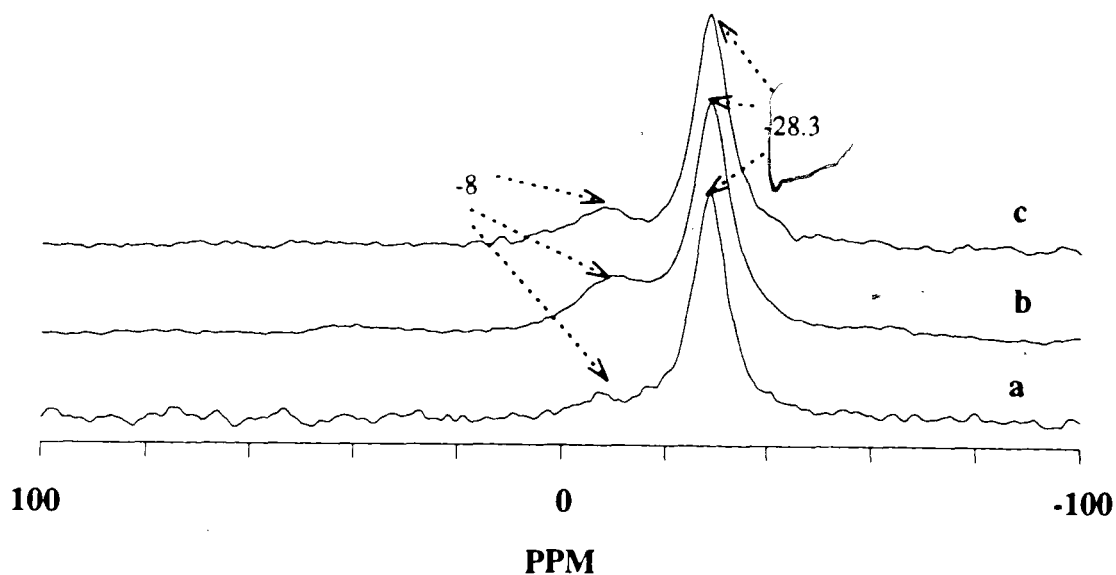


Figure 5.34 ^{31}P MAS NMR spectra of $0.17 \mu\text{mol}/\text{m}^2$ (*o*-Tol) $_3\text{P}$ on the alumina surface with different pulse programs, the alumina was degassed at 450°C and 10^{-5} torr for two hours, adsorbed at 100°C for one hour, 2 s recycle delay. a) 90° pulse, 2.08 kHz MAS rate, 5000 scans; b) cross-polarization flipback, 2.09 kHz MAS, 31480 scans; and c) dipolar dephasing sequence, $70 \mu\text{s}$ delay, 1.87 kHz MAS rate, 28750 scans.

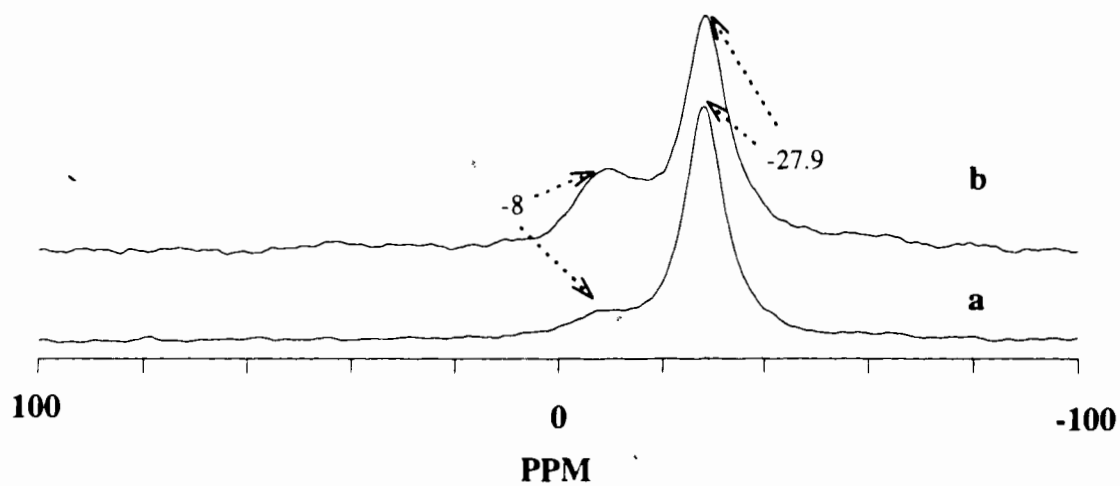


Figure 5.35 ^{31}P MAS NMR spectra of $0.35 \mu\text{mol}/\text{m}^2$ (*o*-Tol) $_3\text{P}$ on the alumina surface, the alumina was degassed at 450°C and 10^{-5} torr for two hours, adsorbed at 100°C for one hour, 2.04 kHz MAS rate, 2 s recycle delay. a) 90° pulse, 82530 scans; b) cross-polarization flipback, 32560

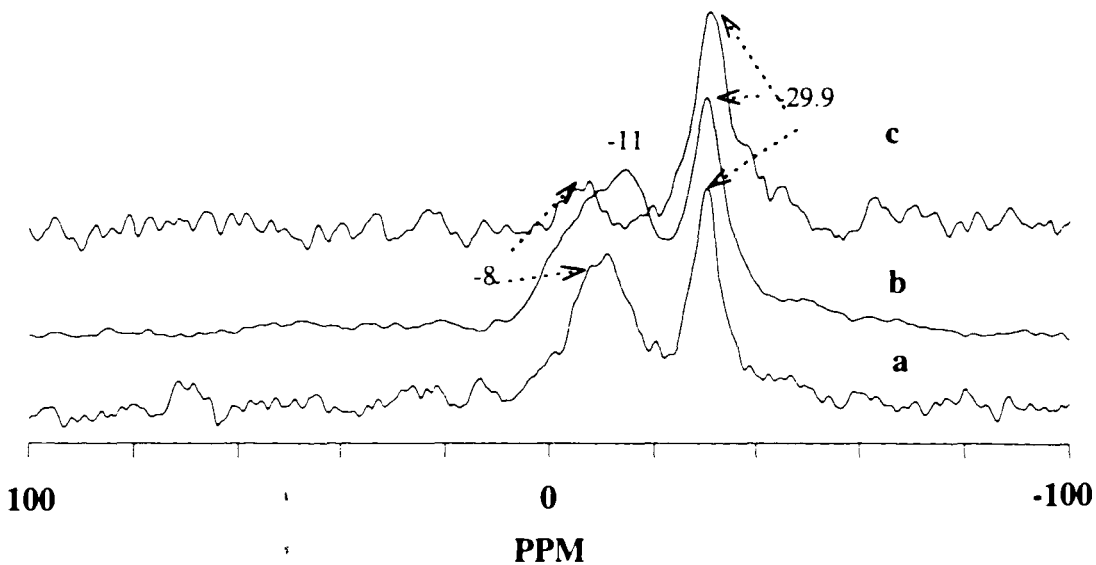


Figure 5.36 ^{31}P MAS NMR spectra of $0.13 \mu\text{mol}/\text{m}^2$ (*o*-Tol) $_3\text{P}$ on the silica-alumina surface with different pulse programs, the catalyst was degassed at 450°C and 10^{-5} torr for two hours, adsorbed at 100°C for one hour, 2.05 kHz MAS rate, 2 s recycle delay. a) 90° pulse, 10000 scans; b) cross-polarization flipback, 28830 scans; and c) dipolar dephasing sequence, 70 μs delay, 3000 scans.

T_1 , less of these molecules were found in Figure 5.34a. However, the spectra of cross-polarization do not depend on ^{31}P T_1 values, so more Lewis acid appeared in figure 5.34b and 5.34c. Using a different coverage of (*o*-Tol) $_3\text{P}$ on the alumina surface (Figure 5.35), similar results were observed.

Figure 5.36 shows the spectra of $0.13 \mu\text{mol}/\text{m}^2$ (*o*-Tol) $_3\text{P}$ on the silica-alumina surface obtained with different pulse programs. The resonance at -29.9 ppm is from the physically adsorbed species, the same as value on the silica (Figure 5.33). The peak around -8 ppm in Figure 5.36a actually consists of overlapping peaks of two kinds of species: Brønsted acid and Lewis acid species. The Brønsted acid species were around -11 ppm, close to -12.9 ppm of the protonated species in HCl (Figure 5.32b). This is confirmed by the spectra in Figure 5.36b and 5.36c. In Figure 5.36b, cross-polarization flipback favors the protonated species, so the -11 ppm peak is prominent. Conversely, the dipolar dephasing sequence in Figure 5.36c discriminates against the protonated species, the -11 ppm peak disappeared and only the -8 ppm (Lewis acid species) peak was left. These results suggest that (*o*-Tol) $_3\text{P}$ is not a good probe, since it cannot easily differentiate between Brønsted acid and Lewis acid sites. It seems that (*o*-Tol) $_3\text{P}$ is easier to approach the Lewis acid sites than the other aryl phosphines. Because this phosphine has a higher value for the cone angle (194°)¹⁶, the different size of the molecules may make the difference. Since the crystal structure of this compound is not found in the literature, an unambiguous explanation cannot be made.

f. Me₂PhP

Figure 5.37 shows the spectra of liquid Me₂PhP and Me₂PhP in HCl. The resonance of protonated species was at -0.7 ppm, with a 512 Hz J_{P-H} coupling.

Figure 5.38 shows the spectra of 2.04 μmol/m² Me₂PhP on the silica gel. The physically adsorbed species resonated at -45.7 ppm on the silica.

Figure 5.39 shows the spectra of 1.01 μmol/m² Me₂PhP on the alumina surface. The peaks around -37.9 should be the Lewis acid species. The resonances were broader than those on the silica gel and the chemical shifts were different.

Figure 5.40 and 5.41 shows the spectra of Me₂PhP on the silica-alumina catalyst surface with two surface coverages. The left peaks around -0.5 ppm (in Figure 5.40a, 5.40b, 5.41a and 5.41b) were the Brønsted acid species, close to the -0.7 ppm of protonated phosphine in HCl (Figure 5.37). This is further confirmed by dipolar dephasing in Figure 5.40c and 5.41c. The resonances at -44.4 ppm in Figure 5.41 were from physically adsorbed species, close to the -45.7 ppm of the same species on the silica (Figure 5.38). The slight difference of chemical shifts was probably due to exchange phenomenon, which had previously been suggested using Me₃P probe². The Lewis acid species were not found in Figure 5.41. In Figure 5.40, the chemical shifts around -36.4 ppm were also from the physically adsorbed species, otherwise the Lewis acid sites would appear in Figure 5.41. Similar to Me₃P², the values of chemical shift for this peak shifted further toward the direction of the Brønsted acid peak with a lower surface coverage.

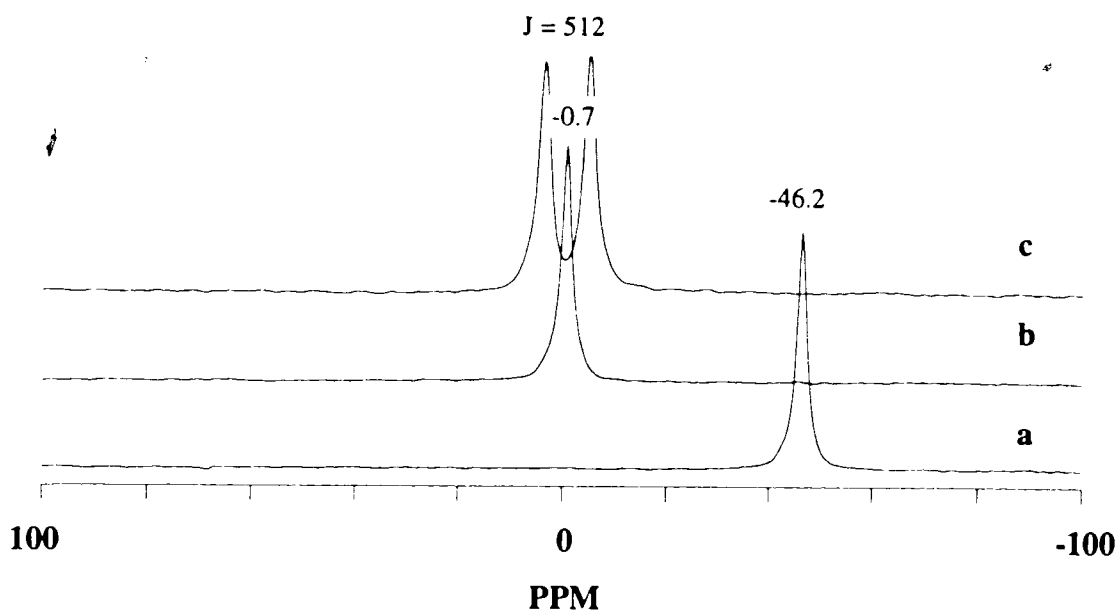


Figure 5.37 ^{31}P MAS NMR spectra of liquid Me_2PhP sample, 90° pulse, 2 s recycle delay. a) pure sample, 1000 scans; b) in concentrated HCl , 1000 scans; and c) in HCl , decoupler off, 2000 scans

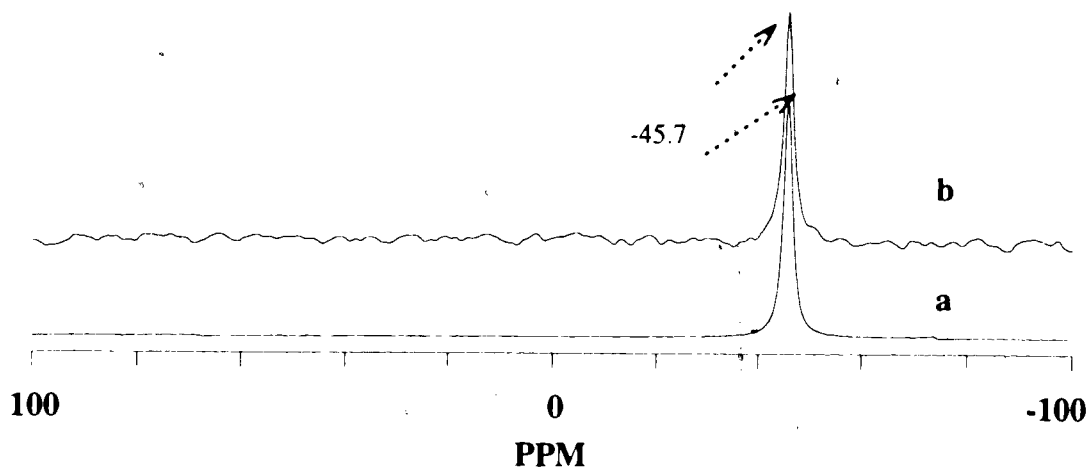


Figure 5.38 ^{31}P MAS NMR spectra of $2.04 \mu\text{mol}/\text{m}^2$ Me_2PhP on silica gel, the silica was degassed at 450°C and 10^{-5} torr for two hours, 1.80 kHz MAS rate, 2 s recycle delay. a) 90° pulse, 200 scans; and b) cross-polarization flipback, 300 scans.

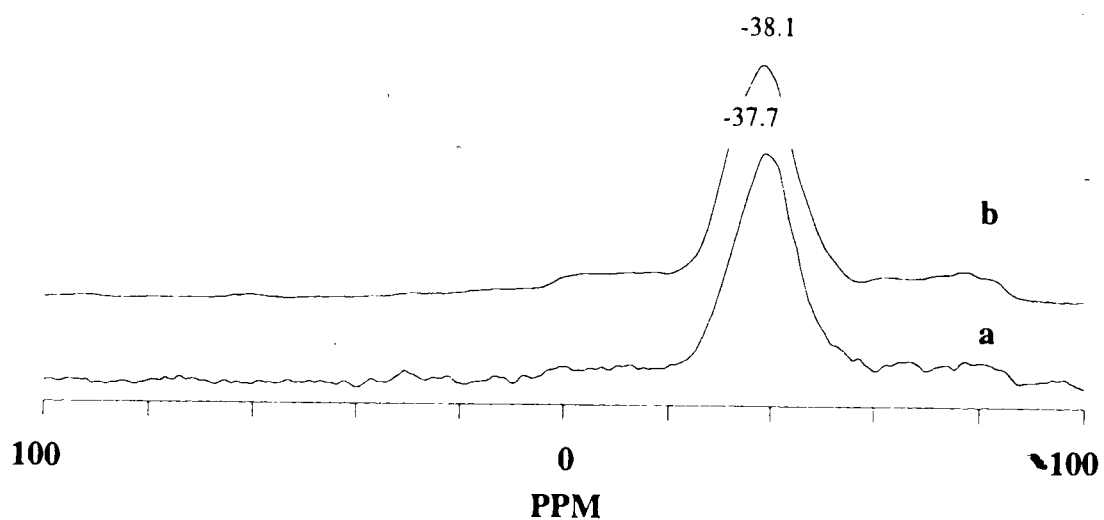


Figure 5.39 ^{31}P MAS NMR spectra of $1.01 \mu\text{mol}/\text{m}^2$ Me_2PhP on the alumina surface, the alumina was degassed at 450°C and 10^{-5} torr for two hours, 1.81 kHz MAS rate, 2 s recycle delay. a) 90° pulse, 2000 scans; and b) cross-polarization flipback, 20580 scans.

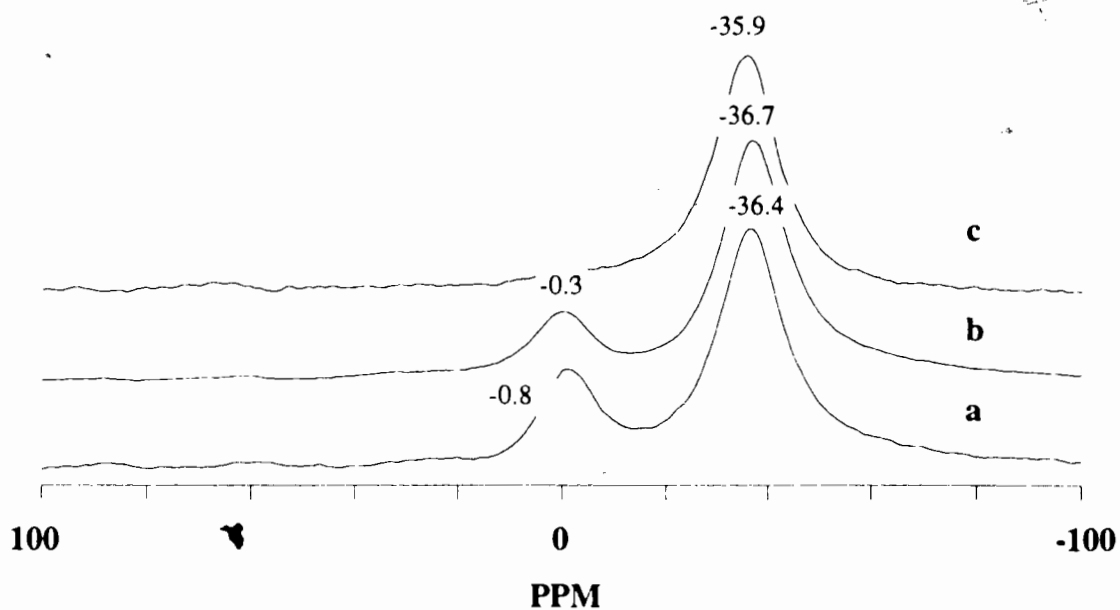


Figure 5.40 ^{31}P MAS NMR spectra of $0.91 \mu\text{mol}/\text{m}^2$ Me_2PhP on the silica-alumina surface with difference pulse sequences, the catalyst was degassed at 450°C and 10^{-5} torr for two hours, 1.80 kHz MAS rate, 2 s recycle delay. a) cross-polarization flipback, 2800 scans; b) 90° pulse, 23900 scans; and c) dipolar dephasing, 2000 scans.

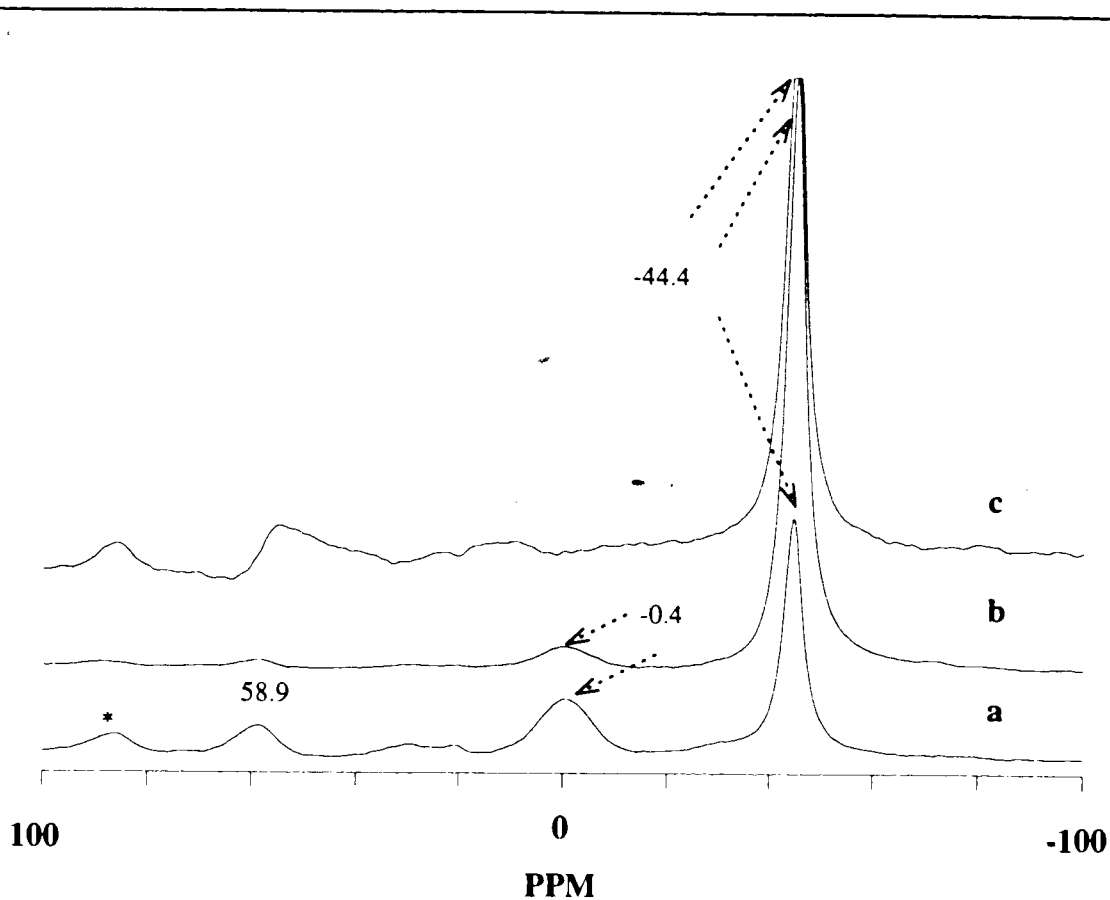


Figure 5.41 ^{31}P MAS NMR spectra of $1.51 \mu\text{mol}/\text{m}^2$ Me_2PhP on the silica-alumina surface with difference pulse sequences, the catalyst was degassed at 450°C and 10^{-5} torr for two hours, 1.80 kHz MAS rate, 2 s recycle delay. a) cross-polarization flipback, 2000 scans; b) 90° pulse, 1500 scans; and c) dipolar dephasing, 2000 scans. (58.9 ppm was from phosphine oxide)
 *= spinning sidebands.

3. Conclusion

Several new aryl phosphine ^{31}P NMR probes (including triparatolylphosphine, trimetatolylphosphine, triphenylphosphine and triparachlorophenylphosphine) have been employed to study surface acidity on silica, alumina and silica-alumina catalyst surfaces. It was found that the phosphines rotate on the surface and that the motions are nearly isotropic. Due to the motions of triphenylphosphine on SiO_2 , the spinning side band intensities have been reduced over 95%. Lewis sites have been detected on alumina by all these phosphines and on the silica-alumina catalyst by triphenylphosphine and triorthotolylphosphine. On the silica-alumina catalyst, the concentrations of Brønsted acid sites were calculated. They appeared to increase on raising the adsorption temperature. At higher coverages a genuine decrease of Brønsted acid was observed from the titration curves. This phenomenon was explained by the presence of a multilayer of physically adsorbed species at higher coverages. At 200°C , using triparatolylphosphine, triparachlorophenylphosphine, trimetatolylphosphine and triphenylphosphine the maximum concentrations of Brønsted acid found are 0.09, 0.13, 0.15 and $0.17 \mu\text{mol}/\text{m}^2$ respectively. These values were controlled by the steric effects.

For quantitative analysis on the silica-alumina surface, a 1 s recycle delay is an excellent choice for efficient noise averaging. However, on the alumina surface, 8 s to 16 s recycle delays have to be used. This is due to paramagnetic impurities in the silica-alumina sample. For this sample, 0.05% Fe_2O_3 (Wt) is present. It will hasten the relaxation processes. The bad aspect is that the peak becomes broad at the same time (T_2 decreases). Mobility of the surface species will affect the T_1 values too. We got a value of 22 s for the crystalline Cy_3P sample. When the phosphines are put on the surface, the motions will greatly reduce the T_1 . On the silica gel, a value of 1.6 s was found for PCy_3 's T_1 .

5. References:

1. J. H. Lunsford, W. P. Rothwell, and W. X. Shen, *J. Am. Chem. Soc.*, **107**, 1540 (1985).
2. T. C. Sheng, and I. D. Gay, *J. Catal.* **145**, 10 (1994).
3. L. Baltusis, J. S. Frye, and G. E. Maciel, *J. Am. Chem. Soc.*, **108**, 7119 (1986).
4. L. Baltusis, J. S. Frye, and G. E. Maciel, *J. Am. Chem. Soc.*, **109**, 40 (1987).
5. B. Hu, and I. D. Gay, *Langmuir*, **11**, 3845 (1995).
6. M. N. Golovin, M. M. Rahman, J. E. Belmonte, and W. D. Giering, *Organometallics*, **4**, 1981 (1985).
7. M. V. Forward, S. T. Bowden, and W. J. Jones, *J. Chem. Soc.*, **3**, S121 (1949).
8. A. A. Grigorev, Y. V. Konchraelev, and A. V. Siworov, *Zh. Obsch. Kh.*, **54**, 1935 (1984).
9. I. D. Gay, *J. Magn. Reson.* **58**, 413 (1984).
10. L. Clark, H. C. Bemi, J. A. Davis, C. A. Fyfe, and R. E. Wasylshen, *J. Am. Chem. Soc.*, **104**, 438 (1982).

11. G. H. Penner, and R. E. Wasylshen, *Can. J. Chem.*, **67**, 1909 (1989).
12. J. Herzfeld, and A. E. Berger, *J. Chem. Phys.*, **73** (12), 6021 (1980).
13. T. Allman, and R. G. Goel, *Can. J. Chem.*, **60**, 716 (1982).
- 13a. J. J. Daly, *J. Chem. Soc.*, 3799 (1964).
14. J. R. Van Wazer, C. F. Callis, J. N. Shoolery, and R. C. Jones, *J. Am. Chem. Soc.*, **78**, 5715 (1956).
15. R. A. Y. Jones and A. R. Katritzky, *Angew. Chem.*, **74**, 60 (1962).
16. C. A. Tolman, *Chem. Rev.*, **77**, No 3, 313 (1977).

Chapter 6 ^{31}P NMR investigation of surface acidity to vapor deposited SiO_2 on Al_2O_3 monolayer catalyst: application to novel catalyst system

1. Introduction

The novel catalysts consisting of SiO_2 on Al_2O_3 monolayer have been prepared by chemical vapor deposition¹⁻³. Compared with mixed oxides made by precipitation, such catalysts possess simple structures. These catalysts will help in understanding the acid properties generated at the interface of the oxides. A simple kinetic model has been proposed to explain the evolution of Brønsted acid concentration as a function of deposited silica. These catalysts permit the development of a controlled level of Brønsted acidity on the catalyst surface. Also, a thin SiO_2 layer on zeolite has been used to control the pore-opening size⁴.

Smaller phosphines and phosphine oxides have been used successfully as probes to study the acidity of silica-alumina catalysts⁵⁻⁶. Recently, we have chosen bulky phosphines to count the acid sites and check steric factors on the commercial silica-alumina cracking catalyst surface (Chapter 4 and 5). In this chapter, three typical phosphines were used as probes to characterize SiO_2 on Al_2O_3 monolayer catalysts prepared by chemical vapor deposition. Triphenylphosphine has a bulky structure⁷ and weak basic strength ($\text{p}K_{\text{a}}=2.73$). Trimethyl phosphine is a small molecule and strong base ($\text{p}K_{\text{a}}=8.65$). Tricyclohexylphosphine is bulky and the strongest base among these three phosphines ($\text{p}K_{\text{a}}=9.70$) (Chapter 3). Brønsted acid concentrations were measured by these phosphines under different treatment temperatures. It is interesting to use these three phosphines to measure the acidity on this monolayer catalyst and later compare the properties with commercial SiO_2 - Al_2O_3 catalyst. We detected more Brønsted acid species on the Al_2O_3 monolayer catalyst of 6.2 SiO_2 per nm^2 than on the commercial silica-

alumina catalyst (25% Al₂O₃). Also the other unique properties of Al₂O₃ monolayer catalyst were observed, which might be partly due to the fact that Al₂O₃ monolayer catalyst has a larger pore diameter than the commercial silica-alumina catalyst.

2. Results and Discussion

a. Ph₃P

Figure 6.1 shows the spectra of 0.40 μmol/m² Ph₃P on the Al₂O₃ catalyst of 6.2 SiO₂ per nm² obtained with different pulse sequences. The peak of "physically adsorbed" species on SiO₂ and SiO₂-Al₂O₃ commercial catalyst was around -5.7 and -6.0 ppm respectively (Chapter 5). So the right hand peaks around -5.2 ppm are mainly due to physically adsorbed species. The left hand peaks around 5.3 ppm are the Brønsted acid species confirmed by the delayed-decoupled program (Figure 6.1a). The 5.1 ppm for Brønsted acid species is different from 7.2 ppm on the SiO₂-Al₂O₃ commercial catalyst (Chapter 5). The reproducibility of chemical shift measurements on different days is better than 0.4 ppm, suggesting that the surface environment for a catalyst prepared by chemical vapor deposition is different from the commercial SiO₂-Al₂O₃ catalyst.

Figure 6.2 shows the spectra of 0.40 μmol/m² Ph₃P on the monolayer Al₂O₃ catalyst of 6.2 SiO₂ per nm² adsorbed at 200°C for one hour with different recycle delays. The integrated results show that the ratios of physically adsorbed species (-5.3 ppm) and Brønsted acid sites (5.3 ppm) were 2.3, 2.2 and 2.2 respectively for Figure 6.2a to 6.2c. These ratios were almost the same, so 1 s recycle delay should be good for this quantitative measurement. More paramagnetic elements (Fe) are present on the silica-

alumina. (0.05% Fe₂O₃ is in the silica-alumina catalyst, but <100 ppm in the alumina from manufacturers' analysis).

Figure 6.3 shows the spectra of 0.40 μmol/m² Ph₃P on Al₂O₃ monolayer catalyst with 6.2 SiO₂ per nm², with different adsorption temperatures. The Brønsted acid concentrations were calculated as 0.15, 0.16 and 0.16 μmol/m² for Figure 6.3a to 6.3c respectively. The Brønsted acid concentrations are almost the same with different temperatures, whereas for the same phosphine probe on the commercial SiO₂-Al₂O₃ catalyst they are different (Chapter 5). The monolayer Al₂O₃ catalyst has almost the same surface area (228 m²/g) as original γ-Al₂O₃ (225 m²/g). So it is reasonable to assume that they have similar pore size distributions. Therefore the Al₂O₃ monolayer catalyst has about 2-fold larger pores than the commercial silica-alumina catalyst. This suggests the diffusion on the Al₂O₃ monolayer catalyst should be much easier.

Figure 6.4 shows the spectra of Ph₃P on Al₂O₃ monolayer catalyst of 6.2 SiO₂ per nm², with different coverages. The adsorption temperature was 200°C. The Brønsted acid concentrations decreased at higher coverages (Figure 6.4c and 6.4d). Figure 6.4 d was amplified to show a small amount of Brønsted acid was detected at this coverage. A similar titration curve was observed for the commercial SiO₂-Al₂O₃ catalyst using the same Ph₃P probe (Chapter 5). The titration curves at each adsorption temperature are plotted in Figure 6.5.

Figure 6.5 shows the titration concentrations of Ph₃PH⁺ on Al₂O₃ monolayer catalyst with 6.2 SiO₂ per nm² at various coverages. Compared with the commercial SiO₂-Al₂O₃ catalyst (Figure 5.8, chapter 5), the maximum Brønsted acid concentration for these two kinds of catalysts are roughly the same (around 0.16-0.17 μmol/m²). At different adsorption temperatures, the titration curves of Al₂O₃ monolayer catalyst were

almost identical. However, the Brønsted acid concentrations increased with adsorption temperatures for the commercial silica-alumina catalyst. This suggests diffusion on the Al_2O_3 monolayer catalyst should be much easier than the commercial catalyst. A 100°C temperature is high enough for Ph_3P molecules to approach Brønsted acid sites.

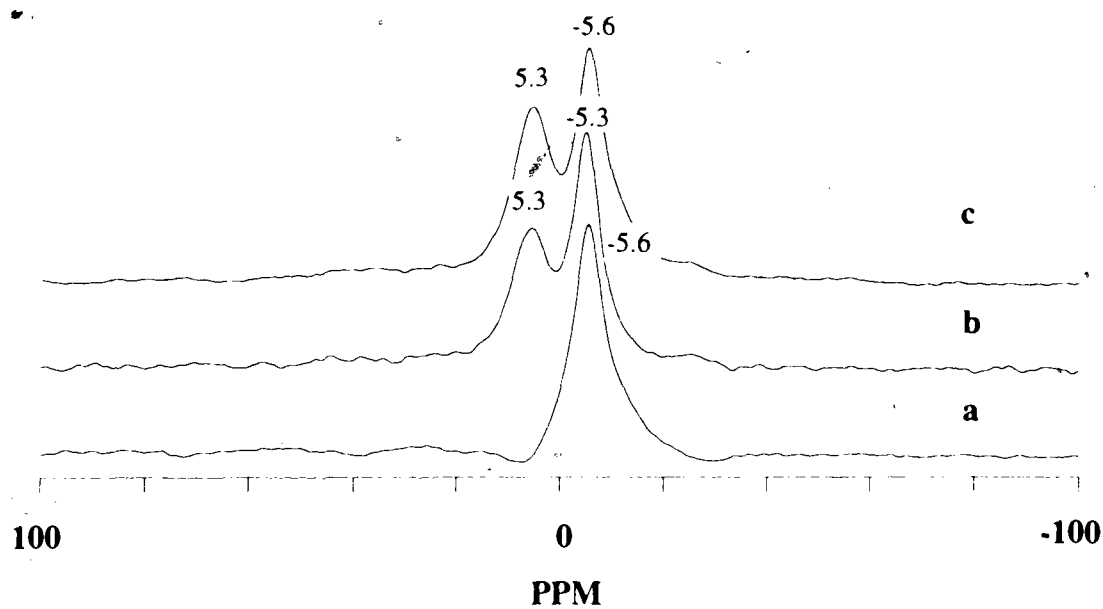


Figure 6.1. ^{31}P MAS NMR spectra of $0.40 \mu\text{mol}/\text{m}^2$ Ph_3P on Al_2O_3 catalyst with 6.2 SiO_2 per nm^2 with different pulse sequences, the monolayer catalyst was degassed at 450°C and 10^{-5} torr for two hours, PPh_3 adsorbed at 200°C for one hour, 1 s recycle delay. a) dipolar dephasing sequence, 1.8 kHz MAS rate, 99518 scans; b) 90° pulse, 1.90 kHz MAS rate, 16900 scans; and c) cross-polarization flipback, 1.80 kHz MAS rate, 81300 scans.

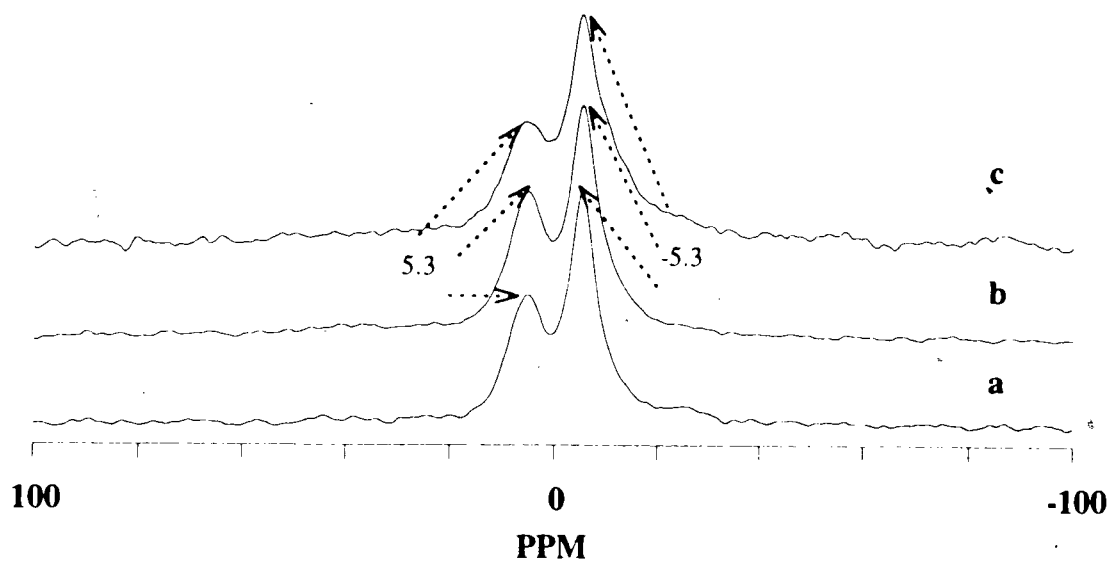


Figure 6.2 ^{31}P MAS NMR spectra of $0.40 \mu\text{mol}/\text{m}^2$ Ph_3P on Al_2O_3 catalyst with 6.2 SiO_2 per nm^2 obtained with different recycle delays, the monolayer catalyst was degassed at 450°C and 10^{-5} torr for two hours, PPh_3 adsorbed at 200°C for one hour, 90° pulse. a) 1.90 kHz MAS rate, 1 s recycle delay, 16900 scans; b) 1.90 kHz MAS rate, 4 s recycle delay, 14418 scans; and c) 1.72 kHz MAS rate, 16 s recycle delay, 7534 scans.

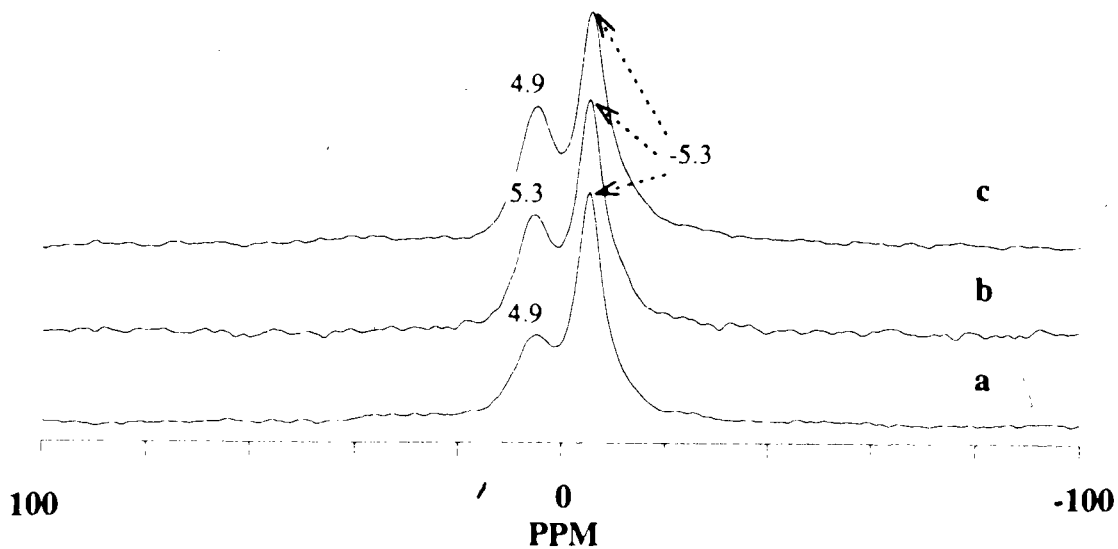


Figure 6.3 ^{31}P MAS NMR spectra of $0.40 \mu\text{mol}/\text{m}^2$ Ph_3P on Al_2O_3 catalyst with 6.2 SiO_2 per nm^2 , with different adsorption temperatures, the monolayer catalyst was degassed at 450°C and 10^{-5} torr for two hours, 90° pulse, 4 s recycle delay. a) 100°C one hour, 1.80 kHz MAS rate, 10713 scans; b) 150°C one hour, 1.85 kHz MAS rate, 4780 scans; and c) 200°C one hour, 1.90 kHz MAS rate, 14418 scans.

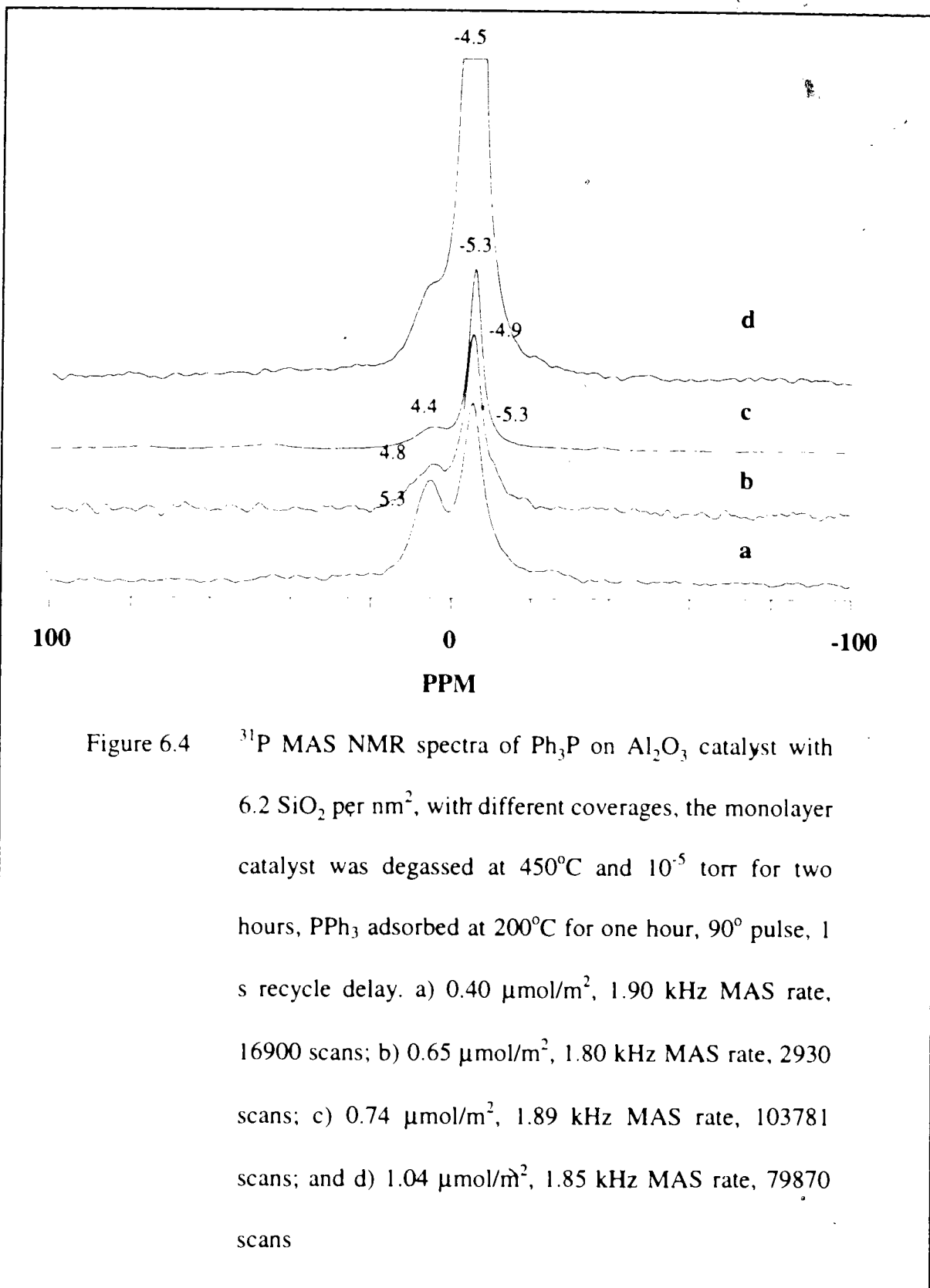


Figure 6.4 ^{31}P MAS NMR spectra of Ph_3P on Al_2O_3 catalyst with 6.2 SiO_2 per nm^2 , with different coverages, the monolayer catalyst was degassed at 450°C and 10^{-5} torr for two hours, PPh_3 adsorbed at 200°C for one hour, 90° pulse, 1 s recycle delay. a) $0.40 \mu\text{mol}/\text{m}^2$, 1.90 kHz MAS rate, 16900 scans; b) $0.65 \mu\text{mol}/\text{m}^2$, 1.80 kHz MAS rate, 2930 scans; c) $0.74 \mu\text{mol}/\text{m}^2$, 1.89 kHz MAS rate, 103781 scans; and d) $1.04 \mu\text{mol}/\text{m}^2$, 1.85 kHz MAS rate, 79870 scans

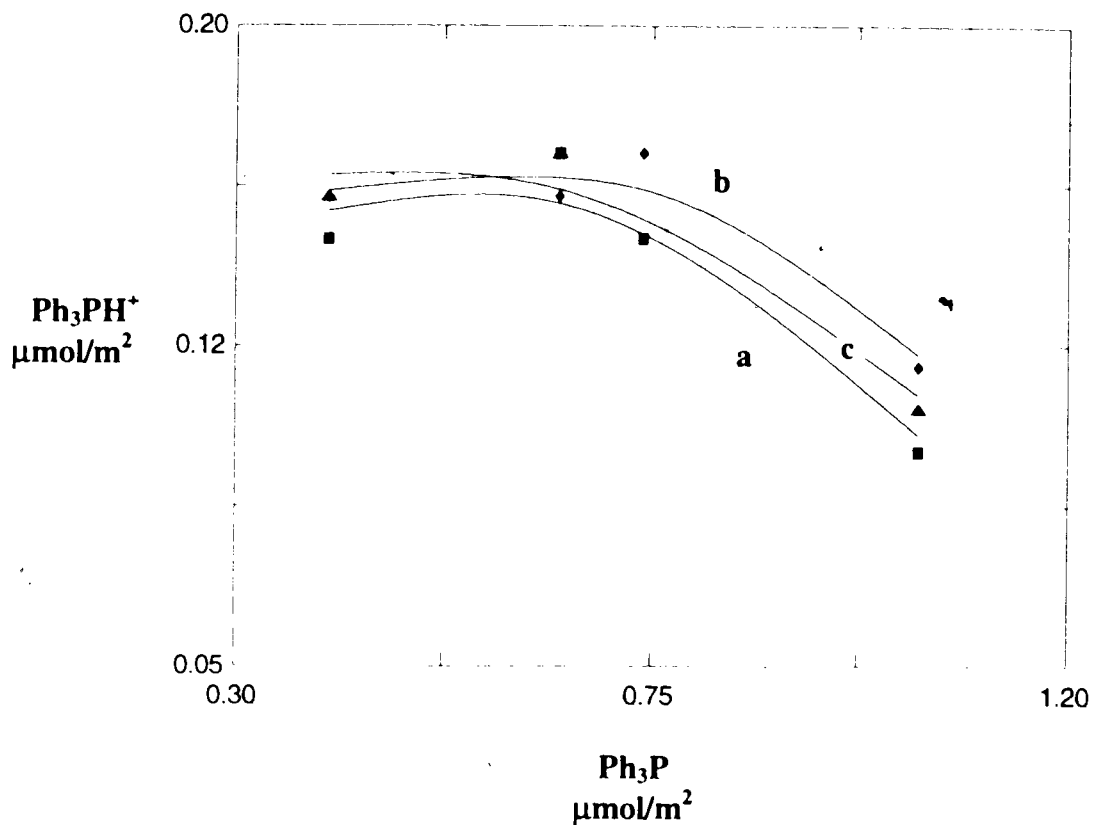


Figure 6.5 the concentrations of Ph_3PH^+ on Al_2O_3 catalyst with 6.2 SiO_2 per nm^2 at various coverages. a) 100°C one hour; b) 150°C one hour; and c) 200°C one hour.

b. Me_3P

Figure 6.6 shows the spectra of $1.10 \mu\text{mol}/\text{m}^2$ Me_3P on Al_2O_3 monolayer catalyst with 6.2 SiO_2 per nm^2 , using different pulse sequences. The peaks around -4.0 ppm arise from the Brønsted acid species. They have been verified by delayed decoupling to be phosphorus with a directly bonded proton (Figure 6.6a). The peaks around -53 ppm were mainly from physisorbed species¹. The new peak around 30 ppm could be the phosphine oxide species on the surface, since the chemical shift of $\text{O}=\text{PMe}_3$ is 36 ppm in solution⁸.

Figure 6.7 shows the spectra of $1.10 \mu\text{mol}/\text{m}^2$ Me_3P on Al_2O_3 catalyst with 6.2 SiO_2 per nm^2 , using different recycle delays. The integrated areas of Brønsted acid peak (-4.3 ppm) were 18% , 20% and 19% of total coverage for Figure 6.7a to Figure 6.7c respectively. This indicates that even a 1 s recycle delay is long enough to quantitatively measure the acid amount. At the same time, we measured the T_1 values for the Brønsted acid and the physically adsorbed species by a 90° pulse sequence with various delay times (Figure 6.8). In Figure 6.8, the spectra were plotted using the same scale and displaced along the X axis. The logarithms of intensities in Figure 6.8 were plotted against the delay time (Figure 6.9), from which the T_1 of Me_3P was calculated as 0.1 and 0.03 seconds for the Brønsted acid and physically adsorbed species respectively. This further confirms that a 1 s recycle delay is long enough.

Figure 6.10 shows the spectra of $1.10 \mu\text{mol}/\text{m}^2$ Me_3P on Al_2O_3 monolayer catalyst with 6.2 SiO_2 per nm^2 , with different adsorption temperatures. Using the exchange model described in¹, we calculated the Brønsted acid concentrations for 23°C , 60°C and 100°C adsorption. They are 0.31 , 0.32 and $0.32 \mu\text{mol}/\text{m}^2$ respectively. Among them the value at room temperature is in agreement with¹. These numbers are higher than those for the commercial catalyst ($0.22 \mu\text{mol}/\text{m}^2$ for each temperature by PMe_3) (Figure 6.11). The

more Brønsted acid species, the higher is the catalytic activity for cumene cracking². The peak at 30 ppm grows with increasing temperature to 100°C. Since the Brønsted acid concentrations are almost the same with different temperatures, the new peaks could be converted from the physisorbed or Lewis acid species.

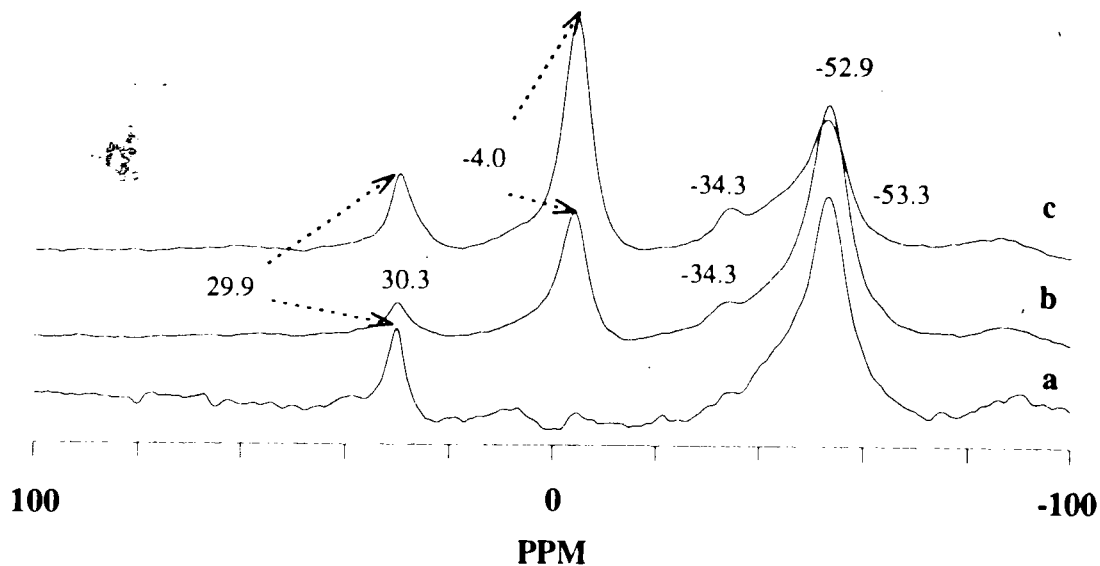


Figure 6.6 ^{31}P MAS NMR spectra of $1.10 \mu\text{mol}/\text{m}^2$ Me_3P on Al_2O_3 catalyst with 6.2 SiO_2 per nm^2 , with different pulse sequences, the monolayer catalyst was degassed at 450°C and 10^{-5} torr for two hours, adsorbed at 60°C for one hour. a) dipolar dephasing, $70 \mu\text{s}$ delay, 1.90 kHz MAS rate, 1 s recycle delay, 18488 scans; b) 90° pulse, 1.80 kHz MAS rate, 4 s recycle delay, 24070 scans; and c) cross-polarization flipback, 1.80 kHz MAS rate, 1 s recycle delay, 77984 scans.

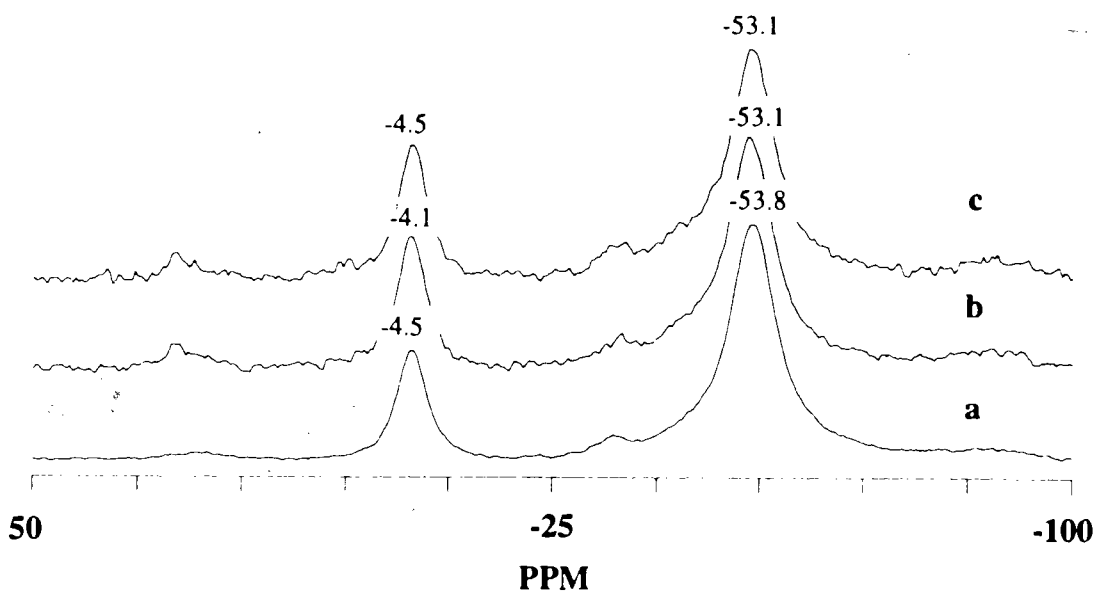


Figure 6.7 ^{31}P MAS NMR spectra of $1.10 \mu\text{mol}/\text{m}^2$ Me_3P on Al_2O_3 catalyst with 6.2 SiO_2 per nm^2 , with different recycle delays, the monolayer catalyst was degassed at 450°C and 10^{-5} torr for two hours, adsorbed at room temperature (23°C) for one hour, 90° pulse, 1.80 kHz MAS rate. a) 1 s recycle delay, 82466 scans; b) 4 s recycle delay, 6348 scans; and c) 16 s recycle delay, 4198 scans.

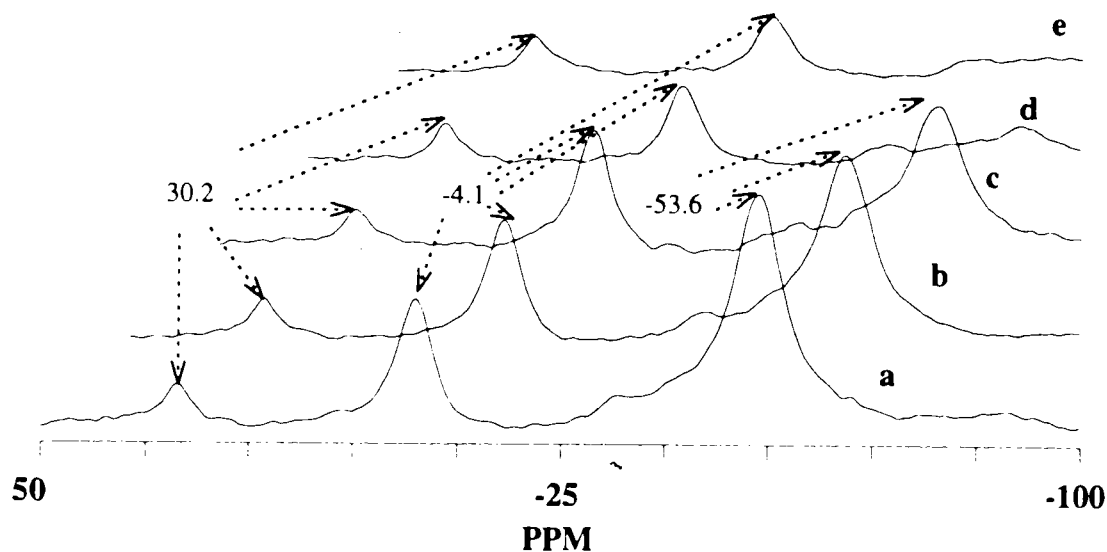


Figure 6.8 ^{31}P MAS NMR spectra of $1.10 \mu\text{mol}/\text{m}^2$ Me_3P on Al_2O_3 catalyst with 6.2 SiO_2 per nm^2 , with different τ values in the $(180^\circ\text{-}\tau\text{-}90^\circ(\text{FID})\text{-}T_d)_n$ pulse sequence (90° pulse), the monolayer catalyst was degassed at 450°C and 10^{-5} torr for two hours, adsorbed at 100°C for one hour, 1.80 kHz MAS rate, 2 s recycle delay, 6000 scans. a) 1 ms ; b) 5 ms ; c) 10 ms ; d) 50 ms and e) 100 ms τ values.

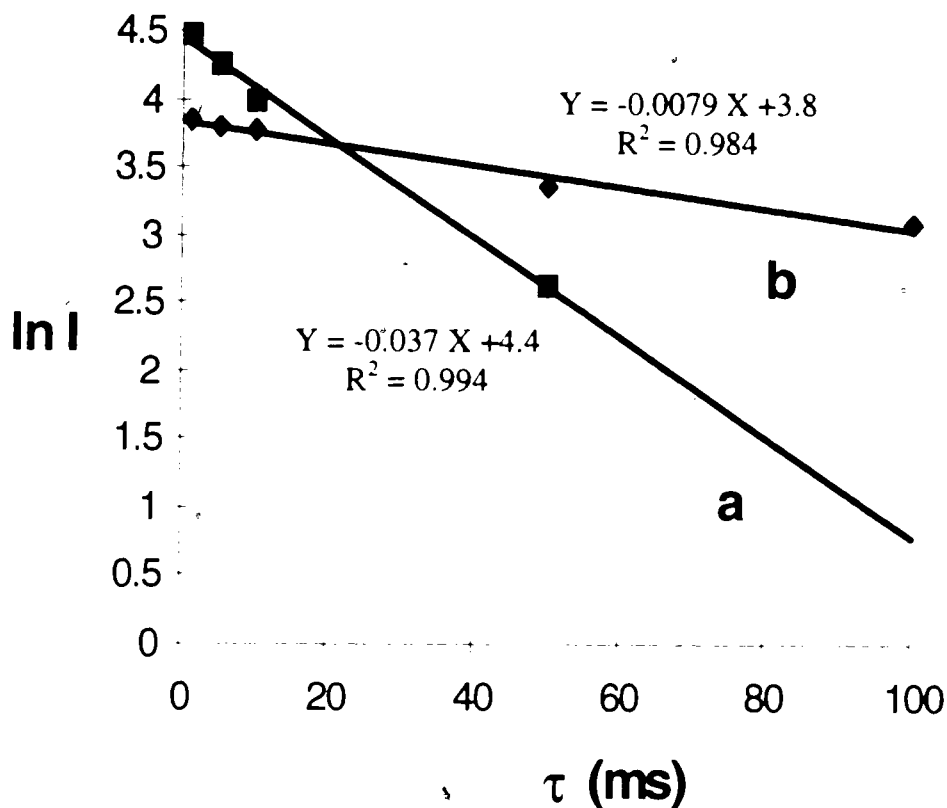


Figure 6.9 Intensity of ^{31}P MAS NMR spectra versus delay time in the 90° sequence (the data were taken from Figure 6.8). a) physically adsorbed species (-53.6 ppm) and b) Brønsted acid species (-4.1 ppm). *R-squared value is a calculated value that indicates how valid a trendline is for forecasting. The R-squared value helps determine the line of best fit. An R-squared value near 0 indicates a poor fit, a value near 1 indicated a good fit and therefore a meaningful trendline.

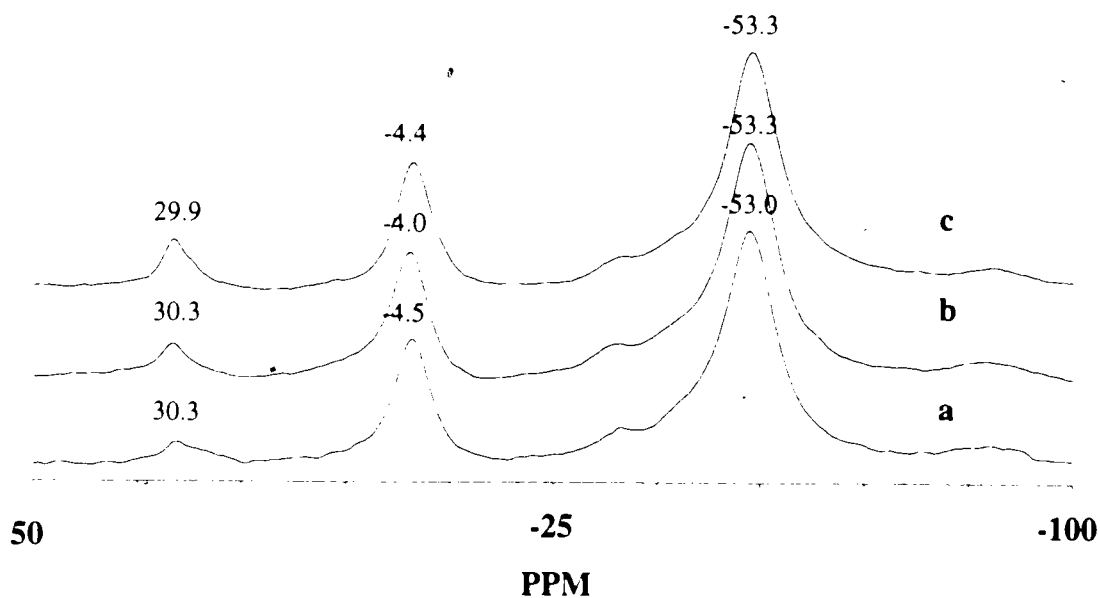


Figure 6.10 ^{31}P MAS NMR spectra of $1.10 \mu\text{mol}/\text{m}^2$ Me_3P on Al_2O_3 catalyst with 6.2 SiO_2 per nm^2 , with different adsorption temperatures, the monolayer catalyst was degassed at 450°C and 10^{-5} torr for two hours, adsorbed for one hour, 90° pulse, 4 s recycle delay. a) 23°C , 1.80 kHz MAS rate, 6348 scans; b) 60°C , 1.80 kHz MAS rate, 24070 scans; and c) 100°C , 1.90 kHz MAS rate, 19038 scans.

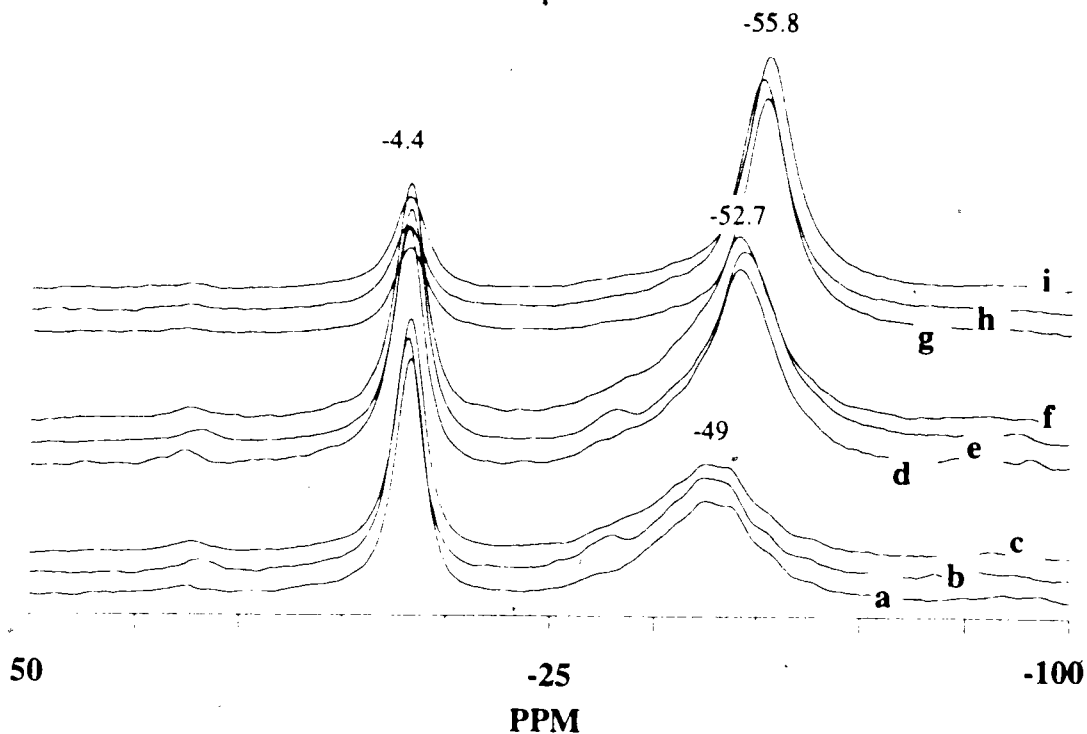


Figure 6.11 ^{31}P MAS NMR spectra of Me_3P on commercial silica-alumina catalyst, with different adsorption temperatures, the catalyst was degassed at 450°C and 10^{-5} torr for two hours, Me_3P adsorbed for one hour, 90° pulse, 1.9 kHz MAS rate, 4 s recycle delay. a) $0.42 \mu\text{mol}/\text{m}^2$, 23°C , 7711 scans; b) $0.42 \mu\text{mol}/\text{m}^2$, 65°C , 5690 scans; c) $0.42 \mu\text{mol}/\text{m}^2$, 100°C , 15000 scans; d) $0.53 \mu\text{mol}/\text{m}^2$, 23°C , 4536 scans; e) $0.53 \mu\text{mol}/\text{m}^2$, 60°C , 16992 scans; f) $0.53 \mu\text{mol}/\text{m}^2$, 100°C , 3818 scans; g) $0.82 \mu\text{mol}/\text{m}^2$, 23°C , 2222 scans; h) $0.82 \mu\text{mol}/\text{m}^2$, 60°C , 1964 scans; and i) $0.82 \mu\text{mol}/\text{m}^2$, 100°C , 3674 scans.

c. **Cy₃P**

Figure 6.12 shows the spectra of 0.41 $\mu\text{mol}/\text{m}^2$ Cy₃P on the alumina catalyst with 6.2 SiO₂ per nm², with different adsorption temperatures. Figure 6.12 a is for the sample that was only mixed under vacuum at room temperature. The main component is the multilayer of adsorbed Cy₃P species, since the 7.1 ppm peak is close to the value of 7.4 ppm of pure crystalline Cy₃P in Figure 4.1 (Chapter 4) but with much smaller spinning side bands. Figure 6.12b shows the results of adsorption at 100°C. There are three peaks: 24.5, 5.9 and -4.6 ppm. The peak at 24.5 ppm, close to 27 ppm (Brønsted acid species on the commercial silica-alumina in Figure 4.10), arises from the protonated phosphine. This is also further confirmed by dipolar dephasing experiment (Figure 6.14).

The peak at 5.9 ppm in Figure 6.12b is almost gone after heating at 150 and 200°C (Figure 6.12c and 6.12d). Therefore the species attributed to this peak must have weaker bonding. It probably arises from the physically adsorbed species. The value of 5.9 ppm is close, but not the same as those for the silica or silica-alumina catalyst (the physically adsorbed species in Figure 4.3 and 4.13). Checking the physically adsorbed species on the coated catalyst versus the coverage (Figure 6.12, 6.17, 6.18, 6.19, 6.20 and 6.21), we found the values of chemical shift change from 5.9 to 9.6 ppm with the increase of coverage on the surface. However, the corresponding species on silica or commercial silica-alumina catalyst have a range of 8.3 to 9.6 ppm (Figure 4.3 and 4.13). This suggests that the H bonding interaction probably is more heterogeneous using this coated catalyst than silica or commercial silica-alumina catalyst. This is reasonable, since the surface of Al₂O₃ is not fully covered with SiO₂ (6.2 SiO₂ per nm² for this coated catalyst) Based on², 95% coverage at 12 Si per nm². Hence roughly 50% Al₂O₃ was covered with SiO₂. The commercial silica-alumina catalyst has 25% Al₂O₃, however we are not sure about the surface composition. At low coverages, the physically adsorbed species may be mostly on

the Al_2O_3 , because 5.9 ppm (Figure 6.12) are about the same as the values for the physically adsorbed species on Al_2O_3 (6 and 6.9 ppm in Figure 4.7 and 4.8). It seems that the phosphine prefers to form H bond with the hydroxyl groups on Al_2O_3 rather than SiO_2 with this coated catalyst.

The peak of -5 ppm in Figure 6.12 b to 6.12d is close to -7 ppm of Lewis acid sites on the commercial silica-alumina catalyst in Figure 4.6. We suggest that this peak arises from Lewis acid species too. The results of dipolar dephasing experiment also support this suggestion (Figure 6.16). Lewis acid complexes should be closer to the surface (containing many OH groups) and less mobile than the physically adsorbed species, since the bond length for the complex must be much shorter than an intermolecular bond. Hence, the degree of discrimination for Lewis acid species by dipolar dephasing must be between those for the Brønsted acid and the physically adsorbed species. This is the true case for the peak of -5 ppm, which has an intermediate slope between Brønsted acid and the physically adsorbed species (Figure 6.16). Figure 6.15 also shows that the Lewis acid line has a smaller slope than that for the Brønsted acid species, consistent with the results of Figure 6.16.

Figure 6.13 shows the spectra of $0.41 \mu\text{mol}/\text{m}^2$ Cy_3P on alumina monolayer catalyst with 6.2 SiO_2 per nm^2 , with various recycle delays. These spectra showed that the relative intensity of -4.6 ppm peaks (Lewis acid species) increases with longer recycle delays. The ratios of integrated areas for Lewis acid and Brønsted acid species (25 ppm) are 0.24, 0.34, 0.39 and 0.42 for Figure 6.13a to 6.13d respectively. The difference among these numbers is due to a longer T_1 for the Lewis acid sites on the surface than for the Brønsted acid species. This could be caused by a) the smaller mobility of the Lewis acid; and b) the P-H bond helps the Brønsted acid species to relax faster. T_1 for the Lewis acid should be longer than that for the Brønsted acid species.

Table 6.1 T_1 values of Cy_3P on coated Al_2O_3 monolayer catalyst

Coverage ($\mu\text{mol}/\text{m}^2$)	Adsorption Temp($^{\circ}\text{C}$)	T_{1H}^* (s)	T_{1L}^* (s)	T_{1P}^* (s)	T_{1C}^* (s)
0.38	100	1.0	1.7		
0.38	150	1.3	2.0		
0.38	200	1.1	1.7		
0.41	200	1.0	2.2		
0.49	200	1.3	1.8		
0.79	RT				2.5
0.79	100	1.3	1.4	1.2	
0.79	150	1.3	1.6	1.2	
0.79	200	1.2	2.3	1.1	
0.94	200	1.1		1.2	
1.99	200	1.5, 2.8**		1.1	
1.30***	100			1.6	

Pure Cy_3P 21

*: T_{1H} , T_{1L} , and T_{1P} stand for T_1 of Brønsted acid, Lewis acid, and the physically adsorbed species respectively. T_{1C} stands for multilayer physically adsorbed or crystalline species.

** : This is for the Brønsted acid species at 33.3 ppm.

*** : The phosphine was on the silica surface.

T_1 values for various species as a function of coverage and adsorption temperature are summarized in Table 6.1. The T_1 values for the coated monolayer Al_2O_3 catalyst do not change with different coverages and adsorption temperatures. T_{1H} , T_{1L} and T_{1P} of Brønsted acid, Lewis acid and the physically adsorbed species are 1.2 ± 0.2 , 1.8 ± 0.5 , 1.2 ± 0.1 seconds respectively. The Brønsted acid and the physically adsorbed species have the same value of T_1 . However, the Lewis species have a higher T_1 . This is probably due to smaller mobility of Lewis acid species. When the coverage is very high ($1.99 \mu\text{mol}/\text{m}^2$), T_1 of the physically adsorbed species is not changed. However, T_1 of the Brønsted acid species becomes larger. This may suggest that high coverage limits the mobility of Brønsted acid species. When the crystalline species were put on the surface, T_1 decreases a lot since the molecule has more mobility. T_1 of the multilayer physically adsorbed species (2.5 s) is still longer than the monolayer's also due to the mobility.

Figure 6.17 shows the spectra of $1.68 \mu\text{mol}/\text{m}^2$ Cy_3P on Al_2O_3 catalyst with 6.2 SiO_2 per nm^2 , with different adsorption temperatures obtained using a 90° pulse. From Figure 6.17 a to 6.17c, the Brønsted acid concentrations were calculated as 0.36, 0.42 and $0.42 \mu\text{mol}/\text{m}^2$ at 100, 150 and 200°C respectively. This indicates that by using various temperature treatments, the differences in concentration are not significant, unlike those on the commercial silica alumina catalyst (see Figure 4.15). From Figure 6.17d, the Brønsted acid concentrations were calculated as $0.40 \mu\text{mol}/\text{m}^2$ using 1 s recycle delay. This is same as the value of Figure 6.17c within integration error. Since the Brønsted acid and the physically adsorbed species have the same T_1 value (1.2 s from Table 6.1), the ratios of their intensities are about the same even though a smaller recycle delay was used.

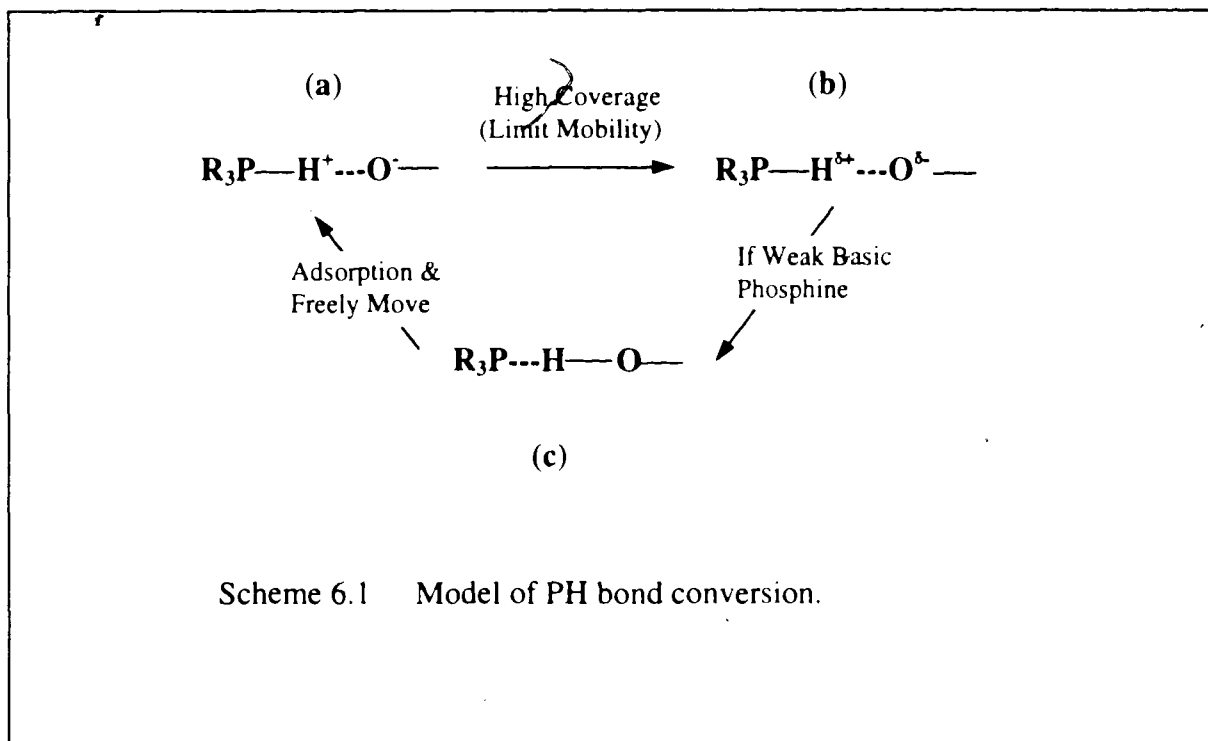
Figure 6.18 shows the spectra of $1.68 \mu\text{mol}/\text{m}^2$ Cy_3P on Al_2O_3 catalyst with 6.2 SiO_2 per nm^2 , with different adsorption temperatures from CP flipback or dipolar

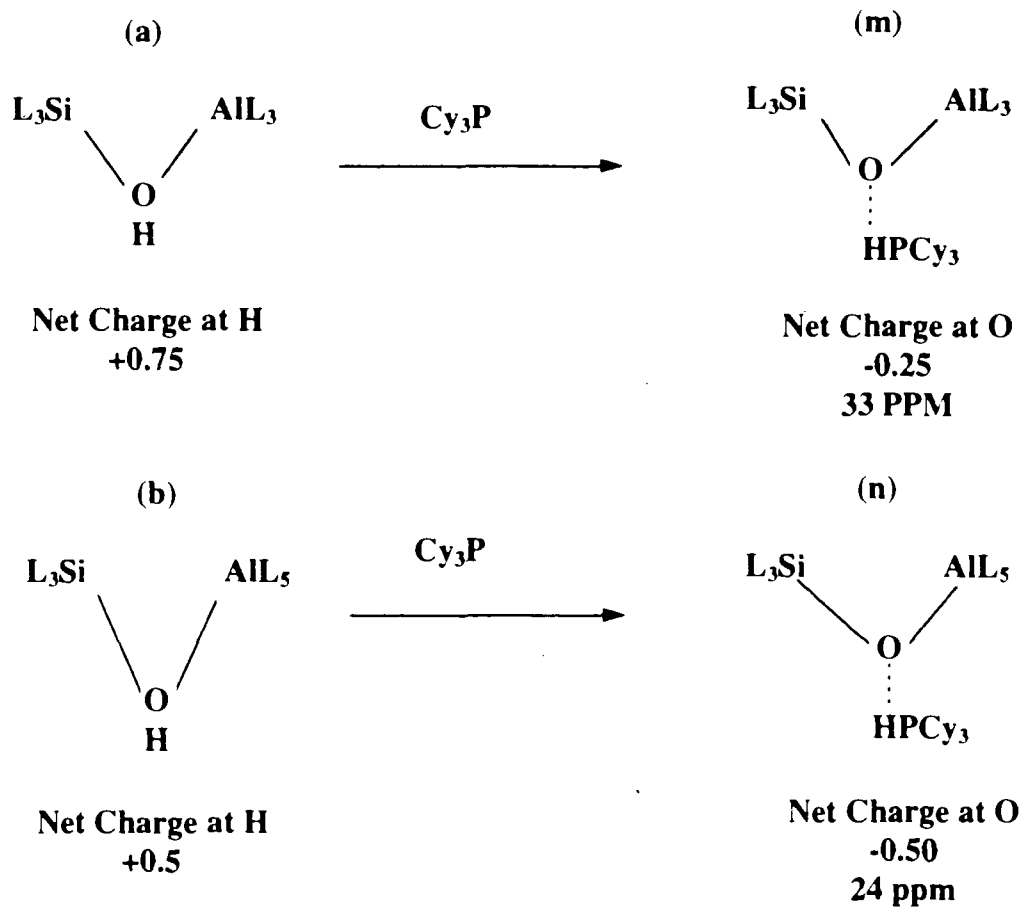
dephasing experiments. Figure 6.18a shows the crystalline Cy_3P species and indicates that no other impurity was present. It is interesting to find a new peak at 32 ppm adjacent to 24 ppm species in Figure 6.18d after adsorption at 200°C . Both of them are Brønsted acid species, since the peaks totally disappear using the dipolar dephasing experiment (Figure 6.18e). This suggests that two kinds of Brønsted acid sites were present on this coated catalyst surface. Since the cross-polarization experiments favors Brønsted acid sites, these two sites are not very obvious in Figure 6.17.

An even higher coverage ($1.99 \mu\text{mol}/\text{m}^2$) sample was prepared to check this new peak at 32 ppm. The spectra are shown from Figure 6.19 to 6.21. Using this coverage the new peak appears more obviously after heating at 150 and 200°C (Figure 6.20 and 6.21). Also it is interesting to find out that these two Brønsted acid signals did not totally disappear using dipolar dephasing experiments (with $70 \mu\text{s}$ delay) (Figure 6.19 to 6.21). Using dipolar dephasing experiments discrimination against Brønsted acid species is based on the dipolar coupling between P and H atoms (Section 3c, Chapter 1). Hence, the residual Brønsted acid peaks suggest that the dipolar interaction is weaker at this coverage. The dipolar coupling depends on $\cos\theta$ and r^{-3} (r is the bond length of PH) (see Equation 1.1, Chapter 1). Other parameters in the equation, such as gyromagnetic ratios, should be constant. Therefore we conclude that a) the bond length r_{PH} of Brønsted acid species is larger than at normal low coverages* or b) $\langle 3\cos^2\theta - 1 \rangle$ is smaller.

The increase of a bond length is rare, but we cannot say it is not reasonable. The following argument may provide an explanation. From Table 6.1, T_1 of Brønsted acid species for this coverage ($1.99 \mu\text{mol}/\text{m}^2$) has higher values. This could increase the P-H bond length (see Scheme 6.1). Since the motion of Cy_3PH^+ must be around HO the intermolecular bond ((a) in Scheme 6.1), the decrease of Cy_3PH^+ mobility may strengthen the HO and eventually weaken the PH bond ((b) in Scheme 6.1). Therefore the Brønsted

acid sites in Figure 6.19 to 6.21 could arise from type (b) species in Scheme 6.1. Cy_3P is strongly basic enough to attract H forming a chemical bond, since they still resonate as protonated species in Figure 6.19 to 6.21. However, other weaker aryl phosphines may give back the proton, so that type (c) species in Scheme 6.1 are formed. In Chapter 5 and section 2a, using the aryl phosphines with higher coverages a genuine decrease in the titration curves for Brønsted acid sites was observed. This phenomenon was explained by the presence of a multilayer of physically adsorbed species at higher coverages. Since the multilayer of physically adsorbed species can limit the mobility of adsorbed phosphines, the formation of type (c) species in scheme 6.1 may further explain why the Brønsted acid sites were lost at higher aryl phosphine coverages. The lower mobility at higher coverage may prevent type (c) shifts to type (a).





Scheme 6.2 Models of Brønsted acid sites for the monolayer Al_2O_3 catalyst coated with SiO_2 ; L = OH, OSi, or OAl.

In Figure 6.20 and 6.21, the peaks at 24 ppm and 34 ppm are two different Brønsted acid sites. Since Brønsted acid species were not observed on the silica or alumina surface, the sites must be adjacent to both silica and alumina. The alumina is built primarily from tetrahedral $[AlO_4]$ and octahedral $[AlO_6]$ groups (see Section 2,

Chapter 2). Two models of Brønsted acid sites are shown in Scheme 6.2. In Scheme 6.2, the net charge is calculated by Pauling's electrostatic valence rule, as in Figure 2.3, Chapter 2. Sites (a) and (b) in Scheme 6.2 are proposed as the two Brønsted acid sites on the monolayer Al_2O_3 catalyst coated with SiO_2 . Site (a) is similar to the cluster model based on the calculation of charge densities (see Figure 2.6, Chapter 2). But our model of site (a) is more reasonable, since the cluster model in Figure 2.6 is too simple for the amorphous catalyst (the metals not only attached to OH group). The Brønsted acid peak shifts to higher frequency in a ^{31}P NMR spectrum compared with a neutral phosphine, so the site (a) with more positive net charge in Scheme 6.2 must shift further than site (b). Hence we assign the peaks at 33 ppm and 24 ppm in Figure 6.19 to 6.21 as the site (m) and site (n) in Scheme 6.2 respectively, based on the values of calculated net charge at H. In Scheme 6.2 the sites (a) and (b) convert to site (m) and (n) respectively after losing the H to the phosphine.

Why is only site (n) observed at low coverages? Due to the higher mobility of protonated species at low coverages, the forming Cy_3PH^+ probably prefer to attach to site (n) in Scheme 6.2 based on net charge at O. The Brønsted acid site on the commercial silica-alumina might be only site (b) or (n) in Scheme 6.2, as we did not observe the 33 ppm peak even with high coverages (Figure 4.13, Chapter 4). Therefore the site (a) may not present on the commercial silica-alumina catalyst. The proposed cluster model (In Figure 2.6, Chapter 2) prefers the structure involving the aluminum tetrahedral group (similar to site (a)) as Brønsted acid site. The cluster model was based on how easy a proton can be lost (electron density). We agree with this aspect ((a) in Scheme 6.2 must more easily lose a proton). However, after proton transfer, the R_3PH^+ probably stays on site (n) instead of (m) in Scheme 6.2. Hence for the commercial acidic catalyst, we suggest the (b) or (n) structure in Scheme 6.2 involving aluminum octahedral group probably is the active center.

Figure 6.22 shows the titration concentrations of C_3PH^+ on Al_2O_3 catalyst with 6.2 SiO_2 per nm^2 at various coverages. Compared with the commercial SiO_2 - Al_2O_3 catalyst (Figure 4.15, Chapter 4), the maximum Brønsted acid concentration for Al_2O_3 monolayer catalyst with 6.2 SiO_2 per nm^2 is higher (around 0.40 - $0.44 \text{ } \mu\text{mol}/\text{m}^2$). This is consistent with the result using Me_3P (see section 2b). At different adsorption temperatures, the titration curves of Al_2O_3 monolayer catalyst were not significantly different. However, the Brønsted acid concentrations increased much more with adsorption temperature for the commercial silica-alumina catalyst. These suggest that diffusion on the Al_2O_3 catalyst coated with SiO_2 is much easier than on the commercial catalyst.

Figure 6.23 shows the concentration of Lewis acid species in the coated Al_2O_3 monolayer catalyst. The titration curves for different adsorption temperatures are about the same within the integration errors. The maximum Lewis acid concentration must be over $0.20 \text{ } \mu\text{mol}/\text{m}^2$.

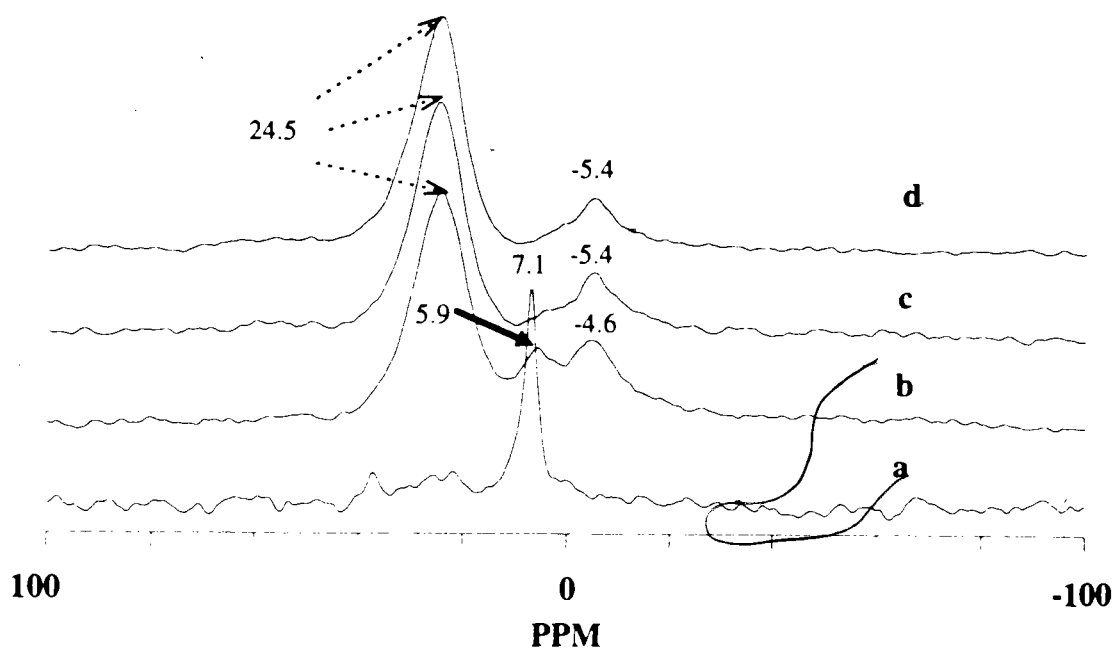


Figure 6.12 ^{31}P MAS NMR spectra of $0.41 \mu\text{mol}/\text{m}^2$ Cy_3P on Al_2O_3 catalyst with 6.2 SiO_2 per nm^2 , with different adsorption temperatures, the monolayer catalyst was degassed at 450°C and 10^{-5} torr for two hours, Cy_3P adsorbed for one hour, 1.85 kHz MAS rate, 1 s recycle delay. a) 23°C mixing, cross-polarization flipback, 1869 scans; b) 100°C , 90° pulse, 61191 scans; c) 150°C , 90° pulse, 45227 scans; and d) 200°C , 90° pulse, 63772 scans.

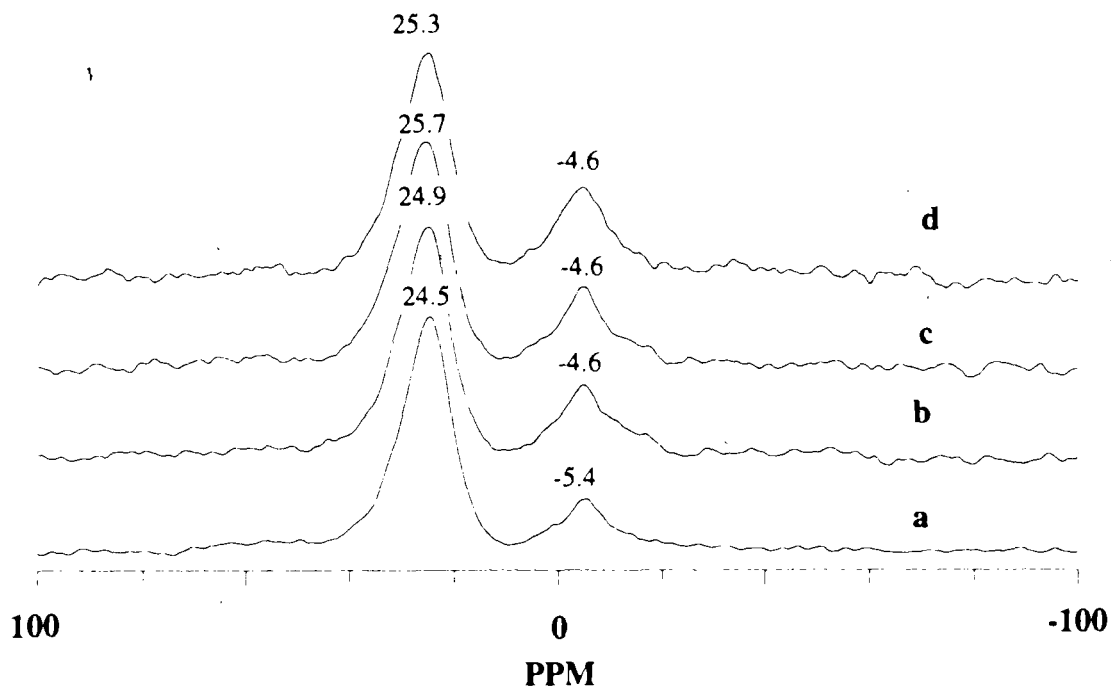


Figure 6.13 ^{31}P MAS NMR spectra of $0.41 \mu\text{mol}/\text{m}^2$ Cy_3P on Al_2O_3 catalyst with 6.2 SiO_2 per nm^2 , with different recycle delays, the monolayer catalyst was degassed at 450°C and 10^{-5} torr for two hours, Cy_3P adsorbed at 200°C for one hour, 1.87 kHz MAS rate, 90° pulse. a) 1 s recycle delay, 63772 scans; b) 4 s recycle delay, 21732 scans; c) 8 s recycle delay, 11860 scans; and d) 30 s recycle delay, 6822 scans.

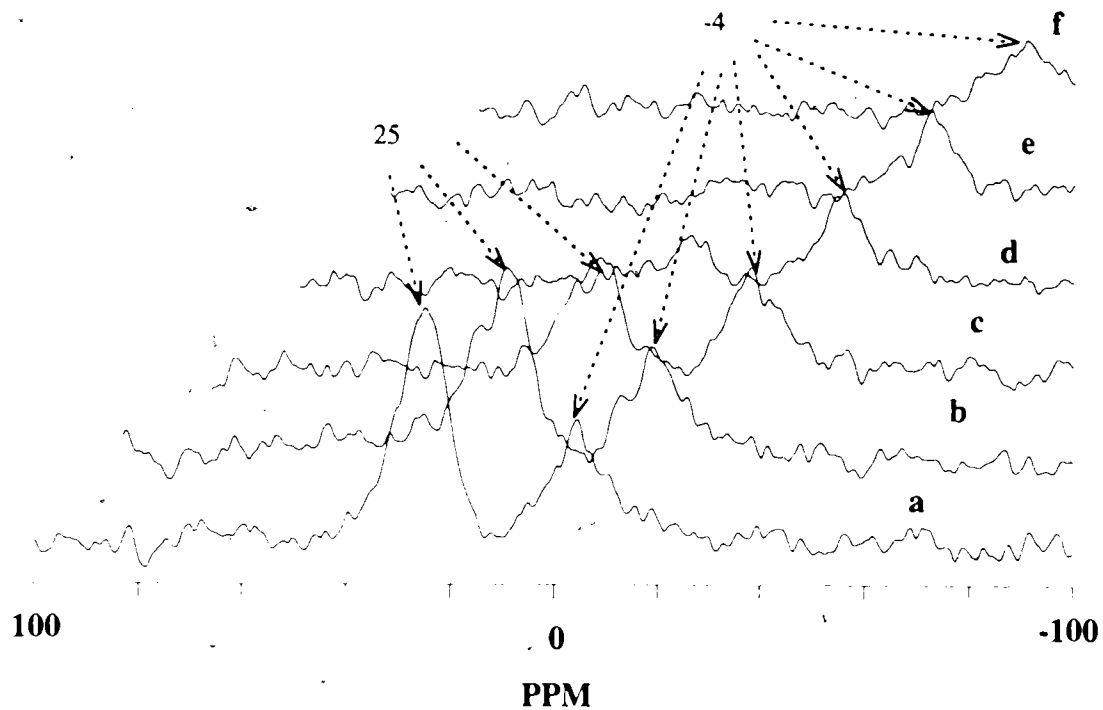


Figure 6.14 ^{31}P MAS NMR spectra of $0.41 \mu\text{mol}/\text{m}^2$ Cy_3P on Al_2O_3 catalyst with 6.2 SiO_2 per nm^2 , with different delays for the dipolar dephasing sequence, the monolayer catalyst was degassed at 450°C and 10^{-5} torr for two hours, Cy_3P adsorbed at 200°C for one hour, 1.80 kHz MAS rate, 1000 scans. a) 10; b) 20; c) 30; d) 40; e) 50 and f) $60 \mu\text{s}$ delay.

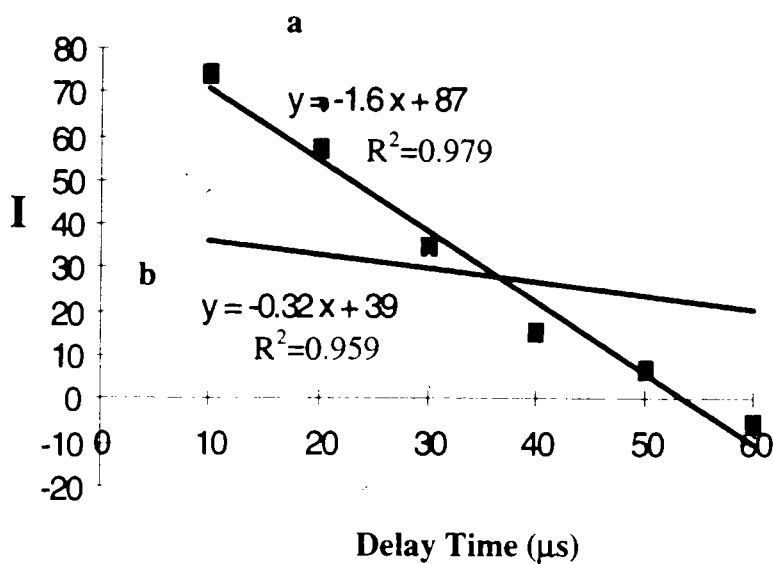


Figure 6.15 Intensity of ^{31}P MAS NMR spectra versus delay time in the dipolar dephasing sequence (The data were taken from adding of several groups of spectra like Figure 6.14). a) Brønsted acid species (25.2 ppm) and b) Lewis acid species (-4.3 ppm). *R-squared value is a calculated value that indicates how valid a trendline is for forecasting. The R-squared value helps determine the line of best fit. An R-squared value near 0 indicates a poor fit, a value near 1 indicated a good fit and therefore a meaningful trendline.

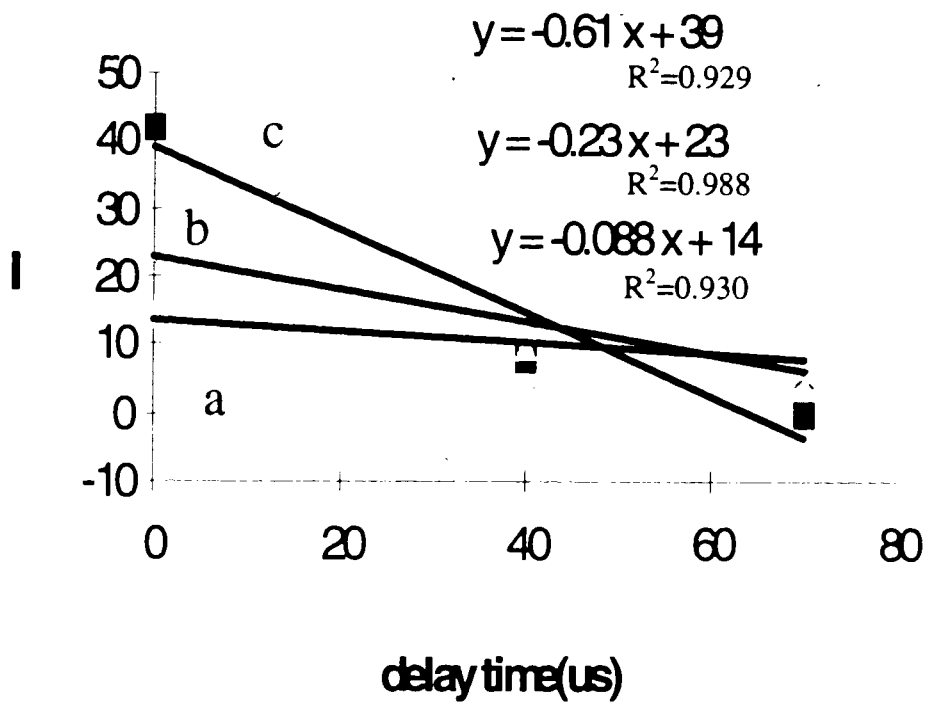


Figure 6.16 Intensity of ^{31}P MAS NMR spectra versus delay time in the dipolar dephasing sequence (The data were taken from $0.41 \mu\text{mol}/\text{m}^2$ Cy_3P on Al_2O_3 monolayer catalyst with 6.2 SiO_2 per nm^2 , adsorbed at 100°C for one hour, same sample as Figure 6.12b). a) physically adsorbed species (5.9 ppm); b) Lewis acid species (-4.3 ppm); and c) Brønsted acid species (25.2 ppm).

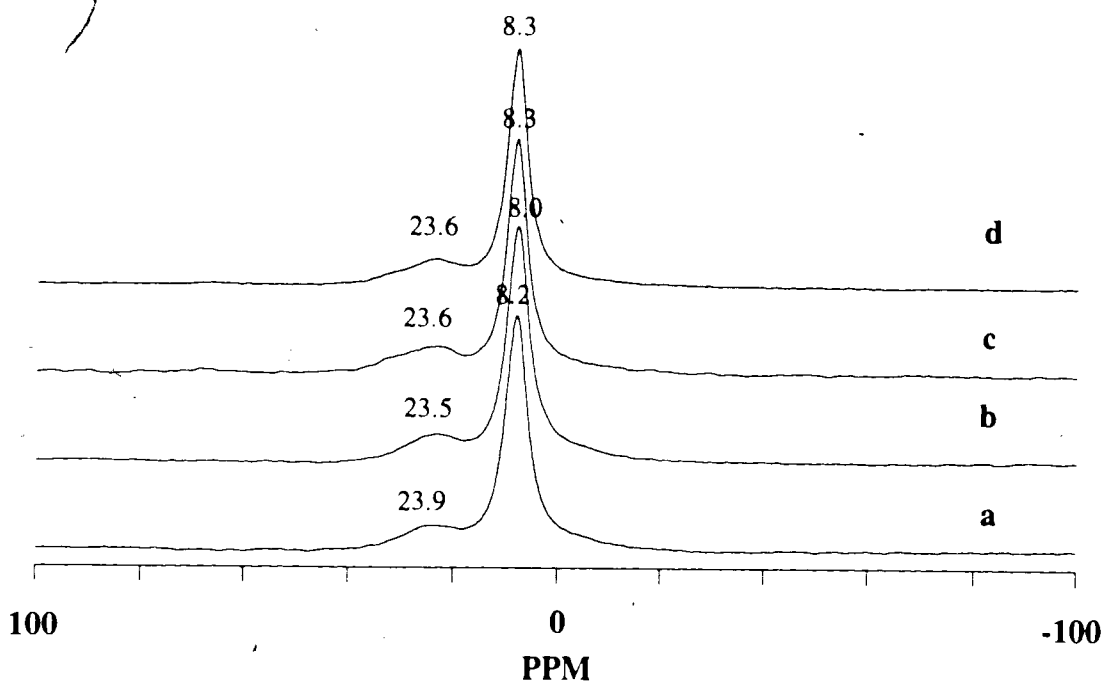


Figure 6.17 ^{31}P MAS NMR spectra of $1.68 \mu\text{mol}/\text{m}^2$ Cy_3P on Al_2O_3 monolayer catalyst with 6.2 SiO_2 per nm^2 , with adsorption at different temperatures for one hour using 90° pulse, the monolayer catalyst was degassed at 450°C and 10^{-5} torr for two hours, 1.87 kHz MAS rate, 4 s recycle delay (if not specified). a) 100°C , 1.88 kHz MAS rate, 16106 scans; b) 150°C , 1.88 kHz MAS rate, 16848 scans; c) 200°C , 1.96 MAS rate, 1584 scans and d) 200°C , 1.96 MAS rate, 1 s recycle delay, 20204 scans.

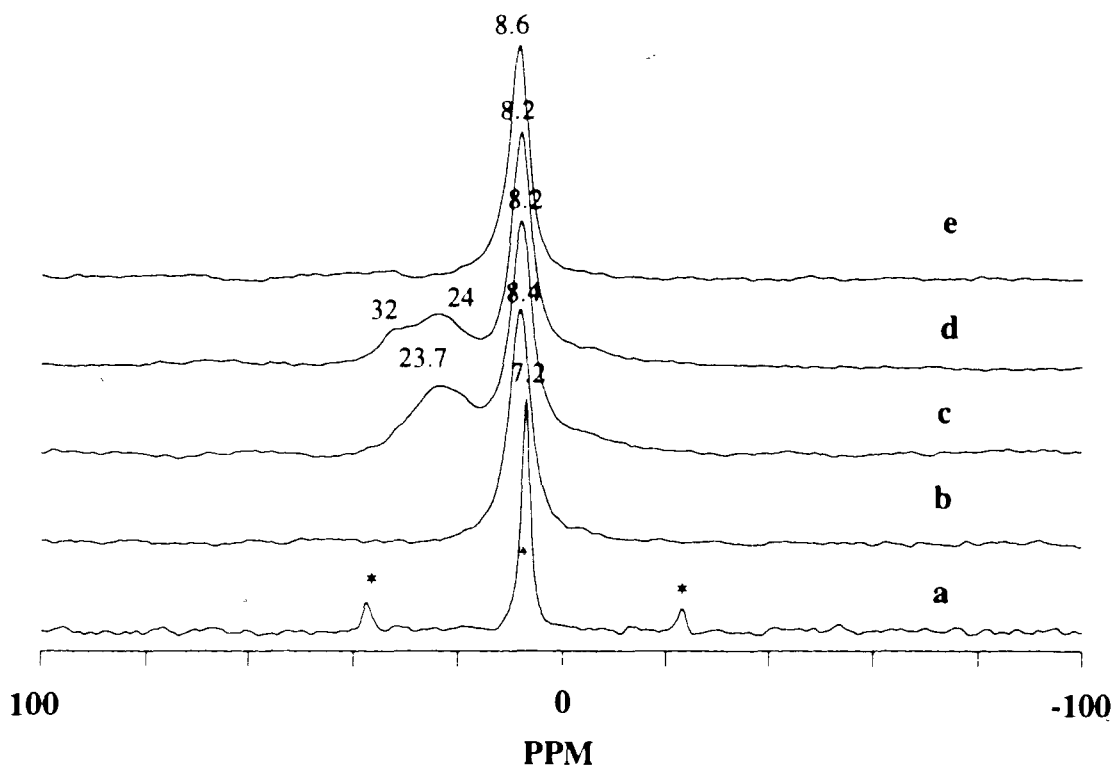


Figure 6.18 ^{31}P MAS NMR spectra of $1.68 \mu\text{mol}/\text{m}^2$ Cy_3P on Al_2O_3 monolayer catalyst with 6.2 SiO_2 per nm^2 , with adsorption at different temperatures for one hour using cross-polarization flipback (if not specified), the monolayer catalyst was degassed at 450°C and 10^{-5} torr for two hours, 1.87 kHz MAS rate, 1 s recycle delay (if not specified). a) RT mixing, 210 scans; b) 100°C , dipolar dephasing, $70 \mu\text{s}$ delay, 5690 scans; c) 150°C , 15790 scans; d) 200°C , 2 s recycle delay, 2880 scans and e) 200°C , dipolar dephasing, $70 \mu\text{s}$ delay, 2 s recycle delay, 3700 scans.

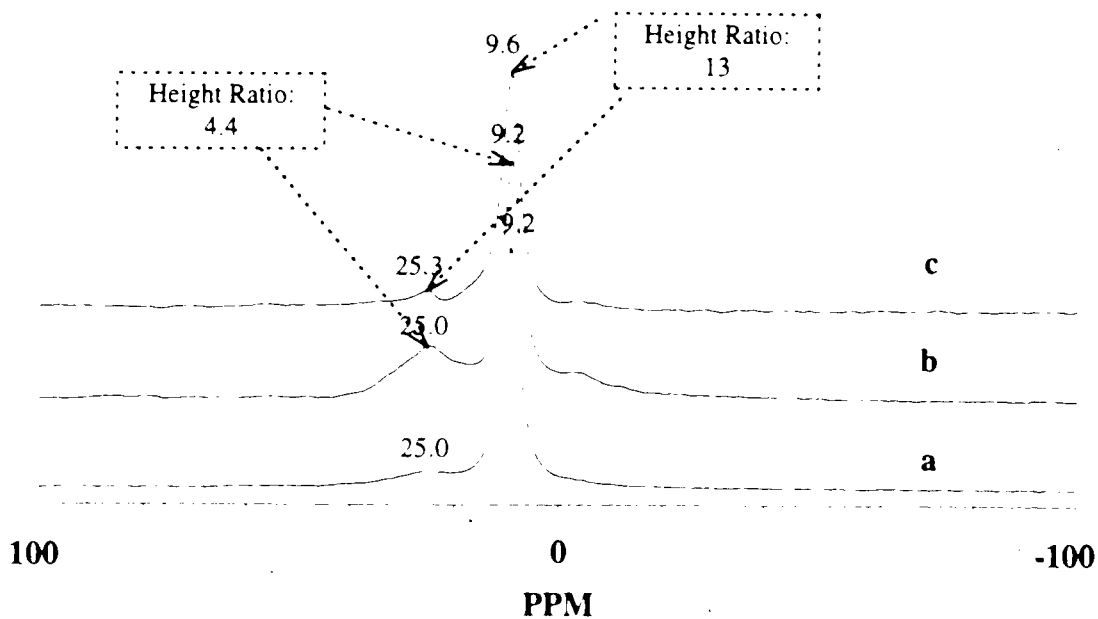


Figure 6.19 ^{31}P MAS NMR spectra of $1.99 \mu\text{mol}/\text{m}^2$ Cy_3P on Al_2O_3 monolayer catalyst with 6.2 SiO_2 per nm^2 , with different pulse sequences, 100°C adsorption for one hour, the monolayer catalyst was degassed at 450°C and 10^{-5} torr for two hours, 1.81 kHz MAS rate, 1 s recycle delay. a) 90° pulse, 26028 scans; b) cross-polarization flipback, 42260 scans; and c) dipolar dephasing, $70 \mu\text{s}$ delay, 20115 scans.

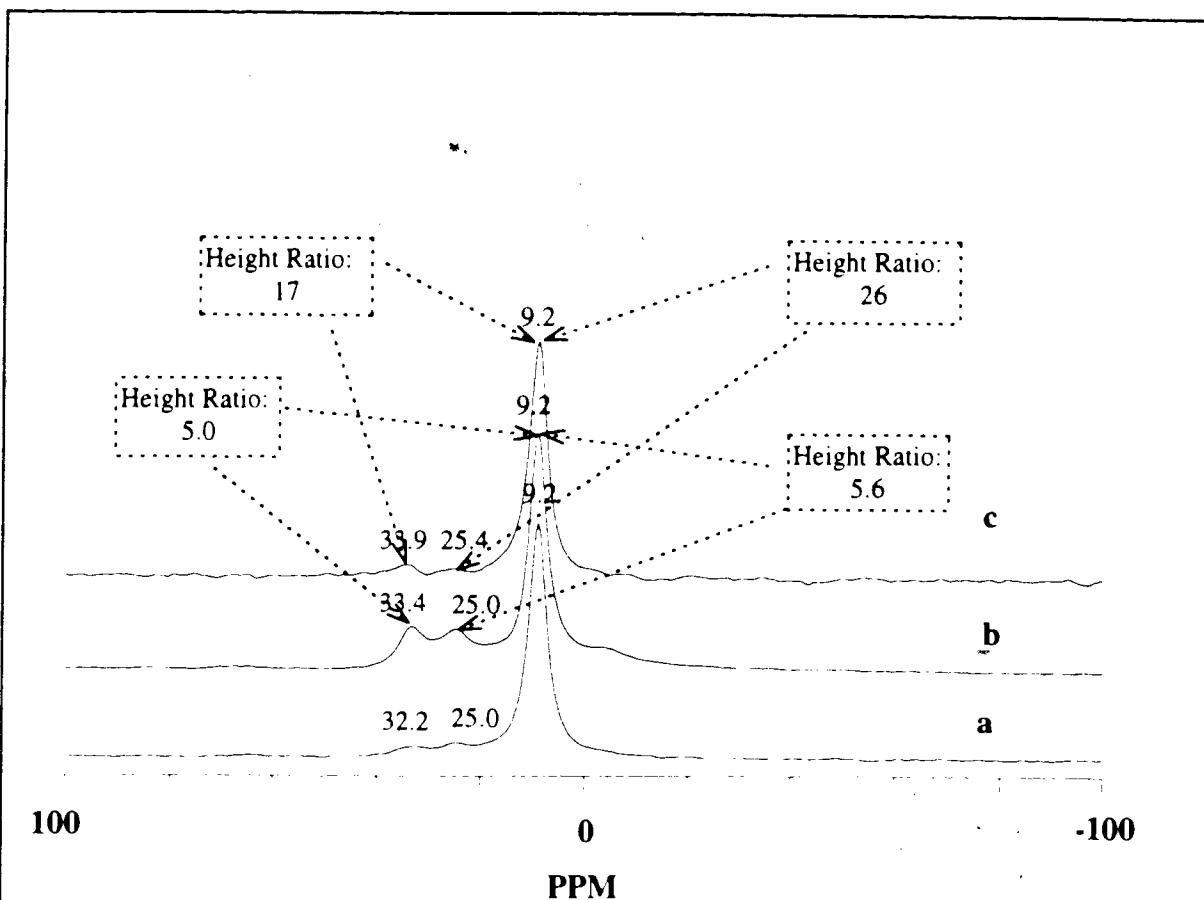


Figure 6.20 ^{31}P MAS NMR spectra of $1.99 \mu\text{mol}/\text{m}^2$ Cy_3P on Al_2O_3 monolayer catalyst with 6.2 SiO_2 per nm^2 , with different pulse sequences, 150°C adsorption for one hour, the monolayer catalyst was degassed at 450°C and 10^{-5} torr for two hours, 1.82 kHz MAS rate, 1 s recycle delay. a) 90° pulse, 5245 scans; b) cross-polarization flipback, 61516 scans; and c) dipolar dephasing, $70 \mu\text{s}$ delay, 4179 scans.

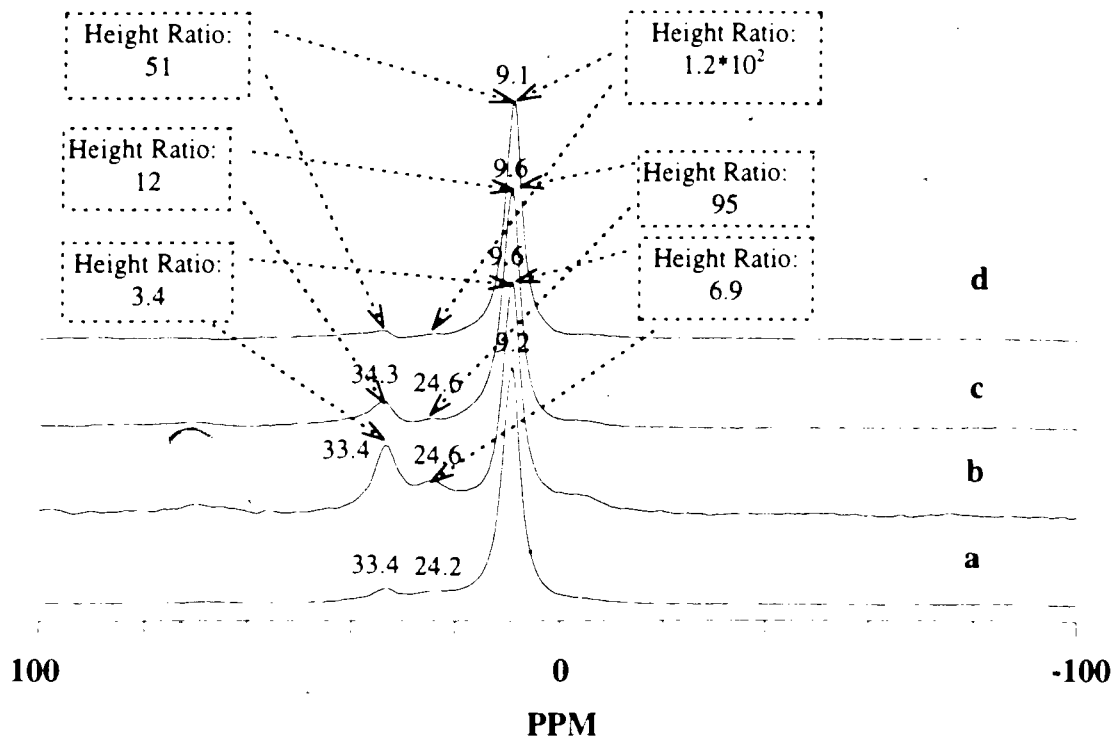


Figure 6.21 ^{31}P MAS NMR spectra of $1.99 \mu\text{mol}/\text{m}^2$ Cy_3P on Al_2O_3 monolayer catalyst with 6.2 SiO_2 per nm^2 , with different pulse sequences, 200°C adsorption for one hour, the monolayer catalyst was degassed at 450°C and 10^{-5} torr for two hours, 1.83 kHz MAS rate, 1 s recycle delay. a) 90° pulse, 66900 scans; b) cross-polarization flipback, 8976 scans; c) dipolar dephasing, $70 \mu\text{s}$ delay, 159419 scans and d) dipolar dephasing, $140 \mu\text{s}$ delay, 95922 scans

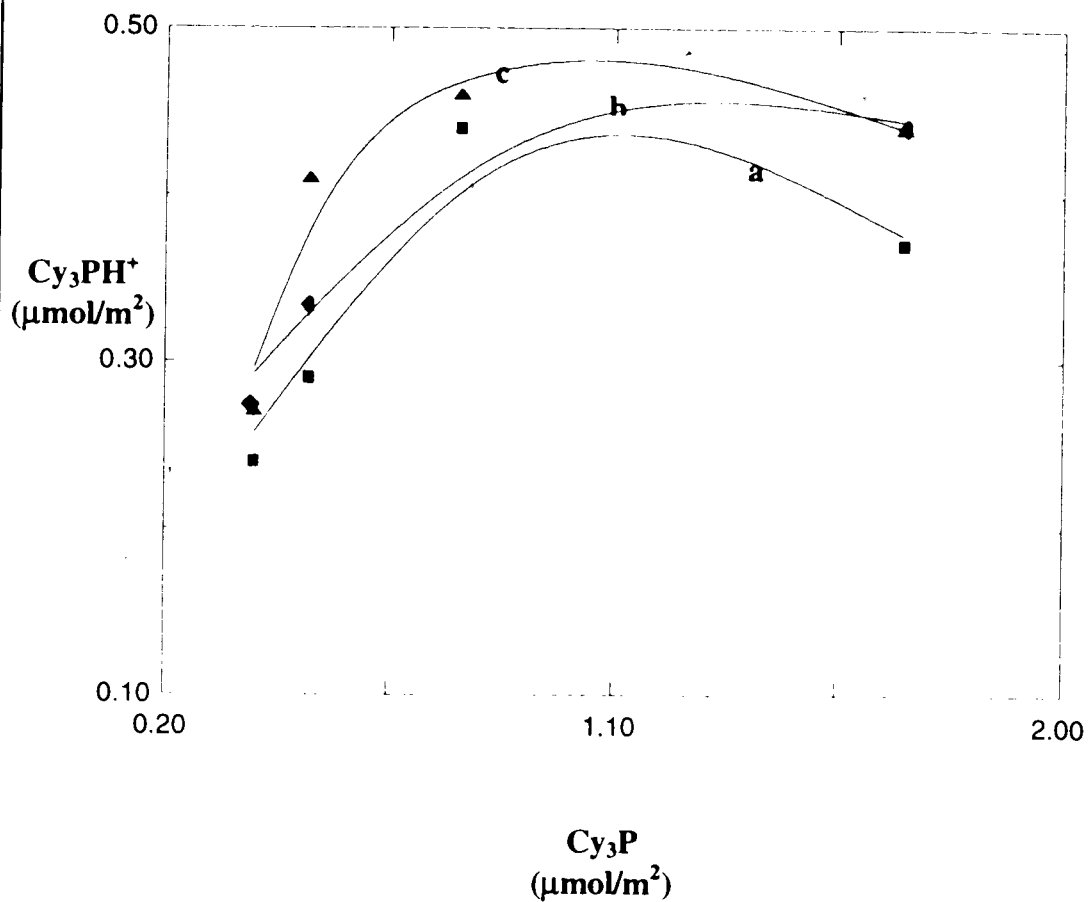


Figure 6.22 the concentrations of Cy_3PH^+ on Al_2O_3 catalyst with 6.2 SiO_2 per nm^2 at various coverages. a) 100°C one hour (■); b) 150°C one hour (◆); and c) 200°C one hour (▲).

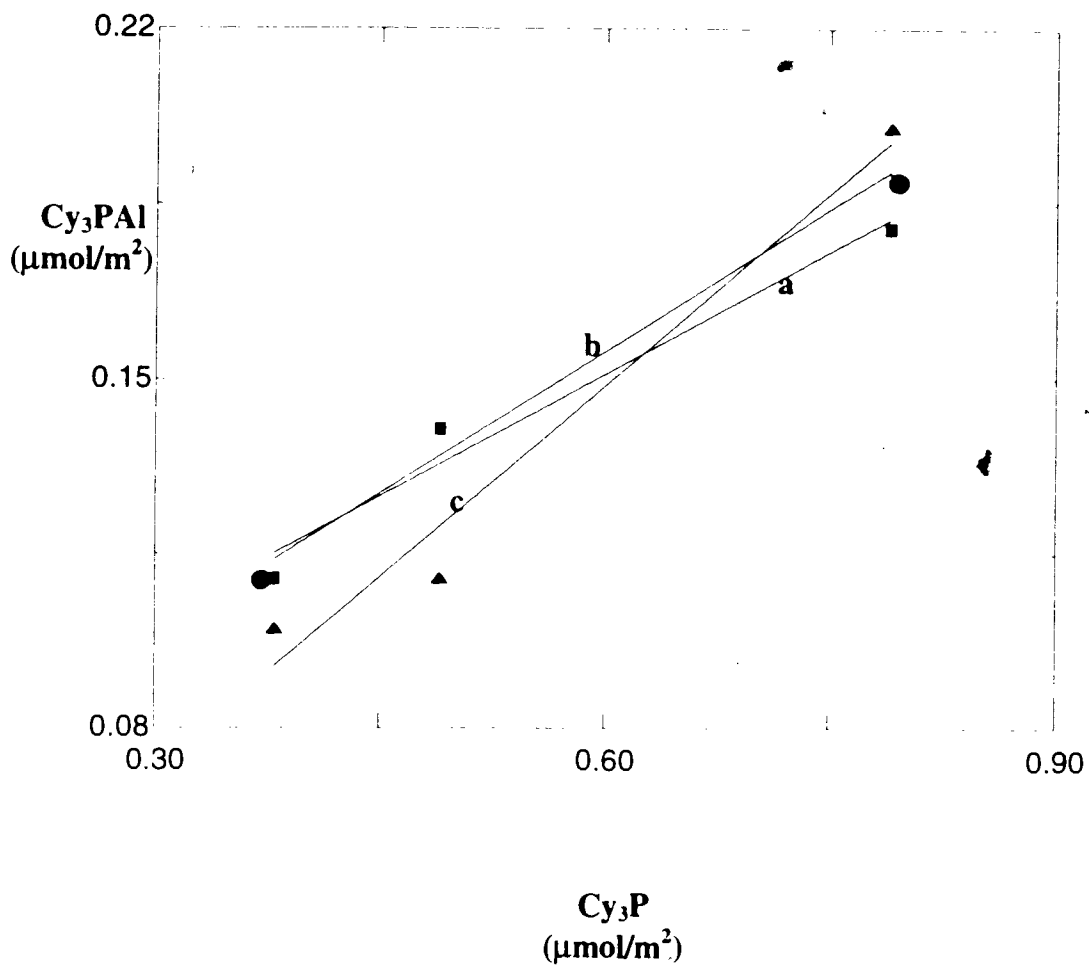
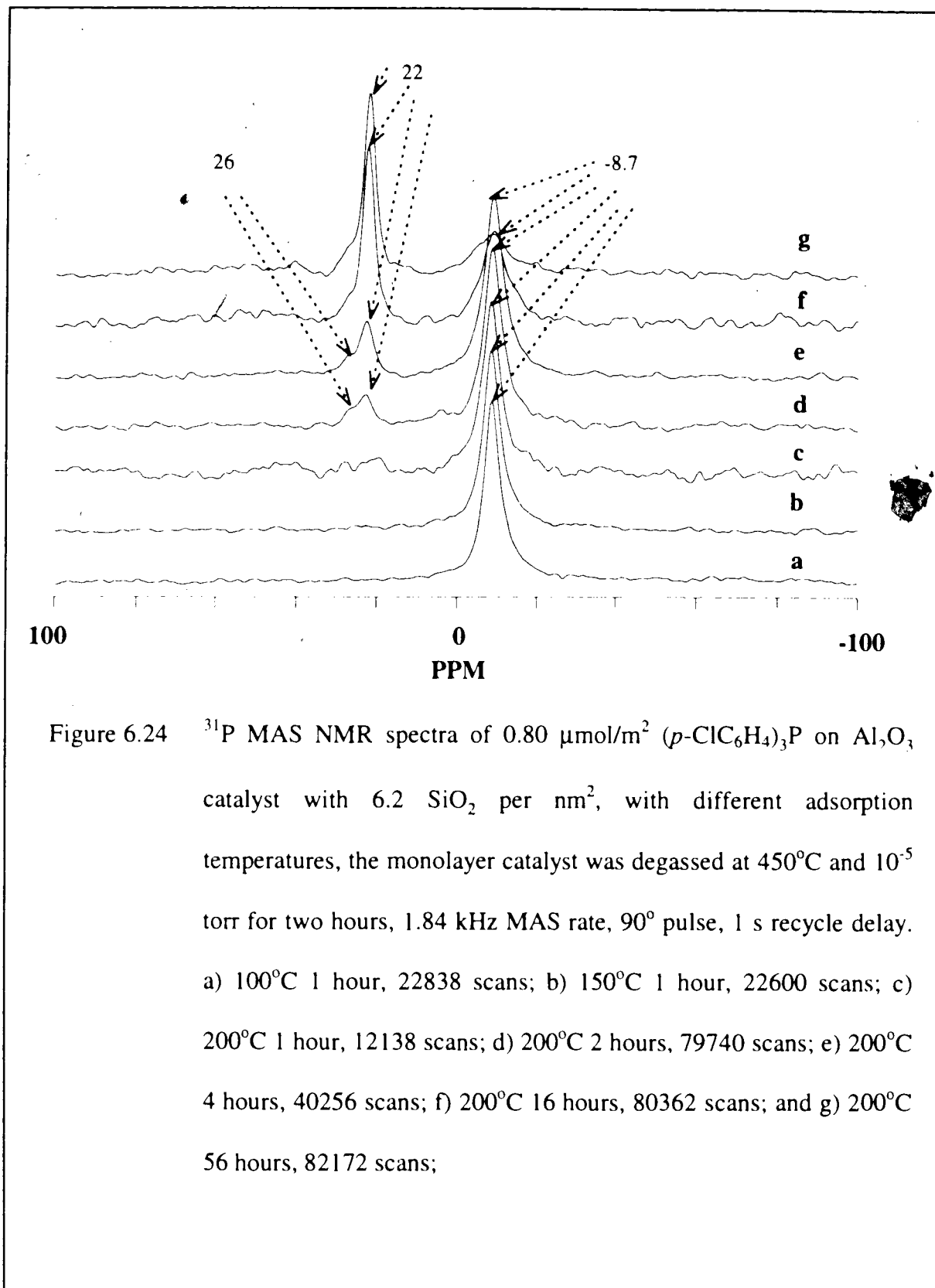


Figure 6.23 The concentrations of Cy₃PAI Lewis acid sites on Al₂O₃ catalyst with 6.2 SiO₂ per nm² at various coverages. a) 100°C one hour (■); b) 150°C one hour (●); and c) 200°C one hour (▲).

d. $(p\text{-ClC}_6\text{H}_4)_3\text{P}$

Figure 6.24 to 6.27 show the spectra of $(p\text{-ClC}_6\text{H}_4)_3\text{P}$ on Al_2O_3 monolayer catalyst with 6.2 SiO_2 per nm^2 . Similar to Figure 5.31, the Brønsted acid site (4 ppm) was hardly found at this coverage range (0.80-1.47 $\mu\text{mol}/\text{m}^2$). The phosphine was rather forming the phosphine oxide on heating for longer times or at higher temperatures. After heating at higher temperatures, the peak of -8.5 ppm (physically adsorbed phosphine) was converted to the peak of 22 ppm (the physically adsorbed phosphine oxide). A peak at 26 ppm was also observed (Figure 6.24d, 6.24e, 6.25c, 6.25d, 6.26d and 6.27c), which was also suggested as the physically adsorbed phosphine oxide.



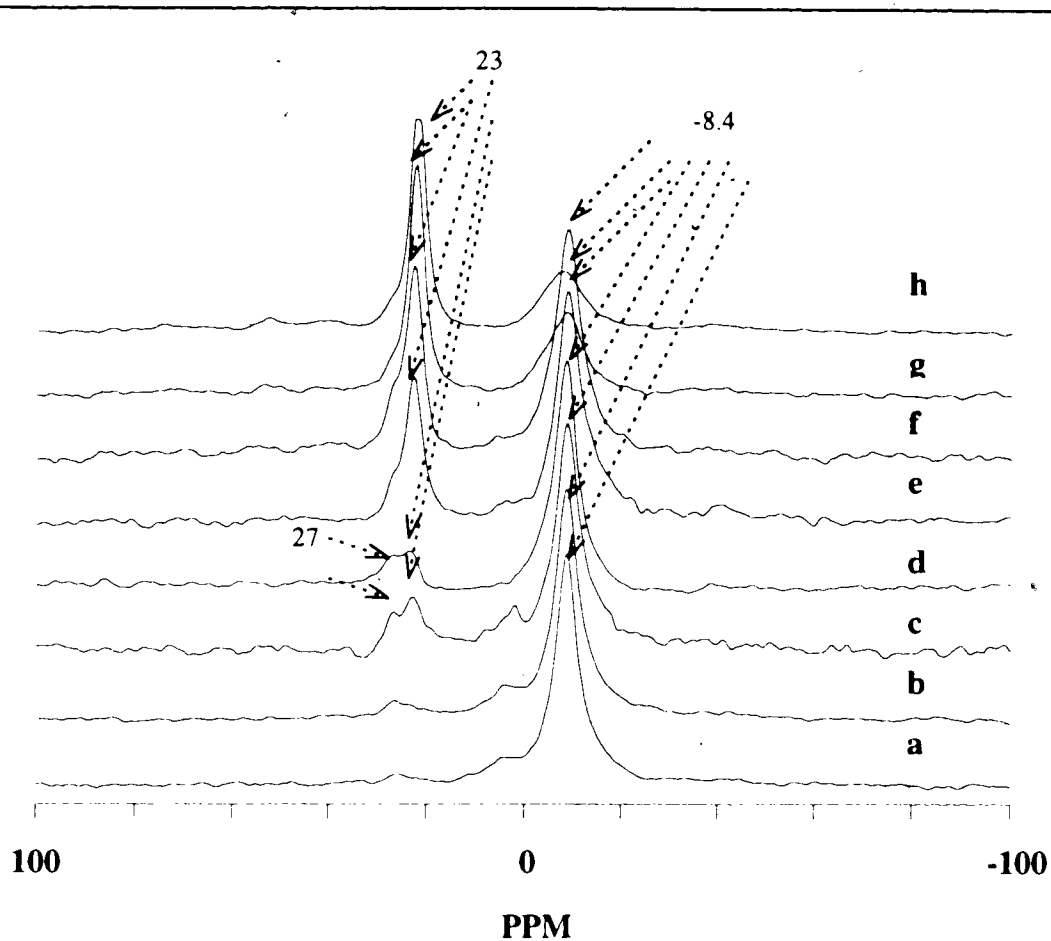


Figure 6.25 ^{31}P MAS NMR spectra of $0.80 \mu\text{mol}/\text{m}^2$ ($p\text{-ClC}_6\text{H}_4$) $_3\text{P}$ on Al_2O_3 catalyst with 6.2 SiO_2 per nm^2 using cross-polarization flipback (except specified), with different adsorption temperatures, the monolayer catalyst was degassed at 450°C and 10^{-5} torr for two hours, 1.84 kHz MAS rate, 1 s recycle delay. a) 100°C 1 hour, 62134 scans; b) 150°C 1 hour, 68360 scans; c) 200°C 1 hour, 66960 scans; d) dipolar depahsing, 200°C 1 hour, $70 \mu\text{s}$, 62892 scans; e) 200°C 2 hours, 141600 scans; f) 200°C 4 hours, 404122 scans; and g) 200°C 16 hours, 80125 scans; and h) 200°C 56 hours, 146751scans

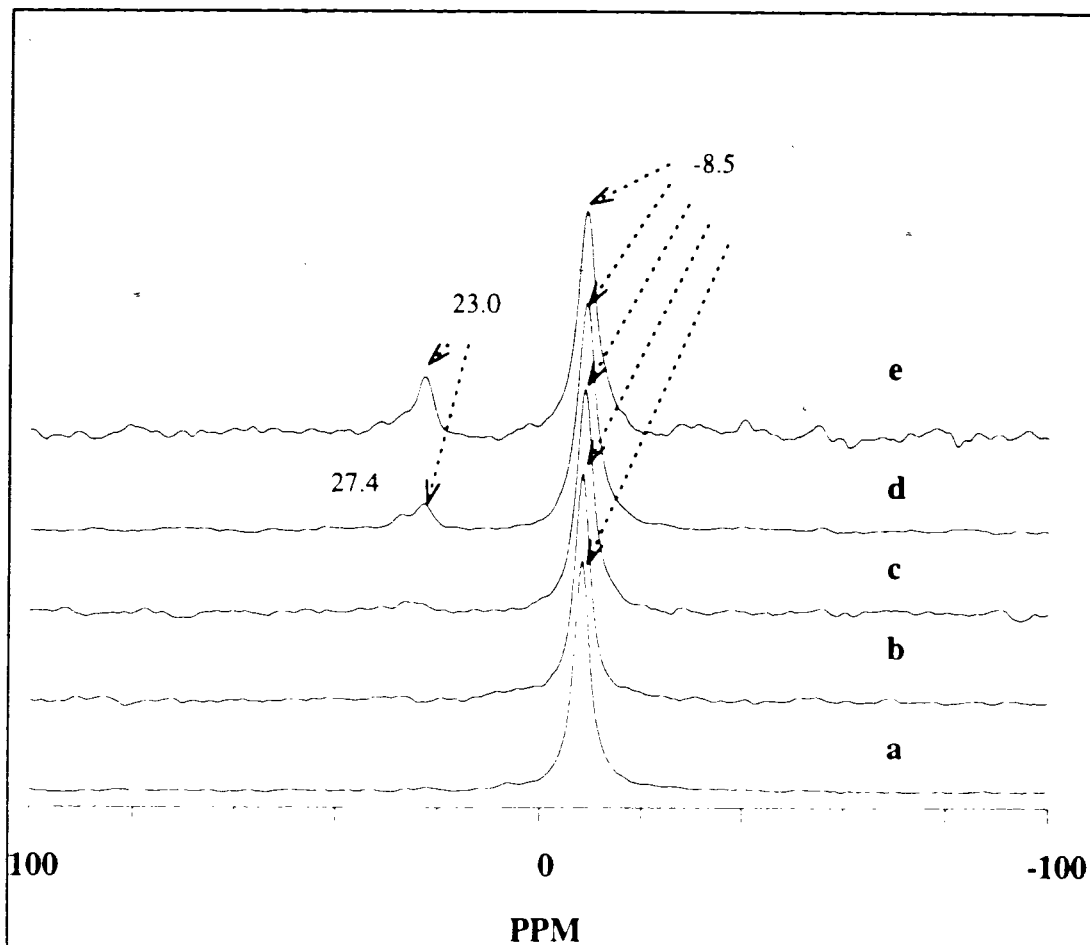


Figure 6.26 ^{31}P MAS NMR spectra of $1.47 \mu\text{mol}/\text{m}^2$ $(p\text{-ClC}_6\text{H}_4)_3\text{P}$ on Al_2O_3 catalyst with 6.2 SiO_2 per nm^2 , with different adsorption temperature, the monolayer catalyst was degassed at 450°C and 10^{-5} torr for two hours, 1.84 kHz MAS rate, 90° pulse, 1 s recycle delay. a) 100°C 1 hour, 83080 scans; b) 150°C 1 hour, 11873 scans; c) 200°C 1 hour, 11120 scans; d) 200°C 2 hours, 58205 scans; and e) 200°C 4 hours, 25135 scans.

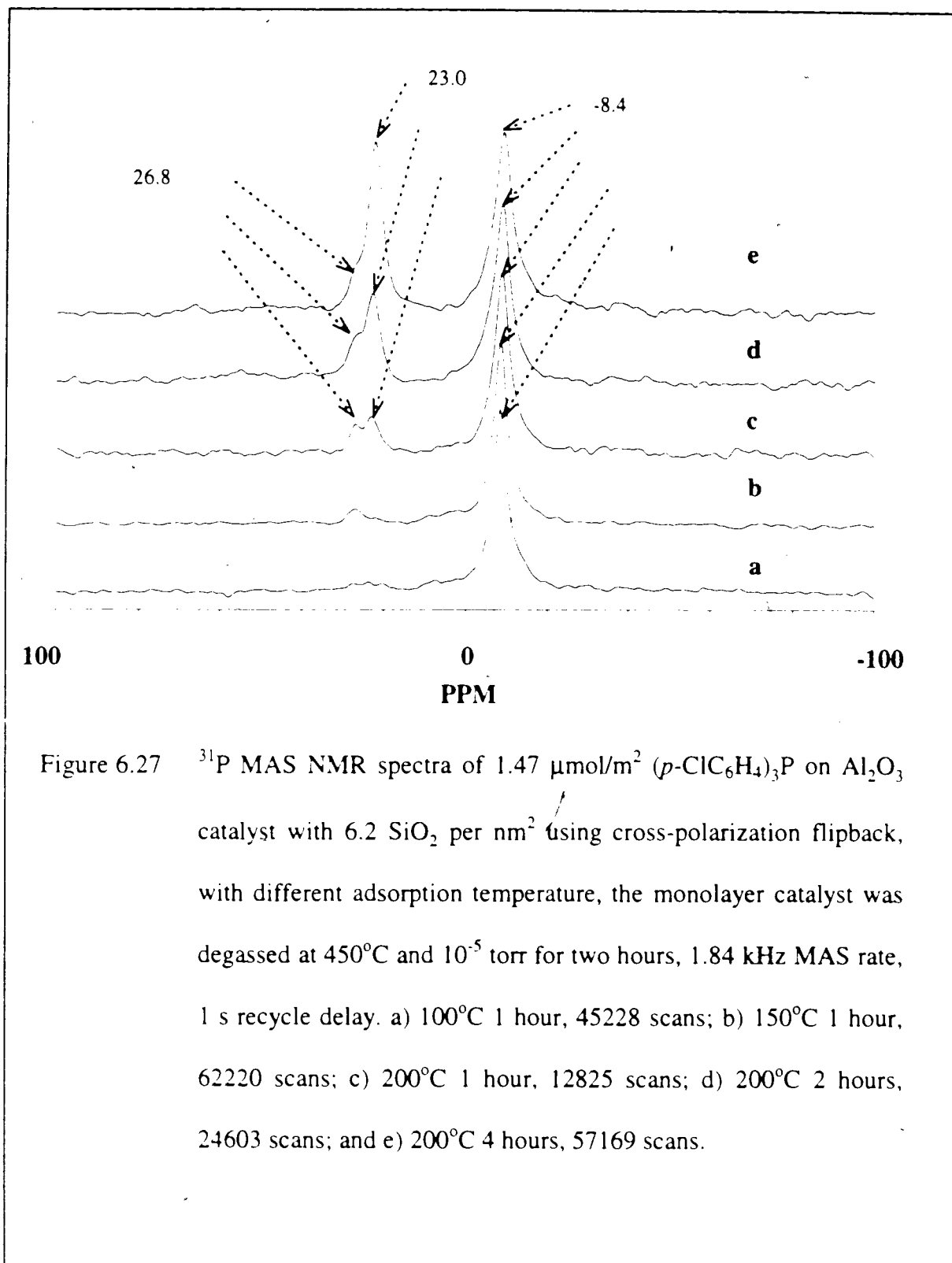


Figure 6.27 ^{31}P MAS NMR spectra of $1.47 \mu\text{mol}/\text{m}^2$ (*p*-ClC₆H₄)₃P on Al₂O₃ catalyst with 6.2 SiO_2 per nm^2 using cross-polarization flipback, with different adsorption temperature, the monolayer catalyst was degassed at 450°C and 10^{-5} torr for two hours, 1.84 kHz MAS rate, 1 s recycle delay. a) 100°C 1 hour, 45228 scans; b) 150°C 1 hour, 62220 scans; c) 200°C 1 hour, 12825 scans; d) 200°C 2 hours, 24603 scans; and e) 200°C 4 hours, 57169 scans.

3. Conclusion

Using Ph_3P , the maximum Brønsted acid concentrations are roughly the same for the coated catalyst and the commercial silica-alumina catalyst. However, using PMe_3 and Cy_3P , the values of the Brønsted acid concentration are higher than those on the commercial catalyst. Since Ph_3P is a weaker base, this suggests that the numbers of strong acid sites probably are the same for these two kinds of catalyst. However, the coated catalyst has more weaker acid sites than the commercial catalyst. The Lewis acid site was observed on the coated catalyst, but not on the commercial catalyst by Cy_3P . This is due to: a) the coated acid catalyst has more Lewis acid sites; b) the Lewis acid sites on commercial catalyst were not accessible due to diffusion difficulties; c) or both. Me_3P finds Lewis acid sites¹ on the commercial catalyst suggesting b).

The diffusion on the Al_2O_3 monolayer catalyst is much easier than on the commercial catalyst. A temperature of 100°C is high enough for Ph_3P molecules to approach Brønsted acid sites. Using Cy_3P and Me_3P at different adsorption temperatures, the titration curves of the Al_2O_3 monolayer catalyst were not significantly different. The monolayer Al_2O_3 catalyst has a similar pore size distribution as compared to the original $\gamma\text{-Al}_2\text{O}_3$. Therefore the Al_2O_3 monolayer catalyst has about 2-fold larger pores than the commercial silica-alumina catalyst.

We suggest that the lower mobility at higher coverage may weaken the P-H bonding. This may further cause a weak basic phosphine to lose the proton. Therefore a genuine decrease of Brønsted acid concentration was observed on both the catalysts. The structure involving the aluminum octahedral group was proposed as the active center on the acidic catalysts.

4. References

1. T. C. Sheng, and I. D. Gay, *J. Catal.* **145**, 10 (1994).
2. M. Niwa, N. Katada, and Y. Murakami, *J. Phy. Chem.* **94**, 6441 (1990).
3. S. Sato, M. Toita, T. Sodesawa, and F. Nozaki, *Appl. Catal.* **62**, 73 (1990).
4. M. Niwa, S. Morimoto, M. Kato, T. Hattori and Y. Murakami, *Proc. Int. Cong. Catal., 8th*, **4**,701 (1984).
5. L. Baltusis, J. S. Frye, and G. E. Maciel, *J. Am. Chem. Soc.*, **108**, 7119 (1986).
6. L. Baltusis, J. S. Frye, and G. E. Maciel, *J. Am. Chem. Soc.*, **109**, 40 (1987)
7. J. J. Daly, *J. Chem. Soc.*, 3799 (1964).
8. M. M. Crutchfield, C. H. Dungan, J. H. Letcher, V. Mark, and J. R. Van Wazer, "P³¹ Nuclear Magnetic Resonance", 283 (1967).

Chapter 7 Lewis acid sites using adducts of the phosphines and AlCl₃ by ³¹P NMR; poisoning effects of adsorbed phosphines on commercial silica-alumina catalyst using 1-butene isomerization reaction followed by GC, and the adsorbed (*p*-ClC₆H₄)₃PO species by Mass Spectroscopy

1. Introduction

The adducts of phosphines and aluminum are useful models of Lewis acid interactions. Adsorbed phosphines on alumina show shifts corresponding to Lewis acid sites (Chapter 4-6). However, those peaks are too broad to identify exact positions. Aluminum chloride can unambiguously show the positions of Lewis acid species. AlCl₃-Me₃P complexes mixed with zeolite have been characterized by ³¹P, and ²⁷Al solid state NMR¹⁻². It has shown that the complexes are present in two forms, AlCl₃:PMe₃ and Me₃P:AlCl₃:PMe₃¹.

For P-Al bonding systems, MAS cannot completely average the dipolar interaction, since Al is a quadrupolar nucleus. The theory of the spectroscopy of spin 1/2 nuclei bound to quadrupolar nuclei in solids has been reviewed³. Analysis of the spinning sideband multiplet in ³¹P spectra was used to measure the P-Al dipolar coupling constant, benefiting from the unique sextet feature of the coupling with a spin 5/2 ²⁷Al¹.

Poisoning experiments with basic molecules have been widely used to determine the number of sites responsible for the catalytic activity on acidic catalysts. Quinoline⁴, pyridine⁵ and 2,6-dimethylpyridine⁶ have been used to react with active sites. Checking the poisoning effects with the same adsorbed phosphines used for NMR studies can relate the apparent acidic concentrations with the active sites for the real catalytic reaction. This is helpful, since the phosphines used for this project have quite different basic strengths.

2. Results and Discussion

a ^{31}P NMR

Figure 7.1 shows the spectra of Ph_3P and AlCl_3 mixture, with 21% (mol) Ph_3P . Figure 7.1a shows the spectrum using 90° pulse program. The peak at -4.4 ppm arises from physically adsorbed species, close to -6 ppm of Ph_3P found on silica gel, Figure 5.2, Chapter 5. The peak at 7.3 ppm was from protonated species, the same shift found for Brønsted acid species on the silica-alumina catalyst, Figure 5.4, Chapter 5. The formation of protonated species probably was caused by small amounts of H_2O present in the AlCl_3 sample. Using 2 s recycle delay in Figure 7.1 a, Lewis acid species were not observed. This is due to much longer T_1 values for Lewis-bound species. A 500 s recycle delay does show the Lewis acid species (Figure 7.2b).

Using cross-polarization flipback experiments, the resonance lines for Lewis acid species with the sextet subpeaks were found, as shown in Figure 7.1 b to 7.1 d, which show repeat spectra at different times after sample preparation. The centers of spectra for the Lewis acid species were at -12 to -9 ppm. This is in the range of the Lewis acid species found on alumina, Figure 5.3, Chapter 5. According to reference³, assuming that none of the multiplet lines are caused to cross over by the second-order shifts (from quadrupolar Al nucleus), the average spacing gives the isotropic J coupling constant. This probably is the case for our spectra, since the spacings of the multiplets are not

significantly different. Therefore the values of J_{P-Al} were averaged as 302, 254, 254 Hz respectively from Figure 7.1b to 7.1d. Since the experimental error of chemical shift is smaller than 0.3 ppm, Figure 7.1 c and 7.1d probably show the same species, but different from Figure 7.1b.

Figure 7.2 shows 28% (mol) Ph_3P and $AlCl_3$ mixture, using 90° pulse experiments. The Brønsted-acid species at 7.4 ppm is very mobile. Without decoupling (Figure 7.2 c and 7.2 d), the spectra gave a J_{P-H} coupling around 500 Hz. The protonated acid species are liquid-like. However a small chemical shift anisotropy was observed using 0 or 90 Hz MAS rate (Figure 7.2 c and 7.2 e). This might just show effects of diamagnetic susceptibility of the sample. This broadening of the line happens if particles are not ellipsoidal, and is removed by MAS.

Figure 7.3 shows 28% (mol) Ph_3P and $AlCl_3$ mixture, using cross polarization flipback experiments measured at different times. Averaging the splitting, we get the values of J_{P-Al} : 259, 264 and 259 Hz respectively from Figure 7.3a to 7.3c, almost same as the species in Figure 7.1 c, 7.1 d and 7.2 b (254 Hz). The centers of the chemical shifts are around -8 to -9 ppm. When the Ph_3P percentage increases to 50% (mol), we also only observe the species with 259 Hz J_{P-Al} (Figure 7.4 d). Using 90° pulse experiments (Figure 7.4 a to 7.4c), the spectra look different from those with smaller PPh_3 percentages. According to T_1 values in Chapter 6, at high percentages of the phosphine, the mobility of the protonated species was anticipated to decrease. Thus the difference of T_1 between

Brønsted acid and Lewis acid species was probably smaller. Figure 7.4a to 7.4c could show the overlapped spectra of these two kinds of species.

Figure 7.5 shows 25% (mol) (*m*-Tol)₃P and AlCl₃ mixture. The peaks around 6 ppm (Figure 7.5a to 7.5c) arise from Brønsted acid species, 5-6 ppm was found for the same species on the silica-alumina catalyst, Figure 5.21 and 5.22, Chapter 5. The peaks at -7.1 ppm with the spinning side bands in Figure 7.5 c and 7.5 d probably arise from crystalline (*m*-Tol)₃P, since the pure sample resonates at -6.7 ppm (Table 3.3, Chapter 3). The centers of the Lewis peaks are at -18 ppm, these were hardly observed on the alumina surface (Figure 5.20, Chapter 5).

Figure 7.6 shows 12% (mol) (*p*-Tol)₃P and AlCl₃ mixture. The peaks at 6 ppm in Figure 7.6 a to 7.6 c probably arise from the protonated phosphine, close to 4-5 ppm found for the same species on the silica-alumina surface in Figure 5.13, Chapter 5. The values of J_{P-Al} were calculated as 337 and 298 Hz based on the average splittings for the sites in Figure 7.6 b and 7.6 c respectively.

Figure 7.7 shows 10% (mol) (*o*-Tol)₃P and AlCl₃ mixture. The peak at -12 ppm (Figure 7.7a) arises from the protonated species, confirmed by the undecoupled experiment in Figure 7.7b. The resonances of the Brønsted acid and Lewis acid sites (-13 ppm) are closer to each other than for other phosphines. This is consistent with the results on the silica-alumina catalyst surface (Figure 5.36, Chapter 5). Again, two kinds of Lewis

acid species were observed with the $J_{P,AI}$ values of 338 and 273 Hz for the sites in Figure 7.7 c and 7.7 d respectively.

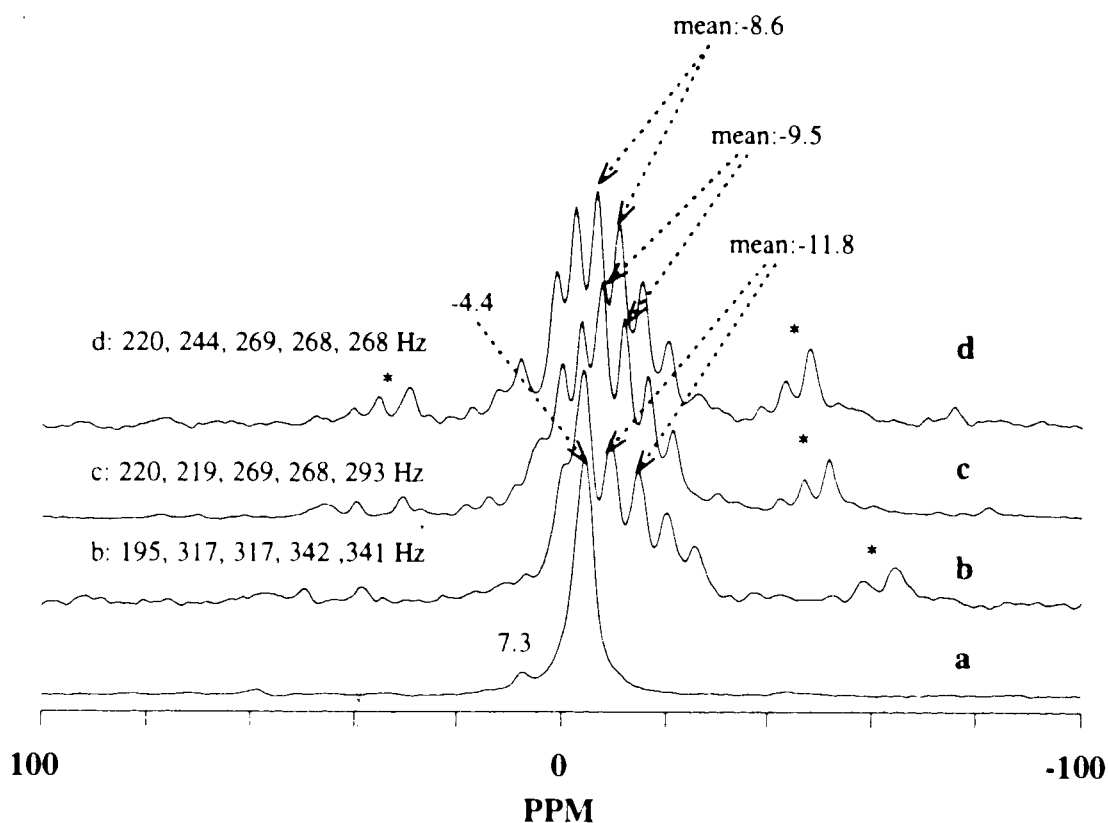


Figure 7.1 ^{31}P NMR MAS spectra of Ph_3P and AlCl_3 mixture, 21% (mol) Ph_3P , heated at 100°C for one hour, cross-polarization filpback (if not specified), 2 s recycle delay (if not specified). a) 90° pulse, same day of sample preparation, 1.83 kHz MAS rate, 2000 scans; b) same day of sample preparation, 2.02 kHz MAS rate, 5000 scans; c) one week later, 1.83 kHz MAS rate, 29160 scans; and d) three years later, 1.67 kHz MAS rate, 1 s recycle delay, 21659 scans; * = spinning side bands.

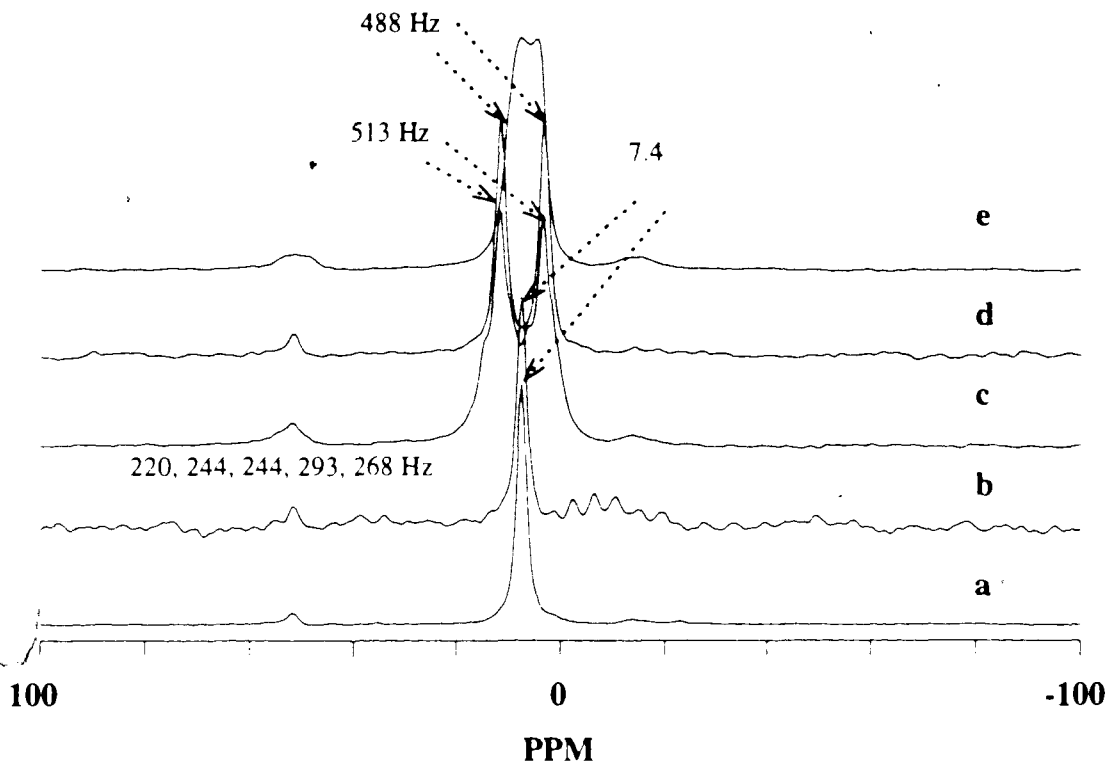


Figure 7.2 ^{31}P NMR MAS spectra of Ph_3P and AlCl_3 mixture, 28% (mol) Ph_3P , heated at 100°C for one hour, 90° pulse, 1 s recycle delay (if not specified). a) 1.74 kHz MAS rate, 51388 scans; b) 1.75 kHz MAS rate, 500 s recycle delay, 312 scans; c) 0.09 kHz MAS rate, decoupler off, 36117 scans; d) 1.75 kHz MAS rate, decoupler off, 8510 scans; and e) 0 Hz MAS rate, decoupler off, 54021 scans.

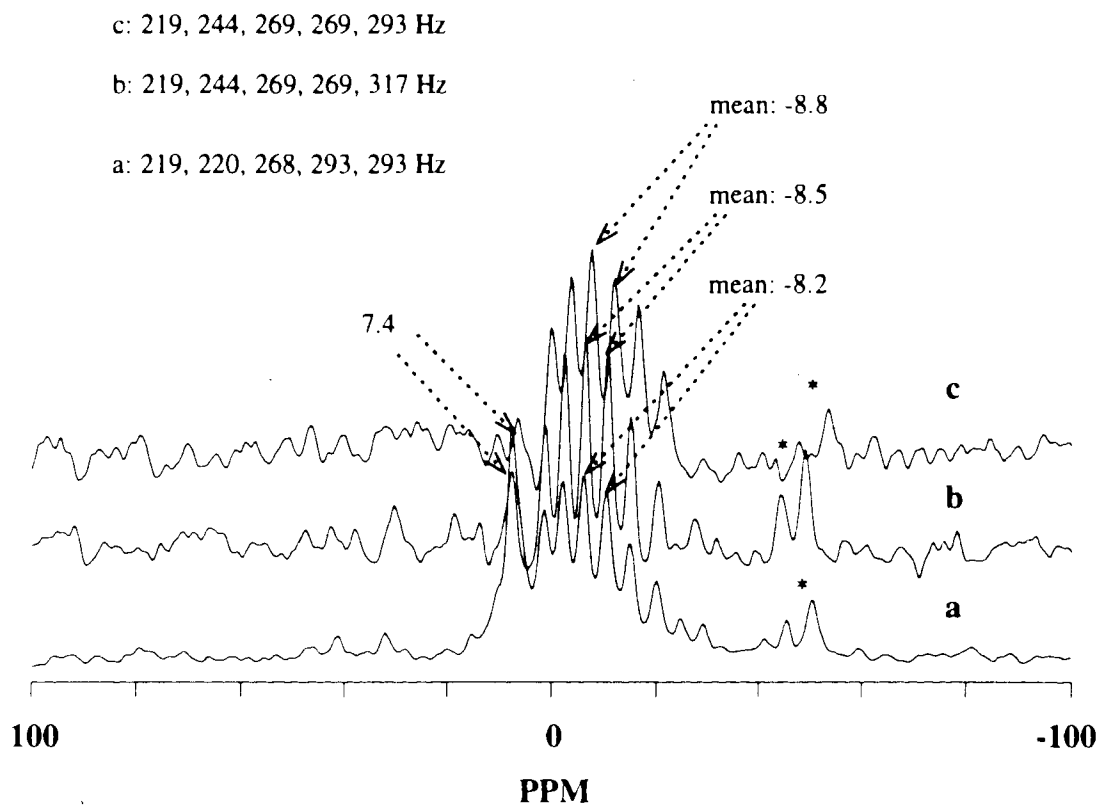


Figure 7.3 ^{31}P NMR MAS spectra of Ph_3P and AlCl_3 mixture, 28% (mol) Ph_3P , heated at 100°C for one hour, cross-polarization filpback, 1 s recycle delay. a) same day of sample preparation, 1.83 kHz MAS rate, 232504 scans; b) one week later, 1.75 kHz MAS rate, 58606 scans; and c) one month later, 1.91 kHz MAS rate, 16745 scans; * = spinning side bands.

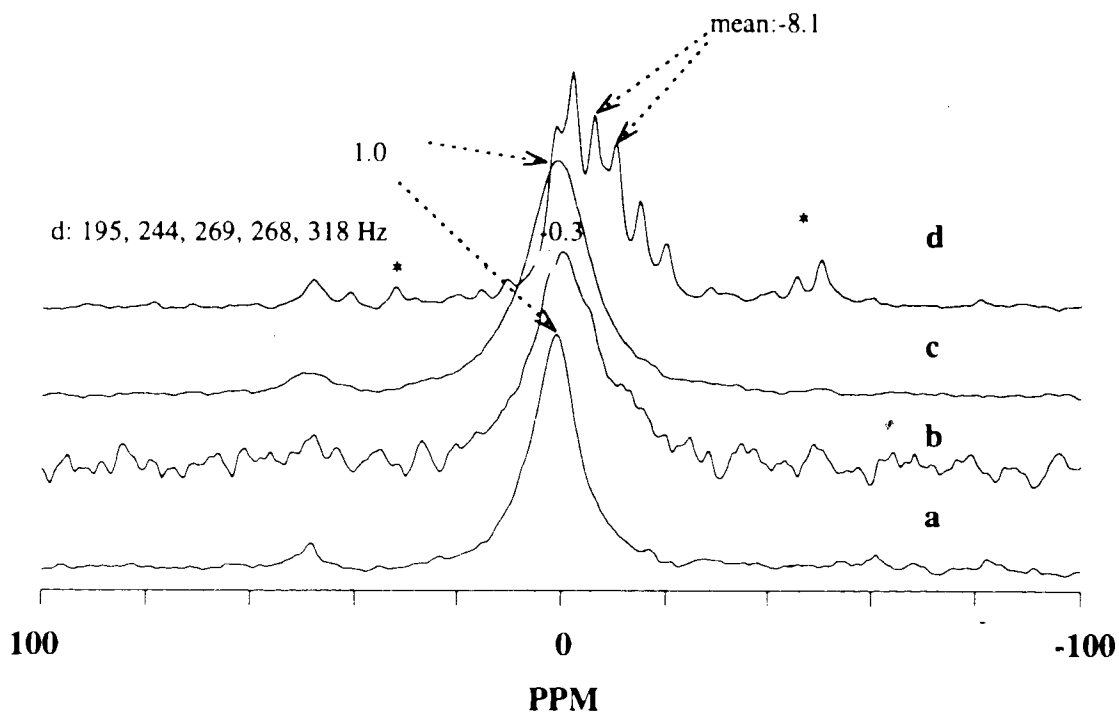


Figure 7.4 ^{31}P NMR MAS spectra of Ph_3P and AlCl_3 mixture, 50% (mol) Ph_3P , heated at 100°C for one hour, 90° pulse (if not specified), 1 s recycle delay. a) 1.84 kHz MAS rate, 14960 scans; b) decoupler off, 1.84 kHz MAS rate, 1990 scans; c) decoupler off, 0 kHz MAS rate, decoupler off, 59821 scans; and d) cross-polarization flipback, 1.83 kHz MAS rate, 65621 scans; * = spinning side bands.

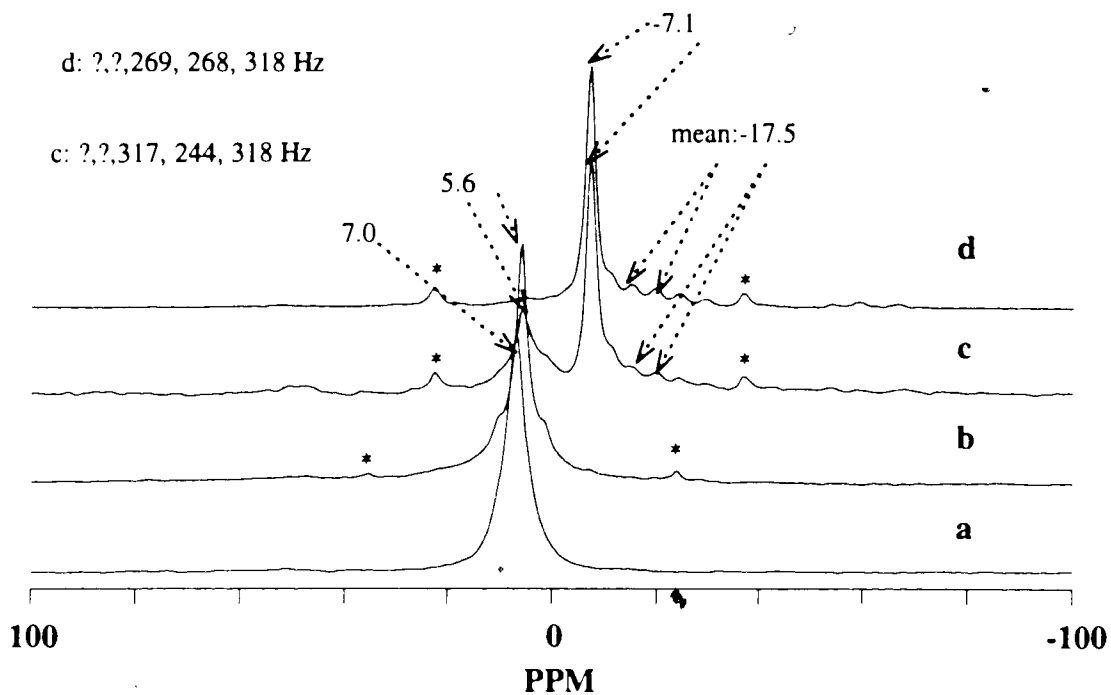


Figure 7.5 ^{31}P NMR MAS spectra of (*m*-Tol) $_3\text{P}$ and AlCl_3 mixture, 25% (mol) (*m*-Tol) $_3\text{P}$, heated at 100°C for one hour, 1 s recycle delay (if not specified), 90° pulse (if not specified). a) 0 Hz MAS rate, 393 scans; b) 1.78 kHz MAS rate, 9230 scans; c) 500 s recycle delay, 1.78 kHz MAS rate, 114 scans; and d) cross polarization flipback, 1.79 kHz MAS rate, 2953 scans; * \pm spinning side bands.

From Figure 7.1 to 7.7, a few peaks seem to show overlapping spectra, such as Figure 7.1 b and 7.6 b. Hence the average J values may be wrong. We can overcome the problem by fitting a line shape to various multiplets³. According to Equation (21) in reference³, $\nu = A + J m + K m^2$, which permits to discard peaks that look bad due to overlap. The results of fitting are shown on Table 7.1.

Table 7.1 shows that average J is about the same as the results from fitting, so the overlapping is not very serious. From Table 7.1, both J and K seem to get smaller with time. The change in K is due to either bond distance becoming longer or the Al environment becoming more symmetrical, because K is proportional to the product of the P-Al dipolar coupling and the ²⁷Al quadrupolar coupling.

Table 7.1 Results of fitting quadratic coupling experiments

Figure	# of peaks	J (Hz)	J _{ave} (Hz)	K
7.1b	6	309	302	14.8
	5 (omit m=-3/2)	304		13.9
7.1c	6	254	254	10.0
	5 (omit m= -1/2)	253		9.0
7.1d	6	256	254	6.0
7.3a	6	259	259	11.8
7.3b	6	263	264	10.5
	5 (omit m= 1/2)	264		10.3
7.3c	6	260	259	8.4
7.6b	6	330	337	4
	5 (omit m=-3/2)	338		5.7
7.6c	6	294	298	0.1
	5 (omit m=-3/2)	296		0.1
	5 (omit m=-1/2)	295		1.3
	4 (omit m= -3/2, -1/2)	298		2.7
7.7c	6	336	338	11.8
	5	337		12.9
7.7d	6	270	273	10.0
	(omit m=-1/2)			
	5 (omit m= 1/2)	271		6.8

b GC

Table 7.2 summarizes the GC results for 1-butene isomerization using the commercial silica-alumina catalyst coated with adsorbed phosphines. With adsorbed phosphines, the conversion ratio is greatly decreased. The stronger the base, the greater the poisoning effects. (*p*-tol)₃P is a stronger base than Ph₃P (see table 3.1, Chapter 3). Hence, the poisoning effect of the (*p*-Tol)₃P is greater. With high coverage of aryl phosphines, a small conversion still was observed, but not with Cy₃P. This suggests that Cy₃P blocks all the active sites. Since we did not detect Lewis acid species on the commercial catalyst, the active centers must be Brønsted acid sites. These results show that weak acid sites (which cannot be poisoned by Ph₃P or (*p*-Tol)₃P) can also catalyze this isomerization reaction.

Table 7.2 Poisoning of 1-butene isomerization on the silica-alumina catalyst

Sample	Weight (mg)	Temp °C.	2-Butene(<i>trans</i>)/1-Butene	2-Butene(<i>cis</i>)/1-Butene
Untreated Catalyst	10.4	76	0.52	0.43
		115	1.8	1.2
		120	2.2	1.4
Preheated Catalyst (350°C 0.5 h)	10.4	105	1.5	0.99
		120	2.2	1.5
Catalyst with Ph ₃ P (0.40 μmol/m ²)	6.0	120	.10	.09
Catalyst with Ph ₃ P (1.00 μmol/m ²)	9.3	120	0.08	0.07
Catalyst with (<i>p</i> -Tol) ₃ P (0.75 μmol/m ²)	8.3	120	0.08	0.07
Catalyst with (<i>p</i> -Tol) ₃ P (1.00 μmol/m ²)	15.3	120	0.06	0.05
Catalyst with Cy ₃ P (1.70 μmol/m ²)	16.4	120	0	0

c Mass Spectroscopy

Chapter 5 shows that adsorbed $(p\text{-ClC}_6\text{H}_4)_3\text{PO}$ species probably exist on the surface. Here we use MS to further confirm this. Table 7.3 shows the MS results of surface adsorbed $(p\text{-ClC}_6\text{H}_4)_3\text{PO}$. These samples were run under similar conditions. A 1 mg sample was put into a melting point tube and sealed under Ar pressure. Later the solid sample was handed to Mr. G. Owen. It was broken and quickly transferred to the machine, evacuated and heated to 250°C followed by MS measurements. The MS data of $(p\text{-ClC}_6\text{H}_4)_3\text{P}$ or $(p\text{-ClC}_6\text{H}_4)_3\text{PO}$ are not available from the literature. Here, we use Ph_3P and Ph_3PO as references to characterize the species (Table 7.4). Checking the data in Table 7.3, we found that a) the mixture of $(p\text{-ClC}_6\text{H}_4)_3\text{P}$ and Me_3NO shows only the $(p\text{-ClC}_6\text{H}_4)_3\text{PO}$ species; and b) the samples of $(p\text{-ClC}_6\text{H}_4)_3\text{P}$ adsorbed on the catalysts show both $(p\text{-ClC}_6\text{H}_4)_3\text{PO}$ and $(p\text{-ClC}_6\text{H}_4)_3\text{P}$ species. These are totally consistent with the corresponding NMR spectra.

The theoretical isotope patterns for $\text{C}_{18}\text{H}_{12}\text{Cl}_3\text{P}$ and $\text{C}_{18}\text{H}_{12}\text{Cl}_3\text{PO}$ are listed in Table 7.5. It is interesting to notice that phosphine oxide has M-1 fragments, whereas phosphine has M fragments (see Table 7.3 and 7.4). Figure 7.8 shows mass spectrum of $0.34 \mu\text{mol}/\text{m}^2$ $(p\text{-ClC}_6\text{H}_4)_3\text{P}$ desorbed from the silica-alumina catalyst. It shows the pattern of both $(p\text{-ClC}_6\text{H}_4)_3\text{PO}$ and $(p\text{-ClC}_6\text{H}_4)_3\text{P}$ species.

Table 7.3 MS results of the adsorbed phosphine and phosphine oxides

Sample	Related MS results: m/z (abundance)	Related NMR spectra
$(p\text{-ClC}_6\text{H}_4)_3\text{P}+\text{Me}_3\text{NO}$	381(100), 379(94), 380(44), 382(43), 383(35), 384(14)	Figure 5.30, Chapter 5
0.24 $\mu\text{mol}/\text{m}^2$ $(p\text{-ClC}_6\text{H}_4)_3\text{P}$ on silica-alumina	381(100), 368(99), 379(91), 380(53), 382(50), 369(50), 383(45), 384(18), 367(17), 364(13), 366(11)	Figure 5.28 c, Chapter 5
0.80 $\mu\text{mol}/\text{m}^2$ $(p\text{-ClC}_6\text{H}_4)_3\text{P}$ on monolayer alumina with coated SiO_2	366(100), 364(89), 368(60), 365(29), 369(26), 367(21), 381(9), 379(8), 382(4), 380(3), 383(2)	Figure 6.49 Chapter 6

Table 7.4 Literature MS results for Ph₃P and Ph₃PO⁷

Sample	Molar Mass	MS results, m/z (abundance)
Ph ₃ P	262	262(100), 183(43), 263(23), 108(21), 107(10), 184(10), 261(7), 185(7)
Ph ₃ PO	278	277(100), 278(57), 77(30), 201(20), 199(13), 183(13), 51(10), 185(9)

Table 7.5 Theoretical isotope patterns of $C_{18}H_{12}Cl_3P$ and $C_{18}H_{12}Cl_3PO$

Chemical	m/z (theoretical abundance)
$C_{18}H_{12}Cl_3P$	364(100.00), 366(99.15), 368(33.39), 365(20.35), 367(19.88), 369(6.51), 370(4.02), 371(0.73), 372(0.07)
$C_{18}H_{12}Cl_3PO$	380(100.00), 382(99.36), 384(33.60), 381(20.38), 383(19.96), 385(6.56), 386(4.09), 387(0.74), 388(0.08)

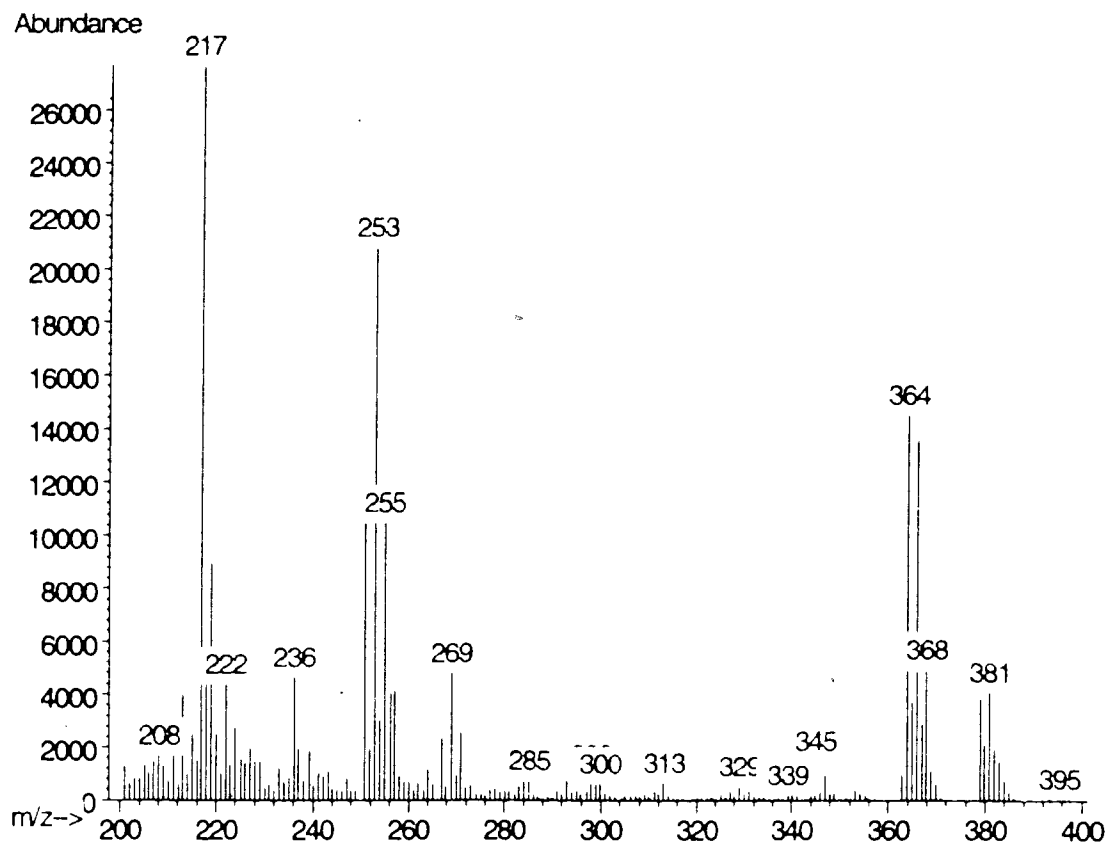


Figure 7.8 the mass spectrum of desorption products from $0.34 \mu\text{mol}/\text{m}^2$ $(p\text{-ClC}_6\text{H}_4)_3\text{P}$ on the silica-alumina catalyst

3. References

1. P. J. Chu, A. de Mallmann, and J. H. Lunsford, *J. Phys. Chem.*, **95**, 7362 (1991).
2. P. J. Chu, J. H. Lunsford, and D. J. Zalewski, *J. Magn. Res.*, **87**, 68 (1990).
3. R. K. Harris, and A. C. Oliveri, *Prog. in NMR spectra.*, **24**, 435 (1992).
4. M. S. Goldstein, and T. R. Morgan, *J. Catal.*, **16**, 232 (1970).
5. P. A. Jacob, H. Leeman and J. B. Uytterhoeven, *J. Catal.*, **33**, 17 (1974).
6. H. A. Bensi, *J. Catal.*, **28**, 176 (1973).
7. J. G. Grasselli, and W. M. Rittley (editor), *ATLAS of Spectra Data and Physical Constants for Organic Compounds*, Vol IV, 105 (1975).

Chapter 8 ³¹P NMR investigation of surface basicity using adsorbed PPh₃ HBr molecules

The previous titration results using some adsorbed phosphines show a genuine decrease of PR₃H⁺ concentration at higher coverages. The argument of multilayer physically adsorbed species was used to explain this phenomenon. The adsorption of HCl (gas) shows that basic OH groups are present on γ -Al₂O₃¹. We wonder whether similar OH groups may exist on the silica-alumina catalyst surface, which react with protonated phosphines at higher coverages. Therefore triphenylphosphine hydrobromide was used to check for this kind of hydroxyl group.

Figure 8.1 shows the ³¹P spectra of a pure PPh₃HBr sample. Three different but close peaks are found at -14, -15 and -17 ppm in Figure 8.1a to 8.1c. They arise from crystalline species with a P-H bond, confirmed by dipolar dephasing experiments (Figure 8.1 d). These probably indicate that three magnetically different species are present in the unit cell of crystalline Ph₃PHBr. When heated to 100°C, these three structures did not undergo any changes (Figure 8.1c). The intensities in Figure 8.1a and 8.1b were about 4 times of those in Figure 8.1c and 8.1d. Figure 8.1c and 8.1d have twice the data points as for Figure 8.1a and 8.1b, which causes 2-fold intensity change after FT.

The preparation procedures for PPh₃HBr/oxides are the same as for the phosphines in section 3a, Chapter 3. Figure 8.2 shows the spectra of PPh₃HBr on silica gel. After adsorption at 100°C (Figure 8.2 b- 8.2e), the crystalline molecules (Figure 8.2 a) were mainly converted to two kinds species at 1 and -5 ppm. Physically adsorbed Ph₃P resonated around -6 ppm (Figure 5.1 and 5.2, Chapter 5). Therefore the species at -5 ppm probably arise from physically adsorbed Ph₃P molecules which were produced by PPh₃HBr reacting with hydroxyl groups on the surface. The species at 1 ppm are

protonated, since they almost disappear using dipolar dephasing (Figure 8.2 e). They are probably physically adsorbed Ph_3PHBr . At 150°C (Figure 8.2 f), more physically adsorbed Ph_3P molecules were formed.

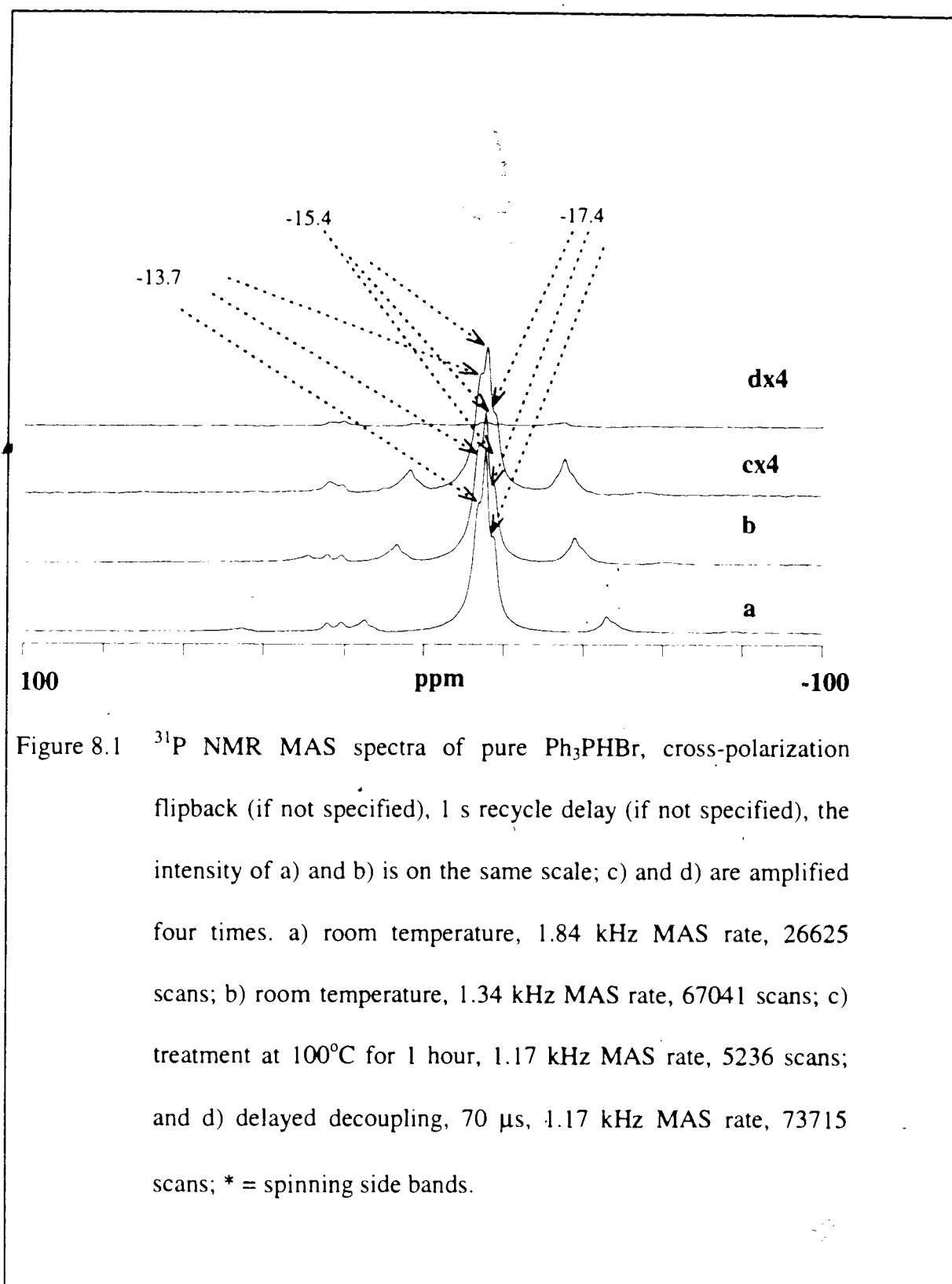
Figure 8.3 shows the spectra of $0.83 \mu\text{mol}/\text{m}^2$ Ph_3PHBr adsorbed on alumina at 100°C . The crystalline Ph_3PHBr was converted to a species resonating at -6.1 ppm (Figure 8.3 a -8.3 d), which is physically adsorbed PPh_3 according to Figure 5.3, Chapter 5. These results show that Ph_3PHBr can easily react with surface OH and form Ph_3P species. These OH groups are basic in nature and this result is in agreement with¹. There is about 0.8 basic OH/nm² ($1.3 \mu\text{mol}/\text{m}^2$) after the sample was dried at 600°C ¹. Our results show that at least $0.8 \mu\text{mol}/\text{m}^2$ basic OH was on the surface after degassing at 450°C .

Figure 8.4 shows the spectra of $0.40 \mu\text{mol}/\text{m}^2$ Ph_3PHBr adsorbed on silica-alumina catalyst at 100°C . The spectra look much like those from Ph_3P molecules (Figure 5.4 and 5.5). The peaks of -5.3 ppm in Figure 8.4 a-8.4 f arise from physically adsorbed species. The peak at 5.2 ppm is from Brønsted acid species, which was confirmed by dipolar dephasing experiments and Figure 8.4 a. The ratio of these two signal intensities changes with the increase in recycle delay (Figure 8.4 e and 8.4 f). However, no changes were found with Ph_3P (Figure 5.5, Chapter 5). The intensity ratios were almost the same with recycle delays after 150°C adsorption with Ph_3PHBr (The ratios are calculated as 0.17, 0.15, 0.14 and 0.16 respectively for Figure 8.5b to 8.5e).

Figure 8.6 shows the spectra of $0.80 \mu\text{mol}/\text{m}^2$ Ph_3PHBr adsorbed on silica-alumina catalyst. The spectra are different at the higher coverage (compared with Figure 8.4 and 8.5). The peak for the Brønsted acid species (5.2 ppm in Figure 8.4 and 8.5) is not observed in Figure 8.6. A new peak at -9.5 ppm is detected using cross-polarization

experiments. The peaks at -6.1 ppm in Figure 8.6 are physically adsorbed Ph_3P species, according to results of Figure 8.2 to 8.5. However the peak is narrower. We heated crystalline Ph_3PHBr at 100°C (Figure 8.1 c) and Ph_3PHBr did not show any phase change. Hence the peak at -9.5 ppm is not crystalline Ph_3PHBr since the spectra in Figure 8.6 c to 8.6 d did not show the typical triple peaks as in Figure 8.1. The species at -9.5 ppm are protonated (Figure 8.6 e). Since 90° pulse experiment did not detect this kind of species (Figure 8.6 a and 8.6 b), at this coverage most of molecules on the surface are probably physically adsorbed Ph_3P species.

Using Ph_3P we observe a similar phenomenon: at higher coverages not much Brønsted acid is detectable (Figure 5.8, Chapter 5). In Chapter 6 we propose that the multilayer physical adsorption causes a low mobility of the adsorbed molecules and further make the Brønsted acid species undetectable. In this Chapter we found that basic OH groups are present on silica-alumina catalyst surface. The basic OH could cause the Brønsted acid species to disappear. However the results do not conflict with the argument in Chapter 6. The presence of basic groups is a more convincing argument. Brønsted acid species may be far away from basic sites, which are only accessible at higher phosphine coverages.



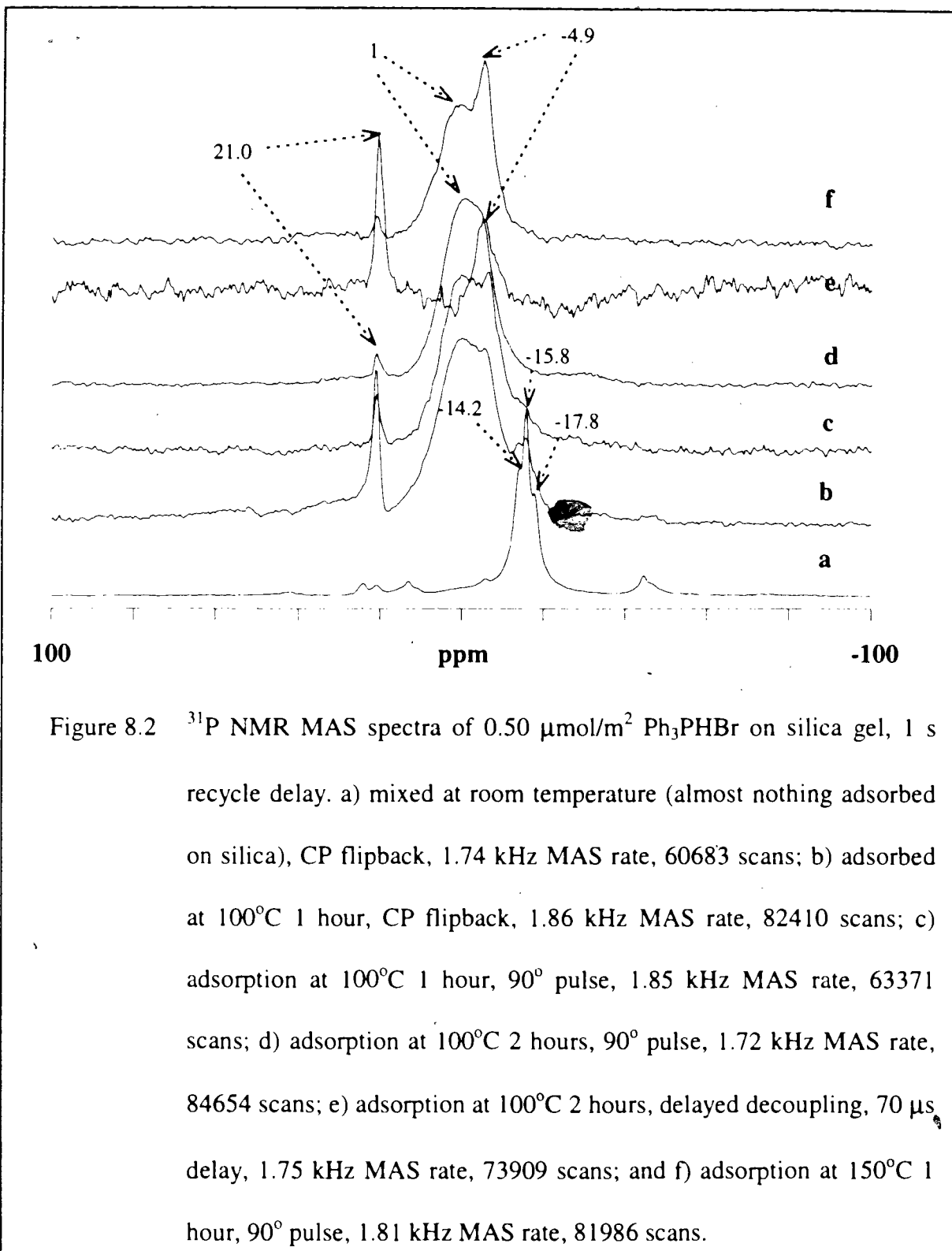


Figure 8.2 ^{31}P NMR MAS spectra of $0.50 \mu\text{mol}/\text{m}^2$ Ph_3PHBr on silica gel, 1 s recycle delay. a) mixed at room temperature (almost nothing adsorbed on silica), CP flipback, 1.74 kHz MAS rate, 60683 scans; b) adsorbed at 100°C 1 hour, CP flipback, 1.86 kHz MAS rate, 82410 scans; c) adsorption at 100°C 1 hour, 90° pulse, 1.85 kHz MAS rate, 63371 scans; d) adsorption at 100°C 2 hours, 90° pulse, 1.72 kHz MAS rate, 84654 scans; e) adsorption at 100°C 2 hours, delayed decoupling, $70 \mu\text{s}$ delay, 1.75 kHz MAS rate, 73909 scans; and f) adsorption at 150°C 1 hour, 90° pulse, 1.81 kHz MAS rate, 81986 scans.

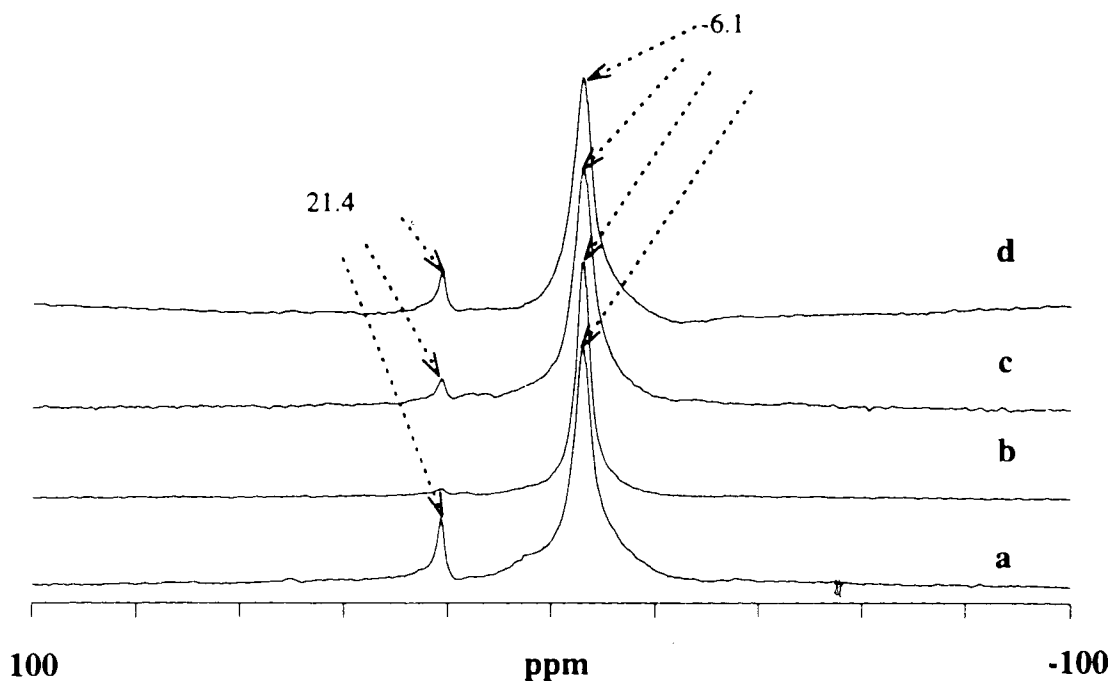
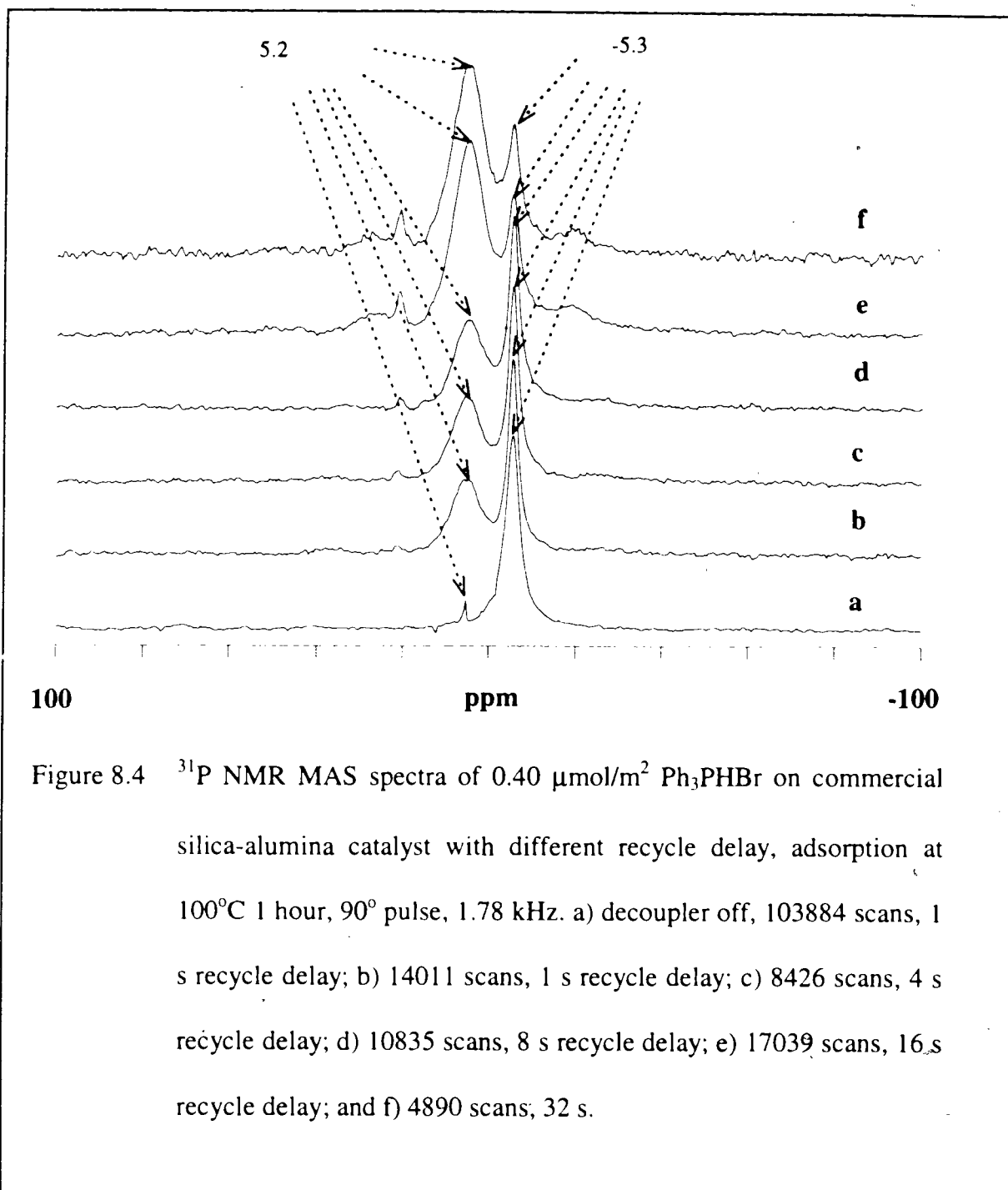


Figure 8.3 ^{31}P NMR MAS spectra of $0.83 \mu\text{mol}/\text{m}^2$ Ph_3PHBr on alumina, adsorption at 100°C 1 hour, 1 s recycle delay (if not specified). a) cross-polarization flipback, 1.73 kHz MAS rate, 65389 scans; b) 90° pulse, 1.75 kHz MAS rate, 27937 scans; c) 90° pulse, 1.25 kHz MAS rate, 13590 scans, 10 s recycle delay; and d) delayed decoupling, $70 \mu\text{s}$, 1.74 kHz MAS rate, 85352 scans.



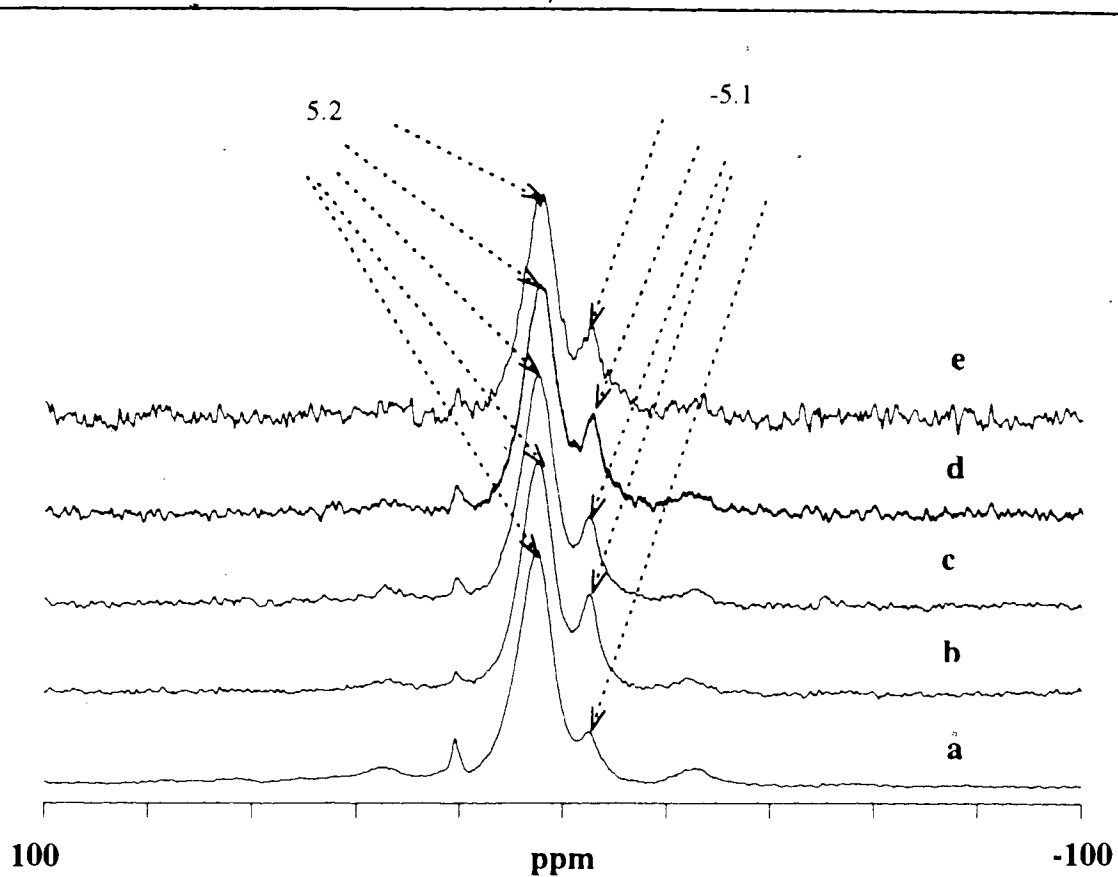


Figure 8.5 ^{31}P NMR MAS spectra of $0.40 \mu\text{mol}/\text{m}^2$ Ph_3PHBr on commercial silica-alumina catalyst with different recycle delay, adsorption at 150°C 1 hour, 90° pulse (if not specified), 1.76 kHz. a) cross-polarization, 169466 scans, 1 s recycle delay; b) 63952 scans, 1 s recycle delay; c) 12293 scans, 8 s recycle delay; d) 4451 scans, 16 s recycle delay; and e) 1334 scans, 32 s recycle delay.

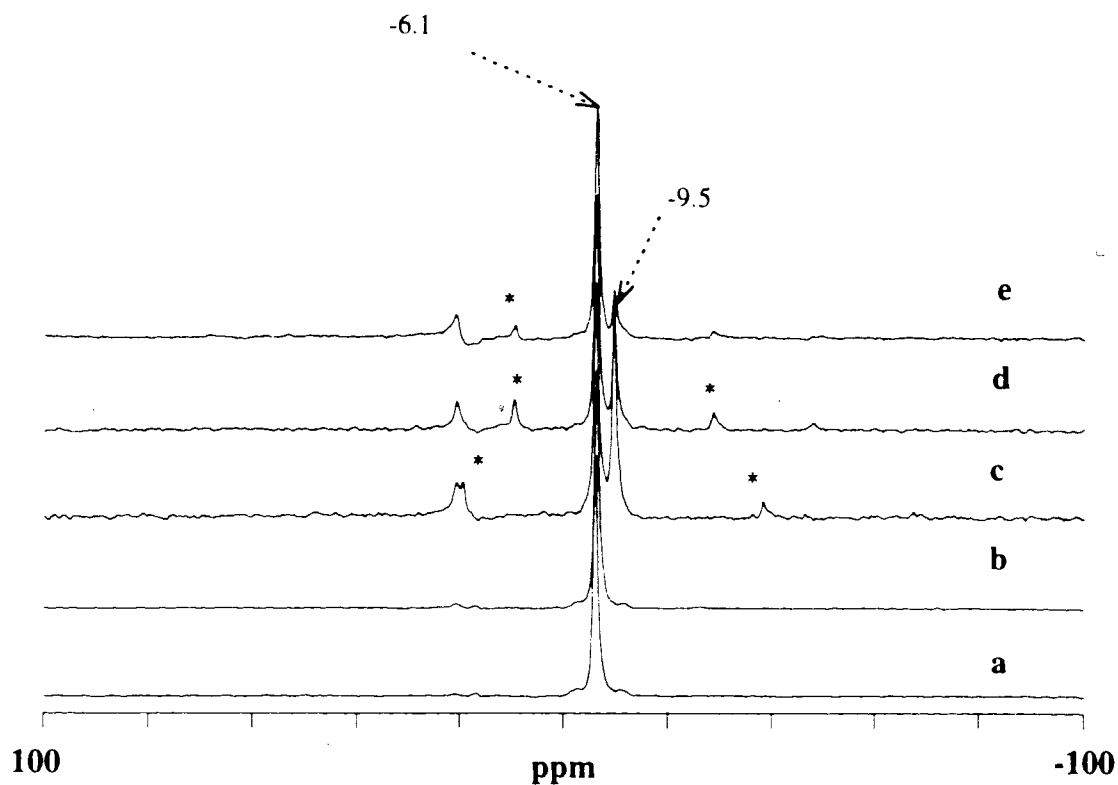


Figure 8.6 ^{31}P NMR MAS spectra of $0.80 \mu\text{mol}/\text{m}^2$ Ph_3PHBr on commercial silica-alumina catalyst, adsorption at 100°C 1 hour, 1.14 kHz MAS rate(if not specified) 1 s recycle delay (if not specified). a) 90° pulse, 3824 scans. b) 90° pulse, 3846 scans, 16 s recycle delay; c) cross-polarization flipback, 1.74 kHz MAS rate, 87423 scans; d)cross-polarization flipback, 78843 scans; and e) dipolar dephasing, $70 \mu\text{s}$, 76068 scans. * = spinning side band.

References:

1. A. Kytokivi, M. Lindblad and A. Root, *J. Chem. Soc. Faraday. Trans.*, **91(5)**, 941 (1995).

Chapter 9 Overall conclusion and future work

1. Facts

In this thesis, we have established some facts. Here we only summarize main aspects.

a **Cy₃P is an excellent ³¹P probe**

Cy₃P is a unique probe: it has high basic strength and bulky structure. Using Cy₃P, the measured Brønsted acid concentration is higher than with Me₃P and other phosphines. On the commercial silica-alumina catalyst, Lewis acid sites were not observed with Cy₃P. However on the monolayer Al₂O₃ catalyst coated with SiO₂, the Lewis acid sites were detected. Hence, Cy₃P is sensitive to different pore sizes.

Pure Cy₃P is a solid at room temperature and under atmospheric pressure. This is an advantage compared with other probes, such as Me₃P. At submonolayer coverages, the molecules are highly mobile. Without spinning side bands, quantitative measurement becomes easier. At monolayer or higher coverages, the mobility of adsorbed species decreases. We observed some special properties due to the mobility change. From these observations, we can make some interesting arguments.

Cy₃P is air sensitive, but it deserves the trouble of sample preparation. We also developed new methods of sample preparation, which did not involve any solvents and always kept the sample under vacuum after degassing.

b. Monolayer Al₂O₃ catalyst coated with SiO₂ is anticipated to be a better catalyst than commercial silica-alumina catalyst

The monolayer Al₂O₃ catalyst coated with 6.2 SiO₂ per nm² is a new catalyst prepared by the chemical vapor deposition method. Compared with commercial silica-alumina cracking catalyst: it has higher Brønsted acid concentration per nm² of the catalyst; more Lewis acid sites; and larger pore size distribution. With different adsorption temperatures, the measured Brønsted acid concentrations on the coated catalyst are not much different, but bigger variations for the commercial silica-alumina catalyst exist. Hence, the monolayer coated catalyst has less diffusion problems than the commercial catalyst. Generally we anticipate that the new catalyst will have better catalytic properties than the commercial catalyst, especially for cracking bulky materials.

c. Steric effects control the apparent Brønsted acid concentrations of the aryl phosphines

Using less basic arylphosphines, at higher coverages a genuine decrease of titration curves for Brønsted acid was observed. This phenomenon was explained by the presence of basic sites and the multilayer of physically adsorbed species at high surface coverages. The

our model was supported by the experimental results, since the argument was partly based on the NMR spectra.

3. Future work suggestions

a. Bulky phosphine oxide as ^{31}P NMR probes to study Lewis sites

For these bulky phosphines, the resonances from Lewis acid sites are still not well separated from those of physically adsorbed species. The bulky phosphine oxides may have the advantages for the quantitative investigation of Lewis acid sites, since some of results related to (*p*-ClC₆H₄)₃PO (Figure 5.29, Chapter 5) show this possibility.

b. ^{19}F NMR to study surface acidity

^{19}F is interesting because of the 100% natural abundance and the high gyromagnetic ratio (higher than ^{31}P). These cause strong dipolar coupling at the same time, which requires homonuclear decoupling for ^{19}F solid state NMR. However, the high gyromagnetic ratio may make it worthwhile to have a try.

p-Fluorobenzophenone may be good to detect Lewis acid sites using solid state MAS ^{19}F NMR. The chemical shift difference between it and the AlCl₃ adduct is about 16 ppm in solution¹, which is much bigger than those for arylphosphines by solid state ^{31}P NMR (1-8

ppm in Table 3.3, Chapter 3). According to reference¹, Al attaches to O (not F) in Lewis acid adduct. This avoids quadrupolar effects of Al on the solid ¹⁹F NMR spectrum. This molecule seems a possibility to directly measure Lewis acid concentrations on the surface.

4. References:

1. R. G. Dews, Y. Tsuno and R. W. Taft, *J. Am. Chem. Soc.* **88**, 3456 (1966).